UNIVERSITY OF READING

Department of Meteorology

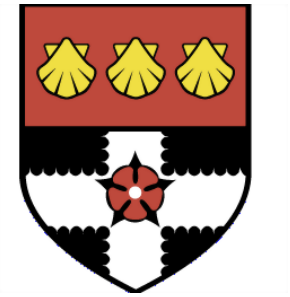

Polar Lows: their climatology, interaction with the ocean and response to climate change

Hélène Marie Emilie Bresson

A thesis submitted for the degree of Doctor of Philosophy

December 2018

DECLARATION

I confirm that this is my own work and the use of all material from other sources has been properly and fully acknowledged.

Hélène Bresson

Abstract

Polar lows (PLs) are intense mesoscale cyclones that form at high latitudes during winter. Their high wind speeds and heavy precipitation can substantially impact offshore infrastructures and coastal communities over regions such as Scandinavia, Russia and Japan. However, large uncertainties regarding their climatology, interaction with the ocean and response to climate change still remain.

Using an automatic tracking method and specific identification criteria, a reliable long-term climatology of PLs and their environment is derived from two atmospheric reanalyses. The mean number of PLs differs significantly between reanalyses, however the inter-annual variability of PL numbers is highly correlated between both datasets. PLs activity from these reanalyses is found consistent with observations and literature. The large-scale environment of PLs is found to play a role in the inter-annual variability of PL numbers.

The possible impact of PLs on the ocean circulation over the Nordic Seas is investigated using high resolution simulations from a coupled global climate model. As seen in previous studies based on an ocean model with parametrized PLs, this thesis shows, in high resolution climate model simulations, a clear positive link between the ocean surface heat fluxes and PL occurrences. However, in this study, no evidence is found that PLs influence on the ocean density is sufficient to destabilize the water column and trigger deep ocean convection over the Nordic Seas.

Finally, for the first time, the representation of PLs and their environment are assessed in a high resolution atmosphere-only global climate model, for both present climate conditions and a future climate scenario. Furthermore, the impact of the resolution of the model on the representation of PLs is assessed using simulations from three different horizontal resolutions for both climate conditions. Overall the PL numbers are expected to decrease in the future, mainly due to an increase in static stability. However, regional differences appear and new areas for PL occurrence emerge over the Arctic Ocean. The horizontal resolution of the climate model is found to affect the mean numbers of PLs but not their activity.

Acknowledgements

I am incredibly grateful to many people who have helped and supported me along this wonderful PhD journey.

Firstly, I owe great thanks to my supervisors, Kevin Hodges, Len Shaffrey and Giuseppe Zappa for their guidance and support during the entire project. They knew how to, with patience, pass on me the scientific approach necessary for the good progress of research works. They were always there to help and encourage me, to help me grow in confidence and ability, and to correct all my English mistakes! I look forward to working with them in the future.

Thank you to the international "Polar low" community, especially Chantal Claud, Thomas Spengler, Gunnar Noer, Günther Heinemann and Christian Melsheimer, who friendly welcomed me and taught me a lot about Polar lows and Polar science.

I am grateful for the help of many people. To Helen Dacre and Tom Frame for useful feedback during our monitoring committee meetings. To Sir Brian Hoskins, Sue Gray, Humphrey Lean and Ted Shepherd and the HHH and Mesoscale research groups, for the interesting questions and discussions. Thank you to Reinhard Schiemann, Allyn Treshansky, Matthew Mizielinski, Malcolm Roberts and Charles Roberts for all their help with the Met Office model data.

Living in a foreign country is never easy but I have made some great friends in Reading who have all contributed to helping me through the PhD. Thanks to my office mates from Harry Pitt 179 - Ying Ying Toh, Davi Mignac, Tom Hall, Will Morrison - and Met 1U08 - Michael Johnston, Kaja Milczewska, Aga Walenkiewicz and Liz Cooper - for always taking time to reply to all my often random (scientific or not) questions, and for putting up with me complaining about the British weather and my IT issues! A special thanks to Joshua Talib, Duick Young, Hannah Bloomfield, Flávia Rodrigues and Rebecca Frew, for all their love, help and support from the first day, and to Jacob Maddison and Ben Courtier, the best housemates ever!

Thank you to Karine Medel and Floriane Tarrou, who showed me that friendship can overcome borders, oceans and a PhD thesis. A huge thank you to César Rondou, for always being at the end of the telephone, and for your endless support and love.

Finally, none of this would have been possible without the continuous love and support of my family. Above all, a tremendous thanks to my parents, who supported me in all possible ways and never stopped believing in me!

CONTENTS

NOMENCLATURE

AMIP	Atmospheric Model Inter-comparison Project
AMOC	Atlantic Meridional Overturning Circulation
ASR	Arctic System Reanalysis
AVHRR	Advanced Very High Resolution Radiometer
CAO	Cold Air Outbreak
CAOI	Cold Air Outbreak Indicator
CISK	Conditional Instability of the Second Kind
ECMWF	European Centre for Medium-Range Weather Forecasts
ERA	ECMWF European Re-Analysis
ERA-40	ECMWF 40-year Re-Analysis
ERA-I	ECMWF ERA-Interim
GCM	Global Climate Model
GFDL	Geophysical Fluid Dynamics Laboratory
GHG	Greenhouse Gas
GODAS	Global Ocean Data Assimilation System
GSI	Gridded Statistical Interpolation
HadISST	Met Office Hadley Center Sea Ice and Sea Surface Temperature data set

IPCC	Intergovernmental Panel for Climate Change
JRA-55	Japanese Reanalysis JRA-55
METAR	Meteorological Aviation Report
MLD	Mixed Layer Depth
MOM	Modular Ocean Model
MSLP	Mean Sea Level Pressure
NADW	North Atlantic Deep Water
NCEP	National Centers for Environmental Prediction
NCEP-CFS	NCEP Climate Forecast Systems (CFS) Reanalysis
NOAA	National Oceanic and Atmospheric Administration
NWP	Numerical Weather Prediction
OSTIA	Operational Sea Surface Temperature and Sea Ice Analysis
PDF	Probability Density Function
PL	Polar Low
PMC	Polar Mesoscale Cyclone
PV	Potential Vorticity
RCM	Regional Climate Model
RCP	Representative Concentration Pathway
SIC	Sea Ice Cover
SIF	Sea Ice Fraction
SST	Sea Surface Temperature
WISHE	Wind-Induced Surface Heat Exchange
Z500	Geopotential height at 500 hPa

Map of the Arctic Ocean and Seas.

CHAPTER 1

INTRODUCTION

1.1 Polar lows

" Weather conditions can shift from calm to storm in minutes with Polar lows. That means people must be particularly alert to such systems. "

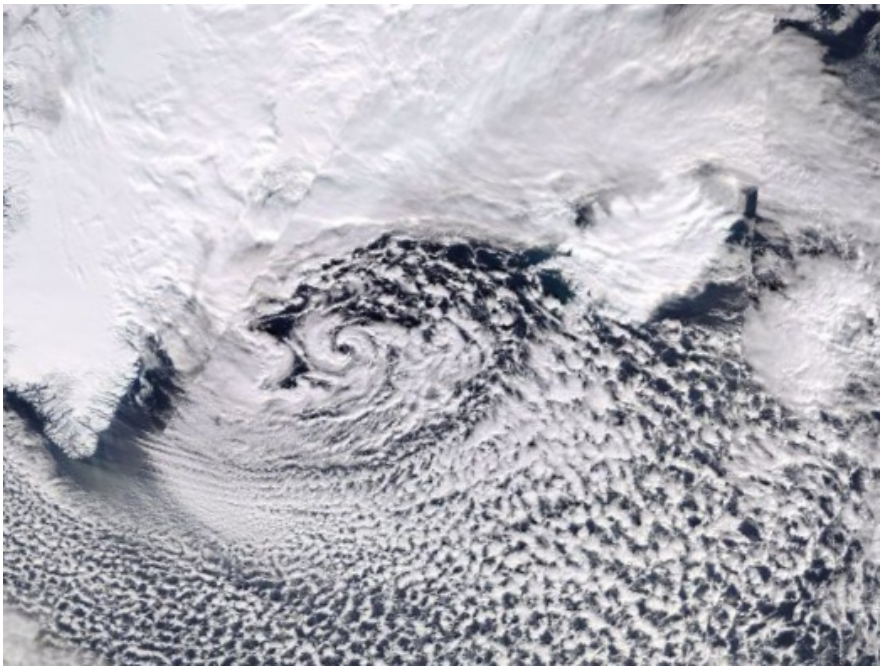

Figure 1-1: A Polar low on 2nd March 2009 over the Irminger Basin (source: NASA Worldview).

As is the advise to the population from the Norwegian Meteorological Institute and

the Barents Watch[1,2]. Polar lows (hereafter PLs) or Arctic hurricanes (see Figure 1-1) are intense mesoscale (from 100 to 1000 km) cyclones that occur at high latitudes. They form a subset of more intense and smaller Polar mesocyclones. Because of their intensity and substantial impact on offshore and coastal communities, PLs are one of the most extreme meteorological events of the Polar regions (Rasmussen and Turner, 2003).

These fairly small but intense systems are often associated with strong wind speeds (usually greater than 10-15 $m.s^{-1}$), poor visibility (with horizontal visibility less than 100 m and vertical visibility less than 30 m) and high precipitation (with often dense snow fall). Therefore PLs can have important effects on offshore and coastal communities (Rasmussen and Turner, 2003). Furthermore, large ocean waves (sometimes up to 9 m, Orimolade A.P. et al. 2016) and strong winds can spray "up to 30 cm snow and up to 25 cm ice" from the sea, causing severe icing to boats (Orimolade et al., 2018). These effects can thus jeopardise the stability and buoyancy of vessels. The strong winds and waves associated with PLs can also have substantial impacts on offshore infrastructure such as gas exploitation (Zahn and von Storch, 2010). Unfortunately, incidents and accidents cannot always be prevented (Noer et al., 2011; Orimolade et al., 2018). Some effects of PLs on human activities can be seen in Figure 1-2.

Figure 1-2: Damaged vessels due to the passage of PLs (from Mallet 2014 and Orimolade et al. 2018).

---

[1] Source: MET/Gunnar Noer/Hanneke Luijting, at `https://www.barentswatch.no/en/services/polar-lows-explained/`

[2] The Barents Watch is a global community (of government agencies, voluntary organisations and private businesses) which collects and shares information about the Norwegian coastal and marine areas, including updates on possible ongoing PL activity. For more information see `https://www.barentswatch.no`.

Due to the sparsity of observational networks, the limited remote sensing data available over the Arctic regions, and the short lifetime of PLs, it is often difficult to observe pre-developing and developing PLs. Furthermore, due to the complex and diverse physical processes involved in their formation, PLs and their associated weather conditions are a challenge to forecast.

Despite the possible importance of PLs, there are still large uncertainties in how frequently they occur, how they are spatially distributed, how they might respond to climate change and what precise impact they have on the ocean circulation. Thus, further studies are required to fully understand how PLs interact with their environment, and under the present and possible future climates. As very few observational datasets of PLs are available (which have large uncertainties), it is important to make use of reanalysis and climate model datasets, with the highest horizontal resolution possible to ensure they capture PLs.

The aim of this first chapter is to survey previous studies and the current knowledge on PLs, and to introduce the motivations of this thesis work.

An overview of PLs and their definition will be presented in Section 1.1.1. The climatology of PLs over the Arctic basin will be reviewed in Section 1.1.2, as well as a quick review of PLs over the Antarctic (although in this thesis we will focus on the Northern hemisphere). The representation of PLs in reanalysis and climate model datasets will be reviewed in Section 1.1.3. PL dynamics will be briefly presented in Section 1.1.4. The study of PLs within the climate system, and how they interact with the large-scale atmospheric and oceanic environment, will be reviewed in Section 1.2. The gaps in current knowledge of PLs will be discussed in Section 1.3. Finally, the specific questions addressed in this thesis will be presented Section 1.4, and the full thesis outline will be detailed in Section 1.5.

1.1.1 The definition of Polar lows

There is a wide range of definitions of PLs due to the diverse ways that they can develop and thus exhibit different visual aspects in satellite imagery (reflecting different structures and cloud patterns). Therefore many names have been used to refer to structures similar to PLs, such as Polar mesoscale cyclones (Condron and Renfrew, 2013; Watanabe and Niino, 2014; Pezza et al., 2016), Polar mesoscale vortexes, Arctic hurricanes (Emanuel and Rotunno, 1989), Arctic instability lows (Dannevig, 1954) and cold air depressions (Rasmussen and Turner, 2003).

Nowadays, the term “Polar low” is usually reserved for the most intense Polar mesoscale systems, which have near-surface winds of at least 15 $m.s^{-1}$.

The most common definition of PLs is stated in Rasmussen and Turner (2003) as:

> " *A polar low is a small but fairly intense maritime cyclone that forms poleward of the main baroclinic zone [...]. The horizontal scale of the polar low is approximately between 200 and 1000 kilometres and surface winds near or above gale force.* "

Hence a Polar low is a small-scale atmospheric low pressure system, found over ocean regions, forming poleward of the main polar front, and associated with relatively high surface wind speeds.

As stated in the definition, PLs have a small spatial scale. Although some PLs may be smaller than 200 km (Rasmussen and Turner, 2003), most of them show diameters usually ranging between 200 and 1,000 km. Hence, PLs are a subset of the meso-α-scale polar mesocyclones. As "Polar meso-cyclone" is the generic term encompassing all meso-α-scale (200 to 2,000 km) and meso-β-scale (20 to 200 km) lows, the term "Polar low" thus refers to the most intense Polar meso-scale cyclones.

If the definition mentions the spatial scale of PLs, it does not include any specification on the region of occurrence, the lifetime and life-cycle of PLs, their formation mechanisms nor their thermo-dynamic characteristics. Even though relatively broad and subjective, this definition from Rasmussen and Turner (2003) is still considered as the primary definition of these systems. However, scientists currently working on PLs[3] often include other characteristics, consistent with the general definition, based on the previous studies and observations.

The main PL characteristics are:

- High surface wind speeds (usually greater than 15 $m.s^{-1}$)
  One of the main issues with this general definition is the lack of specificity related to the intensity of PLs, and how intense should mesoscale cyclones be to be classified as PLs. As near gale or gale force wind speeds (i.e. 13.9 to 17.1 $m.s^{-1}$ and 17.2 to 20.7 $m.s^{-1}$ respectively on the Beaufort Scale) are often observed with PLs (Rasmussen and Turner, 2003), a convention is that a maximum surface wind speed of 15 $m.s^{-1}$ has to be reached to consider the low as a PL. Through observations, maximum wind speeds associated with PLs were even found to reach 25 to 35 $m.s^{-1}$ (Shapiro et al., 1987).

- Strong surface heat fluxes (around 1000 $W.m^{-2}$)
  The strong winds associated with PLs can increase the heat transfer from the

[3] The definition of PLs has been subjected to debates in the last workshops of the European Polar Lows Working Group (Spengler et al., 2017; Heinemann et al., 2018).

ocean. Therefore, large surface heat (latent and sensible heat) fluxes, comparable to the ones from mature tropical cyclones, are also a common characteristic of PLs (Shapiro et al., 1987; Fore et al., 2012).

- A short lifetime (up to 2-3 days) and a rapid development (shorter than 12 hours) Another characteristic of PLs is that they are known to be short-lived phenomenon, lasting usually less than two to three days, and to develop quite rapidly, often within 12 hours (Rasmussen and Turner, 2003; Noer et al., 2011).

PLs are observed in both Northern and Southern hemispheres, mainly at high latitudes (poleward of 50° N and 50° S), but can also develop in lower latitudes, such as the North Atlantic Ocean and the Sea of Japan (Yanase et al., 2016).

PLs are often observed in the presence of a "Cold Air Outbreak" as suggested by Harrold and Browning (1969) and Businger and Reed (1989). As defined by the American Meteorological Society[4], a Polar Outbreak or Cold Air Outbreak (hereafter CAO) is "the movement of a cold air mass from its source region; almost invariably applied to a vigorous equatorward thrust of cold polar air, a rapid equatorward movement of the polar front". This southward incursion of cold Polar air increases the local horizontal air temperature gradient and, when encountering warm open water (compared to a cold sea ice), can help enhance surface heat fluxes (Renfrew and Moore, 1999) and trigger convection. Some years, an increase in PL numbers is even noticed when large numbers of CAO are observed with satellite data (Blechschmidt, 2008). In their climatology of PLs over the Nordic Seas, Bracegirdle and Gray (2008) distinguished PLs from other Polar mesoscale cyclones by the fact that PLs occur during CAO events. Hence, CAOs are one atmospheric feature often associated with PLs (Kolstad, 2007, 2011).

In Chapter 2 of this thesis, some of the above characteristics will be used within an objective method to track and identify PLs, introduced in Zappa et al. (2014).

1.1.2 Polar low observations, case studies and climatologies

As previously mentioned, PLs occur in the Northern and the Southern hemispheres. In this section, a brief climatology of PLs will be presented for the different regions and seas where PLs occur. Only a short summary on PLs over the Southern hemisphere will be given, as this thesis focuses on PLs over the Northern hemisphere.

---

[4] American Meteorological Society, cited 2012: Polar Outbreak. Glossary of Meteorology. [Available online at http://glossary.ametsoc.org/wiki/Polar_outbreak.]

1.1.2.1 Polar lows in the Northern hemisphere

The high latitudes of the Northern hemisphere are largely dominated by the generally sea-ice covered Arctic Ocean. The Arctic Ocean (∼14 million km^2) is composed of a large sea-ice covered ocean basin with several seas along the continental shelves: the Greenland Sea, the Barents Sea, the Kara Sea, the Laptev Sea, the East Siberian Sea, the Chukchi Sea and the Beaufort Sea (see the Arctic map at the beginning of the thesis).

The Arctic region is a place of large variability where the ocean, the ice and the atmosphere interact with each other:

- The sea ice cover over the Arctic Ocean varies considerably between the seasons (and often decreases by half of its winter surface area during summer). The sea ice interacts with the ocean (especially, along the sea ice edge, where shallow baroclinic zones tend to form) and the atmosphere through heat, moisture and radiative transfers. As the Arctic sea ice extent is declining rapidly (Stroeve et al., 2007, 2012), this could have a significant impact on the future climate, and potentially on PLs as well.

- The Arctic region ocean currents interact with the weather and climate of the Northern hemisphere, through large transfers of heat and moisture. For example, the North Atlantic Current (strong warm western boundary current crossing the Atlantic Ocean) warms the surface of the Norwegian and Greenland Seas, while Arctic currents bring cold and dense ocean water masses, through the Baffin Bay and Labrador Sea, over the western part of the North Atlantic Ocean.

- The Arctic inversion[5], the North Atlantic and Pacific storm tracks[6] and the North Atlantic Oscillation[7] are some of the atmospheric patterns that play an important role in shaping the weather and climate of the Arctic region.

The region where PLs occur the most often and which is thus the main studied region for PLs activity (Stoll et al., 2018) is the Nordic Seas region. Depending on the

[5] Extreme temperature inversion (caused by the lack of solar surface heating and the continuous surface heat loss) where the temperature can decrease from 20°C withing 100m.

[6] Narrow zonal regions over the North Atlantic and Pacific Oceans, where large-scale synoptic storms travel driven by the prevailing winds.

[7] Or NAO: variations in atmospheric sea level pressure difference between the Icelandic low and the Azores high. The NAO is the dominant mode of inter-annual and inter-decadal variability of the atmospheric circulation over the North Atlantic Ocean and Europe.

literature the definition of this region changes, including sometimes the North Sea, the Norwegian Sea, the Greenland Sea and the Barents Sea, and even the north-east of the North Atlantic Ocean (and including the Irminger basin). Therefore, in this thesis we consider the Nordic Seas as the region covering the Greenland, the Norwegian and the Barents Seas.

One of the first observational studies of PLs over this region was made by Wilhelmsen (1985). Wilhelmsen found that PLs in the region are more frequent during December and January, that they are often found within the vicinity of a synoptic-scale cyclone and that their propagation speed is round 10 $m.s^{-1}$ over the ocean. The Wilhelmsen study found that PLs tend to originate between Svalbard, the northern coast of Norway and the Barents Sea (where the sea surface temperature (hereafter SST) gradient is enhanced), and move towards or along the Norwegian coast.

In 1984, the first research aircraft measurements within a PL over the Norwegian Sea was undertaken (Shapiro et al., 1987). Important information was retrieved from this observational study, such as values of the surface heat fluxes, vorticity and maximum wind speed, and how the low developed. This study paved the way for other aircraft field campaigns as in Kristjansson et al. (2011) and Sergeev et al. (2017).

Other PL observational studies such as those of Noer et al. (2011), Rojo et al. (2015), Smirnova et al. (2015), Melsheimer et al. (2016) and Sergeev et al. (2017) have used *in-situ* data and remote sensing observations. These studies have provided a large amount of detail on observed PLs.

Case studies have also been used to investigate PLs in other Arctic regions such as the Labrador Sea (Moore et al., 1996; Mailhot et al., 1996; Pagowski and Moore, 2001), the ice-free part of the Hudson Bay (Albright et al., 1995; Gachon et al., 2003), and the Bering Sea and the Gulf of Alaska (Businger, 1987; Businger and Baik, 1991; Bond and Shapiro, 1991; Douglas et al., 1991; Bresch et al., 1997). These studies confirm that the disturbances propagate near the sea ice edge, on the cold side of the baroclinic zone and are usually embedded within a CAO. Whether forward (thermal and mean wind in same direction) or reverse (thermal and mean wind in opposite direction) shear, PLs have strong vorticity and wind speed, and are associated with heavy precipitation and large ocean waves (up to 13 m height in Bond and Shapiro 1991). Although PLs are known to also occur over the regions of the Baffin Bay, the Davis Strait and the Beaufort and Chukchi Seas through reports (Rasmussen and Turner, 2003), no studies of PLs are available.

A brief overview of the case studies and climatologies of PLs so far conducted, using diverse observational data (and sometimes reanalyses and models for comparison),

within different regions of the Northern hemisphere can be seen in Table 1.1.

		Type of data					PL number	
Regions	Authors	Reanalysis/Model	Satellite	Aircraft/Ship	Analysis map Weather station	*In-situ*	Case study	Climatology (PL per year)
Nordic Seas	Wilhelmsen (1985)			✓	✓		33	
	Shapiro et al. (1987)		✓	✓	✓		1	
	Noer et al. (2011)	✓	✓		✓	✓		12.10
	Rojo et al. (2015)	✓	✓		✓			13.60
	Smirnova et al. (2015)		✓					45.50
	Melsheimer et al. (2016)		✓					40.00
	Sergeev et al. (2017)	✓	✓	✓		✓	1	
Labrador Sea	Moore et al. (1996)		✓		✓		1	
	Mailhot et al. (1996)		✓		✓		1	
	Pagowski and Moore (2001)	✓	✓	✓			1	
Hudson Bay	Gachon et al. (2003)	✓			✓		1	
Bering Sea	Businger and Baik (1991)		✓		✓	✓	1	
	Bresch et al. (1997)	✓	✓	✓	✓		1	
Gulf of Alaska	Bond and Shapiro (1991)	✓	✓	✓		✓	2	
	Douglas et al. (1991)		✓	✓	✓	✓	1	
Gulf of Alaska & Bering Sea	Businger (1987)		✓	✓	✓		2	
Sea of Japan	Ninomiya (1989)		✓		✓		1	
	Ninomiya and Wakahara (1993)		✓		✓		1	
	Shimada et al. (2014)	✓	✓		✓		1	
	Watanabe and Niino (2014)		✓		✓		1	

Table 1.1: PL case studies and climatologies over the Northern hemisphere based on observational data.

Finally, one important region for PLs in the Northern hemisphere, which is not a polar region (latitudes between 35°N and 45°N), is the Sea of Japan. PLs in this region have been studied many times. During winter, northerly and northwesterly flows, associated with CAO, descend from the cold Asian continent to arrive over the relatively warm water of the Sea of Japan. The surface heat fluxes from the ocean, associated with the cold flows generate a shallow baroclinic and convective layer, which

is propitious for the formation of PLs (Ninomiya, 1989; Ninomiya and Wakahara, 1993). As they often reach their maximum intensity as they cross of the Sea (Yanase et al., 2016), the Japanese islands are very likely to be affected by them, and PLs can have important impacts on the Japanese transport system (Shimada et al., 2014). Using the Japanese JRA-55 reanalysis (Kobayashi et al., 2015), Yanase et al. (2016) found that PLs over the Sea of Japan have a similar seasonality and inter-annual variability of PL numbers to those from other regions, with a maximum number of PLs between December and February and with a mean number of around 7 PLs per year. Polar mesoscale cyclones (hereafter PMCs) have also been studied over the Sea of Japan (Watanabe and Niino, 2014; Watanabe et al., 2017), as some PLs occurring over this region can be part of the meso-β-scale (20 to 200 km) category of the Polar meso-scale cyclones.

1.1.2.2 Polar lows in the Southern hemisphere

Contrary to the Arctic Ocean, which is an enclosed basin surrounded by continents, the Southern Ocean consists of an ocean body surrounding a large continent encircled by sea ice. Because of the difficulties in retrieving *in-situ* observations over the Southern Ocean, very little detailed information is available on PLs over the Southern hemisphere. This issue results in fewer studies of PLs over the Southern hemisphere compared to the Northern one.

In the Southern hemisphere, mesoscale cyclones have only been investigated in a few regions, mainly over the Weddell and Ross Seas. However, only few systems observed over the Southern hemisphere have been vigorous enough to be classified as PLs (Rasmussen and Turner, 2003). Hence, most of the studies over the Southern Ocean focus on the entire spectrum of mesoscale vorticies and cyclones such as Heinemann (1990), Carrasco et al. (2003) and Verezemskaya et al. (2017). Only few studies, as in Carleton and Carpenter (1990), Heinemann (1996) and Pezza et al. (2016), have focused directly on PLs. These studies showed that PLs mainly form over the Drake Passage and the Ross, Bellingshausen and Weddell Seas (Heinemann, 1996; Verezemskaya et al., 2017). Carleton and Carpenter (1990) found evidence that the inter-annual variability of PLs over the Southern Ocean may be linked to the El Niño - Southern Oscillation[8].

[8] El Niño - Southern Oscillation (or ENSO) is an irregular climate pattern in which variations in winds and SSTs over the tropical Pacific Ocean affect most of the climate of the tropics and subtropics.

1.1.3 Polar lows in other datasets

Since only a few *in-situ* and observational PL datasets are available, several studies used data from reanalyses, operational and climate models. These datasets represent the state of the Earth's climate over long multi-decadal periods, and are used to enhance the knowledge of the weather and climate over these periods in a self consistent way.

Reanalyses are analysis datasets produced by combining historical observations with a short-range forecast using data assimilation. Several previous studies have used operational weather forecast models and reanalyses to examine the climatology of PLs, to assess their representation within these datasets, or to complement information on observational case studies. However except for the following three studies, most of the studies are time and space limited. Using a Numerical Weather Prediction (NWP) model, Bracegirdle and Gray (2008) built a 4-year climatology of PLs to understand some of the dynamical forcings of PLs over he Nordic Seas. Zahn and Von Storch (2008) built a long-term climatology of PLs over the North Atlantic Ocean via the NCEP/NCAR reanalysis over 58 years. Yanase et al. (2016) studies PLs over the Sea of Japan, for 36 years, with the Japanese JRA-55 reanalysis. And Stoll et al. (2018) built a long-term climatology of PLs for both hemispheres, with the ERA-I and the Arctic System Reanalysis (hereafter ASRv1, Bromwich et al. 2016) reanalyses for 37 years. Also using ERA-I reanalysis, Michel et al. (2017) built a climatology of Polar mesoscale cyclones (PMCs) by automatically detecting and tracking them over the Nordic Seas, and assessing the environment of forward and reverse shear PMCs.

Xia et al. (2012a) used reanalysis datasets to compare two methods of tracking and identification methods of PLs. Zappa et al. (2014) used an automatic tracking and identification scheme to assess how well PLs are represented in the ERA-I reanalysis by comparing results with observational data and operational analyses. Similarly, Smirnova and Golubkin (2017) and Stoll et al. (2018) compared PL climatologies within a coarse (ERA-I) and an Arctic-focused (ASR) reanalyses. These studies found that PL numbers differ depending on the tracking and identification method, as well as the horizontal resolution of the chosen reanalysis, but major systems are identified in all datasets.

Climate models are General Circulation Models[9] (or GCMs, McGuffie and Henderson-

[9] General Circulation Models (also known as Global Climate Models) use, similarly as Numerical Weather Prediction (NWP) models, the equations of motion in order to numerically simulate changes in climate, as a result of slow changes in some boundary conditions (e.g. solar constant) or physical parameters (e.g. greenhouse gas concentration). If NWP models are used to predict the short- and medium-range weather (few days to few weeks), GCM models usually run for decadal or centurial periods to study all climate changes (i.e. means and variability).

Sellers (2005) that simulate the atmosphere in atmosphere-only models or the fully coupled system of the atmosphere, ocean, land surface and ice systems. A few previous studies have employed Regional and Global climate models (hereafter RCMs and GCMs) to examine PLs activity. Gachon et al. (2003) (30 km resolution) and Zahn and Von Storch (2008) (50 km resolution) utilised regional climate models to assess the development of PLs. Condron and Renfrew (2013) parametrized the wind speeds associated with PLs in a global ocean circulation model (18 km resolution) to evaluate the possible impact of PLs on the North Atlantic deep ocean circulation. Using downscaling methods, Zahn and von Storch (2010) (50 km resolution) and Romero and Emanuel (2017) assessed PLs in future climate simulations.

Although PLs can be identified in reanalyses, it has been found that some can not be found or are misrepresented (Condron et al., 2006; Zappa et al., 2014). Through investigating different aspects of PLs with different reanalyses, it has been shown that the horizontal resolution of the chosen dataset is one of the main challenges in investigating PLs. The study of PLs is only possible within datasets which can fully capture small mesoscale systems such as PLs. Rasmussen and Turner (2003) defined the "resolution barrier" for PLs at 50 km in horizontal resolution. This indicates that PLs might be missed or misrepresented at coarser resolutions, as they do not fully capture their activity.

The representation of PLs also depends on the so-called "effective resolution" of the dataset. The effective model resolution was defined by Skamarock (2004) as the "scale at which the model spectrum decays relative to the expected spectrum". Both model spectra and effective resolution can be affected by model damping, and are "strongly dependent on the formulation and tuning of implicit and explicit model filters" (Skamarock, 2004). Therefore the effective model resolution can be seen as the effect of all of the "model's numerical filtering and smoothing effects" (Frehlich and Sharman, 2008). The effective resolution of a model is larger than the grid spacing Δx at which the model solves the governing equations of the Earth System. Depending on the model and the model's method used (to prevent non-linear instability), the effective resolution can vary from approximately $L \sim 6\Delta x$ to $L \sim 7\Delta x$ (Skamarock, 2004; Skamarock et al., 2014). Therefore, before investigating PLs with reanalyses and models, one must insure that these datasets represent PLs in an sufficient way. In this study, the effective resolution of the datasets used lies between 150 and 550 km, indicating the ability of the reanalyses and models to resolve PLs.

1.1.4 Polar low dynamics

PLs often develop in regions with strong low-level vorticity (e.g. synoptic-scale troughs), west or south-west of synoptic cyclones or within occluded cyclones (Rasmussen and Turner, 2003). Some pre-existing conditions are often observed to be conducive to the formation of PLs, such as the proximity of warm open water to cold sea ice (i.e. large local temperature differences, where shallow baroclinic zones often form) and CAO (Kolstad and Bracegirdle, 2008; Kolstad et al., 2009; Rojo et al., 2015).

Initial ideas considered PLs to be purely driven by convection, like their tropical cyclone counterparts (Emanuel and Rotunno, 1989; Gray, 1996; Rasmussen and Turner, 2003). This has led PLs to be termed as Arctic hurricanes. However, several case studies have shown that some PLs are often driven by baroclinic processes (Mansfield, 1974). Thus in the 70s and 80s, a debate started to investigate whether PLs should be considered as convective systems or as baroclinic disturbances (Rasmussen and Turner, 2003). Hence, research has been undertaken to try to understand the development and intensification mechanisms of PLs, and to comprehend the differences between PLs and their extra-tropical and tropical counterparts. Some specific differences between PLs and other types of cyclones are still under study, such as why do PLs have a smaller size and a more rapid growth, and why do they tend to only form in regions associated with cold air masses over relatively warm oceans (Rasmussen and Turner, 2003).

Nowadays, it is agreed that PLs are part of a large range of mesoscale systems occurring at high latitude, which cover a range from purely convective to purely baroclinic systems (Bracegirdle, 2006). As previously mentioned, this large spectrum of observed systems reflects the idea that PLs form for various reasons and from different conditions. Furthermore, a variety of "hybrid" systems are also observed (Bracegirdle and Gray, 2008). For these systems, the forcing mechanisms can change significantly during the PLs life-cycle, and both baroclinic instability and convective mechanisms can play a small or large role (depending on the circumstances in which a PL develops).

A brief description of the mechanisms which induce PLs formation will be discussed next.

Baroclinic instability

Baroclinic instability is a mechanism that explains the development and shaping of mid-latitude cyclones (Eady, 1949). It plays an important role in the meridional transport of heat and moisture in the atmosphere.

Baroclinic instability is a type of dynamical instability which is associated with a baroclinic region of the atmosphere (Rasmussen and Turner, 2003). In a baroclinic

region the density of the air depends on both temperature and pressure. A region with a strong temperature gradient, such as the sea ice edge, is an example of such region. The instability arises due to the meridional flow, induced by a small amplitude disturbance moving over the strong temperature gradient (see Figure 1-3).

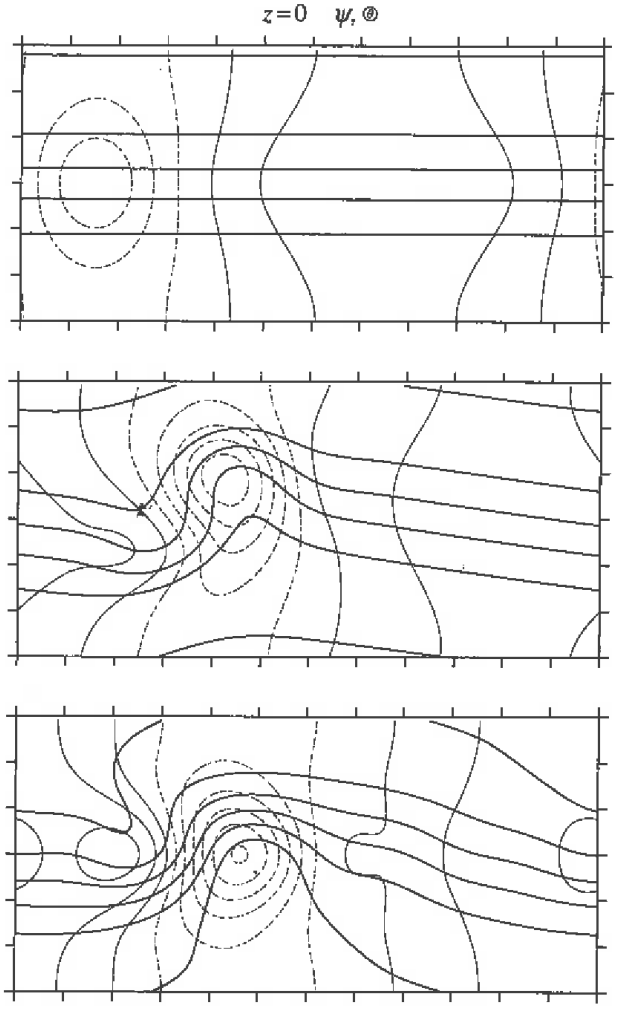

Figure 1-3: Schematic (from Holton and Hakim (2013)) of the development of a localised disturbance in a westerly jet stream. The dashed lines represent the pressure (4 hPa intervals), the solid lines represents the potential temperature (5 K intervals).

The isotherms will bend in a cyclonic direction centred on the disturbance and enhance the amplitude of the temperature gradient (Terpstra, 2014). This disturbance will then grow by converting the potential energy (from the horizontal temperature gradient) into kinetic energy, by the simultaneous ascent of warm air ahead of the disturbance and descent of cold air behind. Thus baroclinic instability is associated with the horizontal temperature gradient, and therefore with the vertical shear of the

mean flow (through the thermal wind equation, see Holton and Hakim 2013)[10].

Another way of describing PLs development is through the dynamic instability at the tropopause (Hoskins et al., 1985), via the Potential Vorticity[11] (hereafter PV) theory. In the "PV thinking" concept, baroclinic instability can be thought of as the interaction between PV anomalies at different levels. A positive feedback mechanism between the PV anomalies at the upper and lower levels induces an increase of the low-level PV anomaly (i.e. action at a distance). This increase of the PV anomaly leads to an increase in the intensification of a cyclone. As PV is conserved for adiabatic and frictionless flow, it can directly be related to the temperature and wind fields. Some studies have applied this concept to PLs, such as Bracegirdle and Gray (2009) who found that the upper-level PV anomaly was the dominating mechanism in the initial phase of the PL development in their case study.

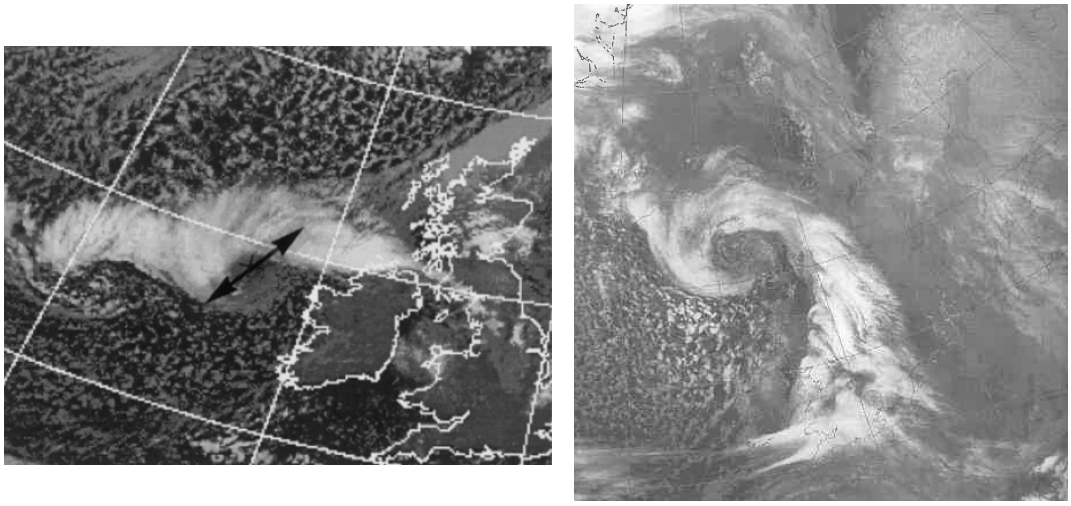

Figure 1-4: Comma cloud PL (left image, from Harold et al. 1999a) and "Instant occlusion" exhibiting a frontal cloud band after the interaction between a comma cloud PL and a synoptic-scale cold front (right image, from Rasmussen and Turner 2003).

A large number of PLs tend to develop on horizontal temperature gradients through

[10] For more information on baroclinic instability see Holton and Hakim (2013) (Chapter 7 on "Baroclinic development") or Hoskins et al. (1985).

[11] The potential vorticity (or PV) is defined by Ertel (1942) as the combination of the kinetic (i.e. absolute vorticity) and thermo-dynamic (i.e. static stability) terms such as:

$$PV = \frac{1}{\rho}\overrightarrow{\xi_a} \cdot \overrightarrow{\nabla\theta}$$

where ρ is the density, $\overrightarrow{\xi_a}$ is the absolute vorticity and $\overrightarrow{\nabla\theta}$ is the gradient of the potential temperature. PV is expressed in PVU unit which corresponds to 1 PVU = 10^{-6} $m^2.s^{-1}.kg^{-1}$.

baroclinic instability. They often have the visual aspect of small frontal depressions such as in Figure 1-4 or in Carleton (1985). The analysis of the vertical velocity derived from radar observation can often provide an indication of PL development (Terpstra, 2014). Previous studies established the predominant role of baroclinic instability with the added influence of latent heating, acting to increase the growth rate of PLs.

Two distinct sub-synoptic environments are associated with the genesis of PLs: reverse and forward shear. Duncan (1978) defined reverse shear as a uniform horizontal flow, in which the mean wind is parallel and in the opposite direction to the thermal wind. Disturbances occurring within reverse shear conditions are able to grow through baroclinic energy conversion. On the other hand, forward shear disturbances appear in conditions when the mean wind of the horizontal flow is parallel and in the same direction as the thermal wind (see Figure 13 in Businger and Reed (1989)). Terpstra et al. (2016) studied the differences in PL development by discriminating between forward and reverse shear conditions[12]. They found that forward shear PLs tend to form in similar conditions to mid-latitudes cyclones (and mainly propagate eastward along this baroclinic zone). Terpstra et al. (2016) showed that reverse shear PLs tend to be stronger than forward shear PLs (as associated with an "intense low-level jet" and a larger temperature gradient between the ocean surface and 500 hPa (i.e. $\Delta T = T500 - SST$).

Restricting the temperature difference criterion may bias the identification towards more reverse shear PLs (Terpstra et al., 2016), delimiting PLs between forward and reverse shear conditions. However, it may limit the PL spectrum considered. Hence, in this thesis, no distinction is made between forward and reverse shear PLs.

Surface thermal instability and air-sea interaction

At the other end of the spectrum, there are PLs with extensive cumulonimbus clouds and often an axisymetric structure, which are mainly generated through convective processes. These PLs are also often associated with cold pools in the mid to upper levels. Similar to tropical cyclones, these PLs can form over the ocean via deep convection.

---

[12] To discriminate forward and reverse shear PLs, the angle between the mean wind and the thermal wind between the low levels at 925 and 700 hPa is calculated.
The thermal wind is defined as: $V_T = \left\{ u_T = -\frac{1}{f}\frac{\partial(\phi_{700}-\phi_{925})}{a\partial\varphi},\ v_T = -\frac{1}{f}\frac{\partial(\phi_{700}-\phi_{925})}{a\cos\varphi\partial\lambda} \right\}$, with ϕ_{700} and ϕ_{700} the geopotential at 700 and 925 hPa, φ the latitude, λ the longitude, f the Coriolis parameter and a the Earth's radius.
The mean wind is defined as: $V_m = \left\{ u_m = -\frac{1}{2f}(\frac{\partial\phi_{700}}{a\partial\varphi} + \frac{\partial\phi_{925}}{a\partial\varphi}),\ v_m = \frac{1}{2f}(\frac{\partial\phi_{700}}{a\cos\varphi\partial\lambda} + \frac{\partial\phi_{925}}{a\cos\varphi\partial\lambda}) \right\}$.
The angle between the mean and thermal wind is defined as: $\cos\alpha = \arccos(\frac{V_T.V_m}{||V_T||\quad||V_m||})$.
In Terpstra et al. (2016) and Michel et al. (2017), forward shear PLs are defined to have an angle between 0° and 45° and the reverse shear PLs to have an angle between 135° and 180°.

Two theories have been proposed to explain the development of "large-scale balanced systems" such as PLs (Rasmussen and Turner, 2003). These two theories are the Conditional Instability of the Second Kind (hereafter CISK) and the Wind-Induced Surface Heat Exchange (hereafter WISHE).

The CISK (Charney and Eliassen, 1964) theory relies on the low-level moisture convergence being a source for latent heat release. The release of latent heat is enhanced by the low level vorticity, and thus reinforces the low level convergence. Hence, this is a positive feedback mechanism, which intensifies and helps maintain systems.

As the effectivness of the CISK mechanism depends on the available amount of Convective Available Potential Energy (or CAPE) (Emanuel, 1986; Rotunno and Emanuel, 1987), Rasmussen (1979) argued that for the CISK mechanism to be active in PL development, a large amount of available CAPE would be needed. Linders and Saetra (2010) analysed dropsonde soundings during PL events, and found that almost no CAPE is present during the development of PLs (and proposed that almost all the CAPE is used at the same time as it is generated). Hence, it seems unlikely that CISK plays an important role in the development of PLs.

Hence, Emanuel (1986) introduced the concept of air-sea interaction instability (WISHE) feedback for tropical cyclones, when it was noted that the atmospheric column for tropical cyclones was not able to provide a large enough reservoir of CAPE. In this WISHE theory, the strong wind speed associated with tropical cyclones (and PLs) would play the major role in the intensification of the surface heat fluxes. The positive feedback in the WISHE theory occurs because the low-level moisture convergence produces latent heating, which enhances the low-level winds and hence the surface heat fluxes, which in their turn provides more low-level moisture. In the case of PLs, the surface sensible heat fluxes help trigger convection for PLs to form, and the latent heat fluxes provide the energy for their intensification (Shapiro et al. 1987, Watanabe and Niino 2014 and Papritz et al. 2015). Craig and Gray (1996) and Gray and Craig (1998), through their simulations (using the non-hydrostatic axisymetric tropical cyclone model from Rotunno and Emanuel 1987), suggested that WISHE is the main process involved in the intensification of PLs[13].

Other processes

Even though they may play a minor role in the development of PLs, other processes can be involved in their generation.

[13] Summary schematics of the CISK and WISK mechanisms can be found in Rasmussen and Turner 2003 (Figure 4.61 p.394-395).

Barotropic instability has been observed in the development of some PL occurrences. A barotropic instability is a type of wave instability associated with horizontal shear in a "jet-like current", which grows by extracting kinetic energy from the mean flow (Holton and Hakim, 2013). Observations as well as theoretical studies have shown that barotropic instability can play a role in the development of PLs, but can not induce PLs formation on its own (Bond and Shapiro, 1991; Rasmussen and Turner, 2003).

PLs can also be associated with orographic waves (Kristjánsson et al., 2011), occlusions or convergence lines. Though little studied, these processes seem to play a role in a few PL occurrences (Rasmussen and Turner, 2003).

Cloud structures

Because of all these different development mechanisms, PLs can range from fully baroclinic to purely convective systems. In the case of "hybrid" PLs, both baroclinic instability and convective processes (such as CISK and WISHE) can play a role with diverse degrees of forcing. Hence, PLs exhibit a large range of cloud structures. Satellite observations of PLs show a wide range of shapes and cloud signatures, as can be seen in Figure 1-5.

For example, cloud-free eye PLs (also known as "Arctic hurricanes") have a primarily convective nature, whereas comma cloud PLs, often caused by a region of upper-level potential vorticity advection (or PVA), tend to develop more through baroclinic instability (Rasmussen and Turner, 2003). Hence, Arctic hurricanes have a large dense convective cloud structure, whereas comma cloud PLs have a comma shape of smaller scale, with a wrapped centre and a denser tail (Mallet, 2014). Spiraliform PLs are distinguished by one or more spiral cloud bands of convective cloud and are often associated with deep convection of CISK type (Rasmussen, 1979). Merry-go-round PLs, consisting in multiple PLs, may form within the centre or in the rim of a large-scale cold core upper-level cyclone (Rasmussen and Turner, 2003).

Comma cloud and spiraliform PLs tend to be the most common (Carleton, 1996). However, PLs may exhibit other cloud structures. Instant occlusions occur when a comma cloud (or sometimes spiraliform) PL merges with a cold front (Carleton, 1985). Baroclinic wave PLs form through baroclinic instability along a secondary baroclinic zone (poleward of the main baroclinic zone) (Rasmussen and Turner, 2003). Their cloud pattern, at a meso-scale, is similar to the one of synoptic-scale extra-tropical cyclones. Finally, warm core systems are characterised by a low-level cyclonic inflow and a upper-level anti-cyclonic outflow (Rasmussen and Turner, 2003). These PLs are often associated, as medicanes (i.e. small but intense cyclones which develop over the Mediterranean Sea), with strong convective cloud structure from intense convection

due to release of latent heat.

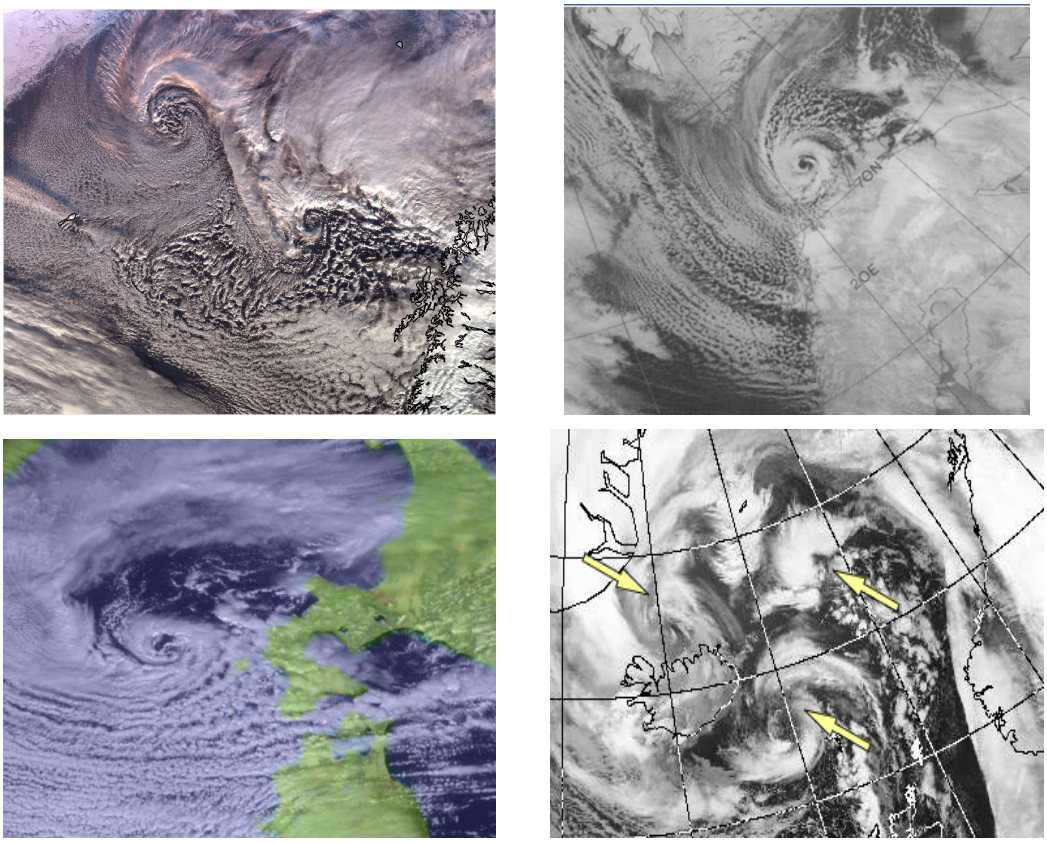

Figure 1-5: Different shapes of observed PLs: comma cloud PL over the Greenland Sea, cloud-free eye PL over the Barents Sea, spiraliform PL over the Sea of Japan and merry-go-round PLs over the Greenland and Norwegian Seas. Sources: NASA EOSDIS Worldview, NOAA, Kochi University Weather Information, and Dundee Satellite Receiving Station.

1.2 Polar Lows and the Climate System

As previously mentioned, the high latitudes are a region, where the atmosphere, the ocean and the ice interact with each other. Although still not fully understood, the interactions between PLs and the large-scale have been analysed by the previously mentioned climatologies of PLs (Laffineur et al., 2014; Terpstra et al., 2016; Mallet et al., 2017). However, research on the possible impact of PLs on the ocean circulation and on their response to climate change has only been of recent interest and questions subsist regarding the role played by PLs in the climate system.

The ocean circulation

The North Atlantic thermohaline circulation (THC), or Atlantic Meridional Overturning Circulation (AMOC), is a part of the large-scale ocean circulation that is driven by global density gradients created by surface heat and freshwater fluxes (Siedler et al., 2001a). Wind-driven surface currents (ex. the Gulf Stream) mainly travel poleward from the equatorial Atlantic Ocean and then sink (as they become denser) at high latitudes. On their journey, the water masses transport both energy (in the form of heat) and matter (solid, dissolved or gas) around the globe. Thus the oceanic circulation has a large impact on the climate of the Earth.

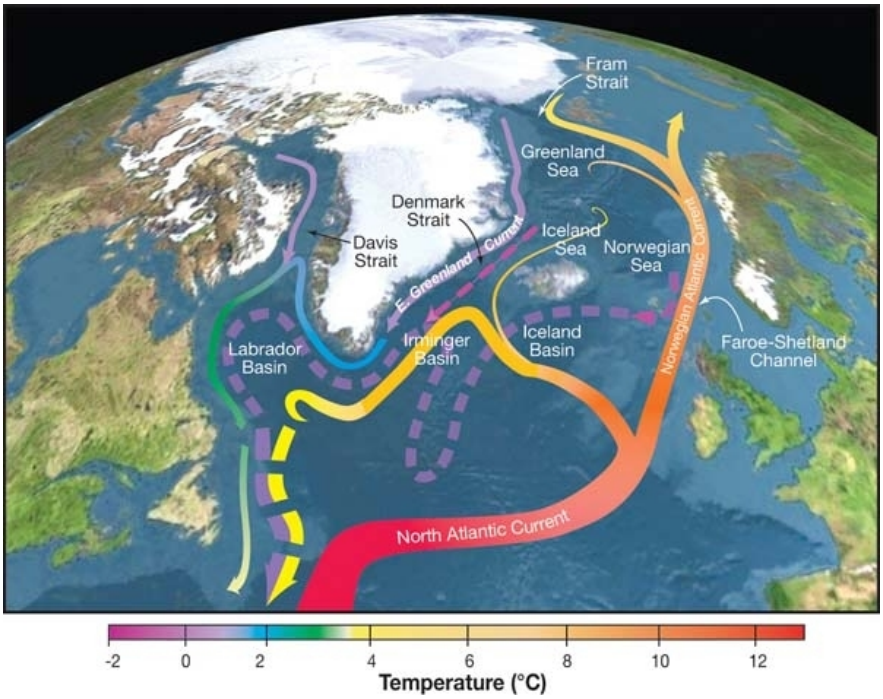

Figure 1-6: Schematic of the North Atlantic Ocean circulation, with the mean temperature of the currents (source: R. Curry, Woods Hole Oceanographic Institution/Science/USGCRP).

In the Northern hemisphere (see Figure 1-6), the deep water formation occurs in two basins: the Greenland and the Labrador Seas[14] (Siedler et al., 2001b). The deep waters are driven by the difference in density (caused by the variations of the water salinity and the temperature), and form through shallow and warm waters of the Norwegian Atlantic Current that cool due to surface wind and low ambient air temperatures and sink. In the Greenland Sea, the evaporative cooling (i.e. decrease in surface sea temperature due to wind-driven evaporation, and related to the latent heat) dominates

[14] In the Southern hemisphere, the two regions of deep water formation are the Ross and Weddell Seas.

and induces the water masses to sink into the basin. These dense deep waters are called the North Atlantic Deep Water (hereafter NADW). The "returning" branch of the dense water (i.e. East Greenland Current) moves southwards at the bottom of the basin, along the coast of Greenland (see Figure 1-7), to then enter the Atlantic abyssal plains through both sides of Iceland, the Denmark Strait and the passage between Iceland and the Faroe Islands (i.e. through the "Greenland-Scotland-Ridge"). It has been recently found that, the warm North Icelandic Irminger Current running northward in the Denmark Strait, cools down when encounters the Icelandic Sea gyre (Våge et al., 2011), north of Iceland (not shown). This confrontation of these water masses, triggers ocean heat loss at the surface and leads to cold, dense and deep waters to overflow southward on both sides of Iceland (Mauritzen, 1996; Våge et al., 2013).

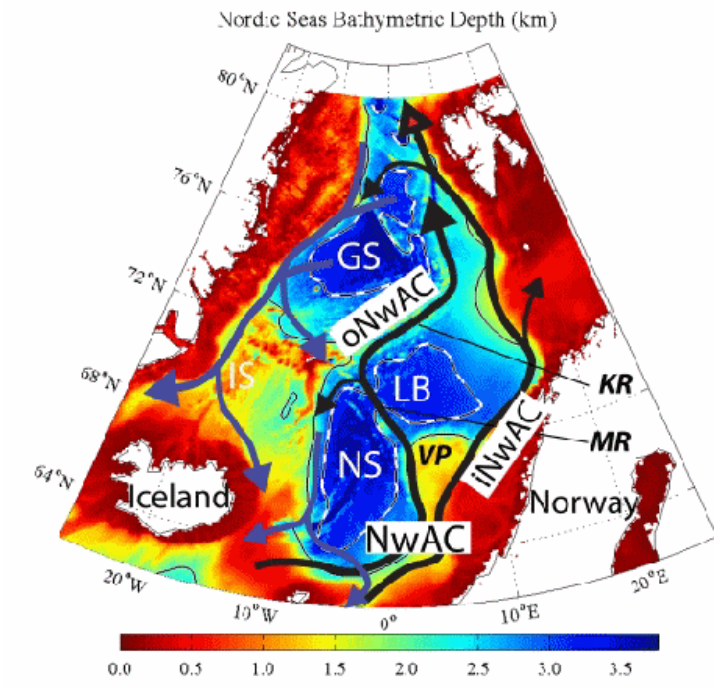

Figure 1-7: Bathymetry (in km) and overturning circulation schemes of the Greenland, Norwegian and Iceland Seas: the warm major surface currents (in black) are transformed into cold and dense bottom currents (in blue). Source: Woods Hole Oceanographic Institution[15].

The second region of deep water formation over the Northern hemisphere lies in the Labrador Sea (Siedler et al., 2001b). The Labrador Sea deep water comes from a combination of cyclonic ocean circulation from the sea currents and atmospheric

[15] Woods Hole Oceanographic Institution: `http://www.whoi.edu/science/PO/people/fstraneo/lofoten/lofoten.html`.

forcing. The Labrador deep water also contributes to the shallower layers of NADW (which supplies the AMOC with cold and dense water masses).

In order to understand the role of the ocean in the climate, it is essential to estimate the ocean transport of volume, heat and freshwater. As the Atlantic Meridional Overturning Circulation (AMOC) is responsible for a large part of the ocean heat transport, it is crucial to monitor and model the AMOC variability and its link with the climate system (Sinha et al., 2018). Through the UK-US RAPID programme (McCarthy et al., 2015), it has been shown that it is possible to accurately monitor the AMOC through direct estimates (from ocean transport) of the strength of the thermohaline circulation. This has been made at 26.5°N in the North Atlantic. This programme showed an estimated strength of the AMOC and meridional heat transport of 17.2 Sv[16] and 1.25×10^{15} W (or PW) respectively from April 2004 to October 2012.

As the AMOC is forecast to decline in the future (Woollings et al., 2012; IPCC, 2013; Robson et al., 2014) due to an increase in freshwater fluxes from the Arctic gates (Gervais et al., 2018) and a possible decrease of the supplied densest overflow waters from the Iceland Sea (Moore et al., 2015), the interaction between the ocean and the atmosphere has an important role to play in the present climate but also in the future under climate change. Condron and Renfrew (2013) suggested that PLs may influence the oceanic circulation and contribute to the atmosphere-ocean interactions, and thus be important for the current and future climate systems.

The future under Climate Change

Climate change is projected to result in a large-scale and long-term shift in the statistical distribution of the Earth's weather patterns and mean temperatures (sources: UK Met Office and NASA[17]). Natural climate change occurs due to various climate forcings and feedbacks, including processes such as solar radiation variation, variation in the albedo or changes in greenhouse gas concentrations. These factors can have different "climate change feedbacks" which can either increase or diminish the initial forcings and their effects. These climate changes are also influenced by anthropogenic greenhouse emissions[18]. Depending on the region and the amplitude of the forcings,

[16] Sverdrup (or Sv) is a unit of the volumetric rate of transport of ocean currents (1 Sv = 10^6 $m^3.s^{-1}$).

[17] See `https://www.metoffice.gov.uk/climate-guide/climate-change` and `https://climate.nasa.gov/`

[18] According the IPPC AR5, due to a combination of continued increase in greenhouse gas concentrations and improved estimates of the radiative forcing, the total radiative forcing due to anthropogenic emission for 2011 is 43% higher than that for 2005 (IPCC, 2013).

these feedbacks may vary[19].

Adopting strategies to adapt to climate change hence requires an analysis of the magnitude of the various possible impacts on different sectors such as agriculture, hydrology, health and industry (IPCC, 2013). A large amount of these impacts are induced by intense weather-climatic phenomena, such as heat waves, droughts, flooding and severe storms (IPCC, 2013). Among all these weather-related threats, PLs are associated with uncertain current and future impacts at high latitudes. Thus investigating the representation of PLs in climate models with present and future climate conditions is an important challenge, as they may have large socio-economic impacts. Furthermore, as the climate warms and the Arctic climate system is undergoing drastic changes such as the decline of the Arctic sea ice extent and thickness (see Stroeve et al. (2007, 2012) and Figure 1-8), PLs might undergo changes too. As new Arctic shipping routes might open (Melia et al., 2016), another important motivation for studying PLs within the future climate is that PLs might be even more of a severe hazard which need to be understood and forecasted.

Climate models are used to improve the understanding of the Earth's climate dynamics and to investigate future changes through climate projections. Global Climate Models help in assessing large-scale climate features and their interactions with each others (ex. assessment of CO_2 increase) whereas Regional Climate Models are employed to focus on specific regions and provide more details on local interactions.

A number of studies have investigated the possible future of extra-tropical cyclones (see Bengtsson et al. (2006) and Table 1.1 from Catto (2009) for an overview of past studies and findings). However, only a few studies have investigated the potential response of PLs to climate change.

Zahn and von Storch (2010) used an RCM nested in a GCM forced with IPCC AR4 emission scenarios, and Romero and Emanuel (2017) used 30 CMIP5 (Coupled Model Inter-comparison Project Phase 5) models forced with the RCP 8.5 scenario (most extreme scenario from IPCC AR5) in order to explore the probable future of PLs. Both studies found that PLs might decrease in numbers in the future over the North Atlantic Ocean and the Nordic Seas. This decrease is hypothesised to be mainly due to the possible future increase in atmospheric static stability, due to a faster increase in mid-tropospheric temperatures compared to the surface ones. Using simulations from a general circulation coupled model with IPCC AR4 scenarios, Mallet (2014) and Woollings et al. (2012) also found a faster rise of the mid-tropospheric temperatures.

[19] Feedbacks such as sea level rise, ocean warming and acidification, variations in precipitation rate, changes in air chemistry, droughts, wildfires, decline of land and sea ice extend and thickness.

This leads them to conclude that PL activity would thus diminish in response to the changes in the large scale environment.

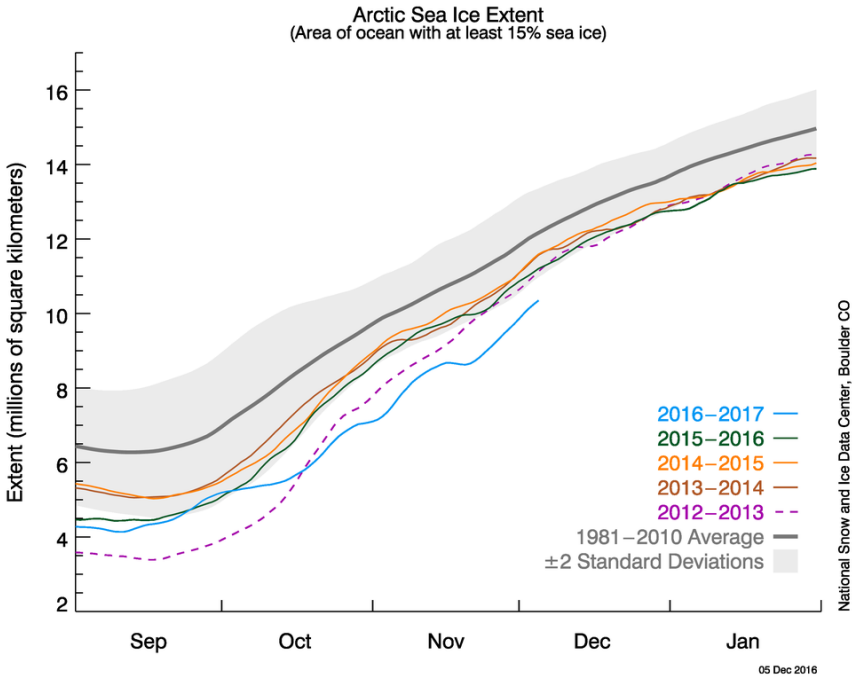

Figure 1-8: Observed sea ice extend over the Arctic Ocean (source: National Snow and Ice Data Center).

1.3 Gaps in the knowledge

1.3.1 Problems related to Polar lows

Because of the short life-cycle of PLs, it is still a challenge to understand their life-cycle and their interaction with the climate system.

As the definition of PLs is ambiguous, delimiting the boundaries of PLs within the polar mesoscale cyclone spectrum is still under investigation (Rasmussen and Turner, 2003). This also implies that PL dynamics is not fully understood yet, as the full three dimensional view of PLs has not been totally determined (Montgomery and Farrell, 1992; Hewson et al., 2000; Terpstra, 2014; Spengler et al., 2017). Therefore, in order to better understand PL activity, as well as to prevent human incidents and damages, increasing the amount of remote sensing and *in-situ* observations of PLs is essential.

In order to improve the current knowledge of PLs, numerous studies have used satel-

lite imagery (Carleton and Carpenter, 1990; Claud et al., 2004; Smirnova et al., 2015, 2016) and reanalysis datasets (Blechschmidt, 2008; Zahn and Von Storch, 2008; Xia et al., 2012a; Zappa et al., 2014; Yanase et al., 2016; Michel et al., 2017; Smirnova and Golubkin, 2017; Stoll et al., 2018) to assess the representation of PLs. However, theses studies have only concerned fairly limited areas and have a short temporal resolution. In addition, these studies often used different sets of criteria to describe PLs. Past studies have shown discrepancies in the representation of PLs in reanalyses, because of their small scale, their short lifetime and the large range of mechanisms involved in their development. Furthermore, most of these studies cover relatively short periods (usually of only a few winter seasons). Thus, an important downside of the current state-of-the-art is the limited number of studies producing long-term climatologies of PLs from reanalyses in order to assess their representation with as many PL cases as possible. Indeed, so far only Zahn and Von Storch (2008) and Yanase et al. (2016) investigated the PLs climatology over the North Atlantic with the 58-year NCEP/NCAR reanalysis and over the Sea of Japan using the 36-year JRA-55 reanalysis, and Stoll et al. (2018) evaluated the representation of PLs in ERA-I for 37 years over both hemispheres. Both studies found no significant long-term trends in PL numbers but show a strong inter-annual variability in PL numbers.
Other studies such as Watanabe et al. (2016) and Michel et al. (2017) have also studied the climatology of PLs but as a part of the larger Polar mesoscale cyclone family.

1.3.2 Problems related to the oceanic circulation

As PLs occur mainly over the ocean, they contribute to the atmosphere-ocean coupling, as they locally increase the heat fluxes at the surface and the mixing of the shallow layer of the ocean (Shapiro et al., 1987; Rasmussen and Turner, 2003; Saetra et al., 2008; Fore et al., 2012).

Condron et al. (2008), Condron and Renfrew (2013) and Jung et al. (2014) showed that PLs could even influence the Atlantic Meridional Overturning Circulation (or AMOC), through increasing the depth, frequency and area of deep convection over the Nordic Seas. This process could happen if the transfer of ocean heat from the ocean surface in to PLs is large, and thus cool the surface water locally, making the water more dense, destabilising the water column. If this were to happen, PLs could have an impact on the large-scale oceanic and atmospheric circulations. Hence the interaction between the atmosphere and ocean may lead to PLs being considered an important component of the climate system. However, the magnitude of this interaction between PLs and the ocean is still uncertain.

1.3.3 Uncertainties regarding climate change

An important question regarding PLs is how PLs activity may change in the future. Indeed, if PLs influence the ocean circulation then the possible future of the ocean circulation may be affected by the future activity of PLs. Hence the interaction with the ocean is an interesting question considered in a limited number of studies (Condron et al., 2008; Condron and Renfrew, 2013). Zahn and von Storch (2010) and Mallet et al. (2017) have suggested that changes in the static stability may affect the generation of PLs, as the temperatures in the mid-troposphere may increase faster than the ocean surface temperatures in future climate scenarios. Hence, this temperature increase could then inhibit the development of PLs and result in a decrease in PL occurrences in the future climate (Zahn and von Storch, 2010; Romero and Emanuel, 2017). As a result, the decline of PL numbers over the North Atlantic Ocean and Nordic Seas could induce a slowdown of the deep water formation in this region. This would mean that PLs could then affect the future climate at a larger scale than the Nordic Seas.

However, the evaluation of the PL response to future changes is challenged by two main difficulties: the rarity of PLs and the uncertainties in the future climate scenarios. Indeed, due to their low frequency of occurrence, extreme weather events such as PLs are difficult to study in climate simulations. The short temporal and spatial scales of PLs mean that their representation depends strongly on small-scale physical processes which are still insufficiently resolved in climate models and subject to large uncertainties depending on the models used (Romero and Emanuel, 2017). Furthermore, investigating the future of PLs implies having a certain knowledge on the possible future climate scenarios. Depending on the future scenario chosen (ex. RCP 4.5 or RCP 8.5), the amplitude of the response of PLs under climate change might be different. Hence this PLs response to climate change is challenged by the gaps in fully understanding our current climate, as well as those in evaluating the future human activities and mitigation strategies. To overcome these problems, more needs to be done to improve the understanding and to reduce the uncertainties, of both current and future climates.

As PLs occur at high latitudes, their future projections are highly dependent on the uncertainties in the response of the Arctic system to climate change, and the response to this change of systems such as the sea ice (Stroeve et al., 2012) or weather patterns (Cohen et al., 2014). Hence, uncertainties in the future of PLs may arise because of uncertainties in their representation as well as uncertainties in the representation of the Arctic system for the present and future climates.

For now, Zahn and von Storch (2010) and Romero and Emanuel (2017) predicted a

future with less PLs over the North Atlantic Ocean. Both of these studies used downscaling to examine PLs over the North Atlantic. Thus, as these studies only illustrate the potential future of PLs over a specific region, there is a lack of knowledge on the global response of PLs to climate change.

1.4 Research questions

The questions addressed by this thesis are:

- What is the representation of PLs when using an objective identification scheme in two reanalysis datasets?

  Because of the shortness of observational datasets of PLs, establishing a clear picture of PLs within reanalysis datasets is essential in order to investigate PL activity. In this thesis, objective and long-term climatologies will be built via an automatic tracking and identification scheme using two atmospheric reanalyses over different PL regions. The behaviour of PLs in both reanalyses will be assessed, and results will be compared with observations where possible. The surrounding environment of PLs will also be investigated.

- What is the impact of the interaction of PLs with the ocean on the ocean circulation over the Nordic Seas?

  The lack of understanding of the interaction between PLs and the ocean leads this thesis to examine how PLs influence the ocean, through their interaction with the ocean surface heat fluxes and the ocean shallow and deep circulation. This work is done with a fully coupled high resolution climate model, with a focus on the Nordic Seas region.

- How might PLs respond to climate change? How might projections of PLs be affected by the model resolution?

  The motivation of this work is to examine how PLs behave under climate change. The observed trends are investigated to see whether previous studies are consistent with those found using an objective PL tracking and identification scheme, applied to a high resolution global climate model. This is achieved by examining a set of global climate model simulations, which are integrated at high enough horizontal resolution to resolve PLs explicitly. Furthermore, the impact of the resolution of the model on the results will be assessed using three different model horizontal resolutions.

1.5 Thesis outline

The outline of this thesis is as follow:

Chapter 2 will detail the observations, reanalysis and model datasets used. The different models from the Met Office will be specified. The PL tracking, identification and statistical methods will be explained and discussed.

In Chapter 3, climatologies of PLs derived from the two atmospheric reanalysis products will be studied and compared to observations. The sensitivity of PLs to the identification criteria, as well as their large-scale environment, will also be explored.

Chapter 4 will detail the representation of PLs in a high resolution coupled climate model. The possible interaction of PLs with the Nordic Seas and North Atlantic ocean circulations will be studied.

In Chapter 5, the PL climatology will be assessed in an atmosphere-only climate model under present and future climate scenarios. The representation of PLs, as well as the environmental factors influencing PLs response to climate change will be explored. The impact of the model resolution on PLs will be evaluate within three different horizontal resolutions.

Finally, Chapter 6 will present some conclusions and answers to the research questions addressed in this thesis. Possible areas for further work that have arisen from this research will also be discussed.

CHAPTER 2

DATA AND METHODOLOGY

The questions addressed in this thesis rely mainly on the ability of reanalyses and climate models to represent PLs, their characteristics and environment. Thus, it is crucial to qualify and quantify these representations prior to answering the main questions.

In this study, four datasets are used: two atmospheric reanalyses, ERA-I and NCEP-CFS, and two global climate models, HadGEM3-GC2 and HadGEM3-GA3. The two reanalysis datasets are used to build a long-term climatology of PLs (in Chapter 3). The STARS observational dataset will be used for comparison with the results from the reanalysis climatologies (in Chapter 3). The coupled climate model HadGEM3-GC2 is used to investigate the potential impact of PLs on the ocean circulation (in Chapter 4). Finally, the atmosphere-only climate model HadGEM3-GA3 is used to analyse the response of PLs to climate change (in Chapter 5).

In the first section of this chapter, the different datasets (observations, reanalyses and climate models) used for this study will be described. The observational dataset will be presented in Section 2.1.1, the two atmospheric reanalysis products will be described in Section 2.1.2 and simulation products from the two climate models will be introduced in Section 2.1.3.

The second part of this chapter will explain how PLs are identified. The automatic feature tracking method used to identify and track PLs will be explained (Section 2.2.1) and a discussion on the limitations of the tracking and identification scheme will be addressed (Section 2.2.2). The identification criteria used to discriminate PLs from other tracked features will be listed and explained (Section 2.2.3). A discussion and sensitivity analysis of PL numbers to the identification criteria will be investigated with ERA-I in Chapter 3 (Section 3.4.3). Finally the statistical tools used for the calculation

of the track, genesis and lysis density of PLs as well as for their distributions, their environment and for hypothesis testing will be described (Section 2.2.4).

2.1 Data

To study PLs over the Nordic Seas, an observational dataset is used. However, since this dataset is only available for limited time and spatial scales, other datasets are used in this thesis. Two reanalyses (ERA-I and NCEP-CFS) and two global climate models (HadGEM3-GC2 and HadGEM3-GA3) are employed to investigate different aspects of PL activity. As seen in the schematic of Figure 2-1, these four datasets have various horizontal grids, varying from high (25 km) to coarse (130 km) resolutions. Therefore, using different datasets, with different horizontal resolutions, will allow a comparison of the dependence of PLs representation to the resolution.

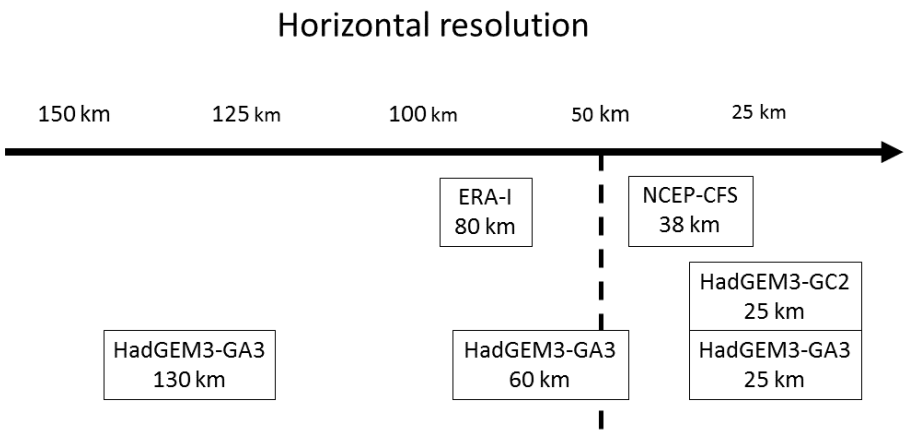

Figure 2-1: The different datasets with different horizontal resolutions used in the thesis.

2.1.1 Observations - the STARS dataset

As PLs are fast-developing systems that usually do not last longer than two or three days, it is a difficult yet essential task to monitor them and study their behaviour. Unfortunately, due to their sparse temporal and spatial distributions and the lack of *in-situ* and satellite information around the Poles, very few datasets of observed PLs and their surroundings are available. Only a few studies have used satellite data to derive PL climatologies, such as Harold et al. (1999a) and Blechschmidt (2008) using satellite infrared imagery and Smirnova et al. (2015) using passive microwave data.

One database of observed PLs, which is currently the longest observational dataset of PLs available, for the Greenland, Norwegian and Barents Seas region, and is called the Sea Surface Temperature and Altimeter Synergy for Improved Forecasting of Polar Lows, or STARS, dataset (Noer et al., 2011). Other datasets may be available upon request from some meteorological services.

The STARS dataset is produced by the Norwegian Meteorological Institute (or MET Norway at Tromso, Norway) and funded by the European Space Agency (ESA). As much information as possible on PLs and their environment is collected, to provide sufficient information for coastal communities and offshore activities (Noer et al., 2011).

In the STARS dataset, observed PLs are followed over the Greenland, Norwegian and Barents Seas from 1st January 2001 (and in the Labrador Sea since 2006) and onward, during the entire year. The process of building the dataset is in two steps. First, PL tracks are identified by an expert, on infra-red satellite images and pressure maps (from synoptic observations and observations from airport networks such as Meteorological Aviation Report or METAR), then additional variables are gathered along the track of the PLs and their surroundings (variables such as wind speed and the surrounding pressure). The data used to produce STARS come from three main sources: *in-situ* data (sea surface temperature (hereafter SST) and surface wind), infra-red satellite data (SST, along-track satellite Sea Level Anomaly (SLA), surface wind speed, Sea Ice Cover (hereafter SIC)[1] and infra-red imagery from the National Oceanic and Atmospheric Administration (hereafter NOAA) Advanced Very High Resolution Radiometer (hereafter AVHRR) , wave height) and Numerical Weather Prediction (hereafter NWP) data (geopotential height, air potential temperature and relative humidity at different pressure levels, SST, precipitation, surface wind speed, Mean Sea Level Pressure (hereafter MSLP)). The large-scale environment associated with PLs is assessed through the static stability[2], the presence of an upper-level advection of potential vorticity and

[1] The sea ice can be expressed by different terms. The sea ice cover (SIC) indicates the region, in km^2, covered by sea ice. The sea ice fraction (SIF) is the sea ice concentration (i.e. amount of area covered by ice), ranging from 0 to 1. For more information see `https://nsidc.org/cryosphere/seaice/data/terminology.html`.

[2] The static stability is a measure of the stability of the atmosphere and its capacity for buoyant convection (i.e. the ability of the air parcel to become turbulent). The air is characterised as statically stable when some less dense (i.e. warmer and/or more moist) air parcel is situated over a more dense air parcel. The atmosphere stratification is often defined through the Brunt-Väisälä frequency such as $N = \sqrt{\frac{g}{\theta}\frac{d\theta}{dz}}$, where g is the local acceleration of gravity, θ is the potential temperature (temperature that a parcel would have if it was adiabatically (process which occurs without transfer of heat or matter) brought to a standard reference pressure $P_0 = 1000$ mbar) and z is the geometric height. For more information on the static stability see textbooks such as Holton and Hakim (2013) and Stull (1988).

low-level baroclinicity. However, in this observational dataset, only the strongest PLs are listed even when a cluster of PLs forms within the same Cold Air Outbreak (CAO) (Zappa et al., 2014; Smirnova and Golubkin, 2017). This means that some PLs not listed in STARS can still be found in reanalysis products (Zappa et al., 2014). Nonetheless, the STARS data is still the largest observational database available for PLs and their environment over the Nordic Seas region.

Although only based on an expert judgement analysis of *in-situ* and satellite observations, this compiled database of PLs has been used in many previous studies to look at PLs over the Nordic Seas. For example, Rojo et al. (2015) and Smirnova et al. (2015) built enhanced climatologies of PLs based on the STARS observations, Zappa et al. (2014) and Smirnova and Golubkin (2017) compared PL characteristics in reanalysis products (and in ECMWF operational analysis) to PLs from STARS and Terpstra et al. (2016) studied the structure and genesis environments of PLs in STARS for forward (thermal and mean wind in same direction) and reverse (thermal and mean wind in opposite direction) shear PLs.

Most previous climatologies of PLs have either used the STARS database of observed PLs, or have been derived from reanalysis datasets such as ERA-40 (Condron et al., 2006), the Japanese reanalysis JRA-55 (Yanase et al., 2016), ERA-I (Michel et al., 2017) or the Arctic System Reanalysis (Smirnova and Golubkin, 2017; Stoll et al., 2018). These studies showed that low resolution reanalyses have limitations in identifying PLs.

For this study, the STARS dataset goes from October 2002 to March 2010 (each extended winter season being from the 1st October of one year to the 31st March of the following year). This will be used to asses the representation of PLs in the reanalyses through quantities such as the numbers of PLs, and their seasonal cycle.

2.1.2 Atmospherics Reanalyses

The main purpose of retrospective analyses, or reanalyses, is to produce global four-dimensional state-of-the-art gridded representations of the state of atmosphere over historical decadal periods. They are generated by combining temporally and spatially irregularly distributed historical observations with a short-range forecast using data assimilation. Having a reliably consistent dataset allows studies of atmospheric features in a statistically robust manner. As atmospheric reanalyses cover a large spatial and temporal resolution of the state of the atmosphere, and since very little observations of PLs are available, reanalyses are the easiest and more robust way to study intense, rare and short-lived systems such as PLs. However, some reanalyses, especially old ones,

might not be at high enough resolution to resolve mesocyclones well (Condron et al., 2006). Hence, using these datasets to study PLs would require them to be downscaled, such as in Zahn et al. (2008), Zahn and Von Storch (2008)(a), Zahn and von Storch (2008)(b) with the NCEP-NCAR.

The two reanalyses used for this study are the European Centre for Medium-Range Weather Forecasts (ECMWF) European Re-Analysis (ERA) Interim or ERA-Interim (hereafter ERA-I) and the National Centers for Environmental Prediction (NCEP) Climate Forecast Systems (CFS) reanalysis or NCEP-CFSR (hereafter NCEP-CFS), which are more recent higher resolution reanalyses.

They have been chosen for their different horizontal resolutions and their already proven ability to represent mesoscale features (Hodges et al., 2011; Tilinina et al., 2014; Bromwich et al., 2016; Smirnova and Golubkin, 2017). Using two different reanalyses with very different resolutions will provide some estimate in the uncertainty in the detection of PLs. Previous studies (Zappa et al., 2014; Rojo et al., 2015; Smirnova and Golubkin, 2017) have shown that, even though some are missed, most PLs are represented in ERA-I. As the NCEP-CFS has a higher spatial resolution (around 38 km or T382 on a spectral grid) compared to ERA-I (around 79 km or T255 on a spectral grid), one might test the impact of the higher horizontal resolution of NCEP-CFS. However, the missed PLs are not only due to the coarse resolution of the reanalysis products, but it is also due to from the sparse observing network within the regions of PL occurrences, as well as PLs transient nature, which make their observation and study more difficult (see Section 1.3.1 from Chapter 1 for some discussion on the knowledge gaps related to PLs nature). Furthermore, some PLs may be missed due to the fact that only short forecasts are run in reanalyses (usually from 6 h up to 5 days), which may give too little time to spin up a PL, and hence miss some occurrence. Therefore, having two reanalysis products, with different setups, will allow this study more robust results.

The characteristics of both ERA-I and NCEP-CFS reanalyses are described in the following two sections of this chapter.

2.1.2.1 The ERA-Interim reanalysis

ERA-Interim (Berrisford et al., 2009; Dee et al., 2011) is a global atmospheric reanalysis produced by ECMWF for the period from 1st January 1979 and onward.

The data products include different 3-hourly surface atmospheric parameters (as well as ocean-wave and land-surface conditions) and 6-hourly upper-air parameters covering the troposphere and stratosphere. The prognostic equations are solved us-

ing a semi-Lagrangian method in the horizontal and a finite element method in the vertical (Berrisford et al., 2009). The dynamical core of the atmospheric model of ERA-I depends on a spectral representation of the basic dynamical variables and on a semi-Lagrangian semi-implicit temporal scheme. The model used is the Integrated Forecasting System (IFS) operational spectral model (Cy31r2). ERA-I has a 30-min time step, a spectral TL255 horizontal resolution (which corresponds to around 79 km horizontal resolution) and 60 hybrid sigma-pressure vertical coordinate levels[3] (i.e. terrain following levels which are interpolated to pressure levels for users) up to 0.1 hPa, with 12 levels below 850 hPa.

The ERA-I reanalysis is produced with a sequential 4D-variational data assimilation scheme for the upper-air atmospheric state, advancing forward in time using 12-hourly analysis cycles with output every 6 hours (Dee et al., 2011). For each cycle, observations are combined with prior information (i.e. temperature, wind speed, humidity, surface pressure, ozone concentration, etc.) gathered from the forecast model, to estimate the evolution of the state of the atmosphere. The observations assimilated in ERA-I mainly come from satellites, and include clear-sky radiance measurements, atmospheric motion vectors, scatterometer wind data, ozone retrievals, as well as surface station observations and other radiosondes and aircraft data. The convection scheme in ERA-I is an enhanced version of the one from ERA-40 (with improved distinction between shallow, mid and deep level convection, and improved computation of the cloud base) and a wave-model component for the forecast model (to include the impact of the ocean waves on the atmosphere, through energy and momentum transfers). For the surface boundary conditions of the atmosphere forecast model, the same SST and SIC inputs are for the ECMWF 40-year Re-Analysis (hereafter ERA-40, Uppala et al. 2005) for the dates prior 2002, and the operational NCEP product for the later period (Dee et al., 2011).

Thanks to its easy availability, large choice of variables and long-term sample (i.e. multi-decadal dataset), the ERA-I product is one of the most commonly used datasets to study PLs.

Laffineur et al. (2014) obtained PL climatologies, using the mean sea level pressure (MSLP) fields from the ERA-40 and ERA-I, over the Nordic Seas. As the MSLP is more influenced by the large-scale environment than the vorticity filed (Xia et al., 2012b), some PLs may have been missed. However, they found that PLs were better captured in ERA-I (T255) than in ERA-40 (T159), and that this difference might be

[3] See Eckermann (2009) for more information on hybrid $\sigma - p$ (sigma-pressure) coordinates.

mainly due to the weaker representation of the synoptic conditions in ERA-40 rather than the representation of the PLs themselves.

Zappa et al. (2014) compared PL characteristics in the ERA-I dataset, the STARS observations and the ECMWF operational analysis. This study was able to objectively identify 55% of the STARS PLs in ERA-I, for a 3-year period over the Norwegian and Barents Seas, and this fraction increased to 70% in the operational analysis dataset. As PLs detection is dependent on the objective criteria used in this study, more PLs may have been found by direct matching (as PLs might be present in the datasets but their properties might be insufficient to satisfy the identification criteria).

More recently, different studies use different identification criteria and datasets. Michel et al. (2017) used the ERA-I dataset to study a 35-year climatology of tracked forward and reverse shear polar mesoscale cyclones (hereafter PMCs), a larger set of mesoscale cyclones which includes PLs. Smirnova and Golubkin (2017) compared the representation of PLs in the 30-km resolution Arctic System Reanalysis version 1 (hereafter ASRv1, Bromwich et al. (2016)) and in ERA-I. Stoll et al. (2018) examined the impact of some identification criteria on the representation of PLs in ERA-I for 37 years over both hemispheres. They found that higher resolution datasets are not necessarily sufficient to give a more accurate assessment of PLs and that the improved representation in ASRv1 is possibly due to the model itself and to its large-scale environment representation. Thus, this suggests that, despite its coarse horizontal resolution, ERA-I might still be suitable for the study of PLs.

Overall, despite its coarse horizontal resolution and thus its possible lack of detail of small-scale features, as well as the difference in PLs identification methods used in these previous studies, PLs can be found in the ERA-I dataset. However, some PLs are difficult to identify, which may be due to ERA-I not representing the weak vorticies well.

2.1.2.2 The NCEP-CFS reanalysis

The NCEP-CFS reanalysis dataset (Saha et al., 2010) uses the NCEP global coupled forecast system model (i.e. a global high-resolution coupled atmosphere - ocean - land surface - sea ice system), to produce a 6-hourly analysis, for the period from 1979 and onward.

The NCEP-CFS consists of a spectral atmospheric model at a resolution of TL382 (which corresponds to around 38 km horizontal resolution) with 64 vertical pressure levels which extend from the surface to 0.26 hPa. The NCEP-CFS uses the Geophysical Fluid Dynamics Laboratory (GFDL) Modular Ocean Model MOM (Cy31r2, Saha et al.

2006) which is a finite difference model at a resolution of around 1/2° with 64 hybrid sigma-pressure levels in the vertical, and the GFDL Sea Ice Simulator, with three ice layers, for the sea ice model. The atmosphere and ocean models are coupled with no flux adjustment. The "global ocean's latitudinal spacing is 0.25° at the equator, extending to a global 0.5° beyond the tropics, with 40 levels to a depth of 4,737 m" (Saha et al., 2010).

The NCEP-CFS uses the Gridded Statistical Interpolation (GSI) scheme to assimilate the atmospheric observations, which is a 3D-variational data assimilation system, and the Global Ocean Data Assimilation System (GODAS) 3D-variational data assimilation system for the ocean to assimilate the oceanic observations. The observations for most of the period of the NCEP-CFS mainly come directly from the NCEP operational Global Forecast System (GFS) analysis, and measurements from aircraft and fixed synoptic surface observations (ex. METAR automated reports), radiosondes (ex. wind and temperature profiles), satellite retrievals (ex. AVHRR infra-red images for the SST) and sounders (ex. temperature and humidity), ocean surface buoys (ex. sea level pressure) and fixed mooring arrays (ex. ocean temperature and salinity profiles).

The NCPS-CFS is known for being able to represent features such as extra-topical (Hodges et al., 2011) and tropical cyclones (Hodges et al., 2017) as well as Arctic cyclones (Tilinina et al., 2014). However, this reanalysis dataset has not been used yet for studying PLs.

As the NCEP-CFS has a horizontal grid resolution that is double that of ERA-I, one might expect larger PL numbers in NCEP-CFS than in ERA-I, and that the NCEP-CFS dataset may represent the properties of PL features better. Such assumptions will be investigated and discussed in Chapter 3.

2.1.3 Climate Models

To help improve the knowledge of the Earth's climate, and how it can be affected by natural and anthropogenic forcings, climate models are utilised to represent the different components of the climate system. Climate models simulate the interactions of climate drivers through different variables for the atmosphere, ocean, land surface and ice. The equations of motion are solved for the atmosphere and the ocean (dynamical part of the model), then semi-empirical methods are used to describe the unresolved processes or diagnoses. Climate models are used to enhance our understanding of the Earth's climate dynamics and to try to create projections of possible future climates. Different types of climate models exist and they are used for different purposes: global climate models, regional climate models, coupled or uncoupled climate models.

Global climate models (GCMs) are used to assess large-scale climate features and their interactions with each other, such as the assessment the impact of increasing CO_2 or the atmosphere-ocean interaction. They are also used to simulate the general circulation of the atmosphere including synoptic scale eddies and, if they are run at high enough resolutions, can also simulate mesoscale eddies such as PLs and medicanes (Tous et al., 2016). Regional climate models (RCMs) focus more on specific regions and local interactions, and usually have a higher spatial resolution to resolve finer spatial features such as fronts and convective storms. However, if GCMs are mainly limited by their coarser resolutions and the limited computer resources available, there are also issues with RCMs that do not occur for GCMs. For instance, as RCMs are constructed for limited areas, they require boundary conditions to be provided from global climate model simulations (i.e. downscaling methods). Hence, the RCM results will depend on the ability of the GCM used to represent the atmosphere and ocean properties at the larger scales.

Atmosphere-only (i.e. non-coupled) climate models simulate the atmosphere only but require surface boundary conditions to be imposed, such as Sea Surface Temperature (SST), sea ice and land properties (e.g. albedo). Ocean-, sea ice- and land-only models also exist and are used in different specific studies. On the other hand, coupled climate models combine atmospheric, oceanic, sea ice and land surface models with coupling between the models in terms of fluxes of heat, moisture and momentum. These coupled climate although more computationally expensive, are more representative of the climate system and are thus required for future climate projections.

In this thesis two climate models are used to assess PLs in two different ways which will be detailed below. The two climate models come from the Met Office climate prediction system Hadley Centre Global Environment Model version 3 (hereafter HadGEM3) family[4], and are named the Met Office HadGEM3-GC2 Coupled Climate Model (hereafter HadGEM3-GC2) and the Met Office HadGEM3-GA3 Atmosphere-only Climate Model (hereafter HadGEM3-GA3).

2.1.3.1 The Met Office HadGEM3-GC2 Coupled Climate Model

The Met Office HadGEM3-CG2 model (Williams et al., 2015) is a global fully coupled (atmosphere-land-ocean-sea ice) climate model which is based on the Met Office Unified Model (hereafter MetUM) system consisting of the Global Atmosphere 6.0 (GA6.0)

[4] More information on the family of the HadGEM3 climate models can be found at: *https://www.metoffice.gov.uk/research/modelling-systems/unified-model/climate-models/hadgem3.*

and the Global Land 6.0 (GL6.0) (Walters et al., 2017), the Global Ocean 5.0 (GO5.0) (Megann et al., 2014) and the Global Sea Ice 6.0 (GSI6.0) (Rae et al., 2015) models. The HadGEM3-CG2 climate model used here has a 25 km atmospheric horizontal resolution (N512 of the MetUM-GC2) and an ocean resolution of 0.25° on a tri-polar grid (ORCA025, Madec and the NEMO team 2008). It also includes the Los Alamos sea ice model (CICE, Hunke et al. 2015) and the Joint UK Land Environment Simulator (JULES, Best et al. 2011).

The vertical resolutions for each of these model components are: 85 levels in the atmosphere (model terrain-following coordinates, expressed in pressure levels for users), 75 depth levels (expressed in height/meter levels for users) in the ocean, 5 sea-ice thickness categories and 4 soil levels (expressed in meter). The grid and level resolutions of each component of the HadGEM3-GC2 model can be found in Table 2.1. The model outputs used for this study come from two long present-day climate simulations, the FEBBRAIO simulations (named "xkjej" and "xklrb"). It is 100-year "free-running simulations with forcings set to use values from the year 2000" (Williams et al., 2015) with outputs every 6 hours. The runs were initialised from restart conditions taken from a 25-year N512-O025 run, itself initialised using EN3[5] climatology (Ingleby and Huddleston, 2006) for ocean temperatures and salinity and sea ice means. The atmosphere and land were initialised from a 20-year N512 Atmospheric Model Inter-comparison Project (AMIP) run (Williams et al., 2015). Despite some SST and heat flux persistent biases over the Northern hemisphere (i.e. hemisphere of interest of this study), the HadGEM3-CG2 model is considered as a reliable fully coupled climate model to study global coupled interactions (Williams et al., 2015).

HadGEM3-GC2				
System	Atmosphere	Ocean	Land	Ice
Model version	GA6.0	GO5.0	GL6.0	GSI6.0
Grid (horizontal reso.)	N512	0.25°	N512	0.25°
Level (vertical reso.)	85	75	4	5

Table 2.1: Summary of the model version, grid and level resolutions of each system component of the HadGEM3-GC2 climate model.

This climate model is used in this thesis to assess the possible impact of PLs on the ocean surface and circulation. The FEBBRAIO simulations used here are very high resolution (25 km) and very long (100 years) compared to what has commonly been

[5] The EN3 is a quality control system for oceanic temperatures as well as temperature and salinity profiles.

used in past studies of PLs (i.e. usually with coarser resolutions and for only a couple of years to a decade). This provides the opportunity to study the interaction of PLs with the ocean at resolutions not previously possible over such a long period of time. Hence it will hopefully provide a greater statistical significance for what are relatively rare systems such as PLs.

2.1.3.2 The Met Office HadGEM3-GA3 Atmospheric Climate Model

The second climate model, used in this study to investigate the response of PLs to climate change (in Chapter 5), is the Met Office HadGEM3-GA3 atmosphere-only Climate Model.

The UK on PRACE - weather-resolving Simulations of Climate for globAL Environmental risk (UPSCALE) - is a series of ensemble simulations of the HadGEM3 global atmosphere-only model (Williams et al., 2015) at horizontal resolutions of 130 km (N96), 60 km (N216) and 25 km (N512). These three resolutions are typical of the resolutions currently used in global climate modelling, seasonal prediction and global weather forecasting respectively. The UPSCALE data have been produced for the recent historical period from 1985 to 2011. In parallel with ensemble climate simulations for the present climate, an ensemble was run (Mizielinski et al., 2014), using a time-slice methodology, to consider atmospheric conditions at the end of this century (2085 to 2110). The potential future climate scenario used for this was the Intergovernmental Panel on Climate Change (IPCC) Representative Concentration Pathway (RCP) 8.5 scenario (hereafter RCP 8.5, Riahi et al. 2011).

The RCPs are a series of greenhouse gas (hereafter GHG) emissions and atmospheric concentrations, air pollutant emissions and land use pathways which are intended to "support research on impacts and potential policy responses to climate change" (Riahi et al., 2011). The different RCPs cover a large range of forcing levels associated with emission scenarios, calculated from future demographic and economic trends and assumptions on possible technological changes (Moss et al., 2008). The RCP 8.5 corresponds to the highest greenhouse gas emissions pathway of the RCPs series as it does not include any specific climate mitigation target. "The greenhouse gas emissions and concentrations in this scenario increase considerably over time, leading to a radiative forcing of 8.5 $W.m^2$ at the end of the century" (Riahi et al., 2011).

The ensemble of climate simulations are produced with the HadGEM3-GA3 model configured with the HadGEM3 Global Atmosphere 3 (GA3) and Global Land 3 (GL3) models that from part of the MetUM. For all simulations there are 85 vertical levels (i.e. model terrain-following coordinates, expressed in pressure levels for users). The

configuration of the UPSCALE ensemble is mainly similar to the Atmospheric Model Inter-comparison Project II (AMIP-II) standard (described in Taylor et al. (2012) as the "historical" climate conditions, using realistic radiative forcings until 2005 and then using RCP 4.5 forcings up to 2011). One difference is that the daily SSTs and the sea ice, come from the Operational Sea Surface Temperature and Sea Ice Analysis (OSTIA) product (Donlon et al., 2012) . The OSTIA dataset has a resolution of 1/20° and is a "synthesis of satellite and *in-situ* observations covering 1985 to the present day" (Roberts et al., 2014). The OSTIA dataset has been chosen because of its high spatial resolution, which allows a more accurate representation of the ocean surface.

For the future climate simulations (the future climate is forced by an atmosphere-land surface model), the SSTs are calculated by adding the SST changes between the 1990-2010 and 2090-2110 in the HadGEM2 Earth System model (hereafter HadGEM2-ES) runs (Collins et al., 2011) under the IPCC (IPCC Fifth Assessment Report, hereafter AR5, Collins et al. 2011) RCP 8.5 (Mizielinski et al., 2014) to the OSTIA SSTs from the present day climate runs (i.e. $SST_{future} = SST_{present} + \Delta SST_{future-present}$). The future sea ice fractions (SIF) were re-gridded from HadGEM2-ES and interpolated from monthly to daily frequency from the same HadGEM2-ES runs. The future SIF is calculated as the present SIF plus the difference between two late century periods (i.e. the difference between 1990-2010 and 2090-2110 as stated in Jones et al. 2011). For the regions of sea which lose the sea ice cover between the present and future climates, the SST values were then interpolated from the HadGEM2-ES results.

The initial conditions for the ensemble members were taken from the N512 simulations from "consecutive days of a testing configuration following a 5-year spin up run starting from a N320 (40 km) resolution" (Mizielinski et al., 2014). A 5-year spin-up period is needed to give time for the land surface properties to adjust to the different (here N512) resolution. This was performed individually for both present and future climate simulations for all three resolutions. The initial conditions of the two coarser resolutions (i.e. N216 and N96) were obtained by re-gridding the N512 simulations.

As the future scenario used here is the most extreme of all RCPs in terms of greenhouse gas emissions and concentrations and warming, it thus gives an idea of how extreme future climate change might be, and thus how extreme the changes in PL frequency might be. The UPSCALE datasets have previously been used by Roberts et al. (2014), to assess possible future changes in tropical cyclones. Increasing the model horizontal resolution from 130 to 25 km was found to increase the frequency of the tracked tropical cyclones, for both present and future climates, but no variation of the intensity of tropical cyclones was found. Also found was a decrease of 50% in the frequency of tropical cyclones in the Southern Hemisphere as well as a decrease

of cyclone numbers over the North Atlantic. In the future simulations, a decrease in weak storms and an increase in strong storms was noted. A previous study from Tous et al. (2016) also used this climate model (N512 resolution only) to study future changes in medicanes (small intense cyclones that develop over the Mediterranean Sea). They found that the representation of medicanes in HadGEM3-GA3 is consistent with observations and that medicanes may decrease in number in the future, but that their intensity would likely experience a future increase.

Zahn and von Storch (2010) and Romero and Emanuel (2017) are the only two previous studies that examine the future of PLs over the North Atlantic region. These studies used global climate model simulations to downscale a set of global climate change scenarios from the IPCC (AR4 and AR5 respectively), and tracked the Mean Sea Level Pressure and the 850 hPa maximum vorticity associated with PLs. Both found a reduction of PLs activity over the North Atlantic Ocean in the future scenarios. These studies attributed this decrease to the change in the large-scale environment of PLs (mainly to the future increase in atmospheric static stability).

However, for the first time here, the representation of PLs is investigated with a high resolution global climate model, with an objective PLs tracking and identification scheme. Results of PL characteristics found with the HadGEM3-GA3 model will thus be important and helpful to assess the current and future representations and environments of PLs, as no previous study has investigated the future of PLs with such a high resolution global climate model.

	Present climate	Future climate
N96	xhqij, xhqik, xhqio	xhqir, xhqis, xgyip
N216	xgxqo, xgxqp, xgxqq	xgyid, xgyie, xgyif
N512	xgxqe, xgxqf, xgxqg	xgxqk, xgxql, xgxqm

Table 2.2: Summary of the simulation names and resolutions from HadGEM3-GA3 model used for the investigation of PLs changes for present and future climates (in Chapter 5).

In Chapter 5 of this thesis, different ensemble members are used for each of the three resolutions for both present and future climates. Since PLs are generally small in number each year, having a large dataset (with more than one ensemble member) is useful for statistical reliability. As the UPSCALE present and future simulations have different numbers of ensemble members for the three resolutions[6], three simulations, have been chosen in each set of simulations. All the simulations are 26-years long. The

[6] From three to five simulations for each resolution for the present climate and only three simulations for each resolution for the future climate because of computational difficulties. For the complete list of simulations, see Table 4 in Mizielinski et al. (2014).

summary of the run IDs used in this study can be found in Table 2.2.

2.2 Polar low tracking and identification

The objective tracking of atmospheric features (such as highs, lows or anomalies of different fields) enables the determination of atmospheric phenomenon characteristics and their climatologies, and to explore their spatial and temporal variability using long-term datasets. Tracking features also allows the study of the formation, lifecycle and decay of storms, including PLs, to be examined.

In this section, the objective feature-tracking algorithm used to track PLs for this study (Hodges 1994, 1995, 1999) will be described. The specific identification criteria used to study PLs will also be described. These are based on the dynamical intensity of the cyclone and the large-scale environment and previously used by Zappa et al. (2014).

2.2.1 Polar low automatic tracking method

Automatic Lagrangian tracking methods are usually composed of three parts: a pre-processing or data preparation first step, a detection step and finally a tracking step often followed by statistical calculations (Xia et al., 2012b). Spatial filtering is often used to remove the large-scale background, to reduce the noise in high resolution data and to focus on the spatial scales of interest (e.g. synoptic or mesoscale). The tracked features are usually local extremes of fields such as the minima of the MSLP (Serreze, 1995), the geopotential height (Blender et al., 1997), the maxima or minima of the relative vorticity (Hodges, 1995) or the geostrophic vorticity (Murray and Simmonds, 1991).

The objective feature-tracking algorithm used to track PLs for this study is named TRACK (Hodges, 1994, 1995, 1999). This algorithm has previously been used to identify and automatically track PLs (Zappa et al., 2014; Yanase et al., 2016; Stoll et al., 2018), medicanes (Tous et al., 2016), extra-tropical cyclones (Hoskins and Hodges, 2002; Catto, 2009; Hodges et al., 2011) as well as tropical cyclones (Roberts et al., 2014), through their maximum vorticity or minimum MSLP. These past studies have proven the flexibility of the method applied to both small and large cyclonic systems.

TRACK is applied to the relative vorticity at 850 hPa (TRACK version for this study: 1.4.7), from the reanalysis (3-hourly data) and climate model (6-hourly data) datasets previously described. Already available for ERA-I, the vorticity for the NCEP-CFS at this level is directly calculated from the u- and v-components of the wind field

at this level. Unfortunately this means that the vorticity is at a lower resolution than the wind speed, which may have an impact on the vorticity values found. The 850 hPa level is chosen as it is above the boundary layer (to avoid taking into account noise and large-scale features from low levels) but low enough (compared to levels such as 500 hPa) to still detect shallow systems. For the reanalyses, the 3-hourly vorticity data is obtained by splicing the relevant forecasts between the 6-hourly analyses. The use of 3-hourly data is useful because of the relatively short lifetimes of some PLs (Rasmussen and Turner, 2003).

Prior to the tracking, the vorticity field is spectrally filtered using a spherical harmonic decomposition. Total wave numbers smaller than 41 and greater than 100 are discarded (later called T41-T100) by setting the spectral coefficients to zero. The spectral coefficients are also tapered to reduced Gibbs oscillations when the inverse transform is performed to real space (Sardeshmukh and Hoskins, 1984). During the inverse transform, the data is output to a common T159 Gaussian grid. This procedure focuses on the spatial scales which are characteristic of relatively small mesoscale systems (between 400 and 1000 km in diameter) which is typical of PLs. This process of spectral filtering has also been applied to the vorticity field of PLs by Zappa et al. (2014); Yanase et al. (2016); Smirnova and Golubkin (2017) and Stoll et al. (2018). These previous PL studies have also used the same T40-T100 spectral truncation as in this study, as it retains the wave-numbers equivalent to mesoscale features with similar scales as PLs (400-1000 km). The spectral filtering technique has proven its ability to constrain the size of the studied features, and has also been applied for extra-tropical cyclones (Hoskins and Hodges, 2002; Jung et al., 2006; Catto, 2009; Dacre et al., 2012; Hawcroft et al., 2012) and tropical cyclones (Roberts et al., 2014; Hodges et al., 2017). Furthermore, as the choice of projections used for the detection can have a substantial impact on the final results (i.e. the use the standard latitude-longitude projection can distort distance and direction from their real values on the surface of a sphere), the choice of a polar stereographic projection (i.e. a conformal projection that preserves angles), which minimises any distortion at high latitudes, is crucial (Hodges, 1999; Zappa et al., 2014).

After the identification of the relative vorticity maxima, the feature points are projected back to spherical coordinates for the tracking to occur directly on the unit sphere. The feature points are initially joined into tracks using the nearest neighbour approach. This method imposes a restriction on the maximum distance between the feature points at consecutive time steps. Then, the tracks are refined to produce the smoothest sets of tracks. This is done by minimising a cost function, which depends on a local smoothness function. The smoothness function is defined in terms of changes

in direction and speed formulated in spherical coordinates (Hodges, 1999) so that the tracking is performed directly on the unit sphere to prevent bias.

Using this tracking approach, thousands of features are tracked over the whole Northern hemisphere in the datasets over the whole period. For all the datasets used, the tracking is carried out for the period between the 1st of October of one year, and the 31st of March of the year after (i.e. from 1st October 1979 to 31st March 1980). This is considered as the extended winter season in which most of PLs occur over the Northern hemisphere (Rasmussen and Turner, 2003).

The number of features identified by the tracking algorithm itself is relatively large compared to PL numbers from observational climatologies. This indicates that besides PLs, other features are present such as other mesocyclones and small-scale synoptic cyclones. Thus, additional criteria are needed to extract PLs from the total number of identified tracks (Zahn and Von Storch, 2008; Xia et al., 2012b; Zappa et al., 2014). Performing the tracking before the identification stage (rather than having the identification stage during tracking) allows more of the life-cycle of the PLs to be obtained.

2.2.2 Polar low identification criteria

In the literature, thresholds and criteria are often applied to different parameters typical of PLs and their environment, to discriminate PLs from other mesoscale systems (Zappa et al., 2014; Yanase et al., 2016; Smirnova and Golubkin, 2017; Stoll et al., 2018). Parameters such as conditions on the environmental static stability, vorticity and wind speed intensities or radius of PLs are typically evaluated at the location and time of the identified tracks.

Here, following the tracking, additional variables are added to the tracks in order to apply specific and commonly used criteria to identify PLs from amongst all tracked features. The additional variables include the sea surface temperature (SST), the 500 hPa temperature (T500) (averaged over 1° radius area) and the 10-m wind speed. A land-sea ice mask is also added to allow the identification criteria to be restricted to the ocean.

In this study, the same identification criteria as in Zappa et al. (2014) are employed:

- The T41-T100 relative vorticity at 850 hPa has to be greater than 6×10^{-5} s^{-1},
- The 10-m wind speed maximum has to be greater than 15 m.s^{-1}, within a 2.5° radius,
- The difference in temperature between the 500 hPa level and the sea surface level (i.e. $\Delta T = T500 - SST$) has to be smaller than -43 K,

- The ocean fraction of the track, averaged over a 1° radius, has to be greater than 75%,

The first two identification criteria focus on the dynamical aspects of the PLs: the maximum vorticity and wind speed associated with PLs.

As Noer et al. (2011) suggested, since Cold Air Outbreaks (CAO) can sometimes have strong background flows (often greater than 15 $m.s^{-1}$) a constraint on the T41-T100 maximum relative vorticity at 850 hPa is required. As a T41-T100 smoothing is applied in this study, the threshold of 6×10^{-5} s^{-1} is chosen. Studies using a similar smoothing often use this value for PLs tracking (Zappa et al., 2014; Yanase et al., 2016; Smirnova and Golubkin, 2017).

Since PLs are intense mesoscale cyclones reaching gale force or near-gale force wind speeds[7] (Rasmussen and Turner, 2003), their surface absolute wind speed maximum, within a 2.5° radius, often exceeds 15 $m.s^{-1}$. Thus as a convention, the maximum wind speed threshold commonly used is also of 15 $m.s^{-1}$, and is here required to be within a 2.5° radius around the PL tracks.

The next two criteria are based on the environment of the PLs.

The fourth criterion is the difference in temperature between 500 hPa and the sea surface, along the track of PLs. The 500 hPa temperature has been chosen, rather than the 200 or 300 hPa temperature, as PLs are shallower systems compared to other extra-tropical or tropical cyclones. Zahn and Von Storch (2008) suggested that the difference between the sea surface temperature and the air temperature at 500 hPa should be lower than -43° in the near surroundings of PLs as a suitable identification criteria. This threshold for the atmospheric static stability was chosen as Zahn and Von Storch (2008) highlighted that, since PLs are systems that often develop in a convectively unstable atmosphere, where the temperature at lower levels is often warmer than at upper levels. The value of -43° has been adopted in many previous studies for different regions (Xia et al., 2012b; Zappa et al., 2014; Yanase et al., 2016) and is the observed threshold for favourable conditions for PLs development used by the Norwegian Meteorological Institute (Noer et al., 2011). However, if the relevance of this static stability criterion is well agreed on, the specific value of -43° is more uncertain. For example, Terpstra et al. (2016) found that applying this particular value may exclude some forward shear PLs, which usually form in an environment of higher vertical stability. Nonetheless, as this

[7] On the Beaufort scale (an empirical measure which relates the wind speed to the observed conditions over the sea, going from force 0, i.e. calm, to 12, i.e. hurricane force) near gale force winds (force 7) are classified between 13.9 and 17.1 $m.s^{-1}$, and gale fore winds (force 8) are classified between 17.2 to 20.7 $m.s^{-1}$.

threshold is still used in almost all the current PLs studies and observational datasets, we here decide to keep this particular value. It will also permit the study to be more consistent, when comparing our results with previous studies and observations.

As PLs occur over the ocean and tend to decay quickly when they reach land (or sea ice), another criterion which is used in this study is that the criteria have to be satisfied only over the ocean, and the ocean fraction of the PLs track has to be greater than 75%.

Finally, as PLs have relatively small diameters and since the maximum wind speed is required to be found in the 2.5° radius circle, a constraint on the radius of PLs is thus applied. This radius threshold has been motivated by the typical mean radius of PLs found in previous studies (Kolstad, 2005; Smirnova et al., 2016; Stoll et al., 2018).

For all PL tracks, the identification criteria detailed above have to be satisfied at the same time step, which is when the vorticity along the track reaches its relative maximum. If not all the criteria are satisfied at the time of the first relative vorticity maximum of the track, then at the time step of the second vorticity maximum, if it exists, the other thresholds are tested. As a pre-criteria step, only tracks with a lifetime of at least six hours are retained (Zappa et al., 2014).

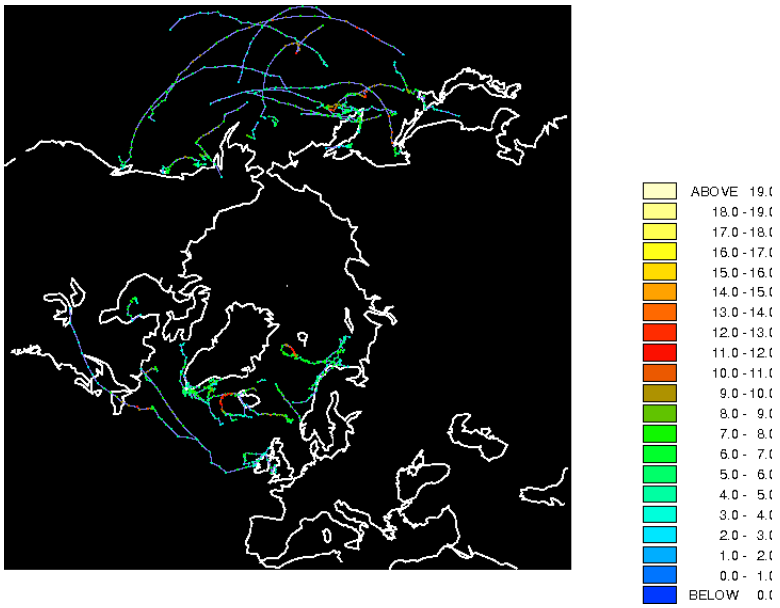

Figure 2-2: 51 PL tracks obtained, after the use of the tracking algorithm and identification criteria for October 1979 to March 1980 from the ERA-I dataset, over the Northern hemisphere. The colour represents the evolution of the vorticity (x10^{-5} m.s^{-1}) at each 3-hourly time step throughout the life cycles.

As PLs might not necessarily be associated with a MSLP minima, due to the dataset

resolution or the background flow, the identification scheme, developed by Zappa et al. (2014), does not require the presence of an associated closed minimum in MSLP. As seen on Figure 2-2, after applying the identification scheme the number of tracks decrease from thousand of tracks, obtained with the tracking algorithm, to around 50 tracks per year in ERA-I, over the Northern hemisphere.

In this study, three main regions are studied: the Northern hemisphere, the Norwegian and Barents Seas and the Sea of Japan (see Figure 2-3). The Northern hemisphere, north of 40°N, is studied as a whole, to get an overview of PL activity over the Northern hemisphere. The other two regions have been chosen in order to compare their results with previous studies using observations or reanalysis datasets. The Norwegian and Barents Seas region is defined as: latitude 64° - 80°N and longitude 15°W - 60°E, as in Zappa et al. (2014). The Sea of Japan's region is defined as: latitude 30° - 55°N and longitude 125° - 150°E, as in Yanase et al. (2016). Only the tracked PLs which reach their maximum vorticity intensity within the regions are considered for this study.

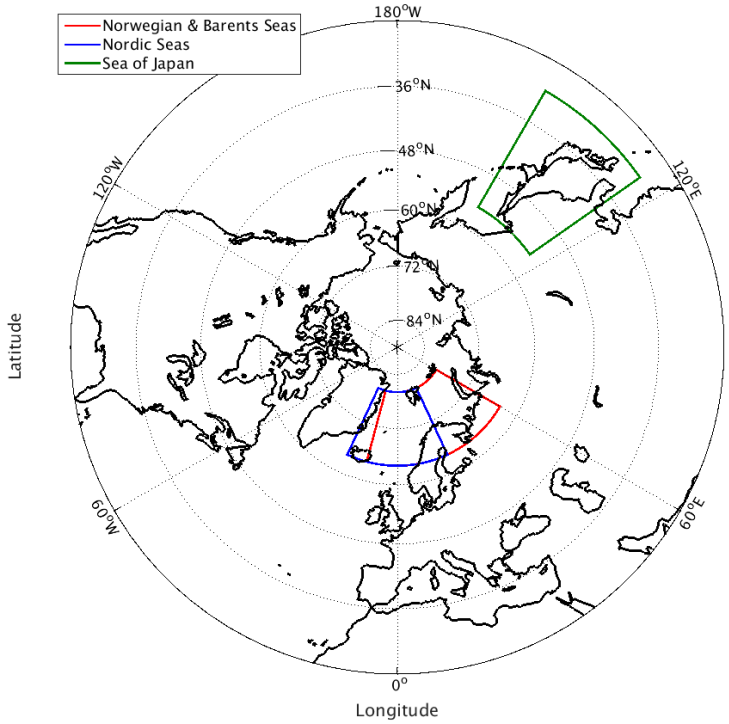

Figure 2-3: Map of the Norwegian and Barents Seas region in red (defined as in Zappa et al. 2014), the Nordic Seas region in blue, and the Sea of Japan region in green (defined as in Yanase et al. 2016).

To avoid repetition, results from Chapter 3 (climatologies from reanalyses) will

mainly focus on the Norwegian and Barents Seas. Later on in Chapter 4, for the investigation of the interaction of PLs with the ocean circulation and the deep water formation over the Nordic Seas, another region is defined as the Nordic Seas region. This region, where the deep water formation occurs over the north-east Atlantic Ocean (Rudels and Quadfasel, 1991), is defined as: latitude 64° - 80°N and longitude 25°W - 25°E. The defined regions can be seen in Figure 2-3. Finally, to investigate global changes in PLs in the future climate, results from Chapter 5 will focus on the whole Northern hemisphere.

2.2.3 Automatic tracking and identification criteria limits

Some PL studies still use manual identification and tracking (Rojo et al., 2015; Smirnova et al., 2015) to investigate numerous satellite images and *in-situ* observations. However, most of the research on PLs is now done thanks to automatic identification and tracking. Even if manual tracking can be a fastidious, time consuming and subjective task, automatic tracking also has its limits. Depending on the tracking method, and especially on the criteria used for identification of PLs (or storms in general), results on feature numbers and their locations can greatly differ.

Xia et al. (2012b) compared two of the main feature tracking methods commonly used for PL studies: the tracking of MSLP minima and the tracking of the vorticity maxima over the Northern hemisphere. Xia et al. (2012b) compared the method from Zahn et al. (2008), which uses a digital bandpass spatial filter of the MSLP field, and the Hodges method (Hodges, 1994, 1995, 1999), which uses a bandpass spatial filter based on the discrete cosine transforms[8] (hereafter DCT, Ahmed et al. 1974) and is used on the vorticity field. As Xia et al. (2012b) study made use of limited area downscaling data, the spherical harmonics could not used. Results from applying the two different filters lead to different numbers and locations of tracks, though actual PLs compared quite well. It is suggested that the DCT method is more precise for separation of scales than the digital filter method. As the detection and tracking parts also have an influence on the track numbers, they concluded that the filtering part of a method seems to be the most crucial step of the whole process.

In this study we are using the Hodges tracking algorithm, which was previously used

[8] A discrete cosine transform (DCT) represents a finite sequence of data points in terms of the sum of cosine functions which oscillate at different frequencies. DCTs are used to compress audio (such as MP3) or image (such as JPEG) files, can produce power spectra from two-dimensional atmospheric fields (Denis et al., 2002), and can also be used for pattern recognition and data filtering (Ahmed et al., 1974).

for mesoscale cyclones in different studies, as previously mentioned in Section 2.2.1. This tracking and identification method has been assessed for PLs in ERA-I and the ECMWF operational analysis by Zappa et al. (2014), and results have been compared to STARS observations. Results showed that around 55% and 70% of the STARS PLs were identified and tracked in ERA-I and the operational analysis respectively, based on the identification criteria stated above. More PLs were identified in ERA-I and the operational analysis than the ones listed in STARS. They suggested that the difference in PL numbers found could be due to the narrow boundary between polar mesocyclones and PLs and the subjectivity of the observed PLs list that is the STARS dataset (i.e. the relatively subjective evaluation of which mesocyclones should be classified as PLs and which should not). The difference in PL climatology also highly depends on how well PLs are represented in the datasets (whether they are observational, reanalysis or model datasets). Furthermore, this difference could be due to PLs being tracked successfully but failing the identification criteria, or could come from the chosen identification criteria have been defined as "being critical, but not universal, properties of polar lows" (Zappa et al., 2014).

As previously mentioned, whether the tracking is made manually or automatically, numerous studies apply criteria and thresholds to discriminate PLs from other tracked features. However, due to the complexity of PLs, specific threshold values are a relatively subjective choice.

The threshold used for the wind speed is the most agreed on criterion for PLs identification. Indeed, having near or above gale force, wind speeds is an attribute that has been pointed out in many PL observations (Rasmussen and Turner, 2003; Blechschmidt, 2008; Noer et al., 2011). Although the specific threshold will depend on the model and reanalysis resolution and other factors (e.g. physical parameterizations), defining PLs as as mesocyclones which have wind speed maxima reaching at least 15 $m.s^{-1}$ can be consider as a robust PL criterion, though it may also discard some less intense PLs.

Using a vorticity threshold to discriminate PLs from other mesocyclones is also a common characteristic of PL studies. If most of PL studies agree that a relative vorticity threshold of 6×10^{-5} s^{-1} is needed for the system to be considered as a PL, some studies use a higher threshold for specific regions. For instance, Yanase et al. (2016) used a 10×10^{-5} s^{-1} threshold over the Sea of Japan since, when using a threshold of 6×10^{-5} s^{-1}, some of the identified features where not actual PLs. Hence, setting a lower criterion value for the Sea of Japan could skew the results. However, having only one value for this criterion will allow consistency and robustness of the results of this thesis.

Finally, the difference in temperature threshold seems to be the most debatable

one. Indeed, as previously mentioned in Section 2.2.2, if the necessity of a vertical stability criterion is conceded, the specific value of -43° is not necessarily reached for all PLs and some studies have preferred to use a -39° threshold (Smirnova and Golubkin, 2017), even though some features identified with this criterion value may not be PLs. Furthermore, as Terpstra et al. (2016) and Michel et al. (2017) showed, some forward shear PLs might not be included in databases when using a static stability criterion of -43°. Stoll et al. (2018) also found that a -43° threshold may discard around 30% of PLs found in ERA-I, and suggested to relax the threshold to a higher value. Hence more work is needed to investigate the threshold value for this criterion through PL observations.

The sensitivity of PL numbers to those specific thresholds (i.e. vorticity, wind speed and static stability thresholds) will be discussed in Chapter 3 (Section 3.4.3) and assessed for PLs found with the ERA-I reanalysis.

2.2.4 Statistical methods

Following the tracking and identification, the climatological statistics of PLs are calculated directly on the sphere using spherical kernel estimators (Hodges, 1996). Some spatial statistics considered in this thesis are the genesis, track and lysis densities.

The track density gives a measure of the number of PLs which pass through a region. It is calculated by using the single track point from each track, which is the closest to the estimation point (Hodges, 1996). Genesis and lysis densities give a measure of where PLs start and decay. The densities are calculated as probability density distributions and scaled to a number density per month per unit area, which is equivalent to a 5° spherical cap, or around 10^6 km^2 (Hodges et al., 2011).

Beside the calculation of the genesis, track and lysis densities, some usual statistical tools are used in this thesis to describe the distributions of PLs and their environment as well as test statistics for hypothesis testing.

In order to describe the key variables, the Pearson's correlation coefficient and non-parametric kernel density estimators, among others, are used. For hypothesis testing, the one-sample and two-sample t-tests, the F-test as well some bootstrap hypothesis testing are used to discriminate hypotheses on PLs and their environment. These statistical tools used in this study are described next.

The Pearson's correlation coefficient indicates the covariance of two $(n \times 1)$ vectors

y_1 and y_2 divided by the product of their standard deviations:

$$\rho\left(y_1, y_2\right) = \frac{\sum_{i=1}^{n}\left(y_{1i} - \overline{y}_1\right)\left(y_{2i} - \overline{y}_2\right)}{\sqrt{\sum_{i=1}^{n}\left(y_{1i} - \overline{y}_1\right)^2 \sum_{i=1}^{n}\left(y_{2i} - \overline{y}_2\right)^2}} \text{ with } \overline{y}_j = \frac{1}{n}\sum_{i=1}^{n} y_{ji} \ , \ j = 1, 2$$

The confidence interval of the Pearson's correlation coefficient is calculated using a Fisher transformation when both datasets follow a multivariate normal distribution. The confidence bounds are based on an asymptotic normal distribution of:

$$0.5 \log\left(\frac{1 + \rho\left(y_1, y_2\right)}{1 - \rho\left(y_1, y_2\right)}\right)$$

with an approximate variance equal to $1/(n-3)$. These bounds are accurate for large samples when y_1 and y_2 have a multivariate normal distribution.

In the context of null hypothesis testing, the p-value (i.e. probability value) is used in order to quantify the idea of statistical significance of evidence. The p-value indicates the probability that a more extreme value than that observed is possible. The null hypothesis is rejected if the p-value is less than some chosen level (e.g. 5%). Here the null hypothesis $H_0 : \rho\left(y_1, y_2\right) = 0$ is that the correlation coefficient is zero (no correlation).

For the Pearson's correlation coefficient, the p-value is computed by transforming the correlation to create a t statistic having $n-2$ degrees of freedom. Working with a 95% confidence level, we will reject the null hypothesis if the p-value is less than 5%.

To statistically describe the distribution of the key variables (i.e. sea surface temperature, heat fluxes, ...), non-parametric kernel densities are computed (which are different from the spherical kernels used for the spatial densities). Statistical density estimation involves approximating a hypothesised Probability Density Function (PDF) from observed data. The kernel density estimation is a non-parametric technique for density estimation in which a known density function (i.e. the kernel) is averaged across the observed data points to create a smooth approximation. For any real values of a $(n \times 1)$ random vector y_1, the kernel density estimator's formula is given by:

$$\widehat{f_h}(y) = \frac{1}{nh}\sum_{i=1}^{n} K\left(\frac{y - y_{1i}}{h}\right)$$

where $y_{11}, y_{12}, \cdots, y_{1n}$ are random samples from an unknown distribution, n is the sample size, $K(.)$ is the kernel smoothing function and h is the bandwidth (Silverman, 1986).

Here, a Gaussian kernel has been chosen:

$$K(\tau) = \frac{1}{\sqrt{2\pi}} \exp\left(-\frac{1}{2}\tau^2\right) \text{ and } h \approx 1.06\widehat{\sigma}n^{-1/5}$$

where $\widehat{\sigma}$ is the standard deviation of y_1. These kernel density estimators are used in Chapter 4 to compare the distributions of PL numbers found with different identification criteria.

In Chapters 4 and 5, tests of zero means and/or differences of means are performed with one-sample and two-sample t-tests.

For example, in Chapter 4, two-sample t-tests are computed to compare pairs of means of PL numbers found per year with FEBBRAIO datasets from the HadGEM3-GC2 model (for 98 years) compared to previous results from ERA-I and NCEP-CFS reanalyses (36 years), for the Northern hemisphere, the Norwegian and Barents Seas and the Sea of Japan. These tests check if the means of PL numbers are similar or different from each other.

The two-sample t-test compares the location parameter of two samples. The test statistic is:

$$t = \frac{\bar{y}_1 - \bar{y}_2}{\sqrt{\frac{s_1^2}{n_1} + \frac{s_2^2}{n_2}}} \text{ with } s_j^2 = \frac{1}{n_j - 1}\sum_{i=1}^{n}\left(y_{ji} - \overline{y}_j\right)^2 \ , j = 1, 2$$

where $\bar{y}_1$ (resp. $\bar{y}_2$), s_1 (resp. s_2) and n_1 (resp. n_2) are the mean, the standard deviation and the sample size of y_1 (resp. y_2).
If equal variances are assumed, then the formula reduces to:

$$t = \frac{\bar{y}_1 - \bar{y}_2}{s_p\sqrt{\frac{1}{n_1} + \frac{1}{n_2}}} \text{ where } s_p = \sqrt{\frac{(n_1 - 1)s_1^2 + (n_2 - 1)s_2^2}{n_1 + n_2 - 2}}$$

The null hypothesis that the two means are equal is rejected if $\mid t \mid > t_{1-\frac{\alpha}{2},\nu}$ where $t_{1-\frac{\alpha}{2},\nu}$ is the critical value of the t distribution with ν degrees of freedom. If equal variances are assumed, then $\nu = n_1 + n_2 - 2$ else we use the Welch-Satterthwaite approximation:

$$\nu = \frac{\left(s_1^2/n_1 + s_2^2/n_2\right)^2}{\left(s_1^2/n_1\right)^2/(n_1 - 1) + \left(s_2^2/n_2\right)^2/(n_2 - 1)}$$

According to the F-test of equality of variances (Storch and Zwiers, 1999), we use the standard formula of the degrees of freedom or the Welch-Satterthwaite approximation for the t-distribution. The two-sample F-test is used to test if the variances of the two

samples are the same (i.e. come from the same population). The F-test is:

$$F = \frac{s_1^2}{s_2^2} \sim F_{n_1-1,n_2-1}$$

where s_1 (resp. s_2) and n_1 (resp. n_2) are the standard deviation and the sample size of the two datasets. The test is the ratio of the two sample variances. Under the null hypothesis of equality of variances, the test statistics F has a Fisher-Snedecor distribution with $(n_1 - 1)$ numerator degrees of freedom and $(n_2 - 1)$ denominator degrees of freedom. The further this ratio is from 1, the more likely the null hypothesis is rejected.

In Chapter 5, series of the difference between the present and future climate conditions of the SIF, the SST and other variables are analysed with the N512 resolution of the HadGEM3-GA3 climate model, over the Northern hemisphere. A standard one-sample t-test is also here used to check if these series are zero (i.e. no difference between present and future climates) or non zero (i.e. the present and future climates have different means of the variables).

Let y be the $(n \times 1)$ vector of difference with n sample size. The t-stat is given by $t = \overline{y}/(s/\sqrt{n})$ where the estimated variance s^2 is defined as $s^2 = (1/n)\sum_{i=1}^{n}(y_i - \overline{y})^2$. Under the null hypothesis $H_0 : \overline{y} = 0$, $\mid t \mid \sim t_{\alpha/2,n-1}$ at the α significance level. If the null hypothesis is accepted, the mean $\overline{y}$ of the difference is statistically not different from zero.

In Chapter 4, when investigating the link between PLs and the ocean, a bootstrap method is used. This bootstrap test is undertaken to assure the significance of a test of differences in anomalies of the heat fluxes and ocean density. Bootstrapping can be defined as any test or metric that relies on random sampling with replacement. So, inference about a population from sample data can be modelled by re-sampling the sample data and inference can be performed from the re-sampled data.

Suppose that we are interested by differences in anomalies of the heat fluxes. We first compute means (from October to March) for each year: $\overline{y}_t = (1/M)\sum_{m=1}^{M} y_{m,t}$. We get a times series of mean heat fluxes of length 98 years and a general mean for the whole period (i.e. climatological mean over the 98 years): $\overline{y} = (1/MT)\sum_{t=1}^{T}\sum_{m=1}^{M} y_{m,t}$ for each grid point of the region of interest.
If two series of five years of mean heat fluxes are defined: $\overline{y}_{1t}$ for years with high PLs and $\overline{y}_{2t}$ for years with low PLs and their means over the five years: $\overline{y}_1 = (1/5)\sum_{t=1}^{5}\overline{y}_{1t}$ and $\overline{y}_2 = (1/5)\sum_{t=1}^{5}\overline{y}_{2t}$. The bootstrap test is defined as followed:

1. From the 98-year heat fluxes series ($\overline{y}_t$), 2000 random samples of five years $\overline{y}^*_t$ are generated.

2. The time mean of each of the 2000 bootstrap series are computed (*i.e.*, $\overline{y}^* = (1/5)\sum_{t=1}^{5}\overline{y}^*_t$).

3. For each grid point, we check if the heat fluxes anomaly for the five specific high years $\Delta F_{high}(=\overline{y}_1-\overline{y})$ is greater or equal to the 95^{th} percentile of the heat fluxes anomaly of the 2000 bootstrap series $\Delta F^*(=\overline{y}^*-\overline{y})$. If it is the case, we keep the lat-lon location and the value of ΔF_{high}, if not we replace by a NaN. We also check if the heat fluxes anomaly for the five specific low years $\Delta F_{low}(=\overline{y}_2-\overline{y})$ is less or equal to the 5^{th} percentile of the heat fluxes anomaly (ΔF^*) of the 2000 bootstrap series. If it is the case, the lat-lon location and the value of ΔF_{low} are kept, if not they are replaced by a NaN. For each grid point, the means over the 2000 samples are computed.
   In other words, for each grid point of the map, only are kept the point locations of where the heat fluxes anomaly for the five specific high/low years is higher/lower than the $95^{\text{th}}/5^{\text{th}}$ percentile of the heat fluxes anomaly of the 2000 bootstrap series. This way, the non-NaN values and their location mean that the heat fluxes of the specific (high/low) years are not representing the climatology as they are higher/lower than the $95^{\text{th}}/5^{\text{th}}$ percentile of the heat fluxes climatology.

Finally, significance testing for the difference of track densities of PLs between the present-day and the future climates have been computed in Chapter 5. Instead of drawing bootstrap resampling with replacement (computed in Chapter 4 and previously explained), the permutation approach to significance, proposed by Hodges (2008), is used here.

With a bootstrap approach, the tracks from both datasets are pooled and then resampled to produce 2000 new paired samples of the same size as the original datasets (i.e. 26 years of present-day and future climates), where each original tracks only appear once in any of the new paired samples. Once the sample pairs have been generated, the statistics are computed for each sample in the same way as for the original samples using the kernel method. The statistics for each pair are then differenced (i.e. future minus present) and the sampling distribution computed. The p-values are then computed using the difference for the original sample pair. To provide the significance of the test, and using the p-values, the track density differences, which are significantly different at a 5% level, are plotted. The p-values of the two-tailed test represent the significance level at which the null hypothesis that $H0 : \theta = \mu_1 - \mu_2 = 0$, is rejected. Storing the

estimate of the statistic $\widehat{\theta}_b$ for the bth bootstrap samples ($b = 1, .., B$, with $B = 2000$), the p-value is given as:

$$p(\widehat{\theta}) = 2 \min \left\{ \frac{1}{B} \sum_{b=1}^{B} I\left(\widehat{\theta}_b \leq \widehat{\theta}\right), \frac{1}{B} \sum_{b=1}^{B} I\left(\widehat{\theta}_b > \widehat{\theta}\right) \right\}$$

where $I\{.\}$, the indicator function, is one or zero, depending on the condition being true or false respectively for the actual statistic θ (see Hodges 2008 for more details). Hodges (2008) showed that the permutation approach is more appropriate than the bootstrap resampling with replacement or the calculation of t-tests according to a Student's distribution for track densities. This approach has also been used in Bengtsson et al. (2006) to study the impact of climate change on storm tracks.

This quick overview avoids repeating the definitions of these statistical tools throughout the chapters of the thesis. More details can be found in Von Storch and Zwiers (1999), Wilks (2005) and Gibbons and Chakraborti (2011) among others.

CHAPTER 3

POLAR LOWS IN ATMOSPHERIC REANALYSES

3.1 Introduction

Being able to provide a reliable climatology of PLs is one of the key starting points to understanding PL dynamics and their interactions with the climate system (Harold et al., 1999a,b). PLs have been previously detected using weather maps and weather station data (Wilhelmsen, 1985) and within satellite images by identifying spiraliform or comma-shaped cloud patterns (Blechschmidt, 2008; Noer et al., 2011). However, the few climatologies based on observations are often short-term, non exhaustive, only for specific regions and often rely on subjective identification. More recently, PLs have been automatically identified and tracked in reanalyses and regional climate model outputs using objective identification criteria based on parameters such as sea level pressure, vorticity or wind speed (Zahn et al., 2008; Xia et al., 2012a; Zappa et al., 2014; Smirnova and Golubkin, 2017). Still there is a large uncertainty in the yearly numbers of PLs detected with these methods. For instance, over the Norwegian and Barents Seas, Noer et al. (2011) found a mean of 11 PLs per extended winter season (from October to March), whereas Blechschmidt (2008) found around 45 PLs per season over a similar region that included the Labrador Sea.

Given the large observational uncertainty in PL numbers, it is important to evaluate whether atmospheric reanalyses are useful for providing an alternative perspective on the climatology of PLs.

Here, the aim is to evaluate the ability of atmospheric reanalyses to represent PLs by contrasting the tracking and the identification criteria of PLs using two atmospheric reanalysis datasets, the ECMWF Interim reanalysis (ERA-I) and the NCEP Climate

System Forecast reanalysis (NCEP-CFS). As previously mentioned in Chapter 2 (Section 2.1.2 on atmospheric reanalyses), ERA-Interim (Dee et al., 2011) is a global atmospheric reanalysis produced by ECMWF, for the period of 1979 and onward based on the Integrated Forecasting System (IFS) operational spectral model. The NCEP-CFS reanalysis (Saha et al., 2010) uses the NCEP coupled forecast system model, to produce the analysis for the period 1979 and onward. These two reanalyses have both been chosen for their different horizontal resolutions, their long-term datasets (36 years) and their ability to represent mesoscale features (Hodges et al., 2011; Tilinina et al., 2014; Bromwich et al., 2016; Smirnova and Golubkin, 2017).

The differences between this study and previous ones are numerous. First, PLs here are tracked and identified over a 36-year period, which makes it one of the longest climatologies produced. The previous longest studies are Zahn and Von Storch (2008) (with a 56-year period of study) using downscaled NCEP-NCAR reanalysis at a resolution of 50 km to track PLs using the MSLP, and Smirnova et al. (2015) and Rojo et al. (2015) (both 14-year period of study), who identified PLs using satellite imagery. Having a longer period of interest increases the sample size of PL cases, which helps to provide more statistically robust results. Secondly, the identically same methodology for all areas of interest, and the same selection of criteria makes the analysis traceable. Hence, PL characteristics can here be compared in a consistent manner between different regions and reanalyses.

In this chapter an overview of PL mean numbers and the spatial density of their tracks over different regions will be given. The seasonal and inter-annual variability of PL numbers obtained for both reanalyses will be explored and compared to observational datasets. In particular PLs identified in the reanalyses will be compared with those from the Sea Surface Temperature and Altimeter Synergy for Improved Forecasting of Polar Lows (or STARS, Noer et al. 2011), described in Section 3.4.2. Later on, the link between PLs and their large-scale environment will be considered and compared with the locations of PLs.

3.2 Characteristics of Polar lows in the reanalyses

In this section, statistics of PLs, such as the mean and variation of their numbers per year, their track density, genesis and lysis across the regions of interest are analysed.

The total, mean and standard deviation of PL numbers found in each extended winter season with both reanalyses are summarised in Table 3.1 for the three main regions of interest. Table 3.1 shows that the numbers of PLs found, with NCEP-CFS is

almost twice those found with ERA-I. These results seems consistent with the fact that the horizontal resolution of NCEP-CFS is almost twice that of ERA-I (i.e. 38 km for NCEP-CFS and 79 km for ERA-I). As expected large numbers are found for the whole Northern hemisphere, compared to the two smaller regions. Unfortunately no previous studies allow a comparison with these results for the Northern hemisphere. However, the mean numbers found appear consistent with the literature, for the Norwegian and Barents Seas (Noer et al., 2011; Rojo et al., 2015) and the Sea of Japan (Yanase et al., 2016). This may give some confidence in the values found for the largest region of interest.

		ERA-I	NCEP-CFS
Northern hemisphere	Mean	65.55	120.81
	Std dev.	13.86	18.32
	Total	2288	4349
Norwegian and Barents Seas	Mean	12.61	23.31
	Std dev.	4.43	6.15
	Total	454	839
Sea of Japan	Mean	2.86	6.42
	Std dev.	2.14	3.71
	Total	103	231

Table 3.1: Statistics of PL numbers found per extended winter season, from October 1979 to March 2014, with ERA-I and NCEP-CFS, for the Northern hemisphere, the Norwegian and Barents Seas and the Sea of Japan.

For the Norwegian and Barents Seas, around 12 and 23 PLs per year are found, with standard deviation around 4 and 6 PLs per year, for ERA-I and NCEP-CFS respectively. Other studies have found relatively similar results for this region, using observations: 12 PLs per year in Noer et al. (2011) (over a 9-year period), 14 PLs per year in Rojo et al. (2015) and 45 PLs per year in Smirnova et al. (2015) (over a 14-year period), 40 PLs per year in Melsheimer et al. (2016) (over a 10-year period).

Another feature to note is that the numbers of PLs found over the Norwegian and Barents Seas region represents nearly 20% of the numbers found with ERA-I and NCEP-CFS for the whole Northern hemisphere, when the Norwegian and Barents Seas region represents around 2% of the Northern hemisphere (and around 28% of the Arctic region). This area is thus a very, if not the most, populated region for PLs and an important place to study their dynamics and interactions with the climate system. This is why in this chapter, results and comments will focus on this particular region.

To see if a common set of PLs is identified in the two reanalyses, the matching of PLs, between the ones found with ERA-I and the ones found with NCEP-CFS, has

been analysed in Table 3.2. The main conditions for tracks to match are that they have to overlap in time by at least 50% of their points, and the mean separation distance have to be less than 2.50° (around 250 km, i.e. mean PLs radius) where they overlap (Zappa et al., 2014).

		Total PLs number	Matched PLs number	Percentage of matched PLs
NH	ERA-I	2288	1422	62.15 %
	NCEP-CFS	4228		33.63 %
N & B Seas	ERA-I	454	309	68.06 %
	NCEP-CFS	819		37.72%
Sea of Japan	ERA-I	119	68	57.14 %
	NCEP-CFS	267		25.47 %

Table 3.2: Total numbers, matched numbers and percentage of matched numbers of PLs found with ERA-I and NCEP-CFS, from 1979 to 2014, over the Northern hemisphere ("NH"), the Norwegian and Barents Seas (N & B Seas) and the Sea of Japan.

Over the Norwegian and Barents Sea and the Northern hemisphere, approximately 60% of the PLs found in ERA-I are matched with those of NCEP-CFS. For this same region (and with the same tracking and identification scheme), Zappa et al. (2014) found that 37.25% of the total PLs numbers identified in ERA-I matched the STARS observed PLs, over a 3-year period. Future tasks could be to match the PLs from NCEP-CFS with the STARS (for the same region and period) to investigate how similar both datasets are, and to investigate if more matches could be found if the matching constraints were relaxed (for example, applying a maximum of 25% or 10% overlapping between the tracks instead of the current 50%).

Similarly, over the Sea of Japan, more than 55% of ERA-I PLs match with the ones from the NCEP-CFS reanalysis. These lower results for the Sea of Japan may be explained by the generally lower numbers of PLs found in this region, or that the criteria used in this thesis are too restrictive for this region. In their 36-year study of PLs over the Sea of Japan, Yanase et al. (2016) found a total number of PLs of 245 with the Japanese reanalyses JRA-55. With a similar tracking and identification scheme (except for a higher vorticity threshold of $10x10^{-5}$ s^{-1}), this value fits within the range of total PL numbers found with ERA-I and NCEP-CFS found here. Again, one interesting analysis to do in the future would be to match PLs from ERA-I and NCEP-CFS with the ones from JRA-55, to investigate the representation of PLs with these three long-term reanalyses.

The tracks of PLs found with both reanalyses are shown in Figure 3-1, for the 36 years for ERA-I (left panel) and NCEP-CFS (right panel) for the Norwegian and

Barents Seas. The box represents the region that we define as the Norwegian and Barents Seas, as previously mentioned.

For both datasets, the tracks cross the Norwegian and Barents Seas box with no obviously preferred path. As mentioned above, fewer PLs are found in ERA-I. Some unusually long tracks crossing the North Atlantic (coming from Canada) can be noted, as well as some tracks going far inland over France, eastern Europe and Russia. As PLs are generally short-lived and usually last less than 48 hours, some of these long tracks (representing less than 15% for tracks longer than 72 hours, for the Norwegian and Barents in both reanalyses), may either be long-lasting PLs, or could also be long tracks containing the part of the track associated with the "Polar low phase" (i.e. the part of the track where all the identification criteria are satisfied within the box) and that the remainder of the track would be the decay phase of the PLs (part of the track where all criteria may not necessarily be satisfied).

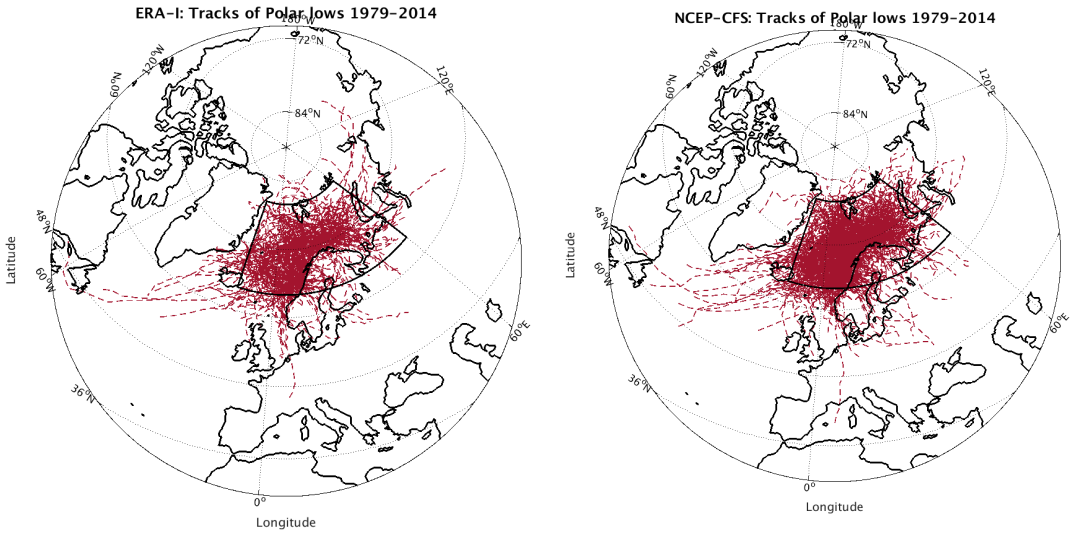

Figure 3-1: Tracks of PLs found with ERA-I (left) and NCEP-CFS (right) from 1979 to 2014, over the Norwegian and Barents Seas (black box, as defined as in Zappa et al. (2014)).

In order to examine the spatial distribution of PLs, statistics for their track density is computed, using non parametric kernel spherical estimators described in Hodges (1995). Using this method, the statistical fields can be determined directly on the sphere which prevents from having "the systematic error introduced when using projections to estimate statistical quantities". Figure 3-2 presents the number of PLs per month per unit area (a unit area is equivalent to a 5° spherical cap, which corresponds to around 10^6 km^2), or track density of PLs that reach their maximum within the box, with ERA-I (left panel) and NCEP-CFS (right panel) for the Norwegian and Barents

Seas, for the 36-year period. The maximum track density over this region is west of Tromso, Norway with a value of around 2.1 and 4.1 tracks per month per unit area for ERA-I and NCEP-CFS respectively. This area represents the region where the largest number of PLs, occur within the Norwegian and Barents Seas box. The density then decreases, almost constantly in all directions, in the rest of the region. For visualisation purposes, the areas where the track density lower than 0.1 has been set in white. The area where the track density is equal or higher to 0.9 corresponds to the region of maximum CAO in Kolstad and Bracegirdle (2008) and Fletcher et al. (2016) (see Section 3.6.2 for further details on CAOs). This reinforces the known fact that CAOs are important for PL formation.

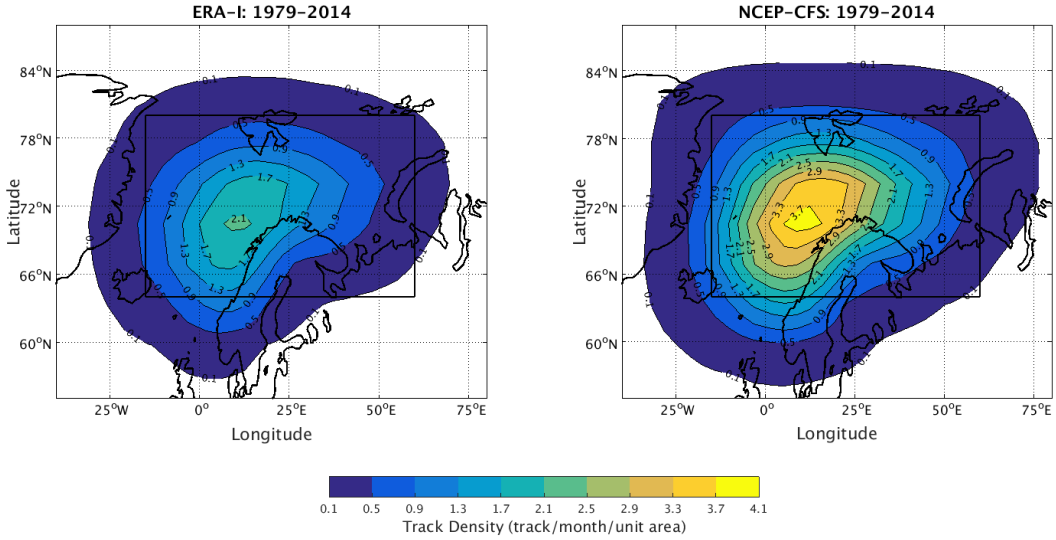

Figure 3-2: Track density (track per month per unit area) of PLs found with ERA-I (left panel) and NCEP-CFS (right panel), over the Norwegian and Barents Seas, from 1979 to 2014.

The same analysis has been performed for the genesis and lysis density of PLs. Figure 3-3 shows the genesis density of PLs identified in ERA-I (left panel) and NCEP-CFS (right panel), from 1979 to 2014 over the Norwegian and Barents Seas. Both reanalyses have similar patterns of genesis density. The genesis density has its maximum over most of the Norwegian Sea with value of 0.9 and 2.1 tracks per month per unit area for ERA-I and NCEP-CFS respectively. This coincides with most of the northerly CAO arriving from the Arctic sea ice, in between Greenland and the Svalbard islands. Most of the domain box has a genesis density of 0.2 track per month per unit area or more, except for the eastern part of the Barents Sea. This may be explained by the presence of less CAOs in this region, or less open water to support PL development.

Figure 3-4 shows the lysis density of PLs identified in ERA-I (left panel) and NCEP-

CFS (right panel), from 1979 to 2014 over the Norwegian and Barents Seas. The lysis density figure looks quite similar to the track density one. The maximum lysis density also lies south-west of Tromso, Norway, with a value of 0.9 and 1.6 track per month per unit area for ERA-I and NCEP-CFS respectively. The main lysis region (lysis density equal or higher than 0.5) tends to spread less than the main genesis region, and stays over the eastern part of the Norwegian Sea.

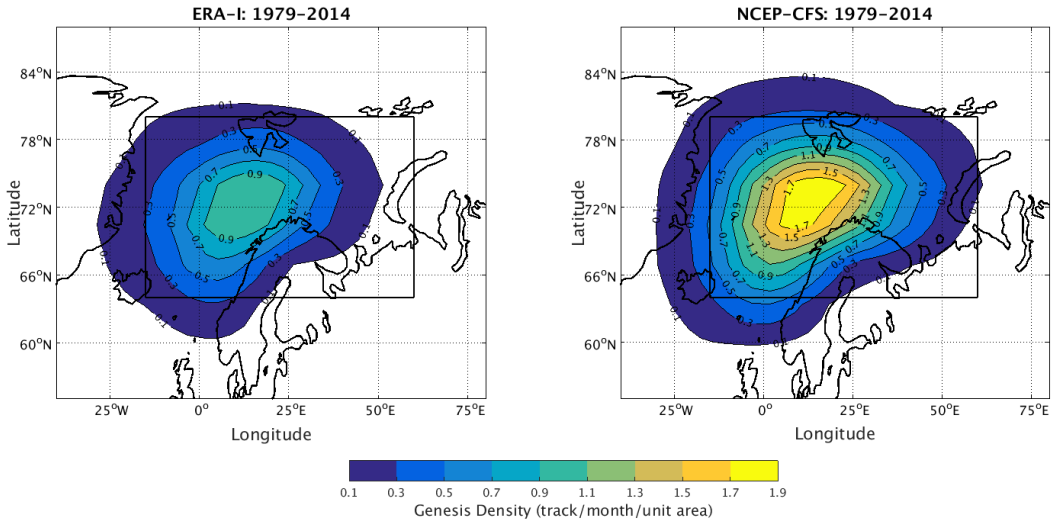

Figure 3-3: Genesis density (track per month per unit area) of PLs found with ERA-I (left panel) and NCEP-CFS (right panel), over the Norwegian and Barents Seas, from 1979 to 2014.

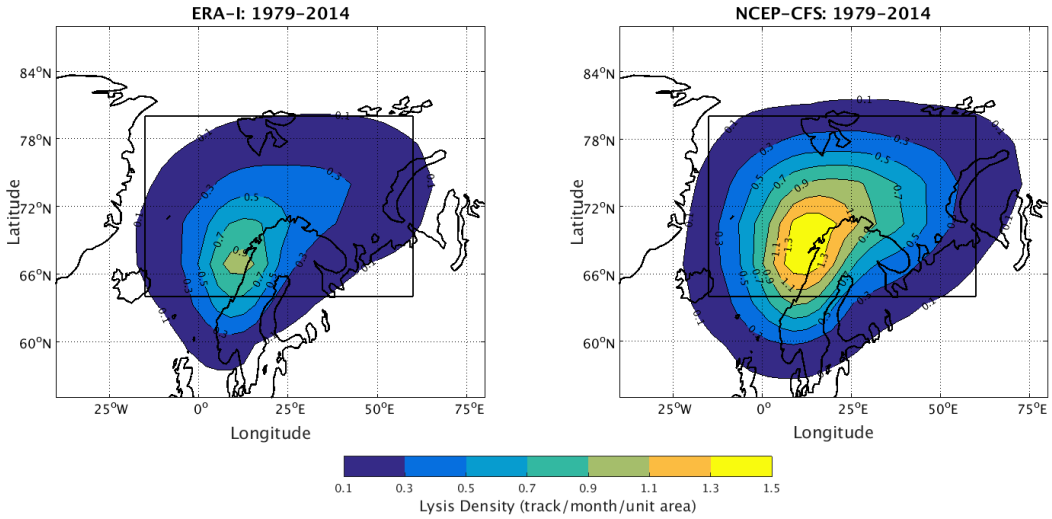

Figure 3-4: Lysis density (track per month per unit area) of PLs found with ERA-I (left panel) and NCEP-CFS (right panel), over the Norwegian and Barents Seas, from 1979 to 2014.

Overall, these results indicate that conditions in this region, along the northern coast of Norway and between north of Norway and south of Svalbard, tend to be favourable for PLs as they tend to develop and decay in this region.

A comparison of the maximum vorticity, maximum wind speed and minimum difference in temperature (between 500 hPa and the surface) at PL track maximum for both reanalyses has also been examined. Table 3.3 shows the mean and the standard deviation of the 850 hPa filtered relative vorticity, 10-m wind speed and the difference between the temperature at 500 hPa and at the surface, at the point of maximum vorticity of each PL found with ERA-I and NCEP-CFS, for the whole period, for the three regions of interest. Overall, the values show that PL characteristics are quite similar in both reanalyses, with slightly larger difference in wind speed values in the datasets. These results suggest that the representations of PLs in the reanalyses are quite similar.

		Vorticity		Wind speed		ΔT	
		ERAI	NCEP	ERAI	NCEP	ERAI	NCEP
NH	Mean	8.12	8.26	18.75	20.47	-45.02	-45.13
	Std dev.	1.76	1.95	2.67	3.51	1.72	1.83
N&B Seas	Mean	8.21	8.41	18.41	20.25	-45.32	-45.46
	Std dev.	1.87	2.01	2.73	3.34	1.83	1.99
Sea of J.	Mean	8.36	8.50	18.28	20.26	-45.15	-45.12
	Std dev.	1.86	2.09	2.48	3.21	1.79	1.92

Table 3.3: Mean and standard deviation of maximum filtered vorticity (in $\times 10^{-5}$ s^{-1}), maximum wind speed (in $m.s^{-1}$) and minimum temperature difference ($\Delta T = T500 - SST$, in °K) found along the PLs track in ERA-I ("ERAI") and NCEP-CFS ("NCEP"), over the Northern hemisphere ("NH"), the Norwegian and Barents Seas ("N&B Seas") and the Sea of Japan ("Sea of J."), from 1979 to 2014.

Finally, one last characteristic of PLs studied here with the reanalysis datasets is is the duration of PLs. Table 3.4 shows the mean, standard deviation, minimum and maximum duration of PLs found in ERA-I and NCEP-CFS, over the Norwegian and Barents Seas, from 1979 to 2014. Results for both reanalyses are very similar. The mean duration of PLs is found to be around 31 h with a standard deviation of around 18 h, a minimum duration of 6 h (as constrained by the identification criteria seen in Chapter 2), and a maximum duration of around 115 h. These results are consistent with the idea that PLs have a mean lifetime of a day or two, and rarely exceed a three- or four-day duration. This mean duration is higher than satellite-based studies (Smirnova et al. 2015, Smirnova et al. 2016) which found an average duration of 12 h. However, in the observations-based study of Rojo et al. (2015), 77% of PLs were found

to last less than 30 h, with a range from a few hours to more than 72 h. Laffineur et al. (2014) found an average lifetime of 15 h in ERA-I and ERA-40 reanalyses.

	Mean	Std dev.	Min	Max
ERA-I	30.81	18.36	6	110
NCEP-CFS	30.74	18.20	6	120

Table 3.4: Mean, standard deviation, minimum and maximum duration (in hours) of PLs found in ERA-I and NCEP-CFS, over the Norwegian and Barents Seas, from 1979 to 2014.

Similar results were considered for the Northern hemisphere and the Sea of Japan, which resulted in mean durations of 31.40 h and 35.36 h respectively, and a standard deviation of 19.02 h and 20.04 h respectively. These results support the idea that even though they may have slightly different characteristics depending on their location, PLs from all regions tend to have a relatively short lifetime compared to synoptic scale cyclones (Catto, 2009; Roberts et al., 2014; Tilinina et al., 2014).

3.3 Seasonal cycle of Polar low numbers

3.3.1 Results from reanalyses

In order to see how PLs are distributed during winter, the seasonal variability of PL numbers in ERA-I and NCEP-CFS is analysed.

Figure 3-5 shows the numbers of PLs found each month (October to March) from 1979 to 2014 over the Norwegian and Barents Seas, represented with boxplots[1]. As seen previously, regardless of the fact that higher PL numbers are found in NCEP-CFS there are similarities between the two reanalyses. Higher numbers of PLs are found in December and January, preceded by a relatively rapid increase of the numbers, and followed by a gradual decrease. For the Norwegian and Barents Seas, a mean of 2 PLs per month was found with ERA-I and a mean of 3 PLs per month was found with NCEP-CFS.

The seasonal evolution of the large-scale environment is found more favourable for PL development. Indeed, the seasonal cycle of PLs is found similar to those of CAOs (Papritz, 2017) and sea ice extent (Stroeve et al., 2012).

Similar results were found for the other regions (not shown), with a mean of 1 and 10 PLs found with ERA-I for the Sea of Japan and the Northern hemisphere

[1] In this study, the boxplots represent the minimum and maximum values and the 25, 50^{th} and 75^{th} percentile of the distributions.

respectively, and 2 and 20 PLs found with NCEP-CFS for the Sea of Japan and the Northern hemisphere respectively.

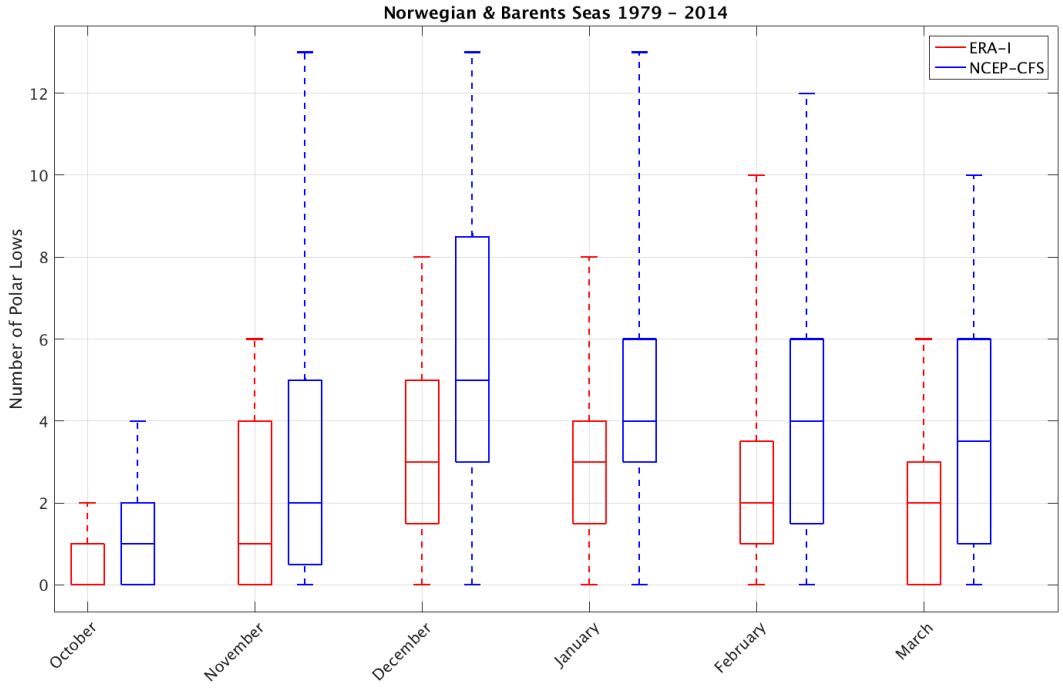

Figure 3-5: Numbers of PLs found each month (October to March) with ERA-I (in red) and NCEP-CFS (in blue), for the Norwegian and Barents Seas, from 1979 to 2014.

3.3.2 Comparison with observational datasets

To perform a validation of the reanalyses against an observational dataset, both ERA-I and NCEP-CFS results were compared to the STARS (Sea Surface Temperature and Altimeter Synergy for Improved Forecasting of Polar Lows) dataset, from 2002 to 2010. As explained in Chapter 2 (Section 2.1.1), the STARS dataset is a satellite and in-situ dataset, gathered by the Norwegian Meteorological Institute (Noer et al., 2011) and used to investigate PL events. Observed PLs are tracked over the Norwegian and Barents Seas since January 2001 (and in the Labrador Sea since 2006). The large-scale environment is also assessed (static stability, presence of a upper-level advection of potential vorticity and low-level baroclinicity). However, only the strongest PLs are listed when a cluster of PLs form within the same CAO (Zappa et al., 2014; Smirnova and Golubkin, 2017). This means that PLs not listed in STARS may be found in ERA-I and NCEP-CFS.

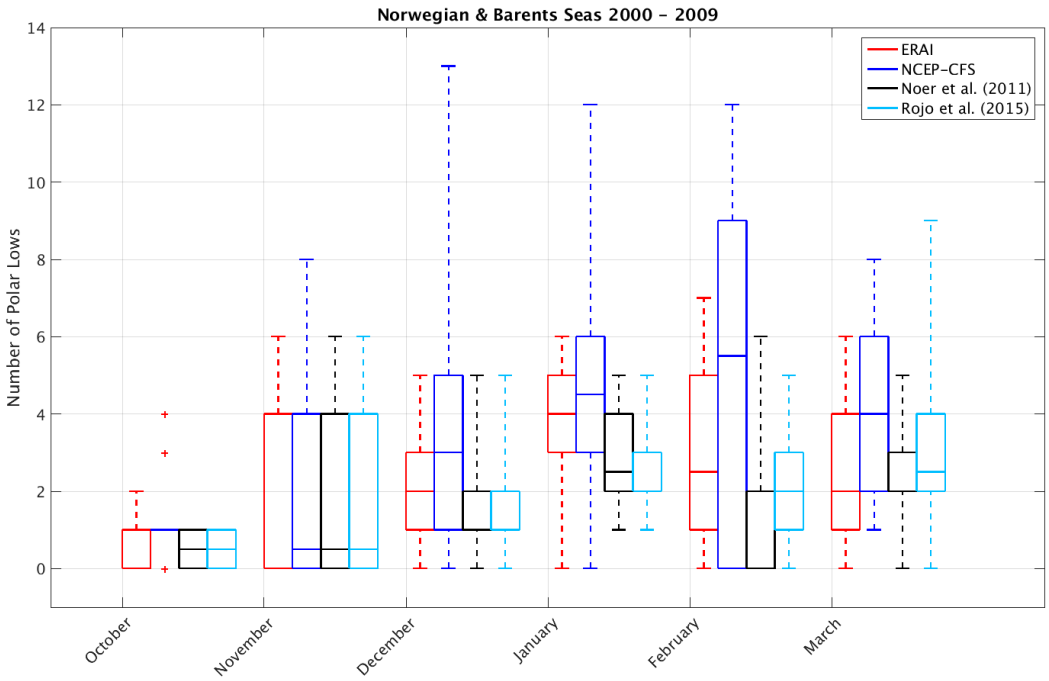

Figure 3-6: Numbers of PLs found each month (October to March) with ERA-I (in red) and NCEP-CFS (in blue), for the Norwegian and Barents Seas, from 2000 to 2009, compared with Noer et al. (2011) (in black) and Rojo et al. (2015) (in light blue).

Figure 3-6 shows the numbers of PLs found for each month (October to March) with ERA-I (in red) and NCEP-CFS (in blue), for the Norwegian and Barents Seas, from 2000 to 2009, compared with satellite-based and radio-sounding observations from Noer et al. (2011) (in black) and Rojo et al. (2015) (in light blue). Both reanalyses tend to have higher numbers of occurrences than the ones from the observations. As previously mentioned, this may be due to the fact that the observation datasets are manually made and only retain the strongest PLs, and thus some PLs may have been missed or discarded. Furthermore since no thresholds[2] were used for these climatologies, some PLs may be missed as the interpretation of the images is only subject to the experts judgement. Another possibility may be that the objective identification scheme used here is too relaxed, and hence identifying too many PLs. When analysing Figure 3-6, a slightly more similar representation of seasonal variability is found between the observation datasets and ERA-I, compared to the NCEP-CFS one. However, though

[2] If no strict threshold are applied in the STARS dataset, on characteristics such as local mean sea level pressure or wind speed, these characteristics are still assessed to insure that the observed features are indeed PLs. See Noer et al. (2011) for more information.

the numbers are relatively small for statistical robustness, there is broad agreement between the number found in the reanalyses and the range of PL numbers found in the literature such as Noer et al. (2011) and Rojo et al. (2015).

Comparisons with observations could unfortunately not be studied for the whole Northern hemisphere and the Sea of Japan as no observation-based climatologies are available for these regions. However, for the Sea of Japan, a comparison with the Japanese reanalysis JRA-55 was made and compared to a previous study from Yanase et al. (2016), which used almost identical tracking method and identification criteria. Despite the really low numbers found for each month, and thus the low statistical robustness, results were quite similar between the three reanalyses, with higher numbers for the months of December, January and February (around 4 PLs per month), and with fewer numbers, less than 2 PLs per month, for the three remaining months (i.e. October, November and March).

3.4 Inter-annual variability of Polar low numbers

3.4.1 Results from reanalyses

One important aspect of the climatology of PLs is the inter-annual variability of their numbers. This facet of the representation of PLs is considered here for both ERA-I and NCEP-CFS.

Figure 3-7 shows a time series of wintertime PL numbers from 1979 to 2014, over the Norwegian and Barents Seas. The upper panel of Figure 3-7 presents the total PL numbers found, with ERA-I (in red) and with NCEP-CFS (in blue). The lower panel shows the normalized PL numbers per winter season. The results show a convergence in PL numbers between the two reanalyses with time, with ERA-I's trend slightly increasing (+0.16 PL per year) and NCEP-CFS's trend slightly decreasing (-0.14 PL per year). This result may be related to changes in the observing system and to how observations are assimilated in the reanalyses over the 36-year period. For example, the drop in PL numbers in both reanalyses (but especially in the NCEP-CFS data), around the early 2000s, may be due to a change in surface wind speed assimilation, as new QuickScat scatterometer satellites were introduced at that time.

A Pearson correlation of PL numbers between both reanalyses of 0.55 was found for the Norwegian and Barents Seas. Similar results were found for the Northern hemisphere and the Sea of Japan, with Pearson correlation coefficients of respectively 0.56 and 0.58 between PL numbers in ERA-I and NCEP-CFS. The 95% confidence intervals of the Pearson correlation coefficients of the PL numbers, and the p-values,

found are statistically significant. A summary of these results can be found in Table 3.5.

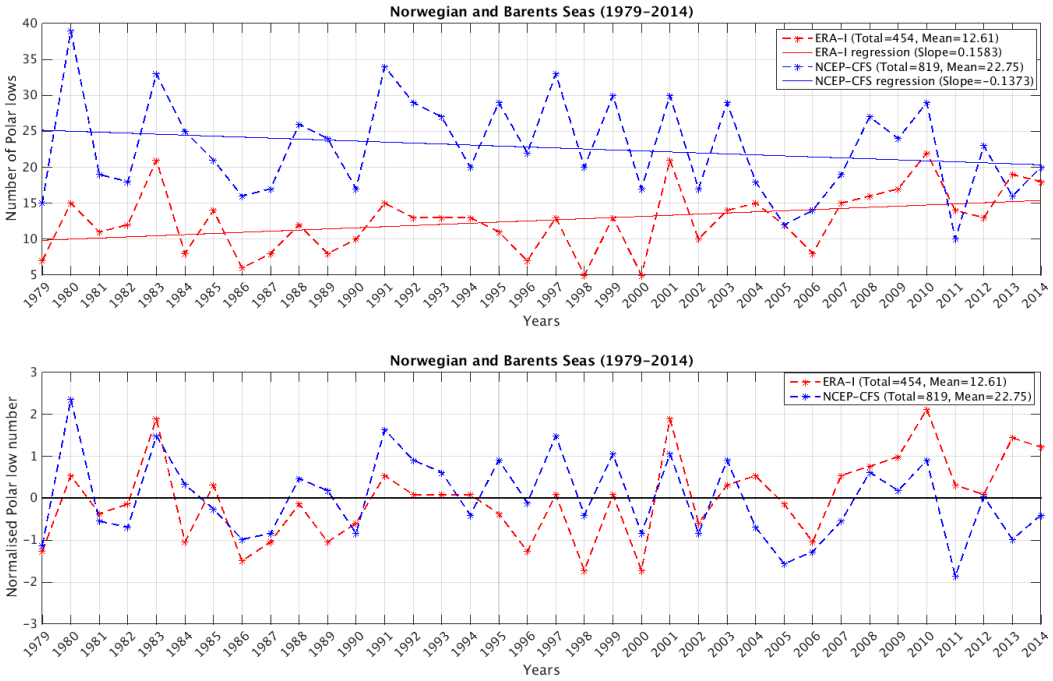

Figure 3-7: Upper panel: Number of PLs found each winter season (October to March) over the Norwegian and Barents Seas, with ERA-I (in red) and with NCEP-CFS (in blue) from 1979 to 2014. Lower panel: Same as the upper panel but with normalized PL numbers.

	N&B Seas	NH	Japan Sea
Pearson corr. coeff.	0.55	0.56	0.58
p-value	$5\text{x}10^{-4}$	$3\text{x}10^{-4}$	$2\text{x}10^{-4}$
95% conf. interval	[0.27 ; 0.74]	[0.29 ; 0.75]	[0.31 ; 0.76]

Table 3.5: Pearson correlation coefficients of PL numbers, p-values and 95% confidence intervals, of PL numbers from ERA-I and NCEP-CFS, from 1979 to 2014 for the Norwegian and Barents Seas ("N&B Seas"), the Northern hemisphere ("NH") and the Sea of Japan ("Japan Sea").

These results confirm that, even if the total numbers of PLs found are different, there is some agreement in the inter-annual variability of PL numbers in the two reanalyses examined here.

3.4.2 Comparison with the STARS observational dataset

To validate the results of PL numbers inter-annual variability found previously with both reanalyses, PL yearly numbers from ERA-I and NCEP-CFS were then compared

with the ones from the STARS observational dataset. This was done for the region of the Norwegian and Barents seas, for the STARS period (i.e. from October 2002 to March 2011).

Figure 3-8 presents the time series of the number of PLs for ERA-I (in red), NCEP-CFS (in blue) and STARS (in black) for the Norwegian and Barents Seas. The number of PLs found with ERA-I are slightly higher compared to the ones observed in STARS, though they are closer compared with NCEP-CFS. This could either be due to the identification criteria allowing more mesocyclones to be identified or, as previously mentioned, that the STARS dataset is missing some PLs. On the contrary, the NCEP-CFS PL inter-annual variability is much higher than the one found with ERA-I, but with a higher and more significant correlation coefficient (0.88) with the STARS PLs than the ERA-I ones (0.74), as can be seen in Table 3.6. If getting PL numbers relatively close to the observational numbers is important, it is even more crucial to have a consistent inter-annual variability of PL numbers in order to build a coherent climatology of PLs. Hence here, if the discrepancy between PL numbers in the NCEP-CFS and STARS datasets is large, the inter-annual variability of PL numbers can be seen as relatively consistent with each other.

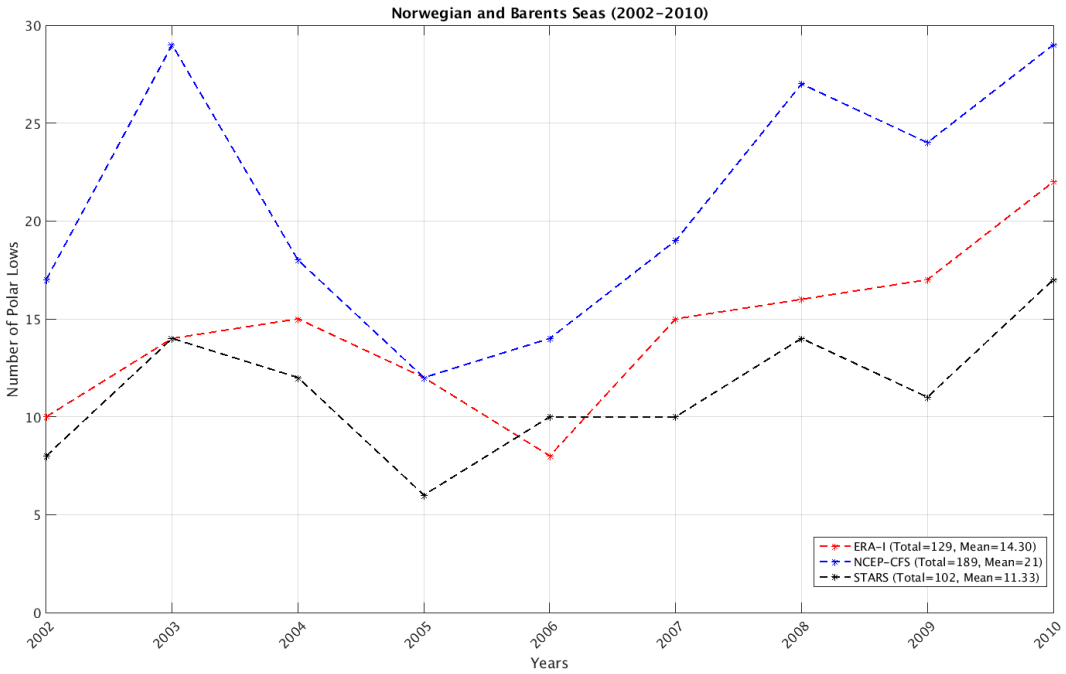

Figure 3-8: Time series of the number of PLs found over the Norwegian and Barents Seas, with the ERA-I (in red) and NCEP-CFS (in blue) reanalyses and the STARS dataset (in black), from 2002 to 2010.

This difference may be because of the higher spatial resolution of NCEP-CFS compared to ERA-I, or because of more similar representation of PL environments between NCEP-CFS and STARS compared to these of ERA-I and STARS.

	ERAI/NCEPCFS	ERAI/STARS	NCEPCFS/STARS
Corr. coeff.	0.740	0.738	0.885
p-values	$2.27\text{x}10^{-2}$	$2.33\text{x}10^{-2}$	$1.5\text{x}10^{-3}$
95% conf. interval	[0.15 ; 0.94]	[0.14 ; 0.94]	[0.54 ; 0.97]

Table 3.6: Pearson correlation coefficients of PL numbers, p-values and 95% confidence intervals of PL numbers time series from ERA-I, NCEP-CFS and the STARS, from 2002 to 2010 over the Norwegian and Barents Seas.

However, these results confirm that both ERA-I and NCEP-CFS are able to represent the inter-annual variability of the PL numbers. Overall, if a disagreement between the reanalyses is found in terms of mean number of PLs (although their range is similar to those found in the literature), more agreement between ERA-I and NCEP-CFS is seen in terms of inter-annual variability and the seasonal cycle of PL numbers, as well as on PLs characteristics and temporal and spatial representations.

3.4.3 Sensitivity of Polar low numbers to identification criteria

As previously mentioned, whether the tracking is made manually or automatically, numerous studies apply criteria and thresholds on PL characteristics (i.e. vorticity, wind speed and temperature difference), to distinguish PLs from other mesocyclone systems. As seen previously in this Chapter, the set of criteria used here to discriminate PLs from other tracked features (as defined in Zappa et al. (2014) and stated in Chapter 2 Section 2.2.2) is able to capture PL characteristics, their seasonal and inter-annual variability as well as their spatial distribution. However, some thresholds (e.g. maximum vorticity and minimum temperature difference) are continuously discussed and tested as the very definition of PLs is still blurred. Hence, in this section, the sensitivity of some of the various criteria used to identity PLs are tested.

The sensitivity of PL numbers to the three main PL criteria (i.e. the 850 hPa relative vorticity, the 10-m wind speed and the temperature difference) is explored. This is done for the three main regions of interest (the Northern hemisphere, the Norwegian and Barents Seas and the Sea of Japan), with ERA-I and NCEP-CFS. Nevertheless, results here will focus on the ERA-I numbers, over the Northern hemisphere and the Norwegian and Barents Seas, to compare them with previous studies.

Table 3.7 presents the mean numbers and inter-annual standard deviations of PLs found over the Norwegian and Barents Seas from 2002 to 2010 (from October to March),

with the observational dataset STARS (i.e. second line of Table 3.6) and ERA-I (i.e. third line of Table 3.6) with the original identification criteria[3] ("Control"). The next six lines present the means and standard deviations of PL numbers when changing one identification criterion at a time: first the maximum vorticity ("ξ") is changed to be higher than 0 s^{-1} and higher than 9×10^{-5} s^{-1}, then the maximum wind speed ("WS") is changed to be higher than 0 $m.s^{-1}$ and higher than 18 $m.s^{-1}$, and finally the minimum temperature difference ("ΔT", i.e. T500-SST) is changed to be lower than -39 K and lower than 0 K. The right column represents the Pearson correlation coefficients (r) and p-values (p) between the STARS and each ERA-I (both "control" and "changed") time series.

	Mean nb.	Std. dev.	Pearson correlation coefficient with control times series
STARS	11.33	3.35	
Control	14.33	4.10	r=0.74, p=2.3x10^{-2}
$\xi > 0\times10^{-5}$ s^{-1}	25.44	5.22	r=0.74, p=3.4x10^{-2}
$\xi > 9\times10^{-5}$ s^{-1}	2.88	2.26	r=0.66, p=5.1x10^{-2}
WS $>$ 0 $m.s^{-1}$	20.11	5.53	r=0.83, p=5.3x10^{-3}
WS $>$ 18 $m.s^{-1}$	6.78	2.82	r=0.91, p=7.0x10^{-4}
$\Delta T <$ -39 K	32.11	11.16	r=0.79, p=1.1x10^{-2}
$\Delta T <$ 0 K	68.67	16.96	r=0.67, p=4.6x10^{-2}

Table 3.7: Mean number and standard deviation of PLs number found each year, over the Norwegian and Barents Seas, with the STARS data and ERA-I, from 2002 to 2010, with the regular identification criteria and when changing one criteria at the time. ξ being the maximum vorticity higher than 0×10^{-5} s^{-1}, 6×10^{-5} s^{-1} and 9×10^{-5} s^{-1}. WS being the maximum wind speed higher than 0 $m.s^{-1}$, 15 $m.s^{-1}$ and 18 $m.s^{-1}$. ΔT being the temperature difference (ΔT=T500-SST) lower than 0 K, -43 K and -39 K. The right column represents the Pearson correlation coefficients (r) and p-values (p) between the STARS and the ERA-I time series (both "control" and "changed" time series).

Mean PL numbers range between 2.88 PLs per year with $\xi > 9\times10^{-5}$ s^{-1} to 68.67 PLs per year with $\Delta T <$ 0 K, with all Pearson correlation coefficients between the STARS data and each of the seven sets of criteria being higher than 0.66. If it does not have the highest correlation with the STARS data (i.e. correlation coefficient of 0.74), the original set of identification criteria ("Control") of ERA-I is the set which gives

[3] As a reminder, the identification criteria used in this thesis, and defined in Chapter 2 are:

- Maximum relative vorticity at 850 hPa greater than 6×10^{-5} s^{-1},
- Maximum 10-m wind speed greater than 15 $m.s^{-1}$,
- Difference between the 500 hPa and surface temperatures lower than -43 K.

the closest mean PL numbers to the ones from STARS (i.e. 14.33 PLs per year for the "Control" and 11.33 PL per year for the STARS). When relaxing the thresholds (i.e. $\xi > 0{\times}10^{-5}$ s^{-1}, WS > 0 m.s^{-1} and $\Delta T < 0$ K), the mean and standard deviation of PL numbers increase quite substantially: they double when changing the wind speed and vorticity thresholds and are multiplied by six when no maximum value is applied to the temperature difference criterion. On the other hand, when higher thresholds than the original ones are applied for the maximum wind speed and the maximum vorticity criteria, the mean numbers of PLs decrease significantly, by two or three times their original value (i.e. value from the "Control"). However, when applying a stability threshold 4 K higher than the original one (i.e. varying from -43 K to -39 K), the mean number of PLs still has a value three times higher than the observed one (i.e. 32.11 PLs per years for the set with -39 K, compared to 11.33 PLs per years with the STARS).

The same analysis was performed with the NCEP-CFS reanalysis. The mean and standard deviation values of PL numbers were found to be more sensitive (from 6.78 PLs per year with $\xi > 0{\times}10^{-5}$ s^{-1} to 92.44 PLs per year with $\Delta T < 0$ K). In addition, the correlations between the STARS data and each of the seven sets of criteria were found higher (i.e. all Pearson correlation coefficients are higher than 0.72) than the ones between the STARS and the ERA-I sets.

These results have several implications. First, the set of identification criteria as originally defined by Zappa et al. (2014) is the one with closest results to the observational dataset for ERA-I (and is also the closest for NCEP-CFS, with the case when increasing the wind speed threshold to 18 m.s^{-1}). Secondly, relaxing any criterion gives rise to annual mean numbers of PLs considerably higher than the ones with the original thresholds or the observations. Subsequently, when using a more restrictive criterion, PL numbers are too small compared to the observations. Finally, even if PL variability seems sensitive to all of the three criteria (vorticity, wind speed and temperature difference), it appears that PL numbers respond strongly to the atmospheric vertical temperature gradient. As the numbers are less sensitive to the vorticity and especially to the wind speed threshold, this indicates that PL numbers appear more constrained by the thermal part of the thermo-dynamics of the atmosphere.

This analysis demonstrates the importance of the definition of PLs and of the identification criteria used. It also confirms that the Zappa et al. (2014) thresholds are suitable criteria for PL identification. Furthermore, when investigating the sensitivity of PL numbers found in ERA-I and ASRv1 to different criteria, Stoll et al. (2018) found that the difference in the potential temperature between the sea surface and the 500hPa level, as well as the difference between the sea-level pressure at the PL centre

and its surroundings and the wind speed (poleward to the PLs) at the tropopause, are the three most effective criteria to identify PLs. Hence, this supports the idea that a threshold for the atmospheric stability is important for PL identification. However, the threshold for this criterion is still under debate.

A similar sensitivity test was performed for the whole Northern hemisphere, over the 36-year period. Table 3.8 presents the mean and standard deviation of yearly PL numbers for ERA-I, with the same sets of criteria tested, but this time for the Northern hemisphere (from 1979 to 2014). With the criteria from Zappa et al. (2014), a mean PL number of 63.55 is found, with a standard deviation of 13.86. As previously seen, when relaxing (constraining) a criterion, the annual mean numbers of PLs increase (decrease) quite considerably compared to the original value. Again, the threshold on the temperature difference is the criterion to which PL numbers are the most sensitive too, with mean numbers probably too large to be considered plausible when this is relaxed to weaker values (i.e. 190 and 506 PLs per year). As previously shown, changing the maximum wind speed has less impact on the PL numbers. As both this criterion and the stability criterion are applied at the time when the maximum vorticity is reached, this means that the detection of PLs is more sensitive to the stability of the atmosphere.

	Mean nb.	Std. dev.	Pearson correlation coefficient with control times series
Control	63.55	13.86	
$\xi > 0\times10^{-5}$ s^{-1}	132.55	30.04	r=0.82, p=0.00
$\xi > 9\times10^{-5}$ s^{-1}	16.47	4.42	r=0.65, p=0.00
WS > 0 m.s^{-1}	83.25	18.17	r=0.95, p=0.00
WS > 18 m.s^{-1}	36.89	9.34	r=0.85, p=0.00
$\Delta T <$ -39 K	190.11	31.16	r=0.75, p=0.00
$\Delta T < 0$ K	506.11	49.50	r=0.57, p=3x10^{-4}

Table 3.8: Mean number and standard deviation of PLs number found each year, over the Northern hemisphere, with ERA-I, from 1979 to 2014, with the regular identification criteria and when changing one criteria at the time. ξ being the maximum vorticity higher than 0×10^{-5} s^{-1}, 6×10^{-5} s^{-1} and 9×10^{-5} s^{-1}. WS being the maximum wind speed higher than 0 m.s^{-1}, 15 m.s^{-1} and 18 m.s^{-1}. ΔT (i.e. T500-SST) being the temperature difference lower than 0 K, -43 K and -39 K. The right column represents the Pearson correlation coefficients (r) and p-values (p) between each "changed" time series and the "control" time series (i.e. with the original criteria).

This analysis has been performed with the NCEP-CFS dataset as well and showed similar results for sensitivity, although with different mean numbers.

The specific criteria defined in Section 2.2.2 have been used in Zappa et al. (2014)

and Smirnova and Golubkin (2017) to study PLs in reanalysis datasets (ERA-I and ASRv1) and operational analysis (ECMWF operational analysis) with conclusive results, leading one to believe those criteria suitable for the identification of PLs. Relaxing these criteria thresholds leads to the number of missed PLs to decrease, but also leads to the identification of additional features which are unlikely to be PLs. Hence this analysis confirms the use, for this study, of the identification criteria as defined in Zappa et al. (2014).

3.5 Large-scale influence on the inter-annual variability of Polar low numbers

3.5.1 Large-scale environment

The previous results found for the inter-annual variability of PL numbers (Figure 3-7) have led to two new main questions: are the large fluctuations in year-to-year PL numbers associated with the variations of the large-scale environment, and if so, what are the main environmental conditions controlling the inter-annual variability of PL numbers?

To answer these questions, the differences in the environmental conditions between years with high and low PL numbers and the locations of PL maximum vorticity for ERA-I and NCEP-CFS have been studied. For this there are two different types of data: the PL tracks and the environmental data which represents a continuous spatial field. For this study, five fields are considered: the mean sea level pressure (MSLP), the sea surface temperature (SST), the sea ice fraction (SIF), the geopotential height at 500hPa (hereafter Z500) and the temperature at 500 hPa (T500). The variables were taken from ERA-I, NCEP-CFS as well as from the Met Office Hadley Center Sea Ice and Sea Surface Temperature data set (hereafter HadISST[4]). Seven years (out of 36 years) with high PL numbers and seven years with low PL numbers were chosen based on the previous time series (as seen on Figure 3-7), and used to generate composites for each of the analysed fields. These fourteen years hence represent the highest and lowest numbers of the distributions. The fourteen years (i.e. seven years with high PL numbers and seven years with low PL numbers) used for ERA-I results were chosen independently of the ones used for NCEP-CFS. However, three years with high PL numbers and three years with low PL numbers were found to be identical in both reanalyses (1983, 2001 and 2010 for the years with high PL numbers and 1986, 2000

[4] `http://www.metoffice.gov.uk/hadobs/hadisst/`

and 2006 for the years with low PLs numbers).

Figure 3-9 shows the December-January-February[5] (hereafter DJF) mean MSLP (left panel) and Z500 (right panel) difference between DJF "years"[6] with high (1983, 2001, 2008, 2009, 2010, 2013 and 2014) and low (1979, 1984, 1986, 1996, 1998, 2000 and 2006) PL numbers, for the Norwegian and Barents Seas. The figure also shows the location of the maximum vorticity of the PLs found with ERA-I, for years with high (dark green plus) and low (black diamond) PL numbers. The black box (latitude 64° - 80°N and longitude 15°W - 60°E) defines the study area as in Zappa et al. (2014). As previously mentioned, only the tracked PLs reaching their maximum vorticity within the box are considered here.

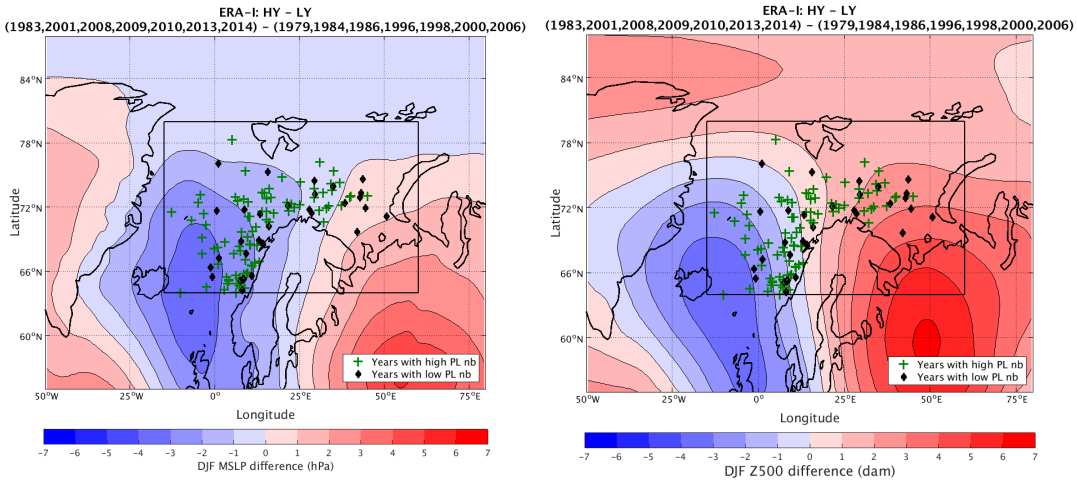

Figure 3-9: DJF mean Mean Sea Level Pressure (i.e. MSLP, left panel) and DJF mean geopotential height at 500 hPa (i.e. Z500, right panel) difference between years with high and lows PL numbers over the Norwegian and Barents Seas. The location of the maximum vorticity of PLs found with ERA-I is represented, for years with high PL numbers (dark green plus) and for years with low PL numbers (black diamond).

On the left panel it can be seen that the MSLP difference is mainly negative over the region of interest. The MSLP difference gradually increases from the Norwegian Sea to the Barents Sea, from a minimum difference of -4 hPa over the Norwegian Sea to a maximum difference of +1 hPa over the eastern part of the Barents Sea. This indicates a lower (higher) MSLP during the DJF period with high (low) numbers of PLs. The southerly flow, associated with the anomalous MSLP, may lead to an increase in warm

[5] The analysis was also performed for the October-March period, showing similar results to the DJF ones, but less contrasted.

[6] Example: the "year" 1983 refers to the mean of December 1983, January 1984 and February 1984.

and moist air flow coming from the North Atlantic. On the other hand, the Arctic northerly flow along Greenland would potentially increase the CAO events. These flows could potentially intensify the surface heat fluxes, inducing low-level convection and potentially help in the formation of PLs. The PLs occurring during years with high PL numbers (dark green plus) are not necessarily closer to the location of the warm southerly winds from the North Atlantic than the ones occurring during years with low PL numbers (black diamond). This may indicate that a low MSLP and a strong southerly flow are important for PL formation but may not be the main factor explaining the location of PLs.

On the right panel of Figure 3-9, a similar "dipole" of the Z500 difference to the one of MSLP can be observed, but with a westerly tilt compared to the composite differences in MSLP. Values of the Z500 difference between the years with high and low PL numbers range between -4 dam, over the southern part of the Norwegian Sea, and +4 dam, over the eastern part the Barents Sea. Almost all the PLs are located on the eastern flank of the "low".

Figure 3-10 shows the DJF mean SIF (left panel) and SST (right panel) difference between DJF "years" with high (1983, 2001, 2008, 2009, 2010, 2013 and 2014) and low (1979, 1984, 1986, 1996, 1998, 2000 and 2006) PL numbers, for the Norwegian and Barents Seas, with the location of the maximum vorticity of PLs found with ERA-I, for years with high (dark green plus) and low (black diamond) PL numbers.

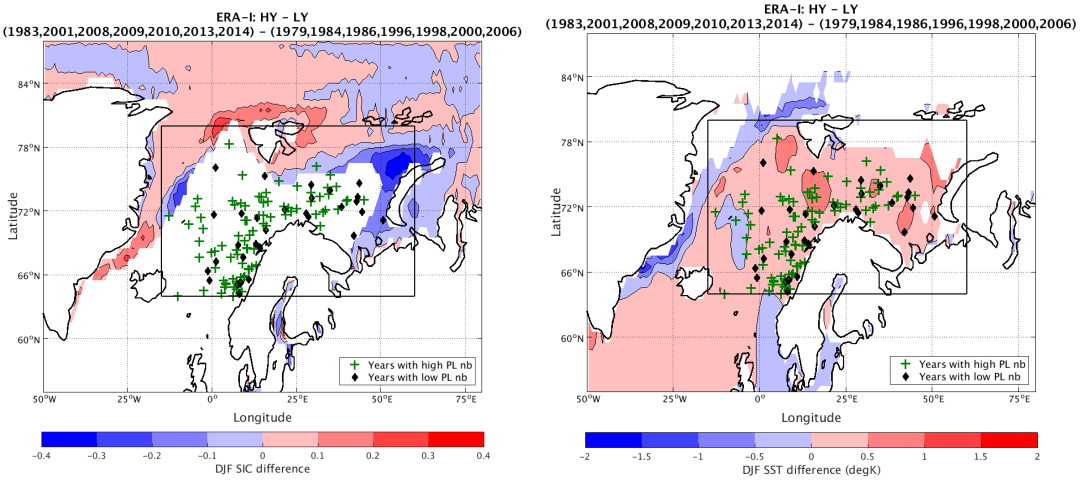

Figure 3-10: DJF mean Sea Ice Cover (i.e. SIF, left panel) and DJF mean SST (right panel) difference between years with high and low PL numbers for the Norwegian and Barents Seas. The location of the maximum vorticity of PLs found with ERA-I is represented, for years with high PLs numbers (dark green plus) and for years with low PLs numbers (black diamond).

Where there is less sea ice during years with high PL numbers (i.e. over the Barents

Sea) the surface is warmer (from +0.5 to +1 K), probably due to the receding sea ice exposing warmer SSTs. However, during the years with high PL numbers, the SST are colder along the sea ice edge between Greenland and Svalbard, but are mainly warmer elsewhere. Comparing this to the locations of PLs, there is less SIF (which increases the open ocean area where PLs can form) and warmer SSTs during the years with high PL numbers. Rojo et al. (2015) found that PL occurrences are enhanced by warm oceanic currents, which is consistent with the findings of this thesis, of having more PLs when there are warmer SSTs and less SIF over the Norwegian and Barents Seas.

Figure 3-11 shows the DJF mean difference of the stability criterion (i.e. the T500-SST field) between DJF "years" with high (1983, 2001, 2008, 2009, 2010, 2013 and 2014) and low (1979, 1984, 1986, 1996, 1998, 2000 and 2006) PL numbers, for the Norwegian and Barents Seas, with the location of the maximum vorticity of PLs found with ERA-I, for years with high (dark green plus) and low (black diamond) PL numbers.

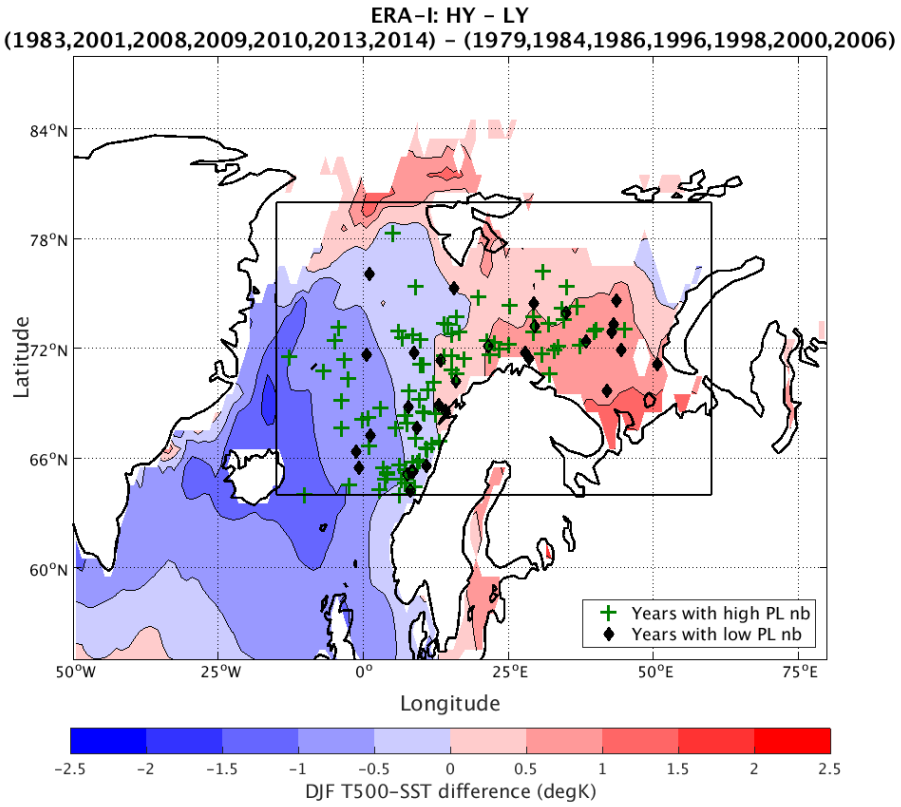

Figure 3-11: DJF mean T500-SST difference between years with high and lows PL numbers over the Norwegian and Barents Seas. The location of the maximum vorticity of PLs found with ERA-I is represented, for years with high PLs numbers (dark green plus) and for years with low PLs numbers (black diamond).

The differences between years with high and low PL numbers range from -2 K, over the Icelandic Sea (north of Iceland), and +1 K, over the eastern part of the Barents Sea. However, the differences of the T500 (not shown) seem to vary more than the SST differences at the location of the PL vorticity maxima. Hence, it appears that the T500 might be the main factor controlling the stability criterion and its relationship to PL numbers. As the SST might increase in the future and SIF might decrease (Parkinson and DiGirolamo, 2016), the interaction between PLs and the ocean is of interest for both current and future climates.

The same method has been applied for the Sea of Japan, and overall results were found similar to the ones found to be for the Norwegian and Barents Seas.

Overall, it appears that the T500, along with SIF and SST might be the most important factors for the fluctuation of PL numbers. As the T500 (and the SST to a lesser extent), is controlled by the atmospheric circulation, these results suggest that the large-scale environment plays an important role in the year-to-year variations of PL numbers.

3.5.2 Cold Air Outbreak

One synoptic feature of the atmosphere which is known to be an important condition for PL formation is the so-called Cold Air Outbreak (CAO). A Cold Air Outbreak is defined by the American Meteorological Society[7] as "the movement of a cold air mass from its source region; almost invariably applied to a vigorous equatorward thrust of cold polar air, a rapid equatorward movement of the polar front". CAOs occur throughout the year in both hemispheres (Fletcher et al., 2016), but tend to be stronger in the Northern hemisphere. As previously seen for PLs, Kolstad et al. (2009) found that atmospheric temperature variability is plays a greater role in controlling the seasonal and inter-annual variability of CAOs compared to the sea surface temperature variability. This incursion of cold Polar air southward creates sharp horizontal air temperature gradients, and when encountering warmer open water (compared to a cold sea ice) can help enhance the surface heat fluxes and trigger convection. Papritz (2017) found that the amount of heat transferred from the ocean to the atmosphere by a CAO depends strongly on the synoptic environment. In a region such as the North Atlantic, where relatively high SST are observed during winter along the North Atlantic Current, CAOs are a common feature. They can often lead to different weather phenomena, such as

[7] American Meteorological Society, cited 2012: Polar Outbreak. Glossary of Meteorology. [Available online at http://glossary.ametsoc.org/wiki/Polar_outbreak.]

Arctic fronts, roll clouds, fog, ice and PLs. Future projections predict a decline of at least 50% of CAO occurrences (Vavrus et al., 2006), especially in the Labrador Sea, and a poleward shift of the mean CAO region in the Nordic Seas (Kolstad, 2007). This possible decrease could then lead to a decrease of PL occurrences.

Hence, in this study, the link between CAO and PL occurrences is explored, in the ERA-I reanalysis.

To estimate the CAO strength, Kolstad and Bracegirdle (2008) defined the Cold Air Outbreak Indicator (hereafter CAOI). The CAOI is defined as the vertical potential temperature gradient between the surface and 700 hPa relative to the pressure.
The CAOI formula is:

$$\frac{\Delta\theta}{\Delta p} = \frac{\theta_{SKT} - \theta_{700}}{SLP - p_{700}}$$

where θ_{SKT} is the skin potential temperature, θ_{700} the potential temperature at 700 hPa, SLP the sea level pressure and p_{700} is the pressure at 700 hPa. The skin temperature corresponds to the SST over the open water and to the soil (or ice) temperature elsewhere. It has been chosen as the temperature of the ocean surface under the ice would be of no use for PL studies (as PLs mainly occur over the ocean). Furthermore, Kolstad and Bracegirdle (2008) divided the vertical temperature difference by the pressure difference to encompass the "large range of climatological sea-level pressure values (and the spatial variations of the typical height of the 700 hPa surface) that occur across different parts of the globe". Hence the CAO indicator allows the "advection of air over open ocean that is cold relative to the SST" (Kolstad and Bracegirdle, 2008) to be observed, and thus allows the rapid fluctuations of the air temperature and surface pressure over the ocean to be observed.

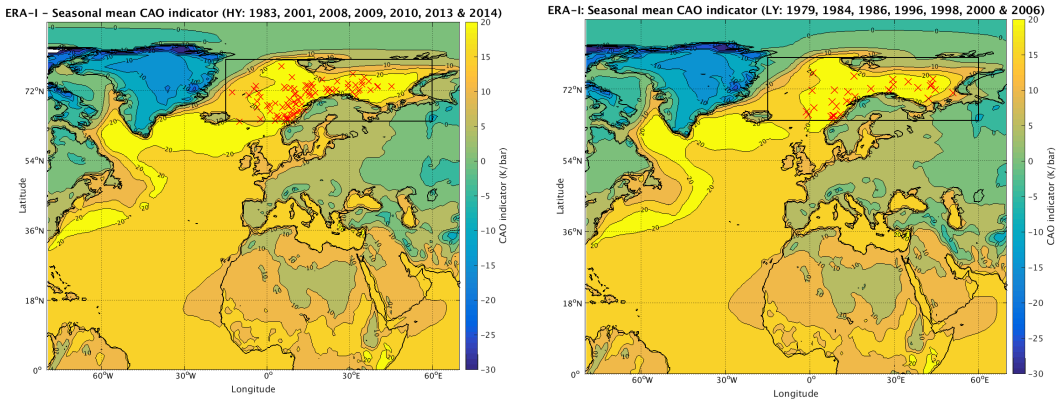

Figure 3-12: DJF mean daily CAO indicator for years with high PLs numbers (left panel) and the years with low PLs numbers (right panel) over the Norwegian and Barents Seas, with the location of the maximum vorticity of PLs found with ERA-I.

Figure 3-12 presents the ERA-I daily mean DJF CAOI for the years with high PL numbers on the left panel (1983, 2001, 2008, 2009, 2010, 2013 and 2014) and for the years with low PL numbers on the right panel (1979, 1994, 1986, 1996, 1998, 2000 and 2006, right panel) over the Norwegian and Barents Seas. The red crosses represents the location of the maximum vorticity of PLs found during these years.

Similar to the results from the IPCC AR4 models and ERA-40 reanalysis (used as an observational reference) obtained in Kolstad and Bracegirdle (2008), a relatively wide range of values of CAOI are found, ranging from -30 to +20 $K.bar^{-1}$ (-50 to +15 $K.bar^{-1}$ in Kolstad and Bracegirdle (2008)).

On the left panel, the same pattern of relatively high values (around +20 $K.bar^{-1}$) is observed along the coast of Eastern Canada, in the Labrador Sea, Denmark Strait, Norwegian Sea and Barents Sea. However the sharp gradient observed along the possible line between sea ice and open water on the east of Greenland is weaker here. The ERA-I PL maximum vorticity points (red crosses) are found along the Scandinavian coast (as in the previous plots) and mainly in the zone of maximum CAOI. This means that the surface potential temperature is larger than the potential temperature at 700 hPa, as expected. On the right panel, the same pattern is observed as on the left one but the zone of high CAOI is cut in two, along the oceanic ridge between Iceland and Scotland. The high value zone over the Norwegian and Barents Seas is also more confined than the previous one. When looking at PL maximum vorticity points, it can be noticed that all but one are within this high CAOI zone.

Comparing both panels, it can be inferred that PLs tend to occur when the CAOI is large. As high values of CAOI means a low stability, this is consistent with the fact that PLs form when strong CAO occur.

Figure 3-13 shows the difference of the 95^{th} percentile of DJF daily mean CAO indicator of ERA-I, between years with high and low PL numbers, over the Norwegian and Barents Seas. This difference in CAOs indicate that during years with high PL numbers, more intense CAOs occur over the Norwegian and Barents Seas, and less intense CAOs occur over the sea ice and land compared to those during years with low PL numbers. This suggests that intense CAOs are more likely to occur over the open-ocean during years with high PL numbers. Therefore these results support the idea that years with high PL numbers are associated with intense CAO events.

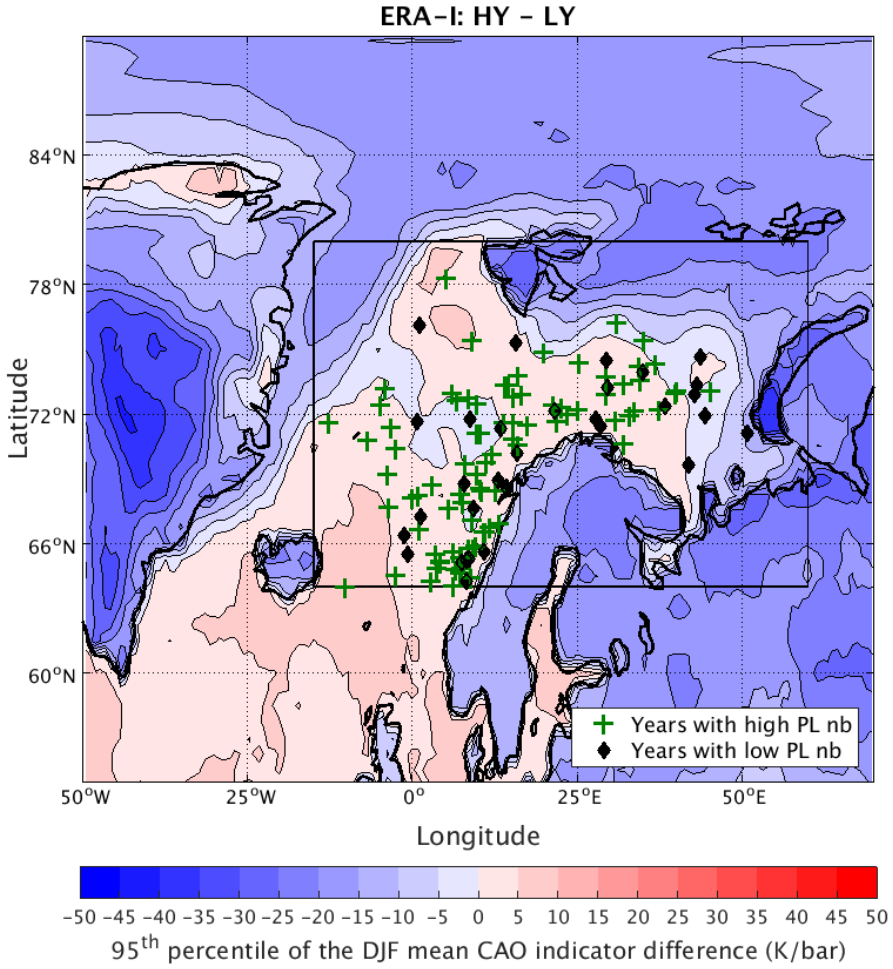

Figure 3-13: Difference between the 95th percentile of DJF daily mean CAO indicator of the years with high PL numbers (1983, 2001, 2008, 2009, 2010, 2013 and 2014) and the years with low PL numbers (1979, 1994, 1986, 1996, 1998, 2000 and 2006) for the Norwegian and Barents Seas. The green crosses and black diamonds represent the location of the maximum vorticity of PLs found with ERA-I, during the years with high and lows PL numbers respectively.

3.6 Conclusions

In this chapter, PL climatologies have been analysed with two atmospheric reanalysis datasets, ERA-I and NCEP-CFS, over the Northern hemisphere, the Norwegian and Barents Seas and the sea of Japan.

PL features were able to be found in both reanalyses. In all three regions, PL numbers are twice as large in NCEP-CFS than in ERA-I. This may be due to the difference in horizontal resolution of the two datasets.

The total and mean PL numbers found in the three regions of interest differ sig-

nificantly. The Norwegian and Barents Seas, covering around 2% of the Northern hemisphere, was found to be the region where almost 20% of total numbers of PLs of the Northern hemisphere occur. This shows the Norwegian and Barents Seas to be an important region to study PLs and to understand their dynamics and future changes. Contrary to the mean numbers, the winter inter-annual and seasonal variability of PL numbers were found to be similar in the two reanalyses, with a maximum of PL occurrences during January.

The duration of PLs found with both reanalysis datasets was found within the range of the observations and literature values, though with a mean lifetime of PLs slightly higher than found in previous studies (30 h in this study against 15 h in Rojo et al. (2015)). However, some PL tracks have a longer lifetime than the typically reported PL lifetimes. This could be related to either the PL representation in the reanalyses, the automatic tracking and identification criteria used here, or the way PLs are identified in the observation datasets. One future suggestion could be to introduce a criterion on the maximum lifetime of the track to discard the longest ones, with a maximum lifetime of 72 h for example.

The track, genesis and lysis densities of PLs have also been studied. For the Norwegian and Barents Seas, the Norwegian Sea was found to be the main area where PLs develop, pass through and decay. In particular, PLs tend to develop and decay in a small region south-east of Tromso, Norway. This area also coincides with the region of maximum CAOI here and in Kolstad and Bracegirdle (2008).

The values of vorticity, wind speed and temperature difference of PLs have been investigated to get further insights into PL characteristics during their life cycles but also when they reach their maximum intensity. Almost identical results were found with both reanalyses, and over each region. This analysis reinforces the definition of PLs as intense mesoscale cyclones and confirms that the automatic tracking and unchanged thresholds can be suitably applied to identify PLs.

The seasonal variability of PL numbers was investigated in all three regions of interest. Different ranges of values were found but all showed higher PL numbers for December, January and February. This period of high numbers is preceded by lower PL numbers during the previous months, followed by a slight decrease in March. These conclusions were supported by the observational STARS dataset for the Norwegian and Barents Seas (Noer et al., 2011; Rojo et al., 2015) and by the PL analysis of Yanase et al. (2016) for the Sea of Japan, based on the JRA-55 reanalysis.

The inter-annual variability of PL numbers was also studied (Noer et al., 2011; Yanase et al., 2016). Numbers of PLs found each year vary substantially, however mean PL numbers were found in concordance with previous studies (respectively for

ERA-I and NCEP-CFS: from 63 to 120 PLs per year for the Northern hemisphere, from 12 to 23 PLs per year for the Norwegian and Barents Seas and from 2 to 6 PLs per year for the Sea of Japan). Some agreement in the time series of PL numbers is found for the ERA-I and NCEP-CFS time series. Correlations of 0.55, 0.56 and 0.58 were obtained between ERA-I and CFS time series of PL number, for the Northern hemisphere, the Norwegian and Barents Sea and the Sea of Japan.

The sensitivity of PL numbers to the vorticity, wind speed and temperature difference criteria was investigated. Results show large variation of PL numbers when changing one criterion at a time, with often mean numbers being too low or too high compared to the observations. These results thus support the values chosen for the identification criteria used in this thesis with ERA-I and NCEP-CFS. However, a recent study from Stoll et al. (2018) also investigated some of the criteria used in this thesis with ERA-I and ASRv1 and found that the maximum 10-m wind speed might not be suitable for identifying PLs in reanalyses. Furthermore, if the temperature difference criterion has been used in different studies (Xia et al. (2012b), Zappa et al. (2014), Yanase et al. (2016) and others), it was recently found by Terpstra et al. (2016) that using this threshold might not capture forward shear PLs, which usually form in an environment with greater static stability. Hence, more work needs to be done to investigate the impact of these identification criteria on PL numbers.

For the first time, the large-scale environment influence on PL numbers was investigated with atmospheric reanalyses using an objective tracking and identification scheme. Results showed that large-scale environment strongly influences PL occurrences. High PL number years are associated with anomalously low MSLP over the Nordic Sea and northerly flow near the east Greenland coast. The northerly flow is also associated with less sea ice, warmer SST and an increase in CAO, all of which act to increase PL occurrences. The seasonal variability of PLs could also be partially explained by the sea ice cover over the Norwegian and Barents Seas, which reaches it maximum during the main winter season (DJF), leading to a higher temperature difference at the surface. This could then culminate in more favourable conditions for PL development toward the end of the winter season (i.e. February-March).

The temperature at 500hPa seems to be the most important factor for the temperature difference criterion, as its variations appear larger than the ones for the SST. As a recent study (Terpstra et al., 2016) has challenged this often used criterion (used in Xia et al. (2012b), Zappa et al. (2014), Yanase et al. (2016), etc.) by showing its application may exclude forward shear PLs, further work would be needed to assess the relevance and influence of this temperature difference threshold.

Finally, the link between CAO and PL occurrences has been studied. The CAO

Indicator (CAOI) results are relatively similar to the ones from Kolstad and Bracegirdle (2008), but with a weaker gradient along the sea ice/open water edge. Higher PL occurrences are observed in the reanalyses when the CAOI is higher (i.e. when the temperature gradient is stronger). This is consistent with the fact that CAO are one of the main crucial conditions for PL formation.

This study could have been expanded by comparing ERA-I and NCEP-CFS climatologies with the Arctic System Reanalysis version 2 (hereafter ASRv2, Bromwich et al. 2017), which has an horizontal resolution of 15 km. The representation of PLs has already been assessed in the Arctic System Reanalysis version 1 (hereafter ASRv1, 30 km) in previous studies (Tilinina et al., 2014; Bromwich et al., 2016; Smirnova and Golubkin, 2017) and has been proven to be more consistent with observations than the representation of PLs in ERA-I, NCEP-CFS and MERRA. Comparing this new version of the Polar Weather Research and Forecasting (WRF) to ERA-I and NCEP-CFS will then give a broader and more complete overview of the representation of PLs in reanalysis datasets, with a wide range of horizontal resolutions. However, since this ASR dataset is of shorter-time range (only 10 years so far compared to the 36-year data of ERA-I and NCEP-CFS), the analysis of PLs in the ASRv2 has not been performed.

Nonetheless, new results were found on the sensitivity of PLs to the identification criteria and the influence of the large-scale environment on PLs inter-annual variability. The long-term climatologies of PLs with ERA-I and NCEP-CFS are seen consistent with observations and literature.

CHAPTER 4

POLAR LOWS AND THE OCEAN CIRCULATION IN A COUPLED CLIMATE MODEL

4.1 Introduction

The interaction between synoptic-scale weather systems such as tropical and extra-tropical cyclones and their atmospheric and oceanic environments have been thoroughly studied (such as in Emanuel 1986, Rotunno and Emanuel 1987, Neiman and Shapiro 1993, Catto 2009). However, these links are less well understood for mesoscale cyclones such as PLs.

In the previous study of Condron et al. (2008), a large number (i.e. 2,500) of "polar mesocyclones" were parametrized in a global ocean-only numerical modelling simulation for a 2-year period (based on the Modular Ocean Model (MOM) from Bryan (1997)), over the North Atlantic Ocean. Their results showed an increase in surface latent and sensible heat fluxes over the ocean as well as a "dramatic increase in the cyclonic rotation of the Nordic Seas gyre by four times the average inter-annual variability". This increase in surface heat fluxes led to an increase of the Greenland Sea Deep Water (GSDW) formation by up to 20% in one month. Hence, the Condron et al. (2008) study indicates an intensification of active open ocean convection associated with the polar mesocyclones.

In a later study from Condron and Renfrew (2013), PLs were parametrized in a global 18-km resolution ocean/sea-ice circulation model (MITgcm; Marshall et al. 1997) to determine the impact of PLs on the ocean circulation. This work showed that in their model PLs have an impact on the depth, frequency and area of deep convection in the Nordic Seas, through the heat fluxes and winds associated with their passage. This

impact of PLs on the ocean surface would then lead to an increase in northward heat transport into the region, and a "southward transport of deep water through Denmark Strait". In both Condron et al. (2008) and Condron and Renfrew (2013) studies, the term Polar lows was used "to encompass all polar mesoscale cyclones" (PMCs), however noting that "in the literature the term polar low is usually reserved for more intense polar mesoscale cyclones with wind speeds > 15 m.s^{-1}" Condron and Renfrew (2013). Hence, more than 60 000 "Polar mesoscale cyclones" were parametrized over 21 years over the north-east Atlantic Ocean in Condron and Renfrew (2013). This leads to around 104 PLs per month in the Condron et al. (2008) study and 230 PLs per month in the Condron and Renfrew (2013) study over the Nordic Seas and the north-east of the North Atlantic Ocean. If these numbers (as well as the winds power spectral analysis) are in accordance with the satellite- and reanalysis-based climatologies of PMCs over the same region (Harold et al., 1999a,b; Condron et al., 2006; Michel et al., 2017), they are relatively large compared to the numbers of PLs observed or detected in reanalyses, which have less than 50 PLs per month in the Nordic Seas region. 12 and 14 PLs were found per October-March season over the Nordic Seas in Noer et al. (2011) and in Rojo et al. (2015) respectively, compared to around 40 PMCs per October-April season in Michel et al. (2017). Hence, one needs to keep in mind that PLs and PMCs, although relatively similar, might show differences in their climatologies and in the impact they have on their surroundings.

The aim of the work in this Chapter is to examine how PLs are simulated in a high resolution coupled climate model, HadGEM3-GC2 N512, and how they might impact the ocean circulation. In order to assess this impact, two 98-year FEBBRAIO simulations are used. These are fully coupled simulations with the MetOffice HadGEM3-GC2 model (Williams et al., 2015). The HadGEM3-CG2 model is a global coupled climate model with a 25 km atmospheric horizontal resolution and an ocean resolution model of 0.25°. The two model experiments (hereafter FEBBRAIO-1 and FEBBRAIO-2), are free runs (6-hourly and monthly outputs for the atmosphere and ocean data respectively) using constant 1990 present-day forcings, initialised in 2007.

First, the climatology of PLs will be studied in both FEBBRAIO runs, to examine how well the climate model represents PLs (Section 4.2). Results on the characteristics of PLs and seasonal and inter-annual variabilities of PL numbers are analysed and compared to the ones found with the reanalyses in Chapter 3. In the last part of the Chapter (Section 4.3), the interaction between PLs and the ocean will be investigated, through the surface heat fluxes and the shallow and deep water circulations.

4.2 Polar lows in the Coupled Climate Model HadGEM3-GC2

The method used to track and identify PLs is the same as the one previously utilised in Chapter 3 (from Zappa et al. 2014), and explained in Chapter 2. The tracking of PLs in both datasets for the 98 years (from October 2008 to March 2105) is first performed and then, further variables are added on to the tracks, to facilitate the identification stage using the criteria defined in Chapter 2 (Section 2.2.2).

4.2.1 Characteristics of Polar lows

The total, mean and standard deviations of PL numbers from the 98-year HadGEM3-GC2 model runs and the reanalyses are shown in Table 4.1, for the three regions of interest (i.e. Northern hemisphere, Norwegian and Barents Seas and Sea of Japan).

When looking at the FEBBRAIO results, it can be seen that both datasets have similar PL numbers and means for each of the studied regions. This tends to support the fact that both FEBBRAIO ensemble members are consistent with each other (i.e. no large discrepancy between their values). The standard deviations of PL numbers found in FEBBRAIO-2 are slightly higher than those of FEBBRAIO-1 (except for the sea of Japan). This indicates that PL numbers from FEBBRAIO-2 may encounter more variations around the means, probably due to natural variability.

		FEBBRAIO-1	FEBBRAIO-2	ERA-I	NCEP-CFS
NH	Mean	127	121	65.55	120.81
	Std dev.	19.2	30.5	13.86	18.32
	Total	12454	11887	2288	4349
N&B Seas	Mean	26.7	25.19	12.61	23.31
	Std dev.	8.51	9.25	4.43	6.15
	Total	2613	2469	454	839
Sea of J.	Mean	7.64	6.73	2.86	6.42
	Std dev.	3.14	3.14	2.14	3.71
	Total	749	660	103	231

Table 4.1: Statistics of PL numbers found, for 98 years (2008-2105), with FEBBRAIO datasets from the HadGEM3-GC2 model compared to previous results from ERA-I and NCEP-CFS reanalyses for 36 years (1979-2014), for the Northern hemisphere (NH), the Norwegian and Barents Seas (N&B Seas) and the Sea of Japan (Sea of J.).

Table 4.1 also shows summary statistics of PL numbers from the 36-years ERA-I and NCEP-CFS reanalysis data. This allows the mean and standard deviations of the HadGEM3-GC2 PL numbers to be compared to the ones from the previous

climatologies from Chapter 3. For all regions, mean and standard deviations of both FEBBRAIO runs are slightly higher than the ones from NCEP-CFS, and almost twice as large as the ones from ERA-I. McInnes et al. (2011) suggested that the horizontal resolution of the model chosen may be one of the factors (along with the synoptic situation) influencing the numbers and representation of PLs. Hence, as the HadGEM3-CG2 model has a higher horizontal resolution than NCEP-CFS (respectively 25 km and 38 km), PL numbers may be expected to be higher than in NCEP-CFS and greater than in ERA-I (whose horizontal resolution is 79 km). The analysis shows that the representation of PLs in HadGEM3-GC2 N512 is in reasonable agreement with those from the NCEP-CFS reanalysis (although numbers are somewhat larger than than those found in ERA-I).

A two-sample t-test for comparing two means is used to test whether the difference in mean values between FEBBRAIO and the reanalyses (from Table 4.1) are statistically significant. Results can be found in Table 4.2. As expected all values from the tests are significantly different at the 5% level when comparing ERA-I and both model ensembles (since there is a larger discrepancy between PL numbers between ERA-I and FEBBRAIO, than NCEP-CFS and FEBBRAIO). However, for all three regions, FEBBRAIO runs are not significantly different from NCEP-CFS at the 5% level, with the only exception of the Norwegian and Barents Seas region for the FEBBRAIO-1. Statistically this means that the model populations correspond more to those of NCEP-CFS than those of ERA-I. This can be partly explained by the similar horizontal resolutions between NCEP-CFS and HadGEM3-CG2. It may also be explained by other hypotheses such as the assimilation of ocean data in both previous datasets (as NCEP-CFS atmospheric component is coupled with an ocean model, whereas ERA-I is not) or similar representation of the atmospheric environment.

		NH		N&B Seas		Sea of Japan	
		ERA-I	NCEP-CFS	ERA-I	NCEP-CFS	ERA-I	NCEP-CFS
FEBBRAIO-1	t-stat	21.067	1.686	12.399	2.139	10.022	1.907
	p-value	0.000*	0.094	0.000*	0.034	0.000*	0.059
FEBBRAIO-2	t-stat	15.003	0.112	10.568	1.307	8.110	0.494
	p-value	0.000*	0.911*	0.000*	0.195*	0.000*	0.694

Table 4.2: Two-sample t-tests comparing two means of PL numbers found per year, with the 98-year FEBBRAIO datasets (FEBBRAIO-1 and FEBBRAIO-2) from the HadGEM3-GC2 model and previous results from the 36-year ERA-I and NCEP-CFS reanalyses, for the Northern hemisphere (NH), the Norwegian and Barents Seas (N&B Seas) and the Sea of Japan (Sea of J.). The stars (*) indicate that the F-test of equality of variances is rejected and the Welch-Satterthwaite approximation (or Welch's t-test) is used to compute the degrees of freedom for the t-test.

The sensitivity of the number of identified PLs in HadGEM3-GC2 N512 to the

identification criteria (vorticity, wind speed and temperature difference thresholds), previously investigated with the reanalyses (see Chapter 3, Section 3.4.3), was also performed with the model datasets (not shown). Similar results were obtained with the model datasets. When changing one identification criterion at a time, a large difference in the year-to-year PL numbers is found. Furthermore a greater sensitivity to the temperature difference criterion was found, confirming that the vertical temperature difference is one of the main variables that PL numbers are sensitive to.

Similarly to the reanalyses, the spatial distribution of PLs in the model was examined, through statistics of their track, genesis and lysis densities (Hodges, 1995).

Figure 4-1 presents the track density as the number of PLs per month per unit area (a unit area is equivalent to a 5° spherical cap, i.e. around 10^6 km^2), from the 98-year FEBBRAIO simulations (left panel) and from the 36-year NCEP-CFS reanalysis (right panel), over the Norwegian and Barents Seas. As previously mentioned, only PLs which reach their maximum vorticity within the box are considered. For visualisation purposes, the areas where the track density is below 0.1 have been set to white. For the HadGEM3-GC2 model (left panel), the maximum track density over this region is found to be north-west of Tromso (Norway), with a value of around 4.1 track per month per unit area. This area represents the region where the largest number of PLs occur. The density then decreases, relatively evenly in all directions, in the rest of the region.

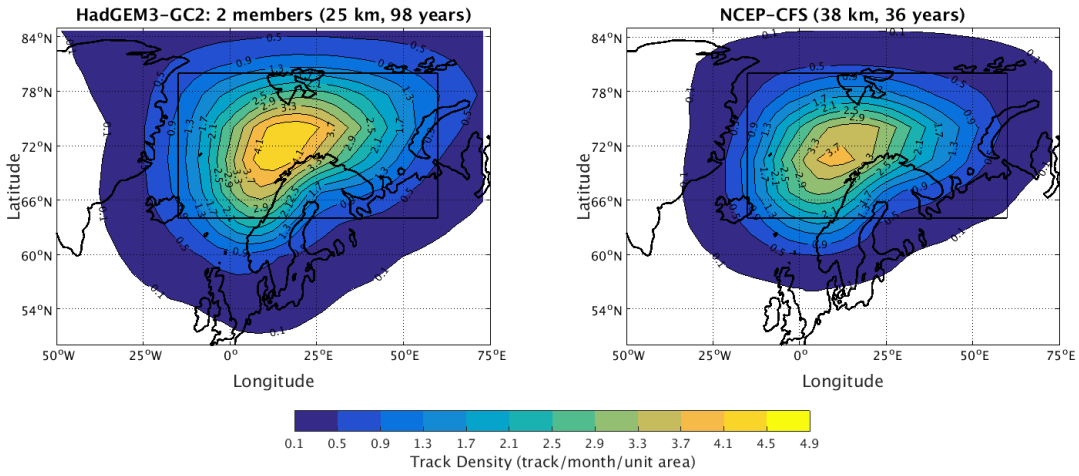

Figure 4-1: Track density (track.month^{-1}.unit area^{-1}) of PLs found over the Norwegian and Barents Seas, with the 98-year FEBBRAIO data (two members) from the HadGEM3-CG2 model (left panel) and with the 36-year NCEP-CFS reanalysis data (right panel).

The track density of PLs identified in the model is quite similar to the track densities

from the reanalyses datasets (shown in Chapter 3 for ERA-I track density and Figure 4-1 right panel for NCEP-CFS track density) in term of the overall pattern, especially when compared with NCEP-CFS. This similarity of track density patterns may be explained, not only by PLs climatology, but also by the winter sea ice distribution as well as the domain size being relatively small. As a reminder, this Norwegian and Barents Seas domain as been chosen this way in order to robustly compare the results of PL climatologies from this thesis with those of Zappa et al. 2014 (see Section 2.2.2 of Chapter 2). If the track density patterns are similar, the maximum values from the model are greater than the ones from the reanalyses, which are of 2.1 and 3.7 tracks per month per unit area for ERA-I and NCEP-CFS respectively. This is in agreement with the fact that mean PL numbers from the model are quite similar to the ones of NCEP-CFS (as seen in Table 4.1). As the differences between the HadGEM3-GC2 model and the reanalyses are relatively small, one can be confident to use this model to study PLs activity.

Tilinina et al. (2014) also studied the track density of PLs over the Northern hemisphere. In this study between 15 and 18 PLs tracks per year per 155 000 km^2 were found over the Norwegian and Barents Seas with the ASRv1 (30km-resolution Arctic System Reanalysis version 1, Bromwich et al. 2016) for a 11-year period (2000-2010). Even though obtaining different values (with different method and model), this study presents a similar pattern of track density as the one from HadGEM3-GC2.

These results support the fact that the HadGEM3-CG2 model is able to represent the PL spatial distribution.

The same analysis was also performed for the genesis and lysis density of PLs found, over the Norwegian and Barents Seas, with the model.

Figure 4-2 shows the genesis density from the 98-year FEBBRAIO simulations (left panel) and from the 36-year NCEP-CFS reanalysis (right panel), over the Norwegian and Barents Seas. The genesis density has its maximum over a similar but easterly shifted region than the region of maximum track density (i.e. between Norway and Svalbard). The maximum value for the genesis in the region is 1.9 tracks per month per unit area and decreases homogeneously around it to a minimum of 0.3 track per month per unit area. These genesis density patterns are analogous to the track densities seen previously, meaning that this area between Norway and Svalbard is an important region for the growth of PLs and that the Norwegian Sea is an important region for the path of PLs that occur over the Norwegian and Barents Seas. Comparing these results to the ones from the NCEP-CFS (right panel), similar patterns are found but lower maximum values are found with the NCEP-CFS reanalysis (max of 1.7 tracks

per month per unit area).

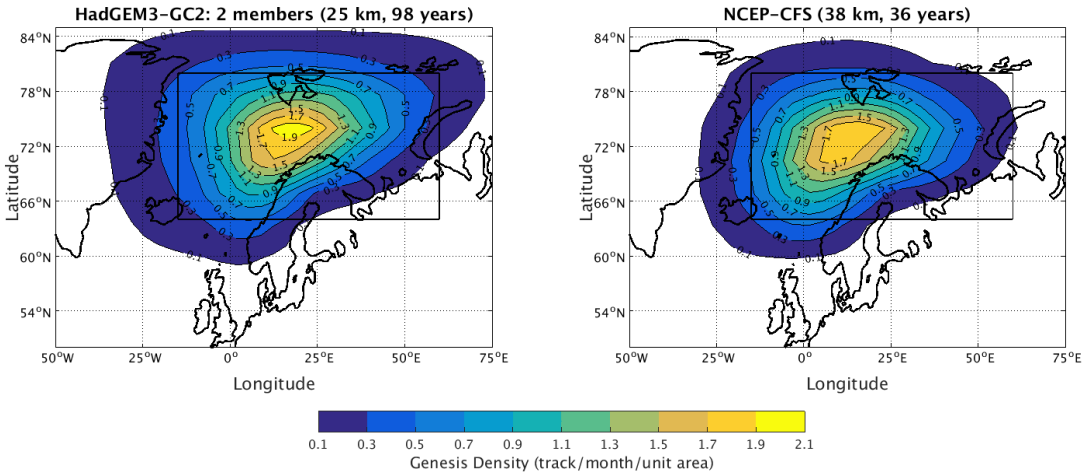

Figure 4-2: Genesis density of PLs found over the Norwegian and Barents Seas, with the 98-year FEBBRAIO data (two members) from the HadGEM3-CG2 model (left panel) and with the 36-year NCEP-CFS reanalysis data (right panel).

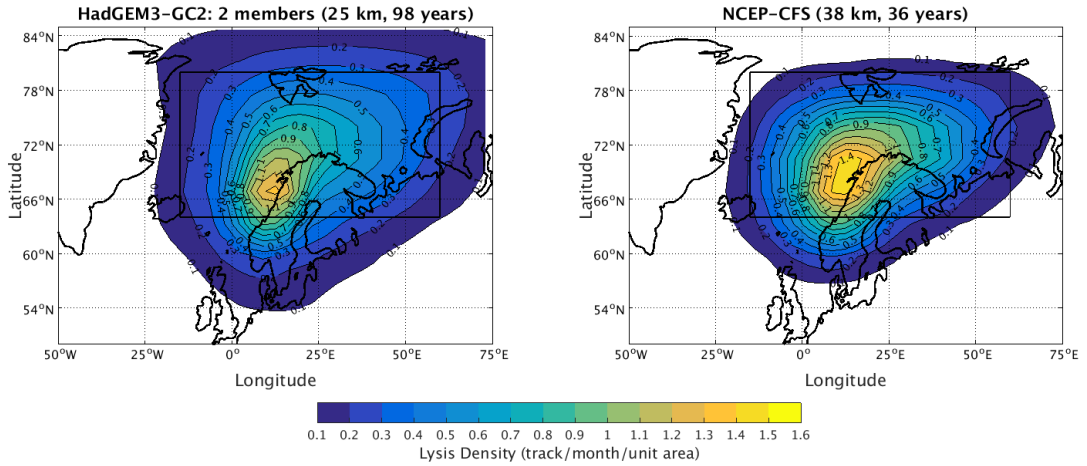

Figure 4-3: Lysis density of PLs found over the Norwegian and Barents Seas, with the 98-year FEBBRAIO data (two members) from the HadGEM3-CG2 model (left panel) and with the 36-year NCEP-CFS reanalysis data (right panel).

Figure 4-3 shows the lysis density from the 98-year FEBBRAIO simulations (left panel) and from the 36-year NCEP-CFS reanalysis (right panel), over the Norwegian and Barents Seas. The lysis density structure is different to the previous track and genesis densities. The maximum lysis density of HadGEM3-GC2 lies in a small location south of Lofoten, Norway. The maximum value of 1.3 tracks per month per unit area

is observed at this point and decays rapidly in the box to reach a minimum of about 0.2 track per month unit area around the edge of the region's box. Lysis density structures show similarities with the ones from the NCEP-CFS, although the region of the maximum lysis density of the reanalysis (which is 1.4 tracks per month per unit area) is larger.

These density results from HadGEM3-GC2 imply that PLs tend to develop, grow and decay mainly over the Norwegian Sea, along the northern coasts of Norway.

4.2.2 Seasonal variability of Polar low numbers

The seasonal variability of PL numbers in the HadGEM3-GC2 model has been investigated.

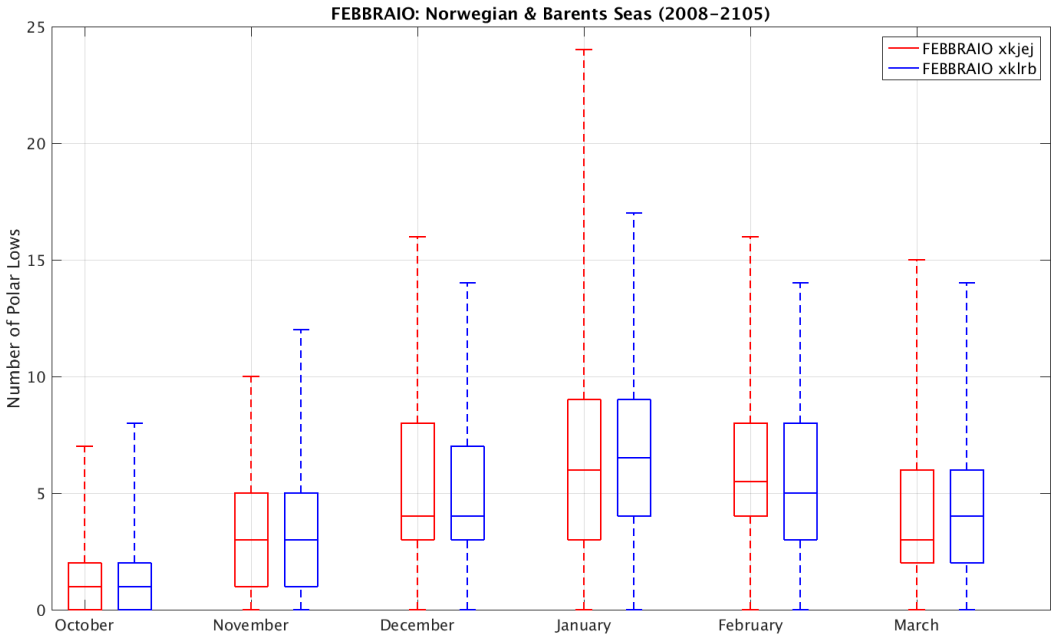

Figure 4-4: Seasonal cycle of PL numbers found over the Norwegian and Barents Seas with the two 98-year FEBBRAIO datasets from the HadGEM3-GC2 climate model.

Figure 4-4 shows for the two 98-year model datasets (FEBBRAIO-1 in red and FEBBRAIO-2 in blue), PL numbers found in each month, from October to March, for the Norwegian and Barents Seas. The first thing to notice is that both HadGEM3-GC2 distributions seem to evolve in a very similar way, with values of mean and quantiles agreeing closely. The same pattern is observed in both samples: PL numbers increase slowly from October (means around 1 PL per month) to peak in January (means around 6 PLs per month) and decrease until March (means around 3.5 PLs per month). This

indicates that PLs within HadGEM3-GC2 occur more often during the winter (i.e. DJF period). However, this period is also the period with the greatest variability in PL numbers (i.e. values between 0 and 24 PLs per month). Nonetheless, these numbers and patterns coincide with the seasonal variability of PL numbers found in previous studies, for the same region, whether they are from observational datasets (Noer et al., 2011; Rojo et al., 2015; Smirnova et al., 2015) or reanalysis products (Tilinina et al., 2014; Zappa et al., 2014; Smirnova and Golubkin, 2017).

The results from the climate model HadGEM3-GC2 have also been compared with those from the reanalysis datasets, presented in Chapter 3.

Figure 4-5 shows for the Norwegian and Barents Seas, the seasonal variability of PL numbers for the FEBBRAIO and NCEP-CFS datasets. The seasonality is comparable between the model and reanalysis, with a slow increase of PL numbers, a peak and then a decrease of these numbers. The month with the highest mean number is January in both cases, and it is also the month with the largest spread between the minimum and maximum numbers. Furthermore, lower numbers are found with the reanalyses for the early period, October to December, compared to the ones of HadGEM3-CG2.

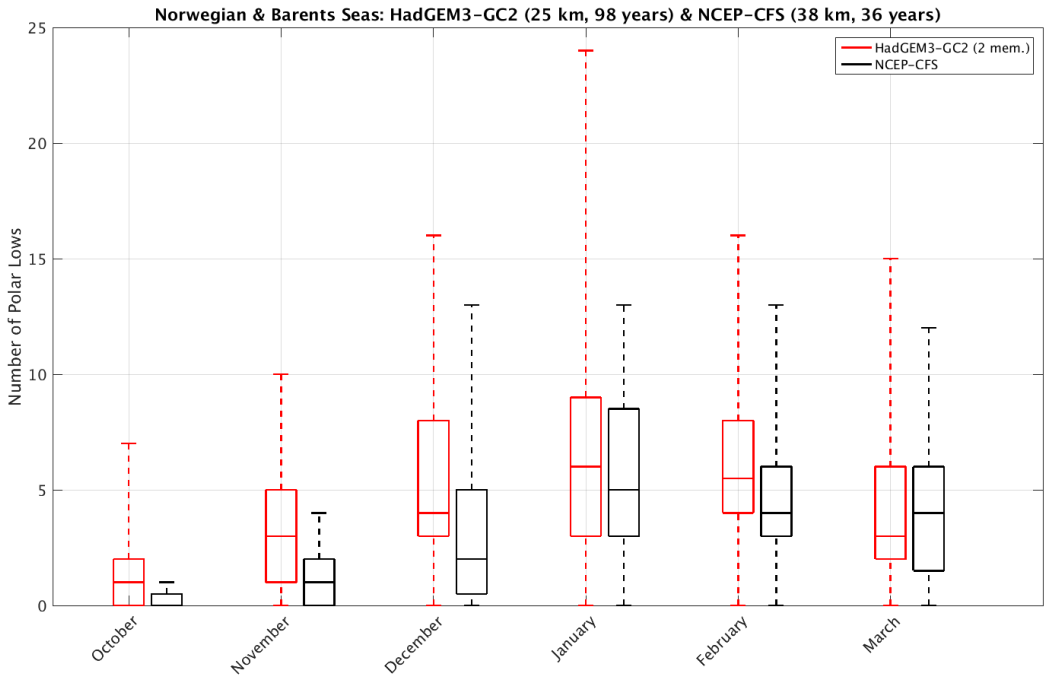

Figure 4-5: Seasonal numbers of PLs found, over the Norwegian and Barents Seas, with the 98-year FEBBRAIO datasets (in red) from the HADGEM3-GC2 model and the 36-year NCEP-CFS reanalysis data (in black).

It can also be seen that there are larger spreads of numbers (of the upper 75%-100%

of the distributions) in the model data compared to the reanalysis, for each month and especially for January. This may be due to the fact that the HadGEM3-GC2 encompasses a longer period than the one of NCEP-CFS (i.e. 98 years for the climate model and 36 years for the reanalysis), and thus has a larger range of PL monthly numbers. Nonetheless, these differences are not inconsistent with the FEBBRAIO simulations being able to represent the seasonal variability of PL numbers.

To fully compare results from the FEBBRAIO simulations and the reanalysis, the seasonality of PL numbers was also investigated for the Northern hemisphere and the Sea of Japan (not shown). Although the numbers of PLs found over the Sea of Japan are relatively low, a similar seasonal variability of PLs numbers to the one for the Norwegian and Barents Seas are found for the Northern Hemisphere and the Sea of Japan (with an slow increase of PL numbers from October to a maximum in January and a decrease until March).

4.2.3 Inter-annual variability of Polar low numbers

The inter-annual variability of PL numbers in the coupled climate model HadGEM3-GC2 has also been explored.

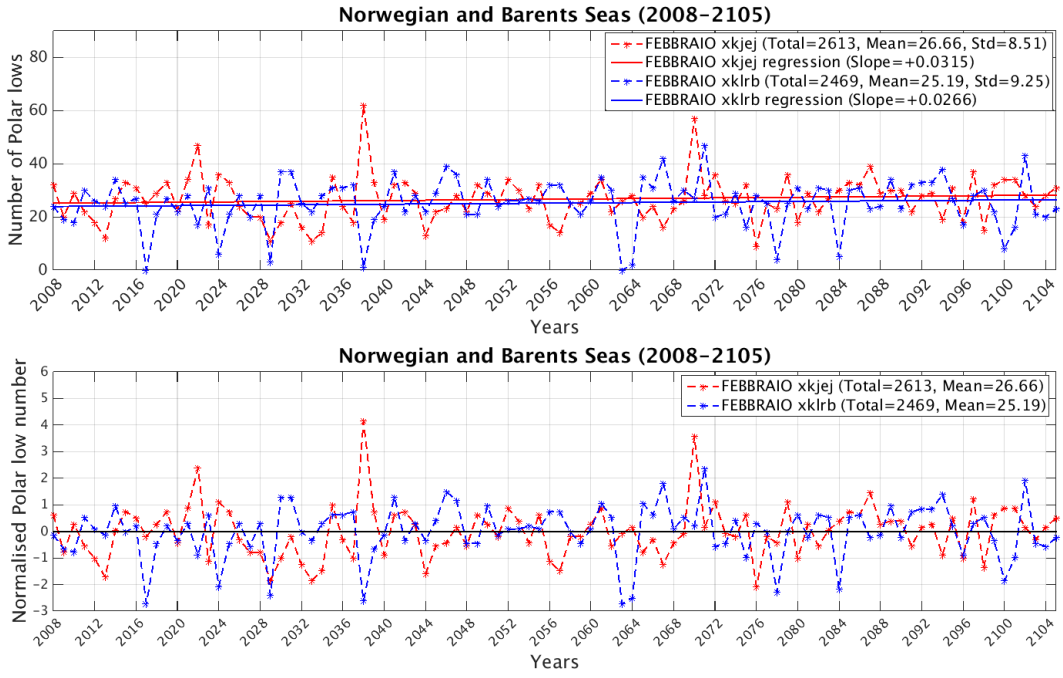

Figure 4-6: Time series of the numbers (upper panel) and normalised numbers (lower panel) of PLs found, over the Norwegian and Barents Seas, with the two 98-year FEBBRAIO datasets.

The upper panel of Figure 4-6 shows a time series of PL numbers, over the Norwegian and Barents Seas, for both model runs (FEBBRAIO-1 in red and FEBBRAIO-2 in blue). The linear trend of both populations is also represented. The lower panel of Figure 4-6 presents the normalized PL numbers of both datasets. The distributions have a range between 0 and 40 PLs per year, with three years with higher numbers. Since the FEBBRAIO simulations are independent and free running the time series of PL numbers are not expected to be correlated (a Pearson correlation of -0.21 is found, with a p-value of 0.034). A very small positive trend of PL numbers appears, with an increase of +0.031 and +0.026 PL per year, for FEBBRAIO-1 and FEBBRAIO-2 respectively. As these variations are relatively small, no clear trend can be deduced.

The same analysis was done for the Northern hemisphere and the Sea of Japan, for both model experiments (not shown). Slightly positive trends were also found with slopes of +0.11 and +0.03, for FEBBRAIO-1 and FEBBRAIO-2 respectively, for the Northern hemisphere. The trends for the Sea of Japan were also found to be positive although very small (+0.0054 and +0.0003 for FEBBRAIO-1 and FEBBRAIO-2 respectively).

In summary, both of the FEBBRAIO runs allow the assessment of PLs representation in a high-resolution fully coupled climate model using present day forcings for a long period of time. The model results show similarities with those from the reanalyses and observations, in term of PL characteristics, for the three regions of interest. As expected, the model results are more alike to those from the NCEP-CFS reanalysis results (compared to the ones from ERA-I) which may reflect that they have similar horizontal resolutions and also possibly because the NCEP-CFS reanalysis has its atmospheric scheme coupled with an ocean component.

The spatial distributions of PLs in the model appear to be similar to the reanalyses ones, with a region of maximum PL tracks along the northern coast of Norway and between the North of Norway and Svalbard. This region has many of the main factors associated with PLs formation (such as CAOs (Kolstad and Bracegirdle, 2008) and warm ocean currents at the surface (Saetra et al., 2008)). The PL spatial distribution found with the climate model seems to be consistent with reanalyses.

The seasonal variability of PL numbers in the model shows a slightly shifted maxima (from December to January) compared to the observations and reanalyses, but is in overall good agreement, in term of numbers, compared to the NCEP-CFS results and the model monthly variations of these numbers are also relatively similar to the reanalyses ones. No general pattern or trends were found in the inter-annual variability of PL numbers in the model. However, mean and standard deviations of PL numbers

per year were found to be really close to the NCEP-CFS ones, and almost double the ERA-I ones.

Overall, the HadGEM3-GC2 coupled climate model showed a satisfactory representation of PLs, in the present-day situation, compared to the reanalysis climatologies.

4.3 Polar lows and ocean circulation in HadGEM3-CG2

PLs are known to be associated with large oceanic sensible and latent heat fluxes (Shapiro et al. 1987, Fore et al. 2012, Yanase et al. 2016). If the link between PLs and the ocean surface has already been seen in previous studies based on observations (Shapiro et al., 1987) and reanalyses (Papritz et al., 2015), there are still uncertainties in how PLs may affect the ocean circulation and fully coupled models may help to understand this interaction. By extracting sufficient ocean surface heat, PLs might locally cool the ocean surface, which will hence become denser. These denser waters could then sink into the less dense waters below it. This could destabilise the water column, and affect the depth and frequency of the deep water formation and convection. If this phenomenon happens over the Nordic Seas, it could also potentially influence the North Atlantic Ocean circulation. However, this possible link between PLs and the shallow and deep ocean circulations is still not fully understood.

The purpose of this chapter is to try to qualify and quantify, in a high resolution coupled climate model, the possible interaction of PLs with the ocean. This link will be investigated through the correlation of PL numbers and surface heat fluxes, as well as with the shallow and deep water circulations, through the correlation of PL numbers and the ocean density.

To investigate the interaction between PLs and the full ocean circulation, a new region of study is defined where deep water formation is known to take place over the North Atlantic Ocean and Nordics Seas.

As previously mentioned in Chapter 1, the warm and salty waters from the Norwegian Atlantic Current (north-east branch of the North Atlantic Current), becomes colder due to large wintertime heat losses while moving poleward. By becoming colder and thus denser, the water masses sink to depth and overflow equatorward through the East Greenland Current (Marshall et al., 1997). These water masses are therefore modified by deep thermal convection (i.e. convection driven by the heat loss) and haline convection (i.e. convection driven by the salt content of the water and by the freezing at the sea surface, see Rudels (1990) and Schmittner et al. (2013)). These deep waters in the Nordic Seas mainly form within the Greenland Sea.

However, it has also been shown that another important place for intermediate and deep convection over the Nordic Seas takes place around the Iceland Sea gyre, north of Iceland Mauritzen (1996). The warm North Icelandic Irminger Current running east and northward in the Denmark Strait, cools down when encounters the Iceland Sea gyre. Triggering important ocean heat loss at the surface, the water masses cool and sink (Våge et al., 2013), leading to a "subsequent circulation of the waters that feed the dense overflows across the Greenland-Scotland Ridge into the North Atlantic" Mauritzen (1996). These currents are therefore supplying the NADW. This supply of dense waters, which has been seen to decrease over the past years (Våge et al., 2015), could as well affects the returning branch of the AMOC, and thus the entire circulation. Therefore, if PLs have a strong impact on the ocean circulation, they may also affect the deep water formation over the Nordic Seas, as seen in Condron et al. (2008) and Condron and Renfrew (2013).

It has to be noted that, if PLs mainly occur during an extended winter season, from October to March (Rasmussen and Turner, 2003), the formation of the deep waters within the region of the Nordic Seas is usually during spring (from March to May). Hence, if PLs are to have an impact on the deep water formation over the Nordic Seas, this effect must be long lasting and strong enough to affect the ocean during this period from March to April (when the sea ice starts to melt and cool the ocean surface). However, since PLs mainly occur during the extended winter, they should also affect the ocean during this period. Therefore for this study, the possible impact of PLs on the ocean circulation is assessed for the period when PLs activity is the most intense (i.e. from October to March). If their effect on the ocean is lagged compared to their time of appearance, then a stronger impact of PLs may be seen during the end of the extended winter period.

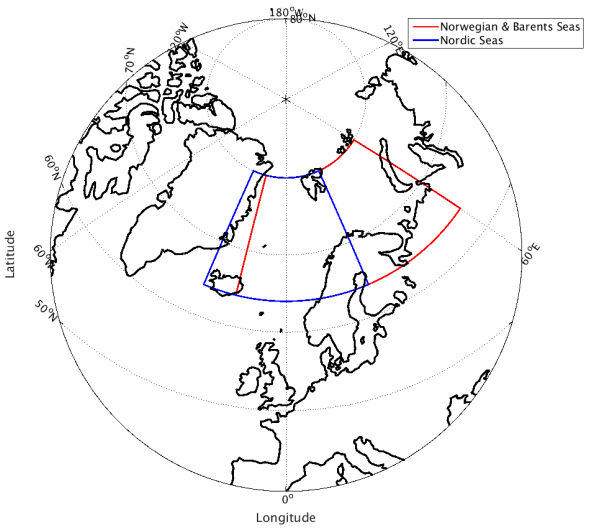

Figure 4-7: Map of the Norwegian and Barents Seas region (in red) as previously defined, and the Nordic Seas region (in blue) newly defined.

In order to focus on PLs interaction with the ocean where the deep water formation occur, a new domain is established. This new region, hereafter called the Nordic Seas, is defined with longitudes from 25°W to 25°E and latitudes from 64°N to 80°N, as

presented in Figure 4-7 (blue box). As for the other regions studied, only the tracked PLs that reach their maximum vorticity intensity within the box are considered here.

Firstly, the representation of PLs over the new region has been studied (not shown). Similar characteristics as for the Norwegian and Barents Seas region are found for the Nordic Seas region, with a yearly mean PL number of 19.8 and 18.9 PLs (and standard deviations of 6.5 and 7.7 PLs per month) for FEBBRAIO-1 and FEBBRAIO-2 respectively, with almost no trend (rate of +0.016 PL per month). These numbers are relatively similar to those found with NCEP-CFS, as the reanalysis shows a mean PL numbers of 18.94 PLs per month and a standard deviation of 8.53 for the same region (when ERA-I shows a mean of 11.08 PLs per month with a standard deviation of 4.57). When looking at PL spatial distributions, similar results to the ones for the Norwegian and Barents Seas were found. The maximum track density is found to be over the North of the Dumshaf Abyssal Plain (i.e. Lat. 68°N, Lon. 5°E). The maximum genesis density is located between the north of Norway and the Svalbard Islands, and the maximum of the lysis density is found in the south of the Norwegian Sea along the coast of Norway. These results appear consistent with previous climatologies, which provide confidence for the results to come.

4.3.1 Relationship between Polar lows and surface heat fluxes

The investigation on the impact of PLs on the ocean circulation begins by examining the relationship between the PLs and the surface heat fluxes.

The time series of both latent and sensible heat fluxes, averaged over the whole Nordic Seas region, was first investigated (not shown). The mean of the latent fluxes was found to be 51.67 and 51.73 $W.m^{-2}$ (with standard deviations of 3.45 and 3.03) for FEBBRAIO-1 and FEBBRAIO-2 respectively, and the mean of the sensible fluxes was found to be 33.53 and 34.25 $W.m^{-2}$ (with standard deviations of 4.55 and 3.71) for FEBBRAIO-1 and FEBBRAIO-2 respectively. Results also showed small positive and negative trends which are not significant for the latent and sensible heat fluxes respectively.

In order to investigate if PLs have an influence on the ocean surface through sensible and latent heat fluxes, the relationship between the numbers of PLs per year and the heat fluxes is studied in the HadGEM3-GC2 model.

Figure 4-8 shows a scatter plot of winter mean surface heat (latent + sensible) fluxes (time and area averaged over the Nordic Seas) against winter PL numbers found with the 98-year FEBBRAIO data (ensemble mean of both simulations). During winter PL numbers ranging from 5 to 32, the values of the surface heat fluxes are found to be

between 150 and 191 W.m^{-2} for both simulations. A positive trend is clearly seen, which is consistent with a positive impact of PLs on the surface heat fluxes: the years with high numbers of PLs are generally also the years with the highest heat fluxes. Indeed, the linear regression of heat fluxes against PL numbers gives a coefficient of +0.74 W.m^{-2} per PL (p-value: 9.1x10^{-5}). Estimated latent and sensible heat fluxes in the vicinity of PL occurrence have been found to be around 200 to 500 W.m^{-2} each (Shapiro et al., 1987). In a more recent aircraft campaign (Sergeev et al., 2017), the heat fluxes associated with the passage of a PL exceeded 500 W.m^{-2}, and the sensible heat fluxes (350 W.m^{-2}) were found to be twice higher than the latent heat fluxes. These values are largely different that what is found in this thesis. However, as the data here are time and area averaged, the relationship between PLs and the surface heat fluxes can be expected to be weaker than found in instantaneous data from individual events.

Hence, a positive relationship is seen between the surface heat fluxes and PL numbers in HadGEM3-GC2, as previously found in Shapiro et al. (1987), Condron and Renfrew (2013) and Papritz et al. (2015). However, a large spread of heat flux values is also observed. This indicates that although a relationship exists between PL numbers and the surface heat fluxes, this relationship might be relatively weak.

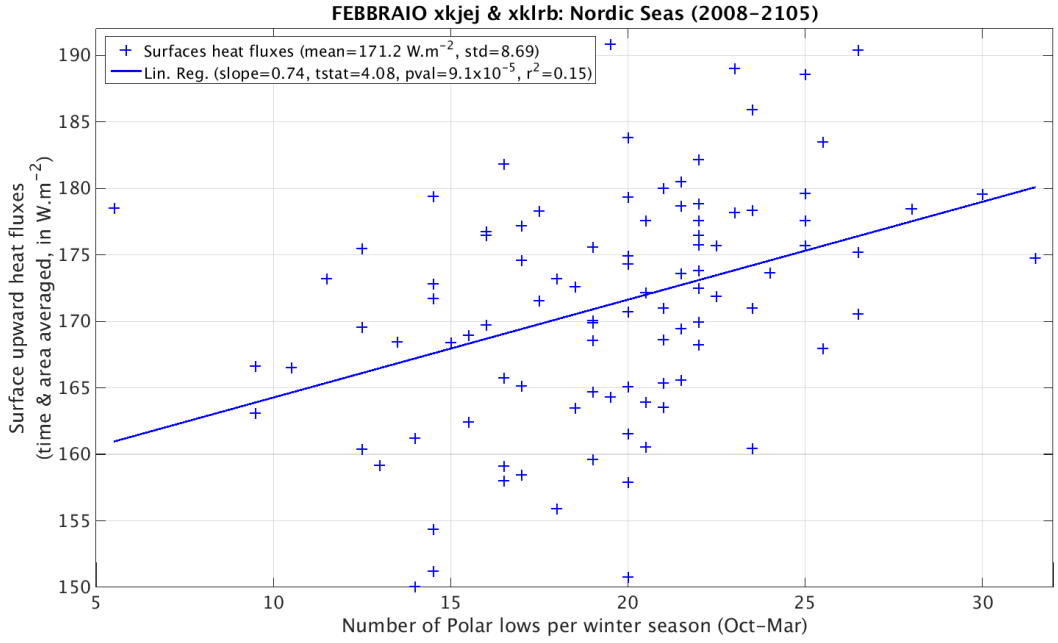

Figure 4-8: Scatter plot of the sum of the latent and sensible surface heat fluxes (time and area averaged) against the mean numbers of PLs found each year, over the Nordic Seas, with the two simulations of the 98-year FEBBRAIO data (ensemble mean).

To explore whether the relationship discussed above is sensitive to the definition of

PLs, the same analysis is performed by changing one of the identification criterion at a time.

Figure 4-9 shows the surface heat fluxes as a function of PL numbers found over the Nordic Seas, with the 98-year FEBBRAIO-1 (left panel) and FEBBRAIO-2 (right panel) simulations. For the plots shown in Figure 4-9, the PL identification criteria for the vorticity and the wind speed have been kept the same as used previously (i.e. 6×10^{-5} s^{-1} and 15 $m.s^{-1}$ respectively) but the temperature difference threshold is varied from 0°C (in red), to -39°C (in blue) to -43°C (in black, the threshold used throughout this study).

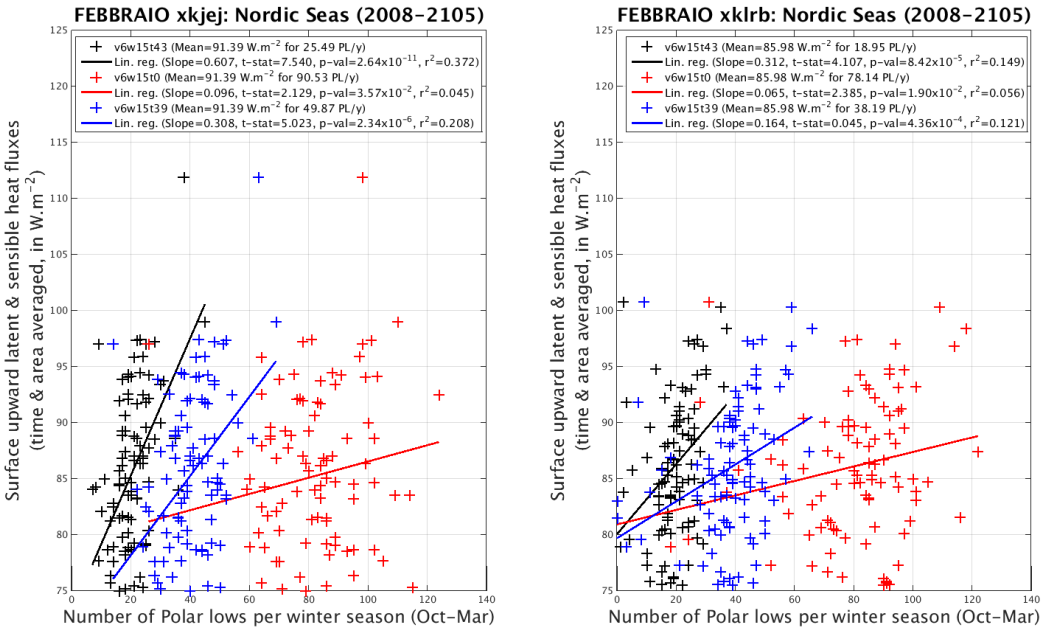

Figure 4-9: Scatter plots of the surface heat fluxes against PL numbers found over the Nordic Seas, with the 98-year FEBBRAIO-1 (left panel) and FEBBRAIO-2 (right panel) data. The PLs identification criteria for the vorticity and the wind speed stay the same (i.e. 6×10^{-5} s^{-1} and 15 $m.s^{-1}$) but the static stability criterion is varied move from 0 C (i.e. no threshold, in red), to -39 C (in blue) to -43 C (in black).

All the distributions show a positive relationship between the PL numbers and the surfaces heat fluxes. Positive trends are present, with linear regression coefficients of +0.61 and +0.31 $W.m^{-2}$ per PL for the -43°C threshold (for FEBBRAIO-1 and FEBBRAIO-2 respectively) and rates of +0.31 and +0.16 $W.m^{-2}$ per PL for the -39°C threshold (for FEBBRAIO-1 and FEBBRAIO-2 respectively). Even in the most extreme case (as with too many PLs per year compared to observation and reanalysis values) of having no criterion for the temperature difference (in red), small positive

trends are found (+0.09 and +0.06 W.m^{-2} per PL for FEBBRAIO-1 and FEBBRAIO-2 respectively). Therefore, even when relaxing the static stability criterion to its maximum, the large spread found in the distribution is weakening, but not suppressed. Hence, even weak, a clear relationship between surface heat fluxes and PL numbers is seen over the Nordic Seas in HadGEM3-GC2.

Similar results where found when changing the values of the maximum vorticity and maximum wind speed criteria (not shown). Therefore, even if the relationship between PL numbers and the surface heat fluxes is sensitive to the definition of PLs and the criteria chosen, a positive link between high PL numbers and high surface heat fluxes is still observed in HadGEM3-GC2. This means that even small and less strong PLs (and polar mesocyclones) have a positive relationship with the surface heat fluxes, as previously suggested by Condron and Renfrew (2013).

To investigate this positive link between PL occurrences and high surface heat fluxes in more detail, the spatial distributions of the heat fluxes was studied, during years with high and low PL numbers.

Figure 4-10 shows for the FEBBRAIO-1 (upper panels) and FEBBRAIO-2 (lower panels) simulations, the difference of surface heat fluxes between five years with high and low (respectively left and right panels) PL numbers and the 98-year climatology, over the Nordic Seas. The black crosses on both maps represent the location of the PLs, during the five years with high and low PL numbers, when they reach their maximum vorticity.

As expected following the previous results, the heat fluxes anomaly is mainly positive (negative) for the left (right) panel. This means that during years with high (low) number of PLs, the transfer of heat from the ocean is higher (lower) compared to the climatology, over the entire region of interest. The heat anomaly ranges between ± 40 W.m^{-2} (mean around ± 10 W.m^{-2}) for the years with high and low PL numbers for both simulations. These results hence indicate that a large transfer of heat from the ocean surface is observed when large numbers of PLs occur.

Some relatively strong heat flux anomalies can be seen on the composites, from the east of Greenland to Svalbard (especially on panels a and c, i.e. during years with high PL numbers). These anomalies tend to follow the winter sea ice edge in this region. Therefore these heat flux anomalies are more likely to be due to the difference of heat transferred between the ocean surface and the sea ice than to the heat transferred from the ocean by PL occurrences.

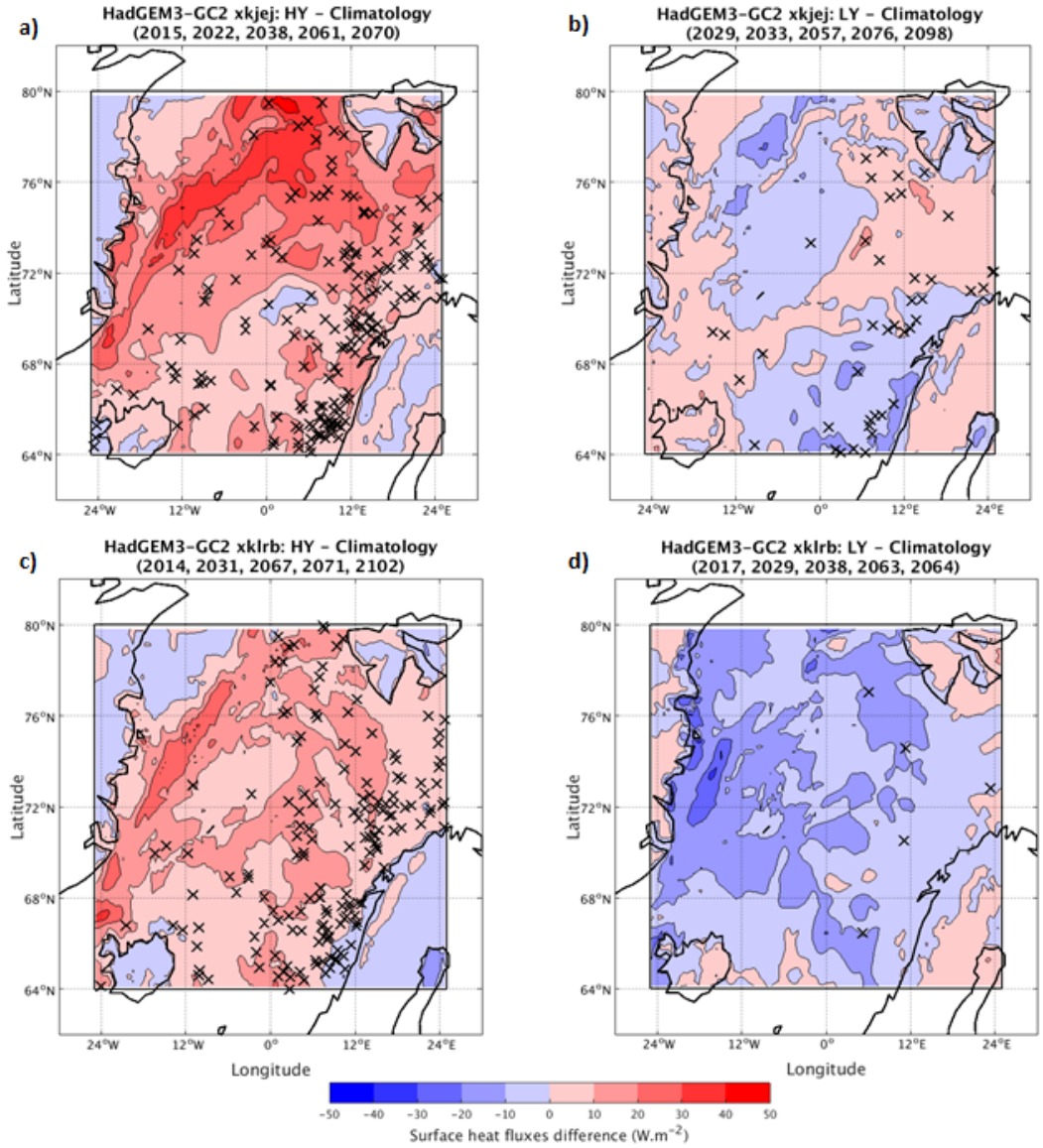

Figure 4-10: Difference between the surface heat fluxes of five years with high (left panels) and low (right panels) PL numbers and the climatology, over the Nordic Seas, with the 98-year FEBBRAIO-1 (upper panels) and FEBBRAIO-2 (lower panels) data, and the location of PLs (black crosses) when reaching their maximum vorticity.

To test the sensitivity of the analysis when including or excluding the ocean-sea ice boundary, the same analysis was performed but over a smaller region, away from this marginal ice zone (MIZ). The new region, over the south of Greenland Sea (over the Icelandic Plateau) and the Norwegian Sea, is defined here from 15°E to 20°W of longitude and from 64°N to 72°N. By defining the new region, winter PL numbers are

slightly changed (i.e. decreased) compared to the ones from the previous region of the Nordic Seas. Thus the five years with high numbers of PLs and the five years with low numbers of PLs have also changed.

Figure 4-11 shows, for the FEBBRAIO-1 (panels a and b) and FEBBRAIO-2 (panels c and d) simulations, the surface heat flux anomalies for five years with high/low (a/b and c/d panels) PL numbers relative to the 98-year climatology, over the new region of interest. The green (previously black) crosses represent the location of PLs during the five years (with high and low PL numbers) when they reach their maximum vorticity. As previously observed, more heat is taken from the ocean by PLs during the years with high numbers of PLs.

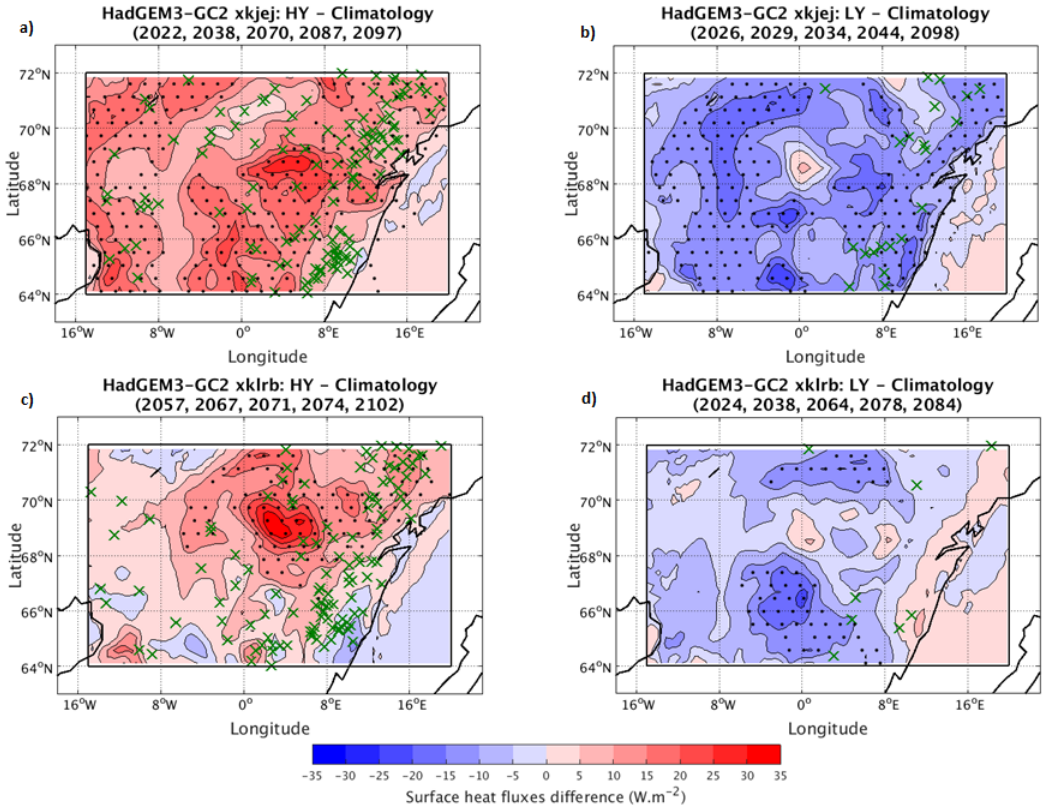

Figure 4-11: Surface heat fluxes anomaly between five years with high (a and c) and low (b and d) PL numbers and the climatology, over the Norwegian Sea, with the 98-year FEBBRAIO-1 (a and b) and FEBBRAIO-2 (c and d) data, the location of PLs (green crosses) when reaching their maximum vorticity, and the location where the bootstrapping test of the difference is significant (black dots).

As the five high (low) years chosen for this new region have changed (compared to the ones for the Nordic Seas region), the anomaly values and range have also changed,

with higher means as the ones for the previous region (around ±20 W.m^{-2}). It should also be noted that the maxima in surface heat flux anomalies are not always collocated with the location of PLs maximum vorticity. This may be due to the passage of PLs when they are not reaching their maximum vorticity, as the green crosses only represent the location of PLs maximum intensity. Another possibility might be that other processes, such as CAOs, may occur over the region and hence also play a role in determining the spatial pattern of surface heat fluxes over the Nordic Seas.

To ensure that the chosen five years with high and low PL numbers were representative of the global PL impact on the surface heat fluxes, a test of differences in anomalies of the heat fluxes was performed via a bootstrapping method (see Chapter 2 Section 2.2.4 for more information). The black dots on both plots in Figure 4-11 thus represent the location where the bootstrap test is significant at a 5% level (i.e. one-tailed test), i.e. where the heat fluxes for the years with high (low) PL numbers are significantly different from those of the climatology.

On all plots, the black dots are located over the maximum (minimum) values of the heat flux anomalies. This means that these values are higher (lower) than the 95$^{\text{th}}$ (5$^{\text{th}}$) percentile of the heat fluxes climatology. The other regions of the plots (i.e. with no dots) indicates that the heat fluxes found during the years with high and low PL numbers are within the range of the climatological values. For the FEBBRAIO-1 simulation (upper panels) the heat flux anomalies are significantly higher (lower) than the climatology over most of the region of interest for the high (low) PL years. This indicates that, as previously seen, high (low) heat fluxes are observed in HadGEM3-GC2 when high (low) numbers of PLs occur. Although still perceptible, the relationship is less clear with the FEBBRAIO-2 simulation (lower panels).

In order to test the sensitivity to the time averaging period, the analysis was repeated but using one month as the averaging period (instead of the six month period previously used). As previously seen for the seasonal cycle of PLs with the reanalyses and the HadGEM3-GC2 climate model, the months with the lowest and highest PL numbers are October and January. Hence, an analysis of the surface heat fluxes anomaly is performed for both months, by examining the difference between five October (January) months with high and low PL numbers and the October (January) monthly climatology, for both FEBBRAIO simulations.

For the FEBBRAIO-1 simulation, a total number of 19 PLs occur during the months with high PL numbers in October while no PL occur during the months with low PL numbers. For January, a total of 41 and 4 PLs occur during the month with high and low PL numbers respectively. For the second FEBBRAIO simulation, a total number of

12 PLs occur during the October months with high PL numbers while no PL happens during the October months with low PL numbers. Finally, for January, 36 (0) PLs occur in total during the month with high (low) PL numbers.

Figure 4-12 presents the heat fluxes anomaly for the five October/January months with high (panels a and c for FEBBRAIO-1 and e and f for FEBBRAIO-2) and low (panels b and d for FEBBRAIO-1 and g and h for FEBBRAIO-2) PL numbers for the FEBBRAIO simulations, over the Norwegian Sea.

For both simulations, the months with high PL numbers (panels a, c, e and g) have higher surface heat fluxes than the months with low PL numbers (panels b, d, f and h). These results indicate that higher heat amounts are transferred from the ocean to the atmosphere when high numbers of PLs occur. During months with high PL numbers, the heat flux anomalies lie around + 80 to +100 $W.m^{-2}$, while the heat flux anomalies during the month with low PL numbers mainly range between 0 and + 60 $W.m^{-2}$. The surface heat flux anomalies found in this study agree with the values of +100 and +200 $W.m^{-2}$, found with the JRA-55 reanalysis in the study from Yanase et al. (2016) (with a similar PLs tracking and identification scheme).

Furthermore, the October and January heat anomalies for the months with high PL numbers are significant at the 5% level for both simulations, whereas almost no significance is observed for the anomalies with the low PL months. Thus, with the FEBBRAIO simulations, a significant difference of heat fluxes can be seen during high PL occurrences.

For all results, a higher heat transfer from the ocean to the atmosphere is observed along the coast of Norway. This may be due to the passage of PLs over the area but also due to the sea-land contrast and the air-sea contrast as the North Atlantic Ocean current is flowing northward along the coast (Schmittner et al., 2013). However, the overall pattern of the heat flux anomaly shows more transfer of heat from the ocean to the atmosphere when a large number of PLs occurs.

Overall, these results clearly indicate that, in the HadGEM3-GC2 coupled climate model, there is a positive link between PL occurrences and the surface heat fluxes of the ocean. Indeed, the more PLs occur the higher the surface heat flux values. This positive transfer of heat from the ocean could then have an impact on the ocean circulation by triggering convection. Hence, in the next section, the potential impact of the cooling associated with PLs on the ocean circulation is investigated.

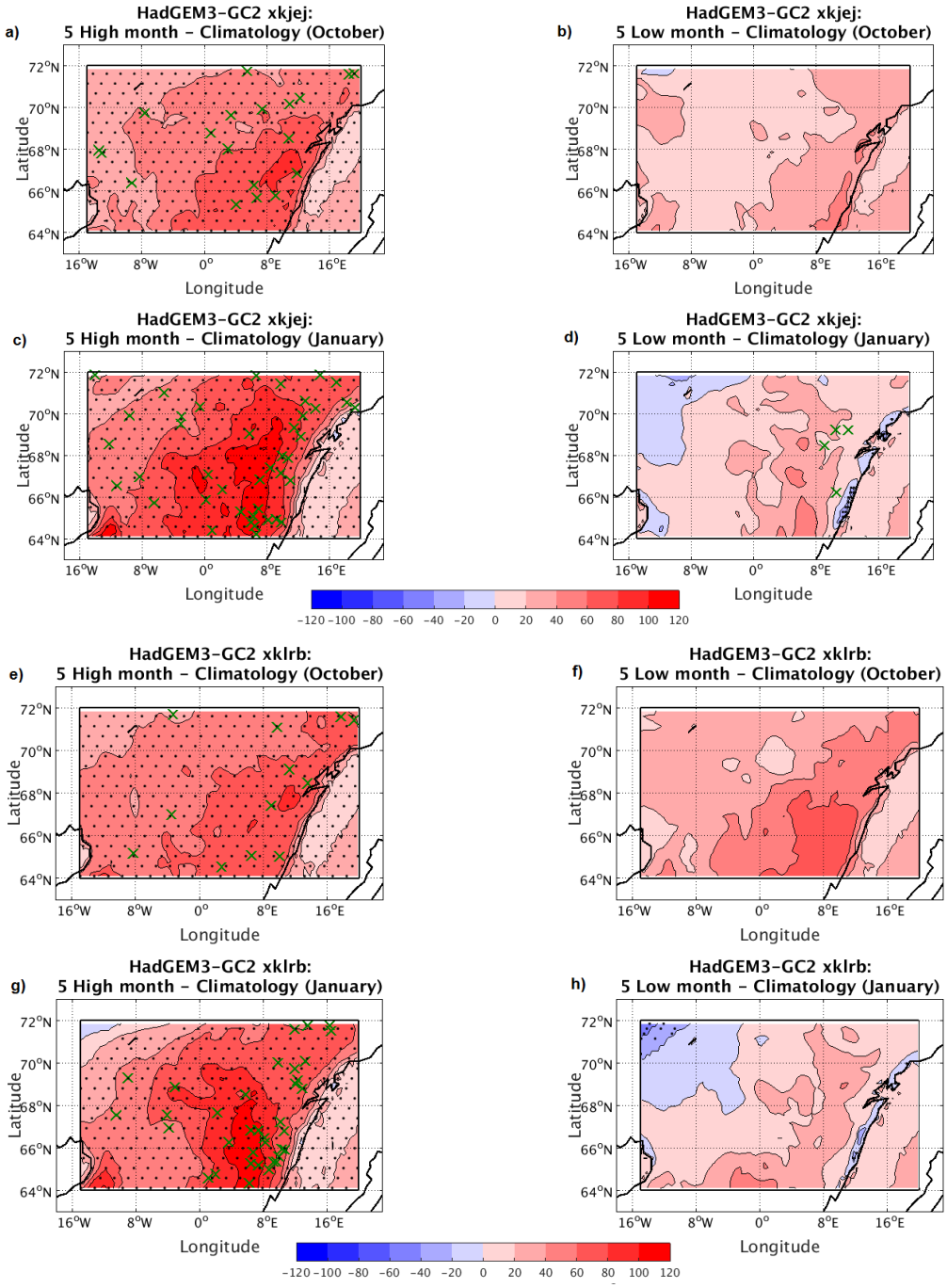

Figure 4-12: Heat fluxes anomaly between five October and January months with high (a, c, d, g) and low (b, d, f, h) PL numbers and the monthly climatology for the FEBBRAIO-1 (a, b, c, d) and FEBBRAIO-2 (e, f, g, h) simulations, over the Norwegian Sea, the location of PLs when reaching their maximum vorticity (green crosses), and the location where the bootstrapping test of the difference is significant (black dots).

4.3.2 Polar lows and the ocean circulation

The next step is to investigate the interaction between PLs and the ocean circulation, at both shallow and deep levels.

The main metric that could show the potential impact of PLs on the oceanic water column is the mixed layer depth (hereafter MLD). The mixed layer depth corresponds to the thickness of the ocean shallow layer, where turbulence is generated through the surface winds and heat fluxes, as well as processes such as thermohaline convection and sea ice formation. As the MLD is in direct contact with the atmosphere, if an atmospheric buoyant forcing would be applied to the water column, it would deepen and increase the depth of the deep waters (Marshall and Schott, 1999). Therefore, the passage of a PL could potentially cool down the ocean surface, and increase the MLD. In Condron and Renfrew (2013), the link between PMCs and the mixed layer depth and area, as well as the number of days of deep convection, were investigated. This study found that PMCs largely influence the depth, the frequency and the area of the deep convection in the Nordic Seas (the higher the PMCs number, the deeper the mixed layer and the higher the number of days of open convection) therefore leading to changes in the ocean circulation.

Unfortunately, due to missing data[1] the link between PLs and the MLD of the Nordic Seas can not be investigated with the HadGEM3-GC2 model simulations. Hence, the interaction between PLs and the ocean circulation is here assessed by examining the ocean density variations, for the shallow and deep ocean layers. Even though limited to this metric, this analysis will give some insight on the potential effect of PLs on the ocean density and the ocean circulation.

To investigate the link between PLs and the ocean density, the 3D potential density[2] is computed thanks to the ocean CDFTOOLS[3] programs from the *Laboratoire des Écoulements Géophysiques et Industriels* (Grenoble, France). First, the *in-situ* potential density is calculated, using the potential temperature and salinity fields from the HadGEM3-CG2 model (for both FEBBRAIO simulations). The potential density is

[1] At the time of the study, no MLD data are available for the second set of the FEBBRAIO dataset (xklrb), and data for some years (including some with the highest and lowest PL numbers) are missing for the first set of the FEBBRAIO dataset (xkjej).

[2] The potential density is the density that the water parcel would have if it was adiabatically brought to a reference pressure (often $P_0 \simeq 1$ bar, i.e. the ocean surface).

[3] `http://www-meom.hmg.inpg.fr/CDFTOOLS/cdftools-2.1.html`

computed using the non-linear equation of state from Jackett and Mcdougall (1995)[4]. The *in-situ* potential density anomaly is computed directly as a function of potential temperature relative to the surface, salinity and pressure. Then the potential density is calculated using each depth level, with 2,000 m as the reference depth.

As the density of ocean water is not globally homogeneous, but varies quite significantly with the depth, four depth levels were chosen for this study. As the deep water formation lies around 1,000 to 2,500 m in the Nordic seas (Rudels and Quadfasel, 1991), these levels were automatically chosen to encompass the entire area where cold and dense water lies. In order to have a view of the possible link between PLs and the full water column, the interaction of PLs and the shallow water circulation was also investigated thanks to the 50 m and 100 m levels. As none of these exact levels exist in the model archived data, the closest upper or lower levels were chosen: 47 m (hereafter 50 m), 97 m (hereafter 100 m), 1,045 m (hereafter 1,000 m) and 2,600 m. As the monthly potential temperature data from the FEBBRAIO-2 simulation was not available for two consecutive years (i.e. 2088 and 2089, corresponding to years number 80 and 81 out of 98), no computation of the potential density was possible. Therefore, these two years were discarded from both datasets, leaving the study for this section to be for 96 years instead of the previous 98 years.

Negative linear trends were found in both simulations in the potential density time series (not shown), due to negative linear trends in the potential temperature data, from the 500 m level down to the lowest ocean level. These trends could arise from the model set-ups (initial conditions) of the deep ocean part of the model, or from some intake of cold and denser water from the Arctic Ocean. Hence, the potential density data were detrended, to avoid the results being biased by the negative trend.

Figure 4-13 shows the normalized time series of the potential density at 50 m (dark green line) and 100 m (light blue line) compared to PL numbers (red dotted line), over the Nordic Seas, for both 96-year FEBBRAIO simulations. The first aspect to notice is that the 50 and 100 m lines look relatively similar to each others. As expected, this implies that that both levels are part of the same water masses, within the mixed

---

[4] The international equation of state of the seawater (Unesco, 1981) defines the density of the water ρ as a function of the salinity S, the *in-situ* temperature T and the pressure of the water p such as: $\rho(S,T,p) = \frac{\rho(S,T,0)}{1-\frac{p}{K(S,T,p)}}$, where $K(S,T,p)$ is the secant bulk modulus (i.e. a measure of the resistance to compressibility of a fluid. See Jackett and Mcdougall (1995) and Safarov et al. (2009) for more information).
In Jackett and Mcdougall (1995), the equation of state of the ocean waters in terms of potential temperature θ is defined as: $\rho(S,\theta,p) = \frac{\rho(S,\theta,0)}{1-\frac{p}{K(S,\theta,p)}}$, where $K(S,\theta,p)$ is the bulk secant modulus.

layer. The second aspect is that the variations in the 50 m and 100 m density seem to partially follow the variations of PL numbers. This seems coherent since the shallow layers are in immediate contact with the atmosphere, and thus with PLs. However, non-significant small positive Pearson correlation coefficients are found: +0.137 (p-value: 0.184) and +0.085 (p-value: 0.407) at 50 m depth for the FEBBRAIO-1 and FEBBRAIO-2 simulations respectively, and +0.095 (p-value: 0.358) and +0.081 (p-value: 0.433) at 100 m depth for the FEBBRAIO-1 and FEBBRAIO-2 simulations respectively.

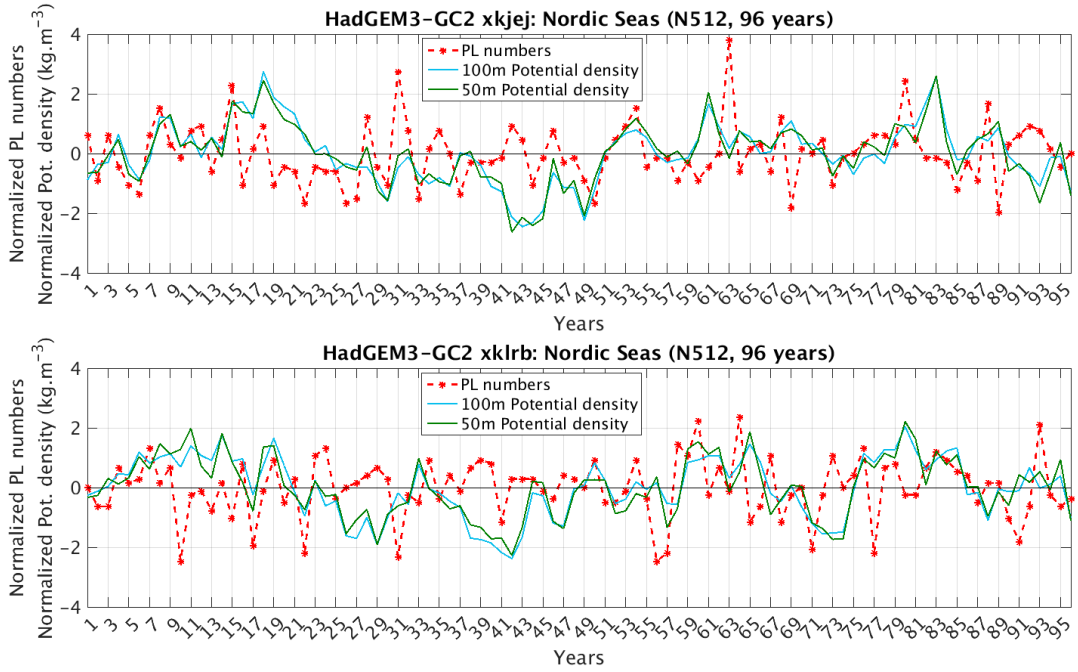

Figure 4-13: Normalised time series of the potential density (referenced to 2,000 m) at 50 m (dark green line), 100 m (light blue line) compared to PL numbers (red dotted line), over the Nordic Seas, from the 96-year FEBBRAIO-1 (upper panel) and FEBBRAIO-2 (lower panel) simulations.

The same analysis is also made for the deep ocean layers, at the level of 1,000 m and 2,600 m, and is shown on Figure 4-14. For both simulations, the time series of the ocean density at 1,000 and 2,600 m seem anti-correlated with each other and do not seem to vary in a similar way as the PL number time series. Non-significant small Pearson correlation coefficients are found between PL numbers and the deep ocean circulation: +0.019 and -0.064 for the 1,000 m depth for FEBBRAIO-1 and FEBBRAIO-2 respectively, and -0.047 and +0.037 for the 2,600 m depth for FEBBRAIO-1 and FEBBRAIO-2 respectively. Hence, it seems that no clear link between PL numbers and the deep water circulation can be inferred from their time series, over the Nordic

Seas in the HadGEM3-GC2 coupled climate model.

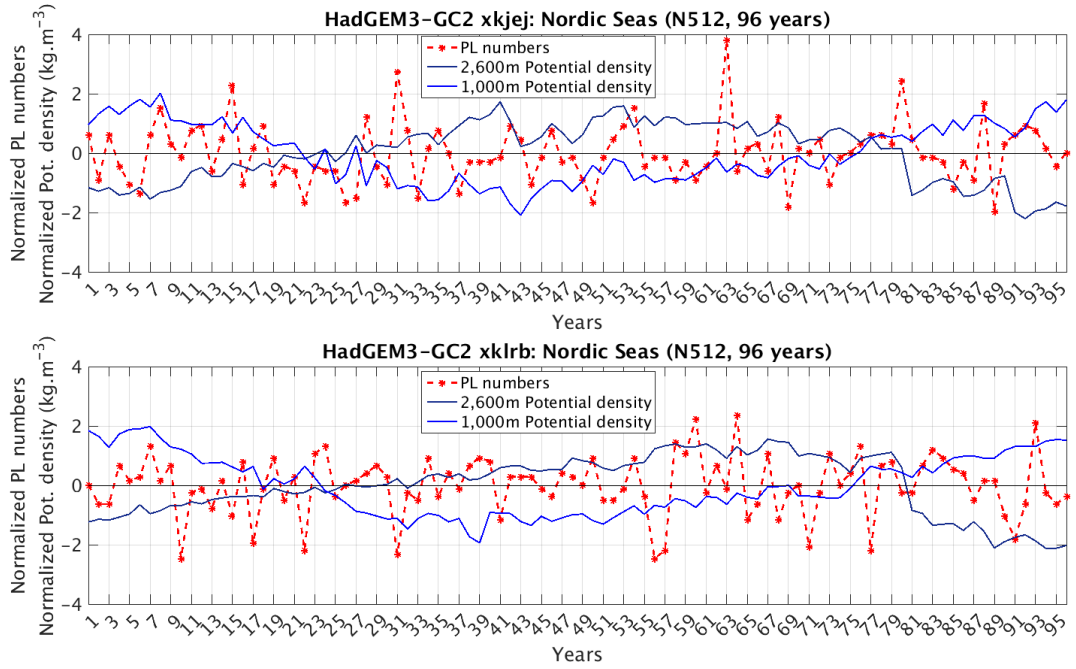

Figure 4-14: Normalised time series of the potential density (referenced to 2,000 m) at 1,000 m (light blue line) and 2,600 m (dark blue line) compared to PL numbers (red dotted line) over the Nordic Seas, with the 96-year FEBBRAIO-1 (upper panel) and FEBBRAIO-2 (lower panel) simulations.

As the ocean takes time to respond to atmospheric forcings, the lag response of the ocean density to PL numbers was also investigated. However, no lag correlation was found between PL numbers and the potential density (year-to-year lag correlation of +0.137 for FEBBRAIO-1 and +0.085 for FEBBRAIO-2 respectively at 50 m).

As previously investigated for the surface heat fluxes, the ocean density differences between years with high and low PL numbers and the climatology has been calculated. Since the previous results for the Norwegian and Barents Seas are influenced by the sea ice edge, the next part of the analysis only focuses on the region over the Norwegian Sea[5], and a test of differences in anomalies of the potential density is performed via a the same bootstrapping method as previously, at different depth levels.

Figure 4-15 shows the potential density difference for years with high (panels a and c) and low (panels b and d) PL numbers, at 50 m, and the location where the

[5] As previously defined the Norwegian Sea corresponds to the region from 20°W to 15°E and from 64°N to 72°N.

bootstrapping test of the difference is significant (black dots) over the Norwegian Sea, for the FEBBRAIO-1 (panels a and b) and FEBBRAIO-2 (panels c and d) simulations.

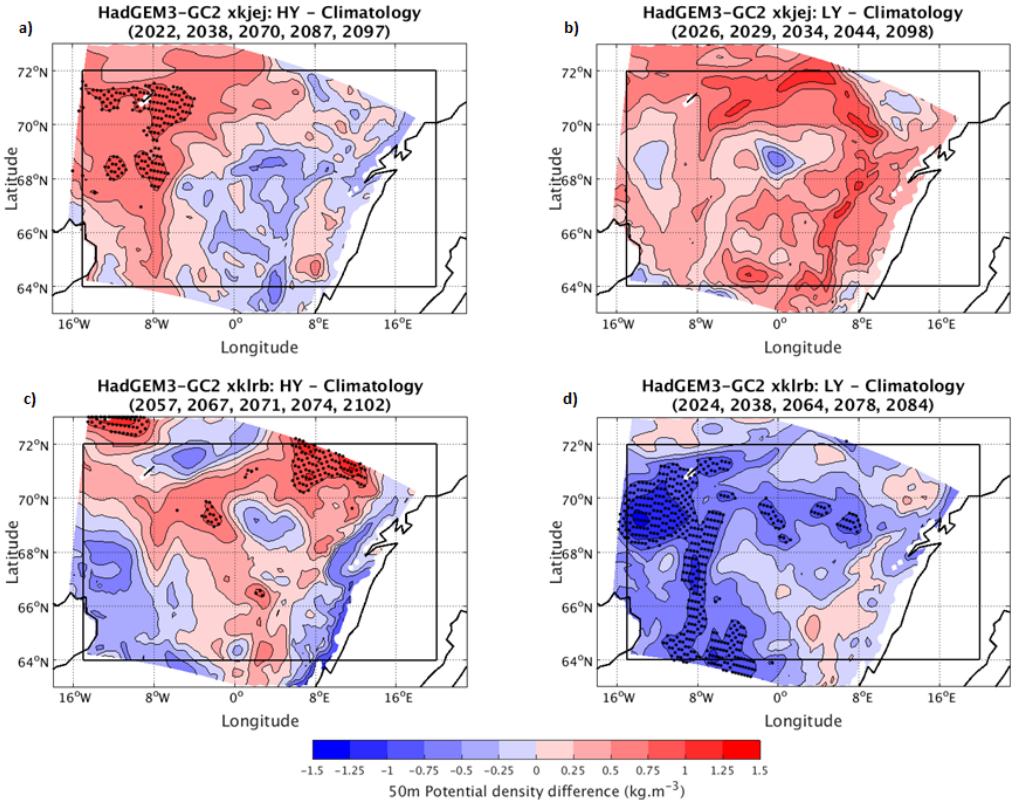

Figure 4-15: 50 m potential density difference between five years with high (a and c) and low (b and d) PL numbers and the climatology, and the location where the bootstrapping test of the difference is significant (black dots), over the Norwegian Sea, with the FEBBRAIO-1 (a and b) and FEBBRAIO-2 (c and d) simulations.

Both simulations show relatively different results. The first simulation (panels a and b) indicates that the potential density of the ocean during years with high PL numbers is slightly less dense (negative anomaly around -0.05 kg.m^{-3}) along the coast of Norway compared to the density over the Icelandic Plateau. This may indicate that when large numbers of PLs occur, the shallow layer of the ocean is less dense than the climatology. These results are only statistically significant in limited regions for the high PLs composite and not significant for the low PLs composite. Hence, this only partially support the hypothesis that PLs have an impact on the ocean density. Furthermore, having a less dense ocean at 50 m during the years with high PL numbers may also be due to other exterior factors such as the transport of warmer (and thus less dense) shallow water masses from the Atlantic Ocean, coming in to the Nordic

Sea through the east branch of the North Atlantic Current. The second FEBBRAIO simulation (panels c and d) indicates that the potential density of the ocean during years with high PL numbers is denser (positive anomaly) than during years with low PL numbers (negative anomaly), over the Norwegian Sea. This result suggests that when PLs occur over the region, the shallow layer of the ocean may be more dense, in response to the surface heat transfer. Therefore with this simulation, the results imply that a relationship between PL numbers and the ocean density at 50 m depth may be inferred. As these doted regions are small, this indicates that, in the FEBBRAIO simulations, there are no large differences in terms of ocean density changes between years with high and low PL numbers and the climatology over the Norwegian Sea.

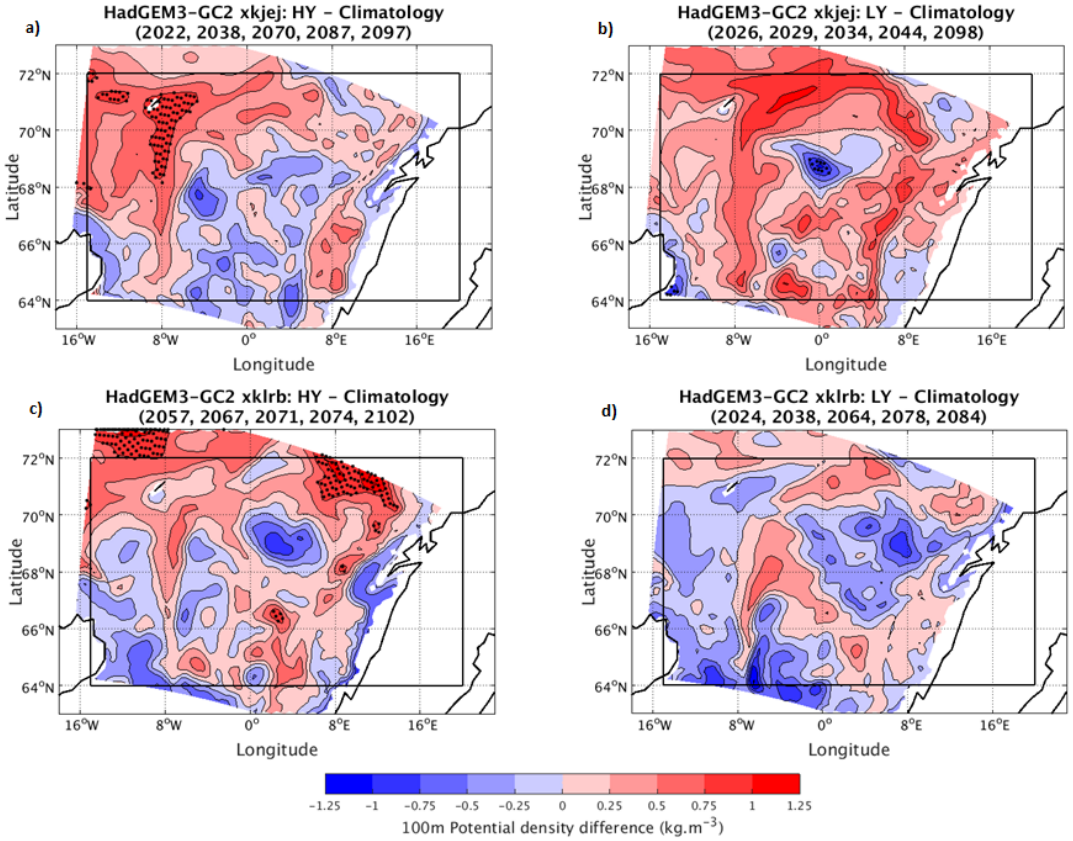

Figure 4-16: 100 m potential density difference between five years with high (a and c) and low (b and d) PL numbers and the climatology, and the location where the bootstrapping test of the difference is significant (black dots), over the Norwegian Sea, with the FEBBRAIO-1 (a and b) and FEBBRAIO-2 (c and d) data.

Figure 4-16 presents, similarly to Figure 4-15, the potential density difference for years with high and low PL numbers but this time at 100 m. Similar results are found compared to those at 50 m, with a slightly less dense (denser) ocean during the years

high PL numbers for the FEBBRAIO-1 (FEBBRAIO-2) simulations. Only small areas of potential density are significantly different from the climatology. Hence, it seems that no impact from PL occurrences on the ocean density can be inferred from these density anomalies from HadGEM3-GC2.

The ocean density anomalies for a shallower level, 50 cm, were also investigated (not shown) and showed similar results to the ones from of the 50 m level but with more local fluctuations. The same analysis was performed for the deep ocean, at 1,000 m and 2,600 m (not shown). Although with relatively different values, both simulations present, for both deep levels, non significant denser ocean waters (i.e. negative density anomalies) during years with high PL numbers compared to those during years with low PL numbers. However, since little or no impact of PLs seen on the shallow ocean density, it is expected that no impact of PLs would be seen at deep levels.

As previously investigated for the surface heat fluxes, the anomaly between five October/January months with high and low PL numbers is also examined for the ocean potential density at 50 and 100 m (and 1,000 and 2,600 m).

Figure 4-17 presents composites of the 50 m potential ocean density anomaly for the five October/January months with high (left panels) and low (right panels) PL numbers for the FEBBRAIO-1 (a, b, c and d) and FEBBRAIO-2 (e, f, g and h) simulations, over the Norwegian Sea, as well as the location where the bootstrapping test of the difference is significant (black dots). No large significant differences in ocean density, between months with high and low PL numbers, can be deduced from the October and January anomalies at 50 m. Similar results were found at 100 m depth (not shown). Thus, these results might suggest that PL occurrences do not too much affect the ocean density within the mixed layer over the Norwegian Sea. A second possible explanation for these results might be that PLs may have an impact on the shallow ocean circulation but at a lower temporal resolution (i.e. hourly or daily) which the monthly average used for the anomaly composites moderates. Unfortunately, as the FEBBRAIO ocean data are only available as monthly outputs (for cost efficiency), the link between PLs and the ocean density at higher temporal frequency can not be examined.

For the deep ocean density (i.e. 1,000 and 2,600 m), similar results (not shown) were found for both simulations and for October/January months (i.e. non significant negative anomalies during years with high PL numbers). However, since no clear relationship can be inferred between PLs and the upper ocean, it is unlikely that PLs will have an impact on the deep ocean if they have no impact at shallow depths.

Hence these results indicate no clear evidence of the impact of PLs on the deep sea water, and thus no statement can be made on PLs influencing the deep water formation,

based on the FEBBRAIO simulations from the coupled climate model HadGEM3-GC2.

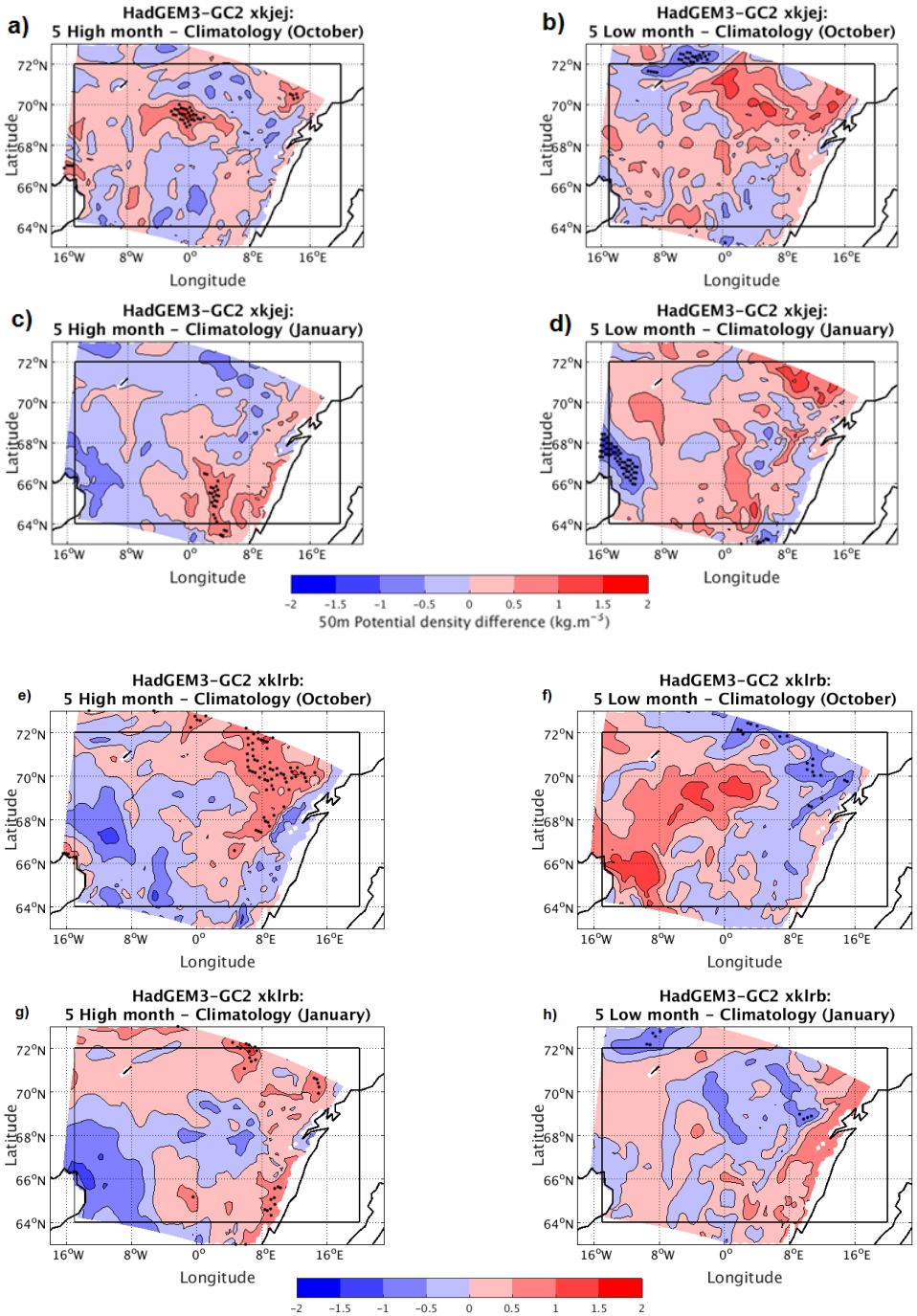

Figure 4-17: 50 m potential ocean density anomaly for five October and January months with high (a c, e and g) and low (b, d, f and h) PL numbers for the FEBBRAIO-1 (a, b, c and d) and FEBBRAIO-2 (e, f, g and h) simulations, over the Norwegian Sea, and the location where the bootstrapping test of the difference is significant (black dots).

4.4 Conclusion

In this chapter, the characteristics of PLs were evaluated in the N512 HadGEM3-GC2 coupled climate model, with two 98-year model simulations, in order to investigate the potential interaction of PLs with the North Atlantic ocean circulation.

The two 98-year FEBBRAIO present day forcing experiments from the MetOffice HadGEM3-CG2 model (Williams et al., 2015) were first used to assess the representation of PLs in the coupled climate model. The model showed similarities with the results from both reanalyses from Chapter 3 for the patterns and numbers of PLs activity, but are closer to those from the NCEP-CFS reanalysis than those from ERA-I. The spatial distribution of PLs (track, genesis and lysis densities) in the model appears similar to those from NCEP-CFS. The PL track density maxima are seen along the western coasts of Norway, and between the northern coasts of Norway and the Svalbard Islands, which is also the region with higher CAO occurrences (Kolstad, 2007, 2011). The seasonal cycle of PL numbers is similar in term of values and pattern to the ones from NCEP-CFS dataset, but with a slightly shifted maxima (from December to January). No trends were found in PL numbers nor in the inter-annual variability of these numbers. The mean numbers and standard deviations of PL numbers were found in correspondence to the ones from NCEP-CFS.

Since the HadGEM3-GC2 model is generally in good agreement with the NCEP-CFS reanalysis in terms of how PLs are represented, it is suggested that the N512 HadGEM3-GC2 model is able to provide a reasonable representation of PLs. However, it is worth noting that there is substantial uncertainty in PL numbers between the observations and reanalyses, and between the reanalyses themselves (e.g. the large discrepancies between NCEP-CFS and ERA-I reanalyses seen in Chapter 3).

The second part of this chapter focused on the possible link between PLs and the North Atlantic Ocean circulation. PLs are known to be associated with surface heat fluxes as previously shown thanks to observations (Shapiro et al., 1987), reanalysis (Papritz et al., 2015) and atmospheric-only model simulation (Fore et al., 2012). In previous studies, to assess the impact of PLs on the ocean circulation over the North Atlantic and Nordic Seas, PLs have been parametrized in a global ocean-only modelling experiment (Condron et al., 2008) and a global ocean/sea-ice circulation model (Condron and Renfrew, 2013). Both studies found that PLs influence the ocean circulation by increasing the ocean density at the surface, thanks to the surface heat being taken from the surface. This increase in surface density "gradually erodes the existing vertical stratification of the water column" (Condron et al., 2008), deepens the depth of

the deep convection in the Nordic Seas (Condron and Renfrew, 2013) and thus impacts the whole North Atlantic Ocean circulation.

In order to evaluate this relationship between PLs and the ocean circulation, the link between PLs and surface heat fluxes and the link between PLs and the ocean density were assessed in the HadGEM3-CG2 coupled climate model, over the Nordic Seas, region where deep water formation occurs (Rudels, 1990; Rudels and Quadfasel, 1991; Mauritzen, 1996; Våge et al., 2013).

A positive link between the PL numbers and the surface heat fluxes was found in both datasets: the more PL occurrences the higher the surface heat fluxes. Indeed, an increase of surface heat fluxes with PL numbers was seen, with a seasonal mean increase of +0.74 $W.m^{-2}$ per PL in the FEBBRAIO datasets. If this positive link between PL numbers and the surface heat fluxes is clear, a large spread in the heat flux distribution is also found. This may suggest that the impact of PLs on the surface heat fluxes may not always be large and that the amount of heat transferred from the ocean may vary depending on characteristics such as PLs large-scale environment, location and intensity. The link between PLs and the ocean surface heat fluxes was even clearer when analysing the year-to-year variability in the heat transfer for the climatological months with the highest and lowest PL numbers (i.e. January and October).

However, a smaller impact was found between PL numbers and the potential density of the upper layers of the ocean (50 cm, 50 m and 100 m). The potential density of years with high PL numbers tends to be only slightly denser than the climatological density. This could mean that the heat fluxes associated with PLs are not strong enough to have an impact on the ocean density or that the monthly temporal resolution used here is too coarse to notice a possible impact of PLs on the shallow ocean density. In order to examine this in a more detailed way, ocean data with higher temporal resolution, as well as other ocean metrics (such as the MLD and the volume of the dense waters), would be needed. Finally, no apparent correlation was observed between PL numbers and the potential density of the ocean at 1,000 and 2,600 m. As only little impact of PLs on the surface ocean was found, there is little possibility that an interaction between PLs and deep water in the Nordic Seas can thus be inferred from this study.

Overall, based the results with the HadGEM3-CG2 coupled climate model, it does not seem as clear as in the Condron et al. (2008) and Condron and Renfrew (2013) experiments, that PLs would cool down the surface layers of the ocean and alter the deep ocean circulation in the North Atlantic Ocean and the Nordic Seas. These thesis results differ from the 2-year and 21-year simulations from Condron et al. (2008) and Condron and Renfrew (2013) which found that the heat transfer from the ocean to PLs

would cool down the ocean surface and trigger deep convection over the Nordic Seas. This discrepancy in the results could arise from several differences in the studies.

First, the models used in the studies are different. Condron and Renfrew (2013) used a 18-km global ocean-sea ice circulation model while this thesis make use of an 25-km coupled climate model. Hence, the different models may respond differently to the surface forcing from PLs.

Secondly, the definitions of PLs in the studies differ. Here PLs are identified via an objective tracking and identification scheme, using the maximum filtered relative vorticity in a coupled climate model. Condron studies used a cyclone detection algorithm (Murray and Simmonds, 1991) to find the maximum of the Laplacian of the MSLP to detect "open-eye" mesocyclones in ERA-40 (Condron et al., 2006). Rankine vortexes (i.e. vortex with a swirling flow) were then inserted into the model wind field at PLs location. Furthermore the studies used the term "Polar lows" to encompass all Polar mesocyclones. The difference in PLs definition hence also induces differences in the total numbers of PLs of both studies. Condron et al. (2008) and Condron and Renfrew (2013) respectively found 1250 and 2857 PLs per year over the North-East Atlantic Ocean their studies while this thesis around 26 PLs per year over the Norwegian and Barents Seas (and 124 PLs per year for the Northern hemisphere). Therefore this discrepancy in PL numbers could also affect the response of the ocean to PLs passage.

Furthermore, the previous studies and this thesis have different methodologies. In the approach of Condron and Renfrew (2013), the only difference between the control and perturbed simulations is the atmospheric forcing due to PLs from the perturbed simulation. Therefore this setup enables to directly and robustly test whether PLs can have an impact on the oceanic circulation.

Finally, the metrics used in the previous studies and this thesis differ, preventing this current analysis to be fully compared with previous results. Condron and Renfrew (2013) investigated the MLD and the volume of the dense water. As these variables were not available in the FEBBRAIO datasets at the time, this thesis made use of the ocean density, which prove itself to be relatively less sensitive to buoyant forcing than the MLD (Marshall and Schott, 1999), and which therefore may be less prone to be influenced by the passage of PLs.

Although limited, this analysis confirms the link between PLs and the ocean surface heat fluxes but shows no evidence that PLs influence on the ocean density is sufficient to destabilize the water column and trigger deep ocean convection over the Nordic Seas. Hence, the role played by PLs on the ocean circulation in the HadGEM3-GA3 coupled model is not seen as clearly as in Condron and Renfrew (2013) in controlling the year-to-year variations of the oceanic circulation.

CHAPTER 5

POLAR LOWS IN THE FUTURE CLIMATE SYSTEM

5.1 Introduction

With the possibility of a future sea ice free Arctic Ocean (Collins et al., 2013), new activities and new shipping routes might become possible (Melia et al., 2016). As PL occurrences in these places may also develop (as more open-ocean surface will be available for them to form), demands for forecast of PLs and PL damage assessments on vessels and offshore infrastructures in the regions might arise. Therefore, knowledge on the future of PLs and their environment might become more and more crucial.

Hence, in this Chapter, PLs activity and the impact of the model resolution on their activity are assessed with an atmosphere-only global climate model under present and future climate conditions.

In Zahn and von Storch (2010), a cyclone detection algorithm was applied to dynamically downscaled (resolution of 50 km) simulations from a regional climate model (forced with IPCC AR4 emission scenarios) in order to investigate PLs under climate change. The study showed a future increase in atmospheric static stability over the North Atlantic Ocean. This increase in stability may be due to a faster increase in mid-tropospheric temperatures compared to those at the surface (as the ocean response to forcings is often slower than the one of the atmosphere). The increase in stability acts to inhibit PL formation and development over the same region. Furthermore, a northward shift of PL activity was also found. As a consequence Zahn and von Storch (2010) observed a reduction of 53% in PL numbers over the North Atlantic Ocean, between the present and future climate conditions, and a poleward shift of PL activity of 2°.

More recently, Romero and Emanuel (2017) looked at PLs, and Medicanes (i.e.

Mediterranean hurricanes), in future climate scenarios. Using most of the 30 CMIP5 climate models in both historical and RCP 8.5 simulations for a recent (1986-2005) and a future (2081-2100) period, they found a possible reduction of around 10% to 15% in the overall frequency of North Atlantic PLs, which would affect both weak and intense mesocyclones. Furthermore, a regional redistribution of PLs was found, with a shift of PL activity "from the south Greenland-Icelandic sector toward the Nordic seas closer to Scandinavia".

In addition to predict a decline of PL occurrences over the Northern hemisphere in the future climate (Zahn and von Storch, 2010; Romero and Emanuel, 2017), other studies have shown a possible decrease of CAO events in the Northern hemisphere (Kolstad and Bracegirdle, 2008) and an increase in North Atlantic atmospheric static stability (Mallet et al., 2017). However, these studies have generally been conducted with relatively low horizontal resolution data at which PLs may not be represented as well as at higher resolutions. Therefore, in this study the response of PLs to climate change, as well as the sensitivity of this response to the resolution, is explored, using an objective PL tracking and identification scheme, in a high resolution global climate model.

This chapter makes use of the UPSCALE dataset (Mizielinski et al., 2014). As introduced in Chapter 2, the UPSCALE dataset is a series of five ensemble simulations of the HadGEM3 global atmosphere-only model (Williams et al., 2015) at resolutions of 130 km (N96), 60 km (N216) and 25 km (N512) for both present climate conditions and a potential future climate scenario, RCP 8.5.

For this study, three ensemble members of each resolutions and climate conditions are used (see Chapter 2 Section 2.1.3.2 for more details). This analysis is done for two distinct climate conditions: the historical climate conditions (period from 1985 to 2010) and a potential future climate scenario (projections for the end of the 21st century). This future scenario is SST and sea ice fraction forced by using the SST and SIF from the HadGEM2-ES (Jones et al., 2011) in response to the RCP 8.5 experiment (Riahi et al., 2011). As the future climate conditions are from the most extreme climate scenario available, it will give an indication of the upper bound of what might happen to PLs. The tracking and identification stage of PLs in each simulation and member is the same as for the reanalysis part of this study. However for this part of the study, instead of highlighting specific PL regions, the focus is on the entire Northern hemisphere, to investigate the global response of PLs to climate change.

The aim of this chapter is to explore how PLs might respond to climate change at

different resolutions. This aim will be addressed by the following objectives:

- Evaluate the representation of PLs for the present climate conditions using the HadGEM3-GA3 high-resolution global climate model,
- Investigate the influence of climate change on PLs characteristics, such as their seasonality, duration and spatial distribution,
- Evaluate the impact of the horizontal resolution of the model chosen on the representation of PLs under the current and future climates.

In Section 5.2.1, the present-day representation of PLs in the high-resolution (N512) simulations of the atmosphere-only climate model HadGEM3-GA3 will be assessed and compared with previous results from the reanalyses (from Chapter 3) and those from the coupled climate model HadGEM3-GC2 (from Chapter 4). The second part of the Chapter (Section 5.2.2) will assess the changes in PLs between the current and future climate conditions with the high-resolution (N512) simulations of HadGEM3-GA3, as well as the changes in the large-scale environment of PLs. Finally, a comparison of PLs activity for both present climate conditions will be investigated with the three horizontal resolutions (N512, N216 and N96) of HadGEM3-GA3 (Section 5.3).

5.2 Polar lows in the high-resolution atmospheric climate model HadGEM3-GA3

5.2.1 Present climate: assessment of the representation of Polar lows

The first part of the work consists in assessing the representation of PLs in the high resolution climate model, for the present-day (i.e. historical) climate conditions. This will provide confidence in using the model to explore how PLs might change in the future. Thus here, the representation of PLs in the current climate is assessed within the three high-resolution (N512) simulations, and compared with previous results from the NCEP-CFS reanalysis (used in Chapter 3) and the coupled climate model HadGEM3-GC2 (used in Chapter 4).

5.2.1.1 Inter-annual variability of Polar low numbers

The first aspect investigated is the present-day representation of the inter-annual variability of PL numbers over the Northern hemisphere in HadGEM3-GA3, and compare it with the previous ones from the reanalyses and coupled model.

Table 5.1 shows the annual mean and standard deviation of PL numbers found with the N512 resolution of the atmosphere-only climate model HadGEM3-GA3, the coupled climate model HadGEM3-GC2 and the NCEP-CFS reanalysis. The mean found with the HadGEM3-GA3 model (93.38 PLs per year) is lower than those found with the coupled model HadGEM3-GC2 (124.19 PLs per year) and the reanalysis NCEP-CFS (120.80 PLs per year). Even though with a shorter period of study, the mean PL numbers found with the HadGEM3-GA3 model can be seen as with a lower sampling error as the ones from HadGEM3-GC2 and NCEP-CFS since the standard deviation is twice smaller (this may be due to having three ensemble members with similar PL numbers, or in having less variability in PL numbers due to the lack of ocean coupling) and the confidence interval is smaller.

	HadGEM3-GA3 (26y - 25km)	HadGEM3-GC2 (98y - 25km)	NCEP-CFS (36y - 38km)
Mean	93.38	124.19	120.80
Standard dev.	8.13	17.31	18.32
95 % conf. interval	[77.44; 109.31]	[90.26; 158.11]	[84.89; 156.70]

Table 5.1: Mean, standard deviations and 95% confidence interval of PL numbers found per year in HadGEM3-GA3 N512 resolution (historical climate conditions, 3 simulations), HadGEM3-GC2 (2 simulations) and NCEP-CFS, over the Northern hemisphere.

5.2.1.2 Seasonal variability of Polar low numbers

In this subsection, the seasonal variability of PLs numbers is studied. This is of particular interest in order to evaluate how well HadGEM3-GA3 represent PLs seasonal variability in the current climate.

Figure 5-1 shows the boxplots of PL numbers found per month for the historical period of high-resolution simulations (mean ensemble) of the atmosphere-only climate model HadGEM3-GA3 (blue), the mean ensemble of the high-resolution (N512) of the two simulations of the coupled climate model HadGEM3-GC2 (light blue), and the reanalysis NCEP-CFS (black), over the Northern hemisphere. As a reminder the periods of study and horizontal resolutions are 26 years and 25 km for HadGEM3-GA3 (with three ensemble members), 98 years and 25 km for HadGEM3-GC2 (with two ensemble members) and 36 years and 38 for the NCEP-CFS (see Chapter 2 for more details on the datasets). For each dataset, a similar seasonal variability of PL numbers is found, with an increase in number from October to December-January and a slow decrease till March. Monthly PL numbers of both climate models are found within the range of the ones from the reanalyses, with a monthly mean around 5 PLs per month for October and around 20 PLs per month for January. The range of PL numbers

found (from minimal to maximal mean values) tends to be smaller for the atmosphere-only climate model HadGEM3-GA3 compared to the other datasets, indicating that the ensemble mean of three members may show less sampling error in the estimated PL numbers.

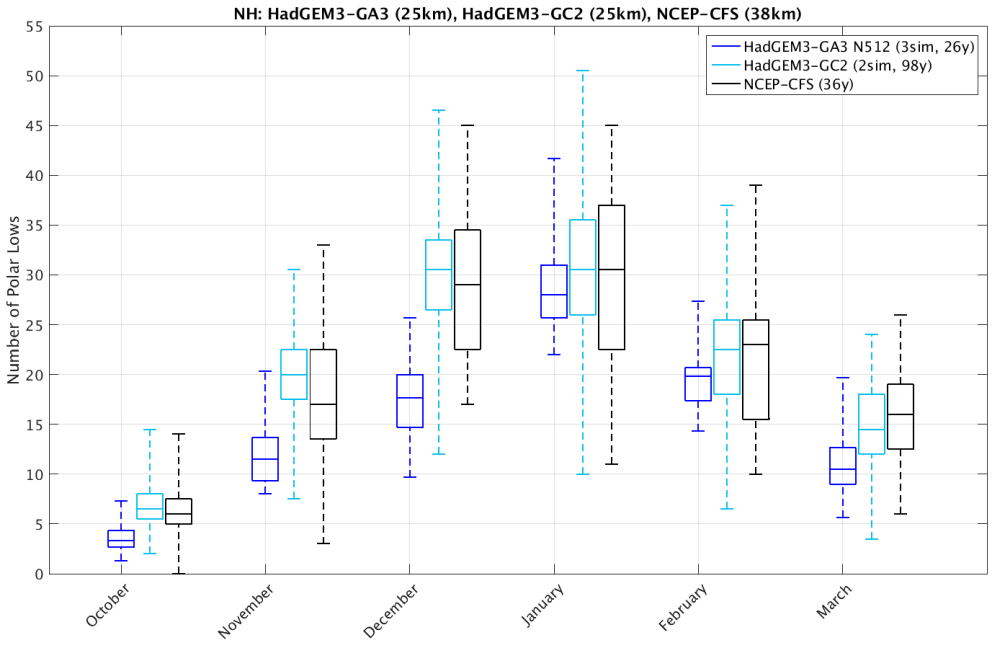

Figure 5-1: Number of PLs found per month for the historical climate conditions of HadGEM3-GA3 (blue), HadGEM3-GC2 (light blue) and NCEP-CFS (black), over the Northern hemisphere.

5.2.1.3 Characteristics of Polar lows

To further investigate the representation of PLs in the HadGEM3-GA3 model, some of their dynamical and thermo-dynamical properties are also explored.

Table 5.2 presents the mean and standard deviation of the maximum along-track vorticity, the maximum wind speed and the minimum temperature difference (found at the time when PLs reach their maximum vorticity) of PLs found with the N512 resolution of the HadGEM3-GA3 climate model, the coupled HadGEM3-GC2 climate model and the reanalysis NCEP-CFS, over the Northern hemisphere. Although they have different temporal ranges and spatial resolutions, all three datasets exhibit very similar results regarding PLs properties. The three datasets indicate the mean of the PLs maximum filtered vorticity to be around 8.40×10^{-5} s^{-1}. The mean of the maximum wind speed is around 20.29 $m.s^{-1}$ and the mean of the minimum temperature difference

is around -45.31 K in all three datasets[1]. All three fields have relatively small variations around the mean. When looking at the coefficient of variation (i.e. $\frac{standard\ deviation}{mean}$), results show that for each dataset, the maximum vorticity is the field with the highest variability (coefficients for the three datasets around 24% for the maximum vorticity, 16% for the maximum wind speed and 4% for the temperature difference).

	Vorticity			Wind speed			ΔT		
	GA3	GC2	NCEP	GA3	GC2	NCEP	GA3	GC2	NCEP
Mean	8.53	8.42	8.26	20.49	19.92	20.47	-45.49	-45.31	-45.13
Std dev.	2.14	2.02	1.95	3.40	3.18	3.51	2.00	1.86	1.82

Table 5.2: Mean and standard deviation of the maximum filtered vorticity (in $\times 10^{-5}$ s^{-1}), maximum wind speed (in $m.s^{-1}$) and minimum temperature difference ($\Delta T = T500 - SST$, in K) of PLs found in the N512 resolution of the atmosphere-only HadGEM3-GA3 ("GA3") climate model, the coupled HadGEM3-GC2 ("GC2") climate model and the reanalysis NCEP-CFS ("NCEP"), over the Northern hemisphere.

These results indicate that the high-resolution simulations of the HadGEM3-GA3 model are able to capture current PL dynamical intensity and environmental properties as seen in the NCEP-CFS reanalysis and in the HadGEM3-GC2 climate model.

5.2.1.4 Spatial distribution of Polar low numbers

The last aspect of PLs representation to be assessed for the current climate conditions before exploring the representation of PLs under climate change, is how they are spatially distributed over the Northern hemisphere in the HadGEM3-GA3 model.

Figure 5-2 shows the track density (track per month per unit area, where a unit area is equivalent to a 5° spherical cap, i.e. around 10^6 km^2) of PLs found with the N512 resolution of the atmosphere-only HadGEM3-GA3 climate model (a), the coupled HadGEM3-GC2 climate model (b) and the NCEP-CFS reanalysis (c).

All three maps have values of track density between 0 and 6 tracks per month per unit area over the Northern hemisphere and with the main PL activity regions being north of the main North Atlantic and North Pacific storm tracks. In all three maps, three track density maximum are observed: one south of Iceland, one over the Norwegian Sea and one east of the Russian Kamchatka region. As previously seen, these regions are the most favourable for PLs formation, with strong temperature and wind gradients.

[1] As a reminder, the thresholds for these identification criteria are: a maximum vorticity greater than 6×10^{-5} s^{-1}, a maximum wind speed greater than 15 $m.s^{-1}$ and a temperature difference lower than -43 K.

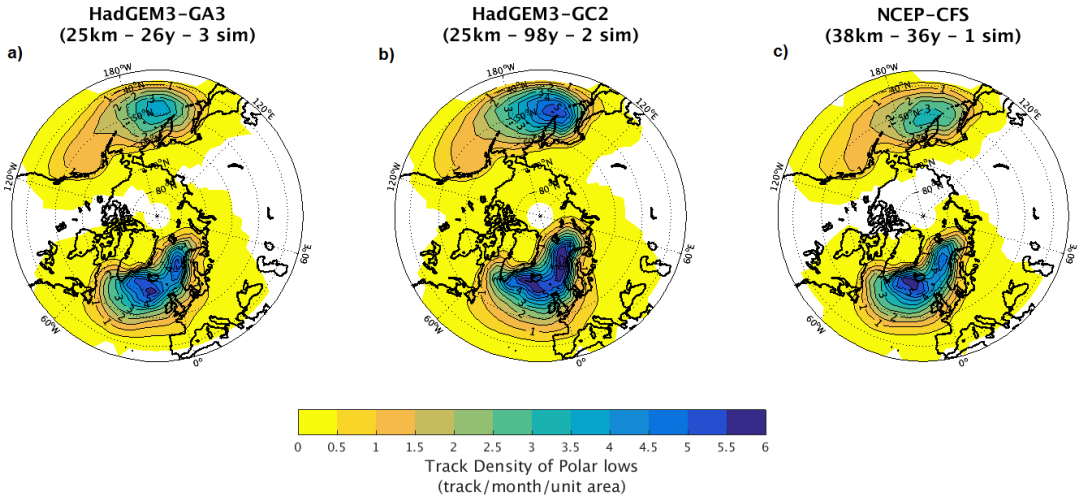

Figure 5-2: Track density (track per month per unit area) of PLs found (from October to March), over the Northern hemisphere with the N512 resolution of the atmosphere-only HadGEM3-GA3 climate model (a), the coupled HadGEM3-GC2 climate model (b) and the reanalysis NCEP-CFS (c).

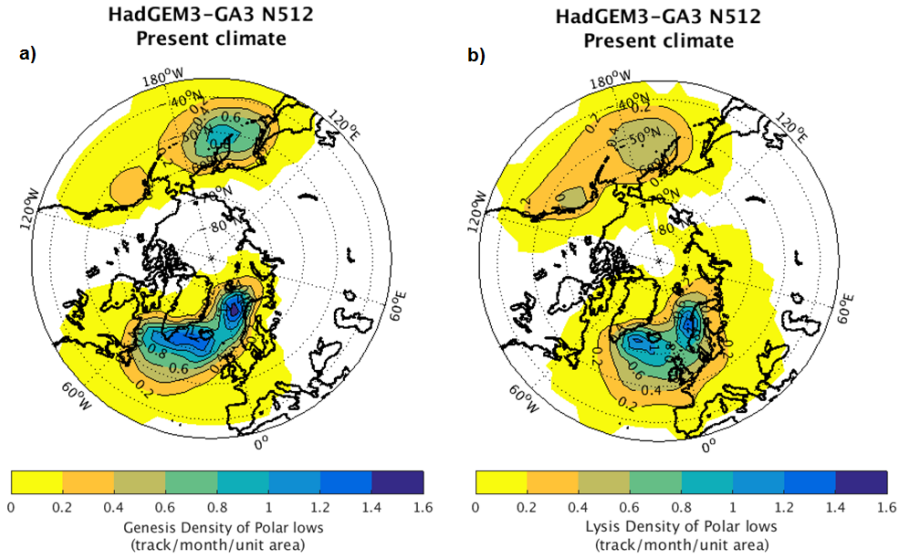

Figure 5-3: Genesis (a) and lysis (b) density of PLs found over the Northern hemisphere with the N512 resolution of the HadGEM3-GA3 climate model.

The genesis and lysis density of PLs in the present climate conditions of the climate model HadGEM3-GA3 (see Figure 5-3) were also analysed and compared to the ones from the HadGEM3-GC2 model and the NCEP-CFS reanalysis (see Chapter 4). Both densities were found within the range of the ones from the coupled climate model and the reanalysis, suggesting that the atmosphere-only climate model HadGEM3-GA3

is capable of representing the regions of genesis and lysis of PLs, over the Northern hemisphere.

Overall, this analysis of the representation of PLs (inter-annual and seasonal variability, environmental properties and spatial distribution) enables one to conclude that, at the horizontal resolution of 25 km, the atmosphere-only climate model HadGEM3-GA3 can reasonably represent present-day PLs within the range of results found with the ERA-I and NCEP-CFS reanalyses and the HadGEM3-GC2 coupled climate model.

5.2.2 The response of Polar lows to climate change in the high resolution N512 HadGEM3-GA3 climate model

As the atmosphere-only climate model HadGEM3-GA3 can reasonably well represent PL characteristics for the present-day climate conditions, the next step of the study is to investigate the PL characteristics under potential future climate conditions, from the RCP 8.5 scenario. In this section, only the results for present and future climates from the highest resolutions of HadGEM3-GA3 (i.e. N512, 25 km) are assessed, since PLs should be better represented at highest resolutions.

This analysis will start by investigating the large-scale environment and the differences between the present and the future climate conditions. As seen in Chapter 3 with the work done using the reanalyses, and as suggested by Zahn and von Storch (2010), the large-scale environment of PLs may influence PLs formation and occurrence. Thus if large discrepancies are found in the large-scale environment between both climate conditions, it is likely that PL occurrences will be affected by these changes.

5.2.2.1 Large-scale environment

The investigation of the synoptic conditions around PLs is analysed by looking at the differences in large-scale fields between the present and the future climate conditions.

Ensemble means of the three present climate and three future climate simulations are assessed for the Sea Ice Fraction (SIF), the temperature at 500 hPa (T500), the Sea Surface Temperature (SST) and the atmosphere temperature difference (i.e. $\Delta T = T500 - SST$). As previously seen for PL climatologies in the atmospheric reanalyses (see Chapter 3), these fields seem to be the ones that PL activity is most sensitive to.

Sea ice Fraction

The first aspect of the environment of PLs to be analysed is the Sea Ice Fraction (SIF).

Figure 5-4 presents the Sea Ice Fraction (SIF, from 0, no sea ice cover, to 1, maximal sea ice cover) from HadGEM3-GA3 N512 from the present and future climate condi-

tions, and for the difference between the future and the present climate conditions which is significant 5% level, for the ensemble mean of three members (each member being 26 years long).

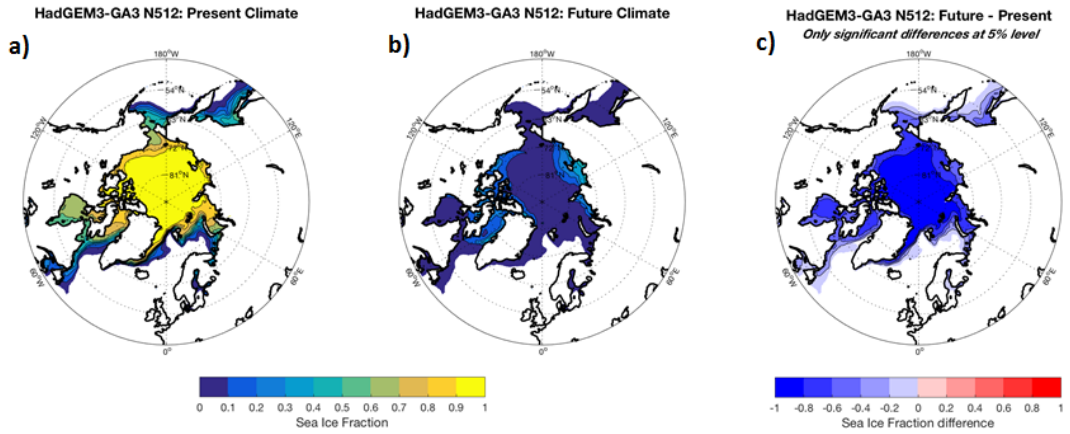

Figure 5-4: October to March Sea Ice Fraction (SIF) from HadGEM3-GA3 N512 (25 km, ensemble mean) from the present (a) and future (b) climate conditions, and for the difference, significant at 5% level, between the future and the present climate conditions (c), over the Northern hemisphere.

Figure 5-4a shows that the Arctic Ocean is almost completely covered with sea ice from October to March during the present climate, with a SIF generally higher than 0.8. This is consistent with current climatologies, as the sea ice starts to build up from October (after the September minimum) to a maximum in March. As expected the sea ice edges are less thick (SIF lower than 0.7) than the sea ice centered around the Pole. Figure 5-4b, representing the SIF for the future climate conditions, shows a clear decrease of the SIF almost everywhere, with a nearly completely ice free Arctic Ocean during the winter months, as seen from results from the CMIP5 multi-model mean showing a reduction of 34% and 94% of the Arctic sea ice extent for February and September respectively, with the RCP 8.5 between the 1986-2005 and 2081-2100 periods (Section 12.4.6 in Collins et al. (2013)[2]). Only a few areas (i.e. the East Siberian Sea, the Beaufort Sea and the Baffin Bay, and the Canadian Arctic Archipelago) are expected to have sea ice during the future extended winter season from HadGEM2-ES SIF forced with the RCP8.5 scenario (i.e. most extreme future climate scenario of the IPCC scenarios).

Figure 5-4c shows the difference between the future and present climate conditions

[2] Collins et al. (2013) corresponds to the Chapter 12 "Long-term climate change: projections, commitments and irreversibility" of the IPCC AR5 (IPCC, 2013).

in HadGEM3-GA3. A clear reduction in the SIF and sea ice extent over the Northern hemisphere in the future climate scenario can be seen, with a complete melting of the sea ice over the Arctic Ocean (with a SIF difference up to -1). Since the sea ice is projected to be much reduced over the Arctic Ocean (Stroeve et al., 2007, 2012), and thus the open ocean will increase, this may then lead to an increase in available area for PLs to develop.

	Mean	Std.
Present	0.4987	0.2552
Future	0.3337	0.2524
Future - Present	-0.1713	0.0677

Table 5.3: Mean and standard deviation values of the sea ice fraction, of the sea ice covered areas, for the present and the future climates, with the N512 HadGEM3-GA3 climate model, over the Northern hemisphere.

Table 5.3 shows the mean and standard deviation of the present, future and difference between present and future climates. A SIF mean of 0.499 (resp. 0.334) with a standard deviation of 0.255 (resp. 0.252) is found for the present (resp. future) climate conditions, over the Northern hemisphere. The N512 HadGEM3-GA3 climate model shows a general significant (p-value: 0.0115) decline of the SIF between the present and the future SIF. Hence a mean October-March decrease of around 32.42% of the SIF is seen in HadGEM3-GA3 between the present-day and the future climates (see Table 5.3). This results is slightly lower (probably due to the six-month average) the range of the CMIP5 multi-model mean, showing a decrease of the SIF of 34% in February and of 94% in September by the end of the century (Collins et al., 2013).

Sea Surface Temperature

As for the sea ice fraction, the Sea Surface temperatures (SSTs) are boundary conditions for the HadGEM3-GA3 model taken from the HadGEM2-ES simulations. The future SSTs are calculated as the present SSTs plus the difference between two late century periods (i.e. $SST_{future} = SST_{present} + \Delta SST_{future-present}$, see Chapter 2.1.3.2 and Jones et al. 2011). For the regions where the sea surface lost its sea ice coverage between the present and future scenario, the SST values were interpolated from the HadGEM2 results (Mizielinski et al., 2014).

Figure 5-5 represents the SSTs from HadGEM3-GA3 N512 from the present (a) and future (b) climate conditions, and for the significant (at 5% level) difference between the future and the present climate conditions (c), for the three 26-year members, over the Northern hemisphere. Figure 5-5a shows that the SSTs of the present climate range from 270 K (mainly along the sea ice edges and the land coasts) to 295 K (at latitudes

lower than 40°N). The future SSTs (b) shows a similar pattern of SSTs, but with a larger gradient of temperature, going up to 300 K (between 30° to 40°N of latitude). As the most of the sea ice is no longer over the Arctic Ocean, this open-water tends to warm up, which now leads the lower temperatures to only be found over the Canadian Arctic Archipelago waters. This increase (c) indicates a clear overall increase of the SSTs in the future, with a larger increase seen around the Arctic ocean (Meehl et al., 2007; Collins et al., 2013). This amplified surface warming over the Arctic might be associated with feedbacks such as the sea ice loss (Kumar et al., 2010; Screen and Simmonds, 2010).

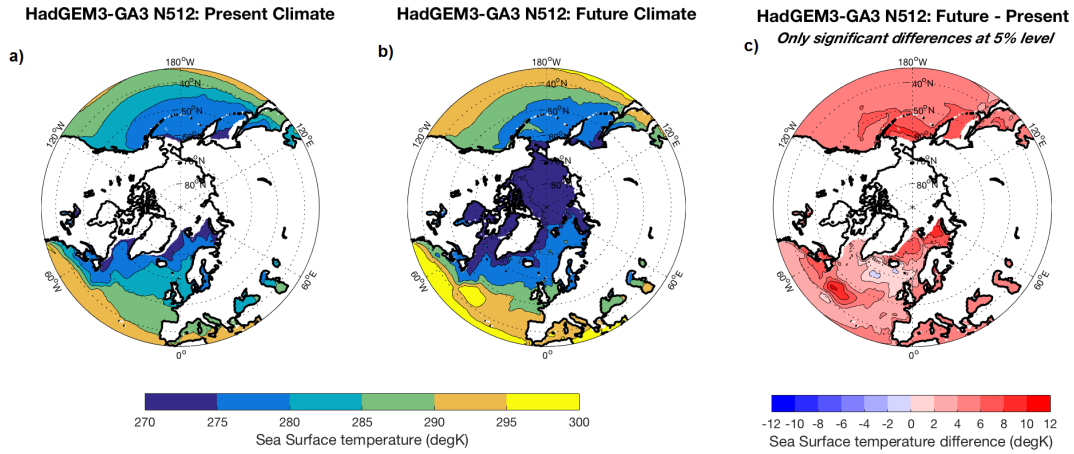

Figure 5-5: October to March Sea Surface Temperature (SST) from HadGEM3-GA3 N512 (25km, ensemble mean) from the present (a) and future (b) climate conditions, and for the difference, significant at 5% level, between the future and the present climate conditions (c), over the Northern hemisphere.

A smaller increase in future SSTs is found over the North Atlantic Ocean, with even a small negative anomaly in the Irminger Basin (c). This slower increase of the North Atlantic SSTs has previously been noted in different studies (Woollings et al., 2012; Collins et al., 2013). Gervais et al. (2018) investigated this temperature anomaly and suggested that this "warming deficit" in North Atlantic SSTs is associated with the interaction between the western current of the North Atlantic Meridional Overturning Circulation (AMOC) and the Labrador and East Greenland currents. As the AMOC slows down, the input of fresh water from the Arctic (through the Labrador and East Greenland currents) to the North Atlantic Ocean will increase and lead to an increase in surface freshening for this region which will reduce the Labrador Sea deep convection. These changes will then lead to "enhanced transport of cooler Labrador Sea surface waters into the interior of the sub-polar gyre" which will result in a "warming deficit"

in the North Atlantic SSTs.

	Mean	Std.
Present	288.3490	1.8636
Future	290.2108	1.8471
Future - Present	1.8618	-0.0165

Table 5.4: Mean and standard deviation values of the sea surface temperature (SST, in K) for the present and future climate conditions, with the N512 HadGEM3-GA3 climate model, over the Northern hemisphere.

An mean increase of +2 K of the SST can be seen between the present-day and future climates (Table 5.4). This positive tendency is in agreement with the increase found with the CMIP5 multi-model mean projections (see Figure 12.12 in IPCC 2013). As the standard deviations of the present and future climates are relatively similar, a relatively constant standard deviation of the SST values is seen between both climates. With a p-value of 0.0016, the general t-test indicates that the future-present difference for the N512 HadGEM3-GA3 model is statistically significant.

Hence, with the highest resolution of the HadGEM3-GA3 climate model, a significant difference is found between the present and future SSTs.

Mid-tropospheric Temperature

The next step is to study the future changes in the 500 hPa temperatures (T500) over the Northern hemisphere.

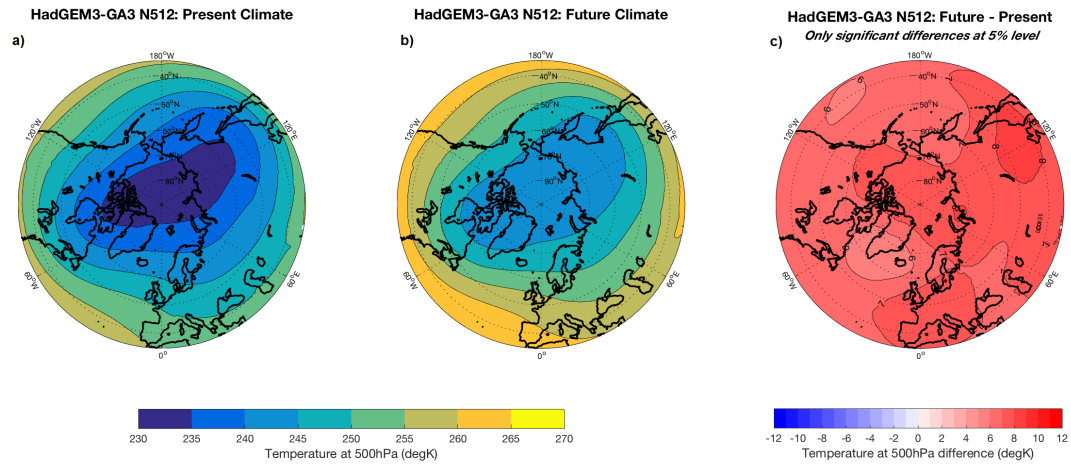

Figure 5-6: Extended winter (October-March) temperature at 500 hPa (T500) from HadGEM3-GA3 N512 (25 km, ensemble mean) from the present (a) and future (b) climate conditions, and for the difference, significant at 5% level, between the future and the present climate conditions (c), over the Northern hemisphere.

Figure 5-6 shows the ensemble mean of the 500 hPa temperature (T500) from the HadGEM3-GA3 N512 simulations for the present (a) and future (b) climate conditions, and for the significant (at 5% level) difference between the future and present climate conditions (c). A clear increase of the mid-tropospheric temperatures can be seen between the present and the future climates. The minimum T500 is observed to increase of almost +10 K (between 230 and 240 K) over the Arctic Ocean (as seen on left and middle panels). On the right panel, an increase between +6 and +11 K, between the present and future climate conditions, is seen. This general increase in mid-tropospheric temperatures over the Northern hemisphere is in accordance with previous studies of future climate projections (Mallet et al., 2017; Collins et al., 2013).

	Mean	Std.
Present	251.4821	1.4092
Future	257.4874	1.2854
Future - Present	6.0051	0.4610

Table 5.5: Mean and standard deviation values of the temperature at 500 hPa (T500, in K) for the present and future climate conditions, with the N512 HadGEM3-GA3 climate model, over the Northern hemisphere.

Table 5.5 presents the mean and standard deviation values of the mid-tropospheric temperature (T500) for the present and the future climates and their difference. A T500 mean value of 251.48 (resp. 257.50) with a standard deviation of 1.41 (resp. 1.28) is found for the present (resp. future) climate conditions, over the Northern hemisphere. The future-present difference between for the high resolution HadGEM3-GA3 climate model is statistically significant (p-value $< 10^{-5}$), with a mean difference of +6 K. Therefore, with the highest resolution of the HadGEM3-GA3 climate model, a significant difference is observed between the present and future mid-tropospheric temperatures.

Atmospheric Static stability

As seen in the above sections, both sea level and mid-level temperatures increase in the future climate climates, but the mid-tropospheric ones rise faster than the surface temperatures. This difference will then lead to a increase in static stability ($\Delta T = T500 - SST$) in the atmosphere in the future scenario.

Figure 5-7 shows the ensemble mean of atmospheric temperature difference for the present (a) and the future (b) climates and the significant (at 5% level) difference between the future and the present climate (c), at 25 km resolution in the HadGEM3-GA3 model.

Present and future climates have atmospheric temperature difference ΔT values

between -24 and -42 K, but an augmentation of the stability can be seen on the future climate map (b). An overall increase of the static stability between the present and future climate for the HadGEM3-GA3 model can be inferred from the temperature difference map (right panel). This increase is particularly apparent over the North Atlantic ocean. As Zahn and von Storch (2010) and Mallet et al. (2017) showed, this increase is due to the future faster increase of the mid-tropospheric temperatures compared to the sea surface temperatures (increase of around +2 to +4 K for the SST and of around +6 to +11 K for the T500 over the North Atlantic Ocean).

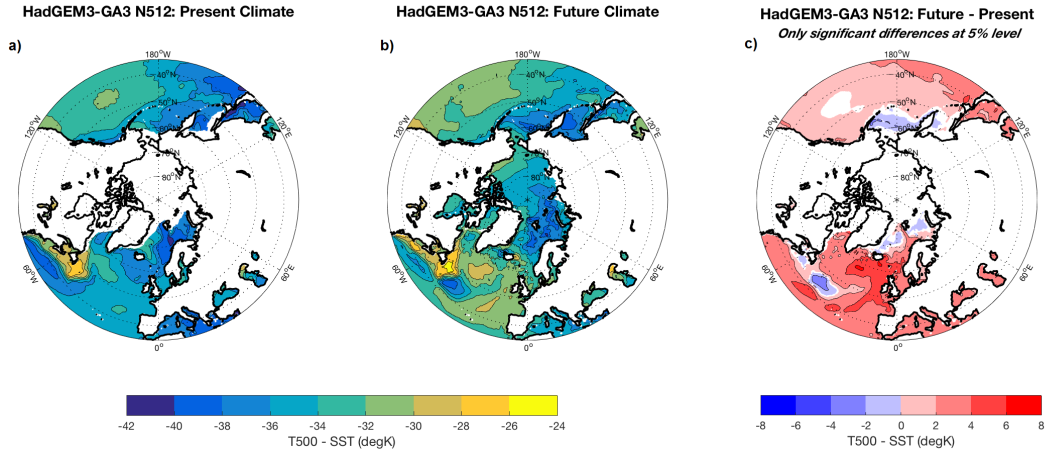

Figure 5-7: Ensemble mean of the difference in temperature between 500 hPa and the surface for the present (a) and the future (b) climates and the difference, significant at 5% level, between the future and the present climate (c), from October to March, with the N512 HadGEM3-GA3 climate model.

In some regions, a decrease in future temperature difference ΔT (i.e. negative anomaly of temperature difference) can be seen, indicating that the surface warming is higher than the mid-troposphere warming (i.e. difference in SST is higher than the difference in T500). This occurs where a sea ice loss is observed (i.e. along the sea ice edge over the Nordic Seas and over the Bering and Okhotsk Seas) and where the SST warming deficit is observed, over the North Atlantic Ocean (Woollings et al., 2012; Gervais et al., 2018).

Table 5.6 shows the mean and standard deviation values of the temperature difference ΔT for the present and the future climates and their difference.

A increase of the mean value of around 2 K is seen between the present and future climate conditions. A mean value of ΔT of -33.03 K (resp. -31.01 K) with a standard deviation of 1.57 (resp. 1.70) is found for the present (resp. future) climate conditions, over the Northern hemisphere. The future-present difference between for the N512

	Mean	Std.
Present	-33.0345	1.5663
Future	-31.0140	1.6960
Future - Present	2.0476	0.8748

Table 5.6: Mean and standard deviation values of the atmospheric temperature difference (ΔT, in K) for the present and future climate conditions, with the N512 HadGEM3-GA3 climate model, from October to March, over the Northern hemisphere.

HadGEM3-GA3 climate model simulations is statistically significant (p-value: 0.0107), with a mean of +2.05 K.

In the region where the static stability increases, the future atmosphere might become more stable than the present one, which could contribute to hindering PL formation. This decrease of PL numbers would be observed in numerous areas, and especially in the North Atlantic as in Zahn and von Storch (2010).

This possible future increase in atmospheric stability has previously been shown in Mallet et al. (2017). This study used a coupled general circulation model to assess PL development over the North Atlantic Ocean under a warmer climate. Mallet et al. (2017) found that favourable conditions for PLs are expected to occur less often in the future climate, due to a strong increase of the North Atlantic static stability (see their Figure 2 based on the SST-T500 wintertime difference between the present and future climate conditions). However, they also noticed that the future large-scale circulation variability would have less influence on the atmospheric stability and thus on PL activity (i.e. the difference of large-scale environment patterns between years with high and low PL numbers will be less clear).

The future increase in static stability over the North Atlantic Ocean was also analysed by Woollings et al. (2012). They suggested that, although the temperature increase at both surface and mid-tropospheric levels is strongly correlated with the global warming, the static stability (i.e. the temperature difference between the surface and the mid-troposphere) might be more related to the changes in the Atlantic Meridional Overturning Circulation (AMOC). Indeed, as the AMOC is projected to weaken under climate change, Woollings et al. (2012) found that this would results in a "local minimum in warming in this region". As this lower increase in warming would be confined to the surface, this would lead to an increase in static stability in the area.

Therefore, the general increase in static stability could be due to the global faster increase in the mid-tropospheric temperatures (compared to the sea surface temperatures), and the local large increase in static stability over the North Atlantic Ocean could mainly be due to this local minimum of the SST which might be explained by the

slow down of the AMOC previously mentioned (Woollings et al., 2012; Gervais et al., 2018).

As seen in this section, the large-scale environment is projected to be different under climate change. With the RCP 8.5 scenario, the Arctic sea ice extent and volume is expected to greatly decline. This decrease could lead to a larger open-ocean area available for PLs to form. Thus some regions (such as the area along the northern Russian coasts or the Hudson Bay) may experience an increase of PL activity. On the other hand, the surface and mid-tropospheric temperatures over the Northern hemisphere, are projected to increase in the future. As the mid-tropospheric temperatures might increase faster than the surface temperatures, an increase in atmospheric static stability is to be expected in the future (especially over the North Atlantic Ocean). This increase of the static stability may inhibit PL formation and may result in a decline of PL occurrences in the future climate.

5.2.2.2 Polar lows in the model

Now that the differences between the present and future large-scale environment have been studied, the response of PLs to those changes is explored.

Inter-annual variability of Polar low numbers

The total number and the inter-annual variability of PL numbers between the historical and future climate conditions is first examined.

Table 5.7 presents the mean number and standard deviation of PL numbers found per year in HadGEM3-GA3 N512, for the historical climate conditions and the future climate scenario, over the Northern hemisphere.

	Present Climate	Future Climate
Ens. mean	93.38	35.22
Standard dev.	8.13	5.15
95 % confidence interval	[77.08; 109.67]	[25.12; 45.31]

Table 5.7: Statistics of PL numbers found per year in the HadGEM3-GA3 N512 climate model, for the present climate conditions and the future climate scenario, for three members of 26 years over the Northern hemisphere.

The numbers of PLs over the entire Northern hemisphere are found to decrease between the present and the future climate scenarios. Numbers are found to decline from 93.38 PLs per year (std: 8.13) in the present climate to 35.22 PLs per year (std: 5.15) in the future climate scenario. This represents a decrease of more than 62% of PL numbers in the high-resolution simulations from the HadGEM3-GA3 model.

The possibility of a decrease of PL numbers in the future over the North Atlantic Ocean has previously been discussed at the beginning of this Chapter. In their downscaling study, Zahn and von Storch (2010) noticed a decrease of almost 53% of PL numbers between the present and future climate scenarios in a smaller domain (North east Atlantic Ocean and Nordic Seas). If both studies have relatively similar lengths (29 years for Zahn and von Storch (2010) and 26 years for this study), they use different tracking algorithms (respectively of the MSLP minima and the relative vorticity maxima), with different horizontal resolutions (50 km for Zahn and von Storch (2010) and 25 km in this study), over different seasons (for a July to June period for Zahn and von Storch (2010) and for an October to March period in this study), and over different regions (North Atlantic Ocean and Nordic Seas for Zahn and von Storch (2010) and the entire Northern hemisphere in this thesis). Furthermore, both studies use different climate projections (from IPCC-AR4 in Zahn and von Storch (2010) and IPCC-AR5 in this study) likely to show different results. However, despite of all these differences, both studies are in accordance regarding the possible future decrease of half of PLs current number. More recently, Romero and Emanuel (2017) found, in 30 CIMP5 models with both historical (1986-2005) and RCP8.5 (2081-2100) simulations, a reduction of 10% to 15% in the overall frequency of PLs (generated via a statisticalâdeterministic method) over the North Atlantic Ocean. If these percentages are lower than those found in this study and in Zahn and von Storch (2010), they still reflect that PLs might encounter a decrease of their number within the end of this century.

Therefore, although different, the numbers of PLs results found with the high-resolution HadGEM3-GA3 over the Northern hemisphere tend to be in accordance with previous studies, and all results converge towards a decline of PL occurrences.

Seasonal variability of Polar low numbers

As well as the inter-annual variability of PL numbers, the present and future seasonal variability of PL numbers is also investigated.

Figure 5-8 shows the mean annual cycle of PL numbers averaged over the three 26-year members of the N512 HadGEM3-GA3 model, for the present (blue) and the future (red) climates, over the Northern hemisphere. As expected, the general decrease of PL numbers is also present in the seasonality of PL numbers. Between the present and future climates, the minimum PLs number goes from 4 to 0 PLs per month and the maximum number of PLs decrease from 28 to 12 PLs per month. Furthermore, less variability is observed in the future climate compared to the present climate (i.e. the ranges between the 25% and 75% percentiles and the minimum and maximum outliers are smaller in the future climate).

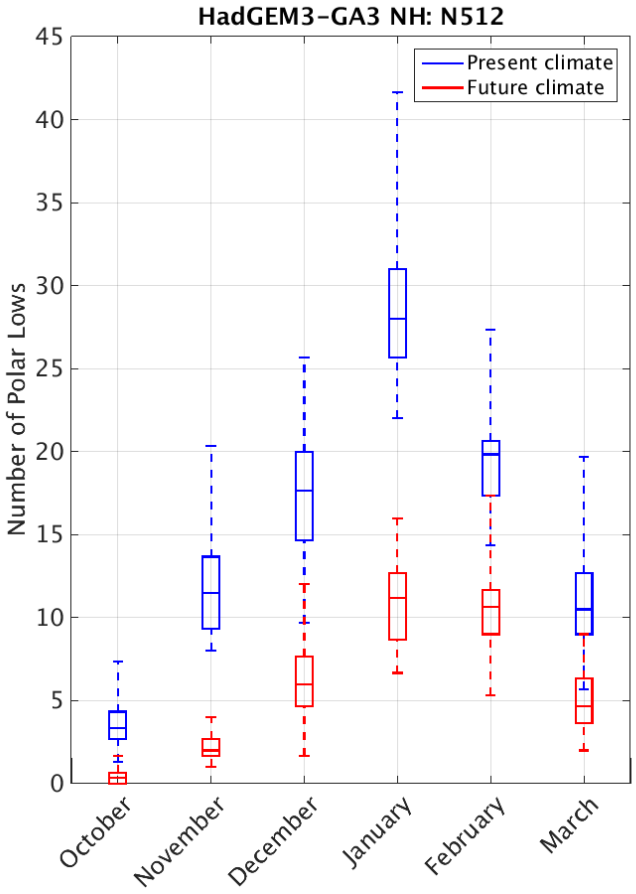

Figure 5-8: Mean seasonal cycle of PL number for the present (blue) and the future (red) climate conditions, with the N512 HadGEM3-GA3 climate model, over the Northern hemisphere.

The seasonality of PL numbers, however, appears relatively similar for both climate conditions, with an increase of PL numbers from October to a maximum PL numbers in January, and then a slower decrease up to March. A slower increase is noted in the future climate in October and November. This slower increase in PLs future seasonal cycle could be due to the pronounced lack of sea ice in the early winter season. Indeed, in the monthly observations of sea ice fraction in the future climate a totally ice free Arctic Ocean can be seen. The sea ice only starts to build up from December (not shown), along the Russian coastlines and around the Canadian Archipelago. This late appearance of sea ice may be associated with the future shift of the main PLs season.

Spatial distribution of Polar lows

As large changes in the future atmospheric large-scale environment are expected in the future climate scenario, a difference in present and future PL regions of activity may

appear. The next step investigates the response of PLs to climate change through their spatial distribution.

Figure 5-9 shows the ensemble mean track density of PLs, for the Northern hemisphere, for the present (a) and the future (b) climate and for the difference, significant at 5% level, between the future and the present climate (c) for the N512 resolution of the HadGEM3-GA3 climate model. As previously discussed in Chapter 2, the track density is shown as the number of PLs per month per unit area (which corresponds approximately 10^6 km^2).

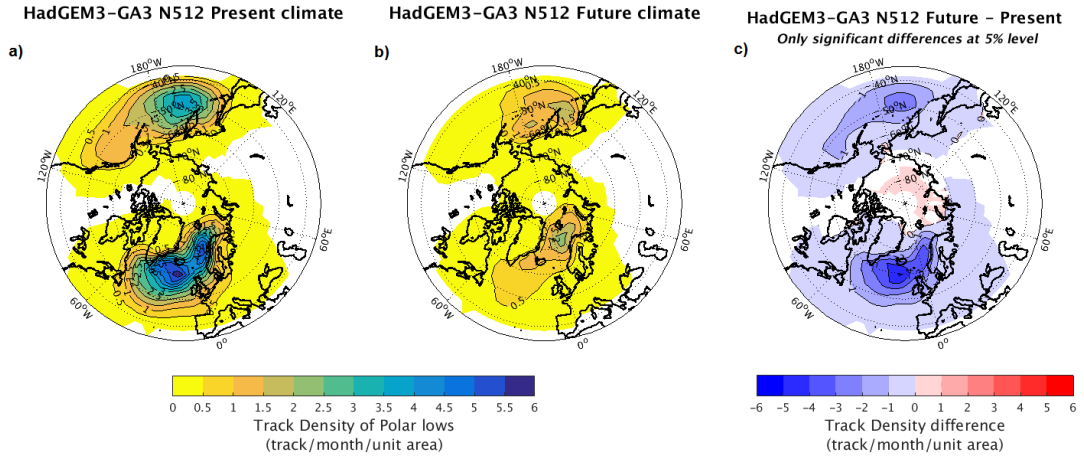

Figure 5-9: Track density (track per month per unit area) of PLs found, from October to March, with the N512 HadGEM3-GA3 model (ensemble mean), for the present (a), the future (b) and the difference, significant at 5% level, between the present and future climate (c), for the three ensemble members of 26 years.

As seen on Figure 5-9a, the historical PLs track density is mainly organised into three main storm tracks, with PLs occurring over the North Atlantic Ocean, over the Nordic Seas (i.e. Greenland, Norwegian and Barents Seas) and over the North - North-West Pacific Ocean. Figure 5-9b shows that in the future climate, the current PL regions will remain active PLs regions, but will experience a reduction in PL numbers.

The difference, at a 5% significance level, between the spatial distribution of PLs in the future and present (Figure 5-9c) indicates a general clear decrease of PL track density over the Northern hemisphere under climate change. This general decline of PL numbers is consistent with the future changes in the large-scale environment discussed previously. The strongest reduction (maximum of -5 PLs per month per unit area) occurs over the North Atlantic Ocean and the Norwegian Sea. This decline can mainly be explained by the increase in atmospheric static stability in this particular region, consistent with Zahn and von Storch (2010). Furthermore, an increase of PLs track

density can be seen over the Arctic Ocean. This increase in PL density may be due to the lack of sea ice coverage in the future in these areas, increasing the available space for PLs to develop. This result thus indicates the possibility of new regions for PLs to occur, as well as a northward shift in PL activity under climate change.

Therefore the change in the future large-scale environments of PLs thus not only affect PL numbers but also the regions they can be found in, with current PL regions encountering a decrease in PL numbers whilst new regions of PL formation might appear.

The future of PL genesis and lysis distributions (i.e. growth and decay regions) has also been investigated.

Figure 5-10 shows the genesis density of PLs for the present (a), future (b) and the difference, at the 5% significance level, between the present and the future climate conditions (c) for the three members of 26 years over the Northern hemisphere.

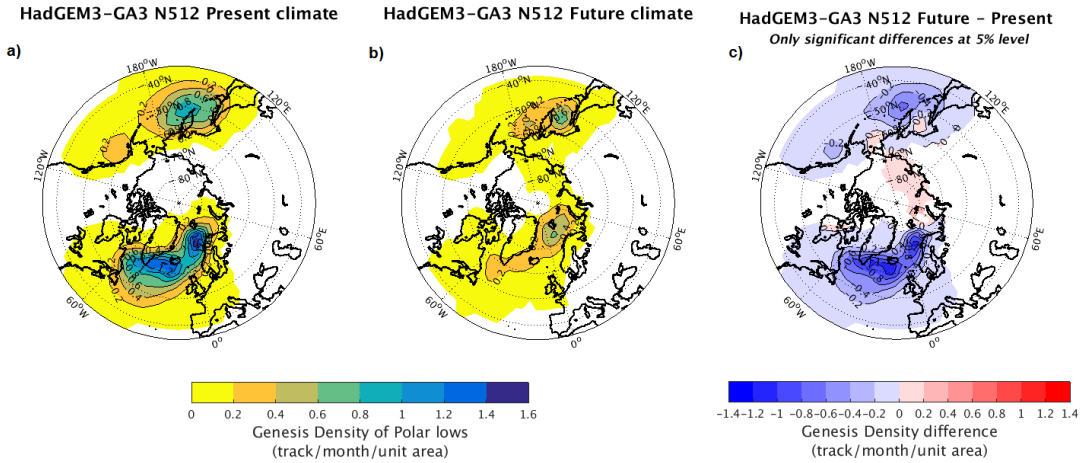

Figure 5-10: Genesis density of PLs found, from October to March, with HadGEM3-GA3 N512 (25km, ensemble mean) for the present (a) and future (b) climate conditions, and the difference, significant at 5% level, between the present and the future climate conditions (c), over the Northern hemisphere.

As for the PL track densities in Figure 5-9, Figure 5-10 indicates large changes between the present-day and future in the amplitude of PLs genesis density. For the historical climate, three regions of maximum genesis density can be observed: one between Greenland and Iceland, one over the Greenland and Norwegian Seas, and one East of the Russian Kamchatka region in the Pacific Ocean. In the future climate scenario (b), the maximum PLs genesis density region between Greenland and Iceland seems to disappear, probably because of the large increase in static stability (i.e. temperature difference ΔT) in this region. The two other genesis density maxima are still

in the same place but their magnitudes have clearly declined. Furthermore, similarly to the track densities, new regions of PL genesis emerge over the Arctic Ocean, mainly along the coasts of Russia, and regions experience an increase in PL numbers, such as the Kara Sea, the Bering Strait or the Okhotsk Sea. All these changes in future PLs genesis can be clearly observed in Figure 5-10c.

Figure 5-11 shows the lysis density of PLs for the present (a), the future (b) and the difference, at the 5% significance level, between the present and the future climate conditions (c) for the three members of 26 years, over the Northern hemisphere.

Consistent with the track and genesis densities, a decrease in the lysis density is observed between the present and the future climate conditions (Figure 5-11 a and b). This is in accordance with the general decrease of PL numbers discussed previously. The current main regions of PL lysis in the Atlantic (Irminger Basin and Norwegian Sea) and Pacific (east of Russian Kamchatka peninsula and south of Alaska state) Oceans are almost negligible in the future. These changes can also be seen on the lysis density difference map (c), where a general decrease is seen almost everywhere, but mainly in the regions previously mentioned. However, as previously remarked for the track and genesis densities, a small future increase of lysis density is perceived over the Arctic Ocean, along the Nansen Basin. These increases are in agreement with the future increase of PL occurrences in those regions.

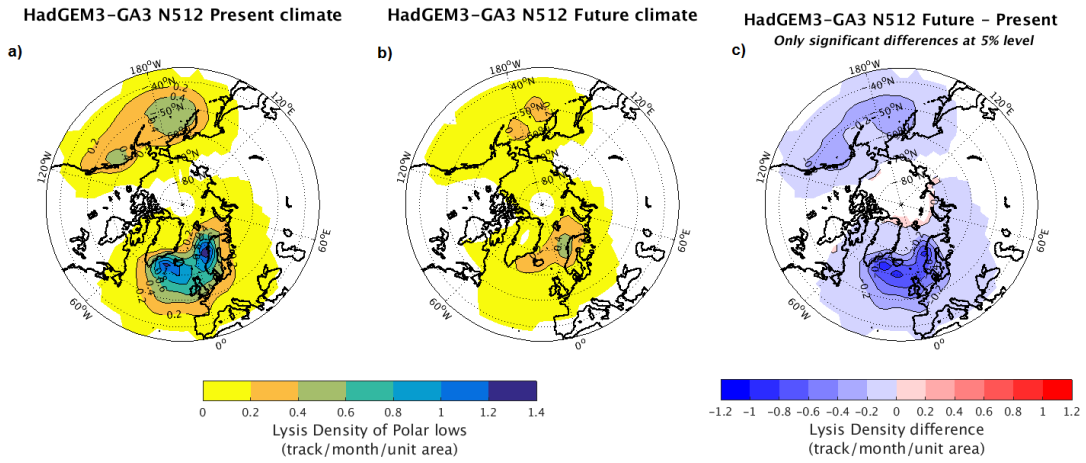

Figure 5-11: Lysis density of PLs found, from October to March, with HadGEM3-GA3 N512 (25km, ensemble mean) for the present (a) and future (b) climate conditions, and the difference, significant at 5% level, between the present and the future climate conditions (c), over the Northern hemisphere.

This part of the study with the high-resolution simulations of the atmosphere-only climate model HadGEM3-GA3 is consistent with previous results from Zahn and von

Storch (2010) and Romero and Emanuel (2017) on the response of PLs to climate change. Within a future climate similar to the RCP 8.5 future climate scenario, it is thus likely that one would observe a substantial decrease (of approximately 60%) of PL occurrences over the Northern hemisphere. This decrease is likely to mainly be due to an increase in the static stability of the atmosphere, due to a faster increase of the mid-tropospheric temperature compared to the increase of the sea surface temperature. This statement will be particularly accurate over the North-Atlantic ocean and the Nordic Seas, as this regions is the one experiencing the strongest increase in static stability in the future. A shift of the seasonality of PLs is also seen in the future, due to the lack of Arctic sea ice and a warmer atmosphere during the beginning of the extended winter season. Finally, even though most of the current PL regions might experience a decrease in PL numbers, some other regions which may have a sea ice free future during winter, might see PLs occur in them, as new open ocean areas will appear.

5.2.3 Present and future sensitivity of Polar low numbers and spatial distribution to Polar lows identification criteria

As previously in Section 5.2, PLs may experience a decline of their occurrences almost everywhere over the Northern hemisphere due to climate change. In the changing climate, one question which could be raised is whether the climate change response in the number of PLs is sensitive to the exact definition used for PLs identification. If so, would the identification criteria used in this thesis still be suitable for PL studies?

As seen earlier in this Chapter, the large-scale environment conducive to PLs will drastically change. Hence, these changes could potentially influence PLs occurrences and their dynamic and thermodynamic characteristics. However, changing the PLs identification criteria would suggest a change in the current definition of PLs. This change in PLs definition would then prevent one to compare the present-day and future PLs in a robust manner.

To investigate the climate change response of PL numbers to the identification criteria, a sensitivity study is performed with the N512 resolution of HadGEM3-GA3. For each simulation of both present and future climate conditions, the yearly numbers of PLs found when changing only one identification criterion are analysed, as well as the ranges of the distributions of these criteria (e.g. the range of vorticity values found for PLs when changing the different criteria) and the spatial distribution of PLs.

Table 5.8 presents the mean numbers and standard deviations of PLs found each year, over the Northern hemisphere, for both present and future climate scenario. The percentage of change between present and future climates, for different thresholds of

the identification criteria is also shown. The first line "Control" represents the original criteria of this study (i.e. a maximum vorticity greater than 6×10^{-5} s^{-1}, a maximum wind speed greater than 15 $m.s^{-1}$ and a minimum temperature difference ΔT lower than -43 K) as defined in Chapter 2. The other lines show the results when changing one criterion at a time: first the vorticity threshold, set at 0, 6 and 9×10^{-5} s^{-1}, then the wind speed threshold, set at 0, 15 and 18 $m.s^{-1}$, and finally the atmosphere temperature difference threshold, set at -43, -39 and 0 K.

As previously seen, a future decrease of 62.15 % of PL numbers is expected over the Northern hemisphere. A decrease of PL numbers is observed, for every set of criteria tested. When looking at the present climate mean numbers of PLs, it is clear that having relaxed thresholds for the three variables (i.e. thresholds set at 0) induces in relatively unrealistic high PL numbers. In the same way, having rather strict identification criteria gives either slightly too low ($\xi > 9\times10^{-5}$ s^{-1} and WS > 18 $m.s^{-1}$) or still too high ($\Delta T <$ -39 K) PL mean numbers.

When looking at future PL numbers, the differences in PL numbers are smaller (as the numbers are lower), except when no stability criterion is applied for the atmosphere.

In addition, regardless of the climate conditions and the threshold value applied, the percentage change between the present and future climates is smaller when relaxing the criterion's threshold compared to when applying a more restrictive threshold. These indicates that, whether changing the thresholds of the identification criteria or not, the future PL numbers are expected to substantially decline by 47% to 88%.

	Present climate		Future climate		Percentage
	Mean nb.	Std. dev.	Mean nb.	Std dev.	of change
Control	93.05	9.70	35.22	5.15	-62.15 %
$\xi > 0\times10^{-5}$ s^{-1}	156.70	14.63	47.32	4.96	-69.80 %
$\xi > 9\times10^{-5}$ s^{-1}	30.55	5.10	3.64	1.33	-88.09 %
WS > 0 $m.s^{-1}$	102.36	10.42	30.19	3.99	-70.51 %
WS > 18 $m.s^{-1}$	69.33	8.86	9.97	1.95	-85.62 %
$\Delta T <$ -39 K	209.93	14.92	60.36	5.57	-71.25 %
$\Delta T <$ 0 K	674.10	22.97	353.85	16.87	-47.51 %

Table 5.8: Mean number of PLs and their standard deviation found each year over the Northern hemisphere with the N512 HadGEM3-GA3 model, for both present and future climate conditions for different identification criteria for the vorticity ("ξ", with values higher than 0, 6 or 9×10^{-5} s^{-1}), the wind speed ("WS" , with values higher than 0, 15 or 18 $m.s^{-1}$) and the temperature difference ("$\Delta T = T500 - SST$", with values lower than -43, -39 or 0 K).

The probability density functions (PDFs) of the distribution of the PL aspects used in testing these criteria (e.g. the PDF of the along-track vorticity found when changing the different criteria, one at a time) were also analysed for both present and

future climate conditions, and compared to the distributions with the original set of criteria.

The PDFs of the maximum vorticity and the maximum wind speed are relatively similar to their PDFs with the original criteria. As expected changing the threshold of the vorticity (wind speed) has a greater impact on the vorticity (wind speed) PDF, as it tends to shift the distributions to lower or higher values. Lowering the stability threshold to -39 K does not seem to affect the vorticity and wind speed distributions (present and future climates), but applying no stability threshold tends to impact the present and future vorticity distributions only, by including higher values of vorticity (not shown). As this statement only applies to the vorticity distributions, this implies an impact of the stability of the atmosphere on the maximum vorticity of PLs.

Figure 5-12 shows the PDFs of the atmosphere temperature difference ΔT of PLs found for the present (left panel) and future (right panel) climate scenarios, for the original set of identification criteria (black dotted line) and when changing one criterion at a time (coloured lines). For the present climate conditions, the temperature difference PDFs lie on the PDF with the original criteria, except for the ones when changing the threshold for the stability criterion (i.e. green and light blue lines). This means that both vorticity and wind speed do not seem to influence the difference in temperature of the present climate. As expected, when relaxing the threshold for the temperature difference, both distributions (i.e. green and light blue lines) encompass larger ranges of temperature differences. For the future climate, the PDFs aspect is relatively the same as the PDFs for the present climate, with larger ranges and lower values of temperature difference values when changing the threshold of the stability criterion, but with a (less large curve). Some small changes can be observed for the future temperature difference when applying a high vorticity threshold (orange line), meaning that high vorticity thresholds would probably decrease the future range of static stability values. However, sensitivity to the different thresholds does not lead to the need to change the identification criteria which have been used to identify PLs in this study.

The last aspect explored here was the present and future spatial distributions (i.e. track density difference between present and future climates) of PLs when changing the identification criteria (not shown). For the different thresholds used, all showed similar results: the numbers of PLs found might change, but no obvious differences in the spatial pattern of PL occurrences is seen when changing one of the identification criteria, whether with the present or the future climate conditions.

Overall, this sensitivity analysis indicates that the substantial decrease in the num-

ber of PLs seen in the future simulations with the N512 HadGEM3-GA3 model, are mainly insensitive to the exact definition used to identify PLs.

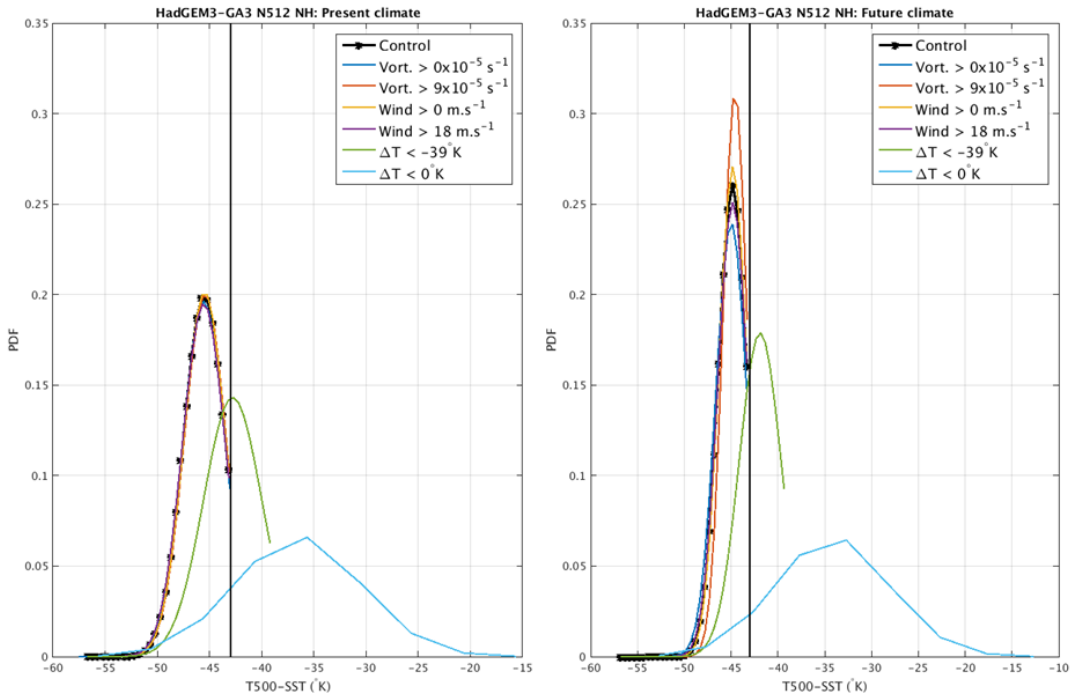

Figure 5-12: Probability density functions of the temperature difference (ΔT=T500-SST) for the present (left panel) and future (right panel) climate conditions, with the original identification criteria (black dotted line) and when changing one criterion at the time (dark blue: $\xi > 0{\times}10^{-5}$ s^{-1}, orange: $\xi > 9{\times}10^{-5}$ s^{-1}, yellow: WS > 0 m.s^{-1}, purple: WS > 18 m.s^{-1}, light green: $\Delta T <$ -39 K, light blue: $\Delta T < 0$ K). The vertical line, at -43 K, represents the threshold used in this study.

5.3 The impact of the horizontal resolution on the representation of PLs in the HadGEM3-GA3 climate model

The last part of the study is to assess the impact of the horizontal resolution of the model on the representation of PLs. PLs activity is thus studied and compared in the present and future climates of the atmosphere-only climate model HadGEM3-GA3, at the horizontal resolutions of N512 ($\sim$ 25 km), N216 ($\sim$ 60 km) and N96 ($\sim$ 130 km), over the Northern hemisphere.

5.3.1 Impact of the model resolution in the present-day climate representation of Polar lows

The impact of the model resolution on PLs representation is first assessed by looking at mean numbers and standard deviations of PL numbers and their characteristics in the present-day climate of the three horizontal resolutions of HadGEM3-GA3.

Table 5.9 shows, for the Northern hemisphere, the mean and standard deviation values of the PL numbers, the maximum vorticity, the maximum wind speed, the minimum temperature difference (ΔT) and of the duration of PLs, as well as the percentage of PLs which have a lifetime shorter than 24 hours, shorter than 48 hours and longer than 72 hours.

PL means range between 38.81 PLs per year (N96 resolution) and 93.38 PLs per year (N512 resolution), with standard deviation of PL numbers of 5.17 and 8.13 for the N96 and N512 resolutions respectively (72.09 PLs per year for the N216 resolution). As seen previously in this chapter, the mean numbers of PLs from the N512 simulations for the present-day climate are relatively close to the ones from the NCEP-CFS reanalysis and the HadGEM3-GC2 coupled climate model. Hence it might be thought that the mean number of PLs for the present climate simulations found with the coarser resolutions of HadGEM3-GA3 might be too small, and therefore show a different representation of PL activity over the Northern hemisphere compared to the ones of the reanalyses. If the mean numbers are different, the standard deviations of PL numbers are relatively small. In a previous study from Jung et al. (2006), the coarser horizontal resolution of the ECMWF model was also found to underestimate the total number of extra-tropical cyclones over the Northern hemisphere. Jung et al. (2006) suggested that at coarse resolutions the misrepresentation of the orography, as well as the "excessive dissipation" of the kinetic energy at meso- and sub-synoptic scales could be at the origin of too few extra-tropical cyclones.

For the maximum vorticity, maximum wind speed and minimum temperature difference (ΔT), all mean values are relatively similar. The largest differences between the mean values is observed for the maximum wind speed, with values going from 18.69 $m.s^{-1}$ to 20.49 $m.s^{-1}$. The mean values of maximum vorticity vary around 8.50×10^{-5} s^{-1}, and those of the temperature difference around -45.50 K. These results may indicate that, whether the chosen horizontal resolution of the climate model HadGEM3-GA3 is high or coarse, the mean values of vorticity and temperature difference are not greatly affected by the resolution. However, an increase of around 10% of the wind speed is seen between the coarser and higher resolutions. These results are in accordance those of Jung et al. (2006), showing that the key characteristics of extra-tropical cyclones in

the ECMWF model were found to also be sensitive to horizontal resolution chosen.

		N512	N216	N96
Number of PLs	Mean	93.38	72.09	38.63
	Standard dev.	8.13	8.20	5.17
Vorticity ξ	Mean	8.53	8.43	8.49
	Standard dev.	2.14	2.04	2.03
Wind speed WS	Mean	20.49	19.55	18.69
	Standard dev.	3.40	3.07	2.80
Temperature difference ΔT	Mean	-45.49	-45.56	-45.52
	Standard dev.	2.00	2.07	2.08
Duration of PLs	Mean	25.60	25.84	22.63
	Standard dev.	14.24	14.12	12.51
	Lifetime $<$ 24 h	50.31 %	49.15 %	59.64 %
	Lifetime $<$ 48 h	91.94 %	92.23 %	95.58 %
	Lifetime $>$ 72 h	0.77 %	0.91 %	0.33 %

Table 5.9: Mean and standard deviation of the numbers of PLs, the along-track maximum vorticity (x10^{-5} s^{-1}), maximum wind speed ($m.s^{-1}$), the minimum temperature difference (K), and of the duration of PLs (h), as well as the percentage of PLs which have a lifetime shorter than 24 and 48 hours and longer than 72 hours, for the present-day climate conditions of the three horizontal resolutions (N512, N216 and N96) of the atmosphere-only HadGEM3-GA3 climate model, over the Northern hemisphere.

The mean and standard deviation of PLs lifetime, for the three horizontal resolutions appear to be relatively similar, with a mean lifetime of PLs around 25.70 h and a standard deviation around 13.60 h. The small difference between the highest resolutions and the N96 resolution may be explained by the coarse horizontal resolution not capturing the entire track of PLs or missing the beginning or the end of PL tracks. However, this could also be due to the fact that PLs captured with the N96 resolution are shorter than those of the N512 and N216 resolutions. In particular, the numbers of PLs lasting longer than 72 hours only represent less than 1% of each distribution. On the other hand, the numbers of PLs lasting less than 24 hours represent more than 49% of each distribution, and the numbers of PLs lasting less than 48 hours represent more than 91% of each distribution. Hence, these results confirm that most PLs are short-lived, usually lasting no longer than two-three days, and that half of them last less than 24 hours. Furthermore, these results indicate that the horizontal resolution of the HadGEM3-GA3 model is not strongly affecting the duration of PLs for the present-day climate.

Finally the present-day spatial distributions of PLs of the three resolutions of HadGEM3-GA3 is investigated.

Figure 5-13 shows the present-day climate conditions of the track density of PLs for the N512 (a), N216 (b) and N96 (c) resolutions, over the Northern hemisphere.

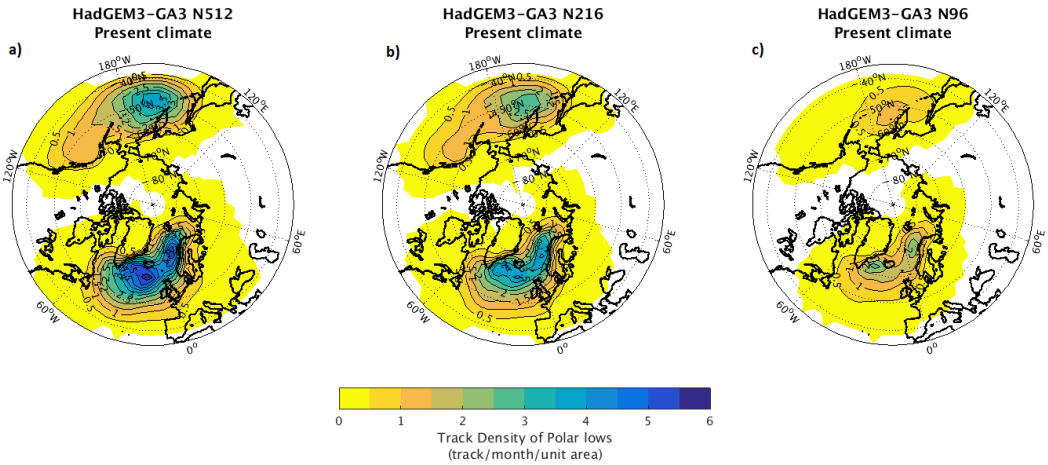

Figure 5-13: Present-day climate conditions of the track density of PLs (track per month per unit area), for the N512 (a), N216 (b) and N96 (c) resolutions of the HadGEM3-GA3 climate model, over the Northern hemisphere.

As previously seen in Table 5-9, the numbers of PLs are different depending on the horizontal resolution. Hence, a variation in the values of the track density is expected, and noticed on the three maps of the track density. However, if the values differ, the pattern of the track densities is the same in the three resolutions, with higher PL occurrences over the Irminger Basin and the north-east of the Atlantic Ocean, the Nordic Seas and the north-west of the Pacific ocean.

Therefore, the horizontal resolution of the present-day climate of the HadGEM3-GA3 model is seen to affect the numbers of PLs found. Furthermore, if the model resolution does not influence on the along-track vorticity and temperature difference, nor their temporal and spatial distributions, the highest resolution of HadGEM3-GA3 is associated with PLs characterised by relatively stronger surface wind speeds.

5.3.2 Impact of the model resolution on the representation of Polar lows response to climate change

In order to assess the impact of the resolution on the response of PLs to climate change, the differences future minus present of PL activity has been evaluated with the three horizontal resolutions of HadGEM3-GA3.

Table 5.10 shows the percentage of the future-present difference of numbers of PLs, their maximum vorticity, maximum wind speed, minimum static stability and duration,

with the N512, N216 and N96 resolutions. Table 5.10 also shows the percentage of PLs which have a lifetime shorter than 24 and 48 hours, and longer than 72 hours, over the Northern hemisphere.

	N512	N216	N96
Number of PLs	-62.28 %	-66.97 %	-73.26 %
Vorticity ξ	-7.62 %	-5.69 %	-1.77 %
Wind speed WS	-7.86 %	-5.93 %	-5.94 %
Temperature difference ΔT	+1.43 %	+1.38 %	+1.27 %
Duration of PLs	+2.62 %	+1.39 %	-10.34 %
Lifetime $<$ 24 h	-4.05 %	-2.36 %	+10.66 %
Lifetime $<$ 48 h	+0.05 %	-0.12 %	+0.34 %
Lifetime $>$ 72 h	+32.47 %	+32.97 %	-63.64 %

Table 5.10: Percentage of change of the numbers of PLs, the maximum vorticity (x10^{-5} s^{-1}), the maximum wind speed ($m.s^{-1}$), the minimum temperature difference (K) and of the duration of PLs (h), as well as the percentage of PLs which have a lifetime shorter than 24 and 48 hours and longer than 72 hours, for the future-present climate difference of the three horizontal resolutions (N512, N216 and N96) of the atmosphere-only HadGEM3-GA3 climate model, over the Northern hemisphere.

For all the three different horizontal resolutions, the yearly number of PLs is found to decrease under climate change. These results confirm the findings of Zahn and von Storch (2010) and Romero and Emanuel (2017). In relative terms, the future decrease observed with HadGEM3-GA3 is larger for the lower horizontal resolution: the percentage difference between present and future climate conditions increase from 62.28% for the N512 resolution to 73.26% for the N96 resolution (66.97% for the N216 resolution). Therefore, the results from the three resolution simulations are different, and indicate that the horizontal resolution of the model has an impact on the representation small mesoscale features such as PLs.

The three resolutions have relatively small percentage of change (up to 8%) between the present and the future climate, indicating that the values of maximum vorticity, maximum wind speed and temperature difference for both climate conditions are relatively close to each other. The results suggest a future decrease of the mean values of the maximum vorticity and wind speed, and an small increase of the temperature difference in the future (i.e. the mean temperature difference increase from -45.49 K to -44.84 K between the present and future climates for the N512 resolution). Therefore, as previously seen for the present-day climate, these changes imply that, regardless of the horizontal resolution of HadGEM3-GA3 chosen, the mean values of these three environmental properties of PLs are not greatly affected by the resolution. Furthermore, although they might slightly differ from the ones of the present-day climate, PL future

characteristics might not be highly affected by climate change.

In contrary to PLs numbers and characteristics, the results on PLs duration differ between the three resolutions. The results indicate that the two highest resolutions predict an increase (1 to 2%, representing around one hour) of PLs mean lifetime in the future, whereas the coarse N96 resolution predicts a decrease (10%, representing two hours) of the lifetime of PLs. This discrepancy in the results mainly comes from the differences in percentage of change of PLs which last longer than 72 hours. The occurrences of PLs which have a lifespan longer than 72 hours are expected to increase in the future climate of in the N512 and N216 resolutions (+30%), while they are expected to drastically decrease (-63%) in the N96 resolution. Therefore, if the numbers of PLs having a shorter lifetime than 48 hours are not anticipated to greatly change in the future, the future of long-lasting PLs is less certain.

Finally the difference between the current and future spatial distribution of PLs is investigated, with the results compared for the three different horizontal resolutions.

Figure 5-14 shows the future minus present difference, significant at the 5% level, of PLs track density, over the Northern hemisphere, for the N512 (a), N216 (b) and N96 (c) resolutions of the HadGEM3-GA3 climate model.

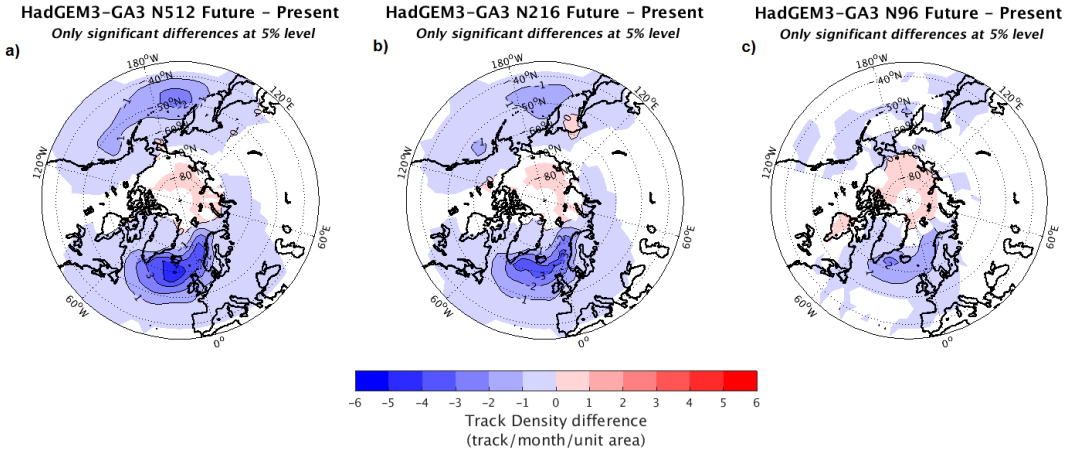

Figure 5-14: Differences between present and future climate conditions of the track density of PLs (track per month per unit area) over the Northern hemisphere, with the N512 (a), N216 (b) and N96 (c) resolutions of the HadGEM3-GA3 climate model.

As previously seen in Figure 5-13, if the values of the track density are expected to change, between the present and future climate, and between the resolutions, the patterns of the differences of track density are similar between the N512, N216 and N96 resolutions.

For the three horizontal resolutions, a decrease is observed almost everywhere over the Northern hemisphere, but especially over the North Atlantic Ocean and the Nordic Seas. As seen in Section 5.2, and found by Zahn and von Storch (2010) and Mallet et al. (2017), this decrease is mainly due to a future increase of the atmospheric static stability. Furthermore, the increase over the Arctic Ocean is seen in the three resolutions.

Overall, the results found for the present and the future climates of the three horizontal resolutions of HadGEM3-GA3 indicate that, the impact of the HadGEM3-GA3 model on the PL characteristics is smaller than that found for the PL numbers.

If increasing the model horizontal resolution from 130 to 25 km shows a monotonic increase in PL numbers, it may not always be the case if the resolution is further increased. Nowadays, most operational forecasts are performed at high horizontal resolutions (around 10 km). If the horizontal resolution is a crucial point for PLs study and if a 10-km horizontal resolution may increase PL numbers, improvement of the dynamics and physics schemes are also essential in order to explicitly resolve PLs at these high horizontal resolutions.

In this thesis, the sensitivity of some of the characteristics of PLs to the model horizontal resolution have been studied. One step further into PLs study would be to assess PLs sensitivity to the vertical resolution of the model, as it will help apprehend the vertical structure of PLs (vertical shear, heat and moisture budgets, etc.).

5.4 Conclusion

As the climate changes, strategic adaptations will be needed to ensure human welfare and sustainability. Being the location associated with the current most rapid changes, the Arctic region is suspected to undergo even more drastic changes in the near future. Among the diverse range of weather-climatic phenomena that the Arctic offshore and coastal communities are and will be facing, PLs are one of the extreme events whose future is not yet fully understood.

Only a few studies (Zahn and von Storch, 2010; Mallet et al., 2017; Romero and Emanuel, 2017) have analysed the possible future of PLs under climate change. These studies have found a possible decrease, between 10 and 45%, of PL numbers in the future. Here for the first time, an ensemble of atmosphere-only simulations of three different horizontal resolutions using the climate model HadGEM3-GA3 are used to assess PLs and their environment under both present and future climate conditions, over the Northern hemisphere. This study has been performed in order to attempt to

answer two main questions: what is the response of PLs to climate change, and will this response be affected by the horizontal resolution of the model?

The first part of the study assessed the representation of PLs in the climate model, to be confident in its ability to capture PLs in the present and future simulations. The study showed that the current representation of PLs (the inter-annual and seasonal variability of PL numbers, the mean vorticity, wind speed and temperature difference (i.e. static stability) of PLs, and their spatial distribution) with the HadGEM3-GA3 model is in accordance with the results from the coupled climate model HadGEM3-GC2 and the reanalysis NCEP-CFS. Although the study revealed that the yearly and monthly PL numbers found with the N512 HadGEM3-GA3 are slightly lower than the ones from HadGEM3-GC2 and NCEP-CFS, similar inter-annual and seasonal variabilities were found, as well as relatively close maximum vorticity, maximum wind speed and temperature difference of PLs. Finally a comparable spatial distribution of PLs over the Northern hemisphere was found with the N512 HadGEM3-GA3, HadGEM3-GC2 and NCEP-CFS datasets.

The similarity of the results found with the N512 HadGEM3-GA3, HadGEM3-GC2 and NCEP-CFS datasets led to the second part of the study: the investigation of the response of PLs to climate change with the high resolution (N512, 25 km) simulations of HadGEM3-GA3.

Firstly, the difference in the large-scale environment between the present-day and future RCP 8.5 scenarios was analysed. The sea ice fraction (used as a boundary condition for the N512 HadGEM3-GA3 experiments) decreases substantially from present-day to future climates, with almost no sea ice present in the Arctic during winter. The sea surface temperatures and the mid-tropospheric temperatures were found to increase in the future climate compared to the current climate. A faster increase (around +6 K) of the mid-tropospheric temperatures was found, compared to a slower increase (around +2 K) of the sea surface temperatures, over the Northern hemisphere. This difference in temperature increase leads to an increase of the atmospheric static stability. This increase in the stability is found over most of the Northern hemisphere, and is especially strong over the North Atlantic Ocean.

Associated with changes in the large-scale environment in the highest resolution (N512) of the HadGEM3-GA3 climate model, a decrease of around 62% of PL numbers was found between the present and the future climate conditions over the Northern hemisphere. A seasonal shift of the PL activity was found during the extended winter season, with the maximum PL monthly counts changing from December-January to January-February. This shift may be explained by the Arctic Ocean being almost

sea-ice free during the early period of the extended winter season. The duration of PLs does not seem to change substantially between the present and future climate conditions (with the mean duration of PLs around 25 hours). A change in the spatial distribution of PLs with the N512 resolution of HadGEM3-GA3 between present and future climates was observed. A general decrease in PL activity was observed over the Northern hemisphere, mainly due to an increase in static stability (especially over the North Atlantic Ocean). Furthermore, a small increase in PL occurrences was found over the Arctic Ocean and over the Hudson Bay, mainly due to a decrease in sea ice extent and indicating a northward shift of PL activity. These results reinforce the findings from previous studies, all agreeing that under climate change, PL activity over the Northern hemisphere will be reduced and will shift poleward, towards the sea ice free Arctic Ocean.

Finally, the third part of this chapter analysed the impact of the horizontal resolution on the representation of PLs in both climate conditions.

PLs numbers for the present-day climate between the three resolutions are found different, with a difference of 22% between the two highest resolutions and a difference of 59% between the highest and the coarser resolutions. The horizontal resolution of HadGEM3-GA3 does not seem to impact PL characteristics or their spatial and temporal representation, but surface winds become slightly stronger with increasing resolution.

When investigating the impact of the model resolution on the response of PLs to climate change, a stronger future decrease of PLs was found with the coarser resolution (decrease of 73.26 % (62.28 %) with the N96 (N512) resolution). Similar temporal and spatial PL distributions, and PLs characteristics were found with the three resolutions for both present and future climates. These findings indicate that, for both present and future climate conditions, the horizontal resolution chosen may not be drastically affecting PLs characteristics but that the number of PLs found is strongly dependent on the model horizontal resolution chosen.

Overall, the present and future conditions of PLs and their surroundings were studied with the atmosphere-only climate model HadGEM3-GA3 with three different horizontal resolutions. Under climate change, if PL numbers and their environment are expected to undergo important changes, PL main characteristics are not anticipated to vary too much. Further work on PLs future could investigate PLs vertical structure, or the impact of an ocean component on PLs future activity.

CHAPTER 6

CONCLUSIONS AND FUTURE WORK

6.1 Overview of the study

Polar lows (PLs) are small intense mesocyclones occurring at high latitudes in both hemispheres and can often be associated with significant damage to offshore infrastructures and coastal communities (Rasmussen and Turner, 2003). PLs are difficult systems to observe and study because of their occurrence in remote locations and of their short life cycle. Hence, there are very few available observational datasets (Noer et al., 2011).

Previous studies of PLs have been limited to specific case studies and temporally and spatially short climatologies, with global studies being rather limited (Stoll et al., 2018). The limited information on PLs and on their properties contributes to the lack of understanding of their activity. Hence it is important to improve our understanding of PLs by exploring their climatologies in atmospheric reanalyses. In this thesis, the representation of PLs when using an objective identification scheme in two different reanalysis datasets was thus investigated.

As PLs are maritime systems, it is expected that they will interact with the ocean through heat and moisture transfers at the surface, as highlighted by the observational study of Shapiro et al. (1987). In addition to influencing the ocean surface heat fluxes, Condron and Renfrew (2013) suggested that PLs may also impact the ocean deep water formation over the North Atlantic, by destabilising the water column. However, this interaction of PLs with the ocean, and thus their potential impact on the ocean, is still not fully understood. Therefore in this thesis, the impact of the interaction of PLs with the ocean on the ocean circulation over the Nordic Seas was examined in a fully

coupled climate model.

Due to human activities, the Arctic climate is undergoing rapid changes, such as the decline of the sea ice extent and thickness (Stroeve et al., 2007), the warming of the troposphere (Perlwitz et al., 2015), and the weakening and northward shift of Cold Air Outbreaks (Kolstad and Bracegirdle, 2008). As the Arctic climate changes and new human activity appears in the region (Melia et al., 2016), the response of PLs will be of particular importance, both in terms of number and location. In order to assess the possible future of PLs and their interaction with their surroundings, it is crucial that climate models are able to represent PLs and their behaviour, as well as the key processes which regulate their formation and intensification. Hence this thesis aimed at quantifying the response of PLs to climate change, and how the horizontal resolution of the model may impact projections of PLs.

In this chapter, the answers to the research questions raised in Chapter 1 - and which have been addressed in Chapters 3, 4 and 5 - will be presented and summarised. It will be followed by the limitations and implications of this work, as well as suggestions for future work.

6.2 Summary of the key findings

What is the representation of PLs when using an objective identification scheme in two reanalysis datasets?

In Chapter 3, the long-term climatology of PLs was examined in two modern atmospheric reanalyses, ERA-I (Dee et al., 2011) and NCEP-CFS (Saha et al., 2010), over the Northern hemisphere, the Norwegian and Barents Seas and the Sea of Japan. Due to their availability and high temporal and spatial resolutions, reanalyses are the main alternative to observational datasets for studying PLs. In this study, PLs are analysed using an objective identification and tracking scheme (Zappa et al., 2014). This allows PLs to be detected, tracked and separated from other tracked mesoscale systems.

PL features were found to be represented in both reanalyses. In all three regions of interest (i.e. Northern hemisphere, Norwegian and Barents Seas and Sea of Japan), the identified PL numbers are twice as large in NCEP-CFS than in ERA-I. This may be due to the difference in horizontal resolution of the two reanalyses impacting differently on the representation of small dynamical features such as PLs. While only covering 2% of the Northern hemisphere, the Norwegian and Barents Seas were found to encompass almost 20% of PLs in the Northern hemisphere. This suggests that this area is an

important region to study PL climatologies and to understand their dynamics and future changes.

The temporal and spatial distributions of PLs identified in both reanalyses were found to be within the range of these from observations and literature (Laffineur et al., 2014; Rojo et al., 2015). PLs were found to last around 30 hours and to mainly occur over the Norwegian Sea (which coincides with the region of maximum Cold Air Outbreaks). Similar mean values for the vorticity, wind speed and static stability associated with PLs were found with both reanalyses, for each region. The sensitivity of PL numbers to the identification criteria (vorticity, wind speed and static stability) showed large variations of PL numbers when changing one criterion at a time, with often too large or too low mean numbers when compared to the STARS observations or literature. These results reinforce the chosen definition of PLs as intense mesoscale cyclones and indicate that the automatic tracking and chosen thresholds can be suitably applied to identify PLs in the reanalyses and models.

The seasonal variability of PL numbers was investigated in all three regions of interest. Different ranges of values were found but all showed higher PL numbers occur for December/January. This peak is preceded by an increase of the number from October until December/January, and followed by a slower decrease until March. These conclusions were supported by the observational STARS dataset for the Norwegian and Barents Seas (Noer et al., 2011; Rojo et al., 2015) and by the PLs analysis over the Sea of Japan of Yanase et al. (2016) based on the JRA-55 reanalysis. The inter-annual variability of PL numbers was also studied. Numbers of PLs found each year vary greatly, however mean PL numbers in ERA-I and NCEP-CFS were found in accordance with previous studies: around 18 PLs per year were found with ERA-I and NCEP-CFS over the Norwegian and Barents Seas when 12 and 14 PLs per year where found by Noer et al. (2011) and Rojo et al. (2015) respectively, and around 5 PLs per year were found with ERA-I and NCEP-CFS over the Sea of Japan whereas Yanase et al. (2016) found around 7 PLs per year. Furthermore, similar inter-annual variability of PL numbers in the two reanalyses was also found, for the three regions of interest.

The large-scale environment appears to influence PL events over the Norwegian and Barents Seas in both reanalyses. Extended winter seasons with high PL number years are associated with low MSLP, a low sea ice extent, warmer SSTs and an increase in strong CAO events, all of which act to increase PL occurrences. The seasonal variability of PLs may also be partially explained by the sea ice cover, which reaches its maximum during the winter season (DJF), leading to a higher meridional surface temperature difference. Finally, the link between CAOs and PL numbers was investigated in ERA-I, by using the CAO Indicator defined in Kolstad and Bracegirdle (2008). Results

show that years with high PL numbers are associated with higher strong CAO events (i.e. when the temperature gradient between the surface and 700 hPa is stronger), confirming the fact that CAOs are an important condition for PLs formation.

Overall, Chapter 3 adds to the literature on developing climatologies of PLs by showing, i) that PL numbers differ substantially between reanalyses and, ii) that there is some agreement between reanalyses on the lack of trends seen in PL numbers over the past few decades and in the inter-annual variability, iii) that the large-scale environment is seen to influence the inter-annual variability of PL numbers.

What is the impact of the interaction of PLs with the ocean on the ocean circulation over the Nordic Seas?

The second part of this thesis has focused on the interaction of PLs with the ocean. In an ocean circulation model, Condron and Renfrew (2013) found that PLs may influence the surface and deep waters of the ocean. Here in Chapter 4, an investigation of PLs and their interaction with the ocean, was made with a fully coupled atmosphere-ocean model, HadGEM3-GC2 (Williams et al., 2015). The impact of PLs on the ocean surface heat fluxes and on the shallow and deep ocean densities was studied, in order to see if similar results to those of Condron and Renfrew (2013) on PLs impact on the ocean surface heat fluxes and MLD, can be found in a high resolution coupled climate model. This thesis focuses on the Nordic Seas region where a large number of PLs are found to occur and also where the deep water formation is known to take place.

PLs are known to be associated with strong surface heat fluxes (Shapiro et al., 1987; Fore et al., 2012). However, the link between PLs and the ocean circulation is not yet fully understood. Previously, Condron et al. (2008) and Condron and Renfrew (2013) assessed the impact of PLs on the ocean circulation over the North Atlantic and Nordic Seas. Both studies predicted that PLs influence the ocean circulation by increasing the ocean density at the surface (through increasing the surface heat fluxes by cooling the surface water). This increase in surface density could inhibit the existing vertical stratification of the water column, and increase the depth of the deep convection in the Nordic Seas.

The two 98-year FEBBRAIO present day forcing experiments from the HadGEM3-CG2 model were first used to evaluate the representation of PLs (though their temporal and spatial distributions, their seasonal and inter-annual variability, and their thermodynamics characteristics) and compare the results with those of the reanalyses. Results show similar characteristics of PLs as the NCEP-CFS reanalysis.

A positive link between the year-to-year variations in PL numbers and surface heat fluxes was found using the ensemble mean of the PL numbers from the FEBBRAIO datasets: higher PL occurrences are associated with higher surface heat fluxes. The link between PLs and the ocean surface heat fluxes was also confirmed within individual months when considering the surface heat fluxes during the months with the highest (January) and lowest (October) PL numbers.

Although a relationship between PLs and the ocean surface heat fluxes is clear, the same can not be inferred for the link between PLs and the ocean density. Only a weak correlation between PL numbers and the potential density of the first layers of the ocean was observed (correlation coefficient of +0.11 at 50 m). The ocean density of the years with high PL numbers was found to be slightly denser than the climatological density, but anomalies were not significant. Since a small impact of PLs on the shallow waters is observed, it is unlikely that PLs may have an impact at a deeper level. This was also confirmed by looking at the density during years with high and low PL numbers, as no influence of PLs was detected at deep levels.

The difference in PLs impact on the deep water formation and their influence on the AMOC over the North Atlantic Ocean seen in this thesis and in Condron and Renfrew (2013) could be due to differences in the definition of PLs, in the datasets and models used as well as differences in the methodologies of each study. Furthermore, due to data availability, different metrics were used in Condron and Renfrew (2013) (ocean MLD and dense water volume) and in this thesis (ocean potential density). Therefore, the respective impact of PLs on the ocean circulation of both studies could not be fully compared. Hence, more work would be needed to gain insight into the interaction of PLs with the ocean.

Overall with the HadGEM3-CG2 coupled climate model, the impact of PLs on the ocean circulation in the Nordics Seas and on the AMOC is not seen as clear as that found in Condron et al. (2008) and Condron and Renfrew (2013).

How might PLs respond to climate change? How might projections of PLs be affected by the model resolution?

Only a few studies (Zahn and von Storch, 2010; Romero and Emanuel, 2017) have investigated how PLs might respond to a warming climate. As the climate changes and new Arctic shipping routes open up (Melia et al., 2016), the future of PLs is one of the Arctic phenomena that the offshore and coastal communities will have to consider for their future strategic adaptations.

Hence, the third part of the study was to explore how PLs and their environ-

ment might be affected by climate change, and how the representation of PLs and their changes may be influenced by the model horizontal resolution. This was investigated using historical and climate change simulations performed with the same atmosphere-only climate model HadGEM3-GA3 (Mizielinski et al., 2014) at three different spatial resolutions. This thesis hence is the first high resolution global model analysis exploring the future of PLs. In order to assess the representation of PLs in HadGEM3-GA3, the present-day simulations of PLs was first examined and compared with the HadGEM3-GC2 coupled climate model (FEBBRAIO) and the NCEP-CFS reanalysis. Zahn and von Storch (2010) suggested that PL numbers might decrease in the future because of changes in their synoptic surroundings. It is from this perspective that here, the differences between the present and future PL activity, as well as their large-scale environment, have been evaluated with the highest resolution (N512, 25 km) of HadGEM3-GA3, for the present-day climate conditions (historical, 1985-2010) and for those expected by the end of the century in a high emissions scenario (from RCP 8.5 scenario) over the Northern hemisphere. Finally, the results obtained with the highest horizontal resolution were compared to the two coarser resolutions (N216/N96, i.e. 60/130 km) of the HadGEM3-GA3, to assess the impact of the model resolution on PL representation.

Before investigating the PL activity in the future climate, the representation of PLs in the current climate was assessed. The results from the high resolution (25 km) simulations of the atmosphere-only climate model HadGEM3-GA3 were found similar to the ones from the coupled climate model HadGEM3-GC2 (25 km) and the reanalysis NCEP-CFS (38 km), indicating that HadGEM3-GA3 is able to represent PLs well and their environment for the current climate.

The difference in the environment of PLs between the present and future climate conditions show large differences in the Northern hemisphere, for the highest resolution (N512) of the climate model. A large future decrease of the sea ice fraction is observed, as well as an increase in sea surface and mid-tropospheric temperatures, and hence of the atmospheric static stability. These results suggest that PLs could also undergo major changes under the RCP 8.5 scenario.

As a result of these changes in the large-scale environment, a decrease of 62% of PL numbers was found between the present and the future climate conditions over the Northern hemisphere, with a seasonal shift of PL activity towards late winter. Indeed, the maximum of PL occurrences shifts from December-January to January-February in the N512 HadGEM3-GA3 model. This shift may be linked to the larger future Arctic sea ice loss at the beginning of the winter season.

Whilst these changes do not seem to affect the distribution of lifetimes of PLs (around 25 h), they do seem to affect the PLs spatial distribution. Between the present and future climate scenarios, the historical regions of PL occurrences (i.e. mainly around the Atlantic and Pacific storm tracks) experience a decline of PL numbers, while new regions of PL formation appear (in places such as the East Siberian Sea or the Beaufort Sea). If the general decrease in PL activity observed over the Northern hemisphere is mainly due to the atmosphere becoming more stable (especially over the North Atlantic Ocean), the new increase in PL occurrences found over the Arctic Ocean may be due to the large decrease in sea ice extent (leading to a large open-ocean area where PLs can form). These results reinforce the findings from previous studies, all agreeing that under climate change, PL activity over the Northern hemisphere might decline.

Finally, the third part of Chapter 5 studied the impact of the horizontal resolution on PL representation, for both climate conditions. The future-present differences in PL characteristics were analysed and compared for the three horizontal resolutions of the atmosphere-only HadGEM3-GA3 climate model: the N512 (25 km), the N216 (60 km) and the N96 (130 km) resolutions.

A strong future decrease of PL numbers was found with all three resolutions (decrease of 73.26% (62.28%) with the N96 (N512) resolution). The shift in PL occurrences towards the end of the extended winter season, and similar temporal and spatial PL distributions, were observed with the three resolutions. Hence, if the horizontal resolution might influence PL numbers, it does not seem to impact the PL characteristics in the HadGEM3-GA3 model. This indicates that the horizontal resolution of HadGEM3-GA3 has an impact on the number of detected features but does not affect the characteristics of these features.

Overall, PLs under present and future conditions were studied with the atmosphere-only climate model HadGEM3-GA3 running at three different horizontal resolutions. Under climate change, if PL activity (numbers and location) and their large-scale environment are expected to drastically change, as seen in Zahn and von Storch (2010) and Romero and Emanuel (2017), the main characteristics of PLs (duration, maximum vorticity, maximum wind speed and minimum static stability) are not found to undergo too much change.

6.3 Limitations of the study and future work

Whilst this study provides a comprehensive analysis of PLs in climate models and reanalyses, there are some limitations and caveats that should be considered. Two of the main issues with this work, which cannot be easily addressed, are the definition of PLs and the lack of PL observations.

6.3.1 Definition of Polar lows

Because of the large spectrum of systems covered by "Polar lows", their definition is relatively broad (e.g. "fairly intense" maritime cyclone according to Rasmussen and Turner 2003). It is now common to track PLs through their maximum vorticity and to use criteria to identify PLs. But the fields and values used for some of the criteria are still unclear. For example, the value of the static stability criterion is still under debate. Indeed, if the difference value of -43 K has been adopted in many previous studies for different regions (Xia et al., 2012b; Zappa et al., 2014; Yanase et al., 2016) and is the observed threshold for favourable conditions for PLs development used by the Norwegian Meteorological Institute (Noer et al., 2011), it has been questioned by Terpstra et al. (2016). Terpstra et al. (2016) found that applying a threshold with this particular value may exclude some forward shear PLs, which usually develop in an environment of higher vertical stability. Another issue comes from the lack of *in-situ* observations of PLs. Indeed, as PLs are fast-developing and short-lived systems, occurring often in remote locations, observations of PLs are limited and only for specific regions. The Nordic Seas and the Sea of Japan are the two main areas where PLs information is available. Hence, in order to gain further knowledge of PLs, more needs to be done on collecting observational data of PLs.

6.3.2 Regarding reanalyses

In Chapter 3, the climatology of PLs and their representation was evaluated within atmospheric reanalyses. Reanalysis datasets are not observations and are generally too coarse to well represent the observed properties of small mesoscale features such as PLs. However, they are a good substitute for the lack of long-term observational data. In this study, a coarse (ERA-I) and a high (NCEP-CFS) resolution atmospheric reanalyses were used to study PLs over the Northern hemisphere. The work done with these two global and long-term datasets could be enhanced by investigating PLs in Arctic-focused reanalyses, such as the Arctic System Reanalyses (ASR). By being Arctic centered and with high resolutions (15 and 30 km, Bromwich et al. 2016, 2017),

this "polar-optimised version of the Weather Research and Forecasting" (WRF) would be of interest to study PLs. Results of the climatologies from Chapter 3 could then be compared and assessed to a dataset supposedly more representative of the Arctic system. Comparing the results from ASR (with the same tracking and identification method) with previous results with ERA-I and NCEP-CFS from Chapter 3, as well as a comparison with observations, could give more insight on PLs activity seen with datasets with different horizontal resolutions.

Because PLs only occur in small numbers, the variables used to study PLs in this thesis have been averaged over the six-month period (i.e. from October to March) to gain more statistical confidence in the results. However, this seasonal average may induce some smoothness when looking at the link between PLs and the large-scale environment for example (as PLs only last for a few days). As most of the reanalysis products are available at a 3- or 6-hourly resolution, it would be of interest to investigate in a more detailed way the interaction between PLs and their surroundings, as in Chapter 3, at a higher temporal resolution than a seasonal mean.

Moreover, further investigation on the spatial and temporal distribution of PLs could be done, in order to get more insight into PL activity and to help establish a more precise definition of PLs. For instance, assessing the impact of having a threshold on the maximum duration (e.g. 3/4 days) and distance travelled (e.g. 1000 km, as observed in Michel et al. (2017) and Smirnova and Golubkin (2017)) of PLs.

An interesting aspect of PLs which has not been investigated here in the climatologies of PLs in reanalyses (Chapter 3) is their vertical structure. As most studies on PLs focus on the horizontal structure of PLs, looking at the vertical structure of PLs would be of great interest to understand how they form, and how "hybrid" PLs transition. Montgomery and Farrell (1992) studied the vertical structure of developing PLs through case studies. Sergeev et al. (2017) analysed the vertical structure of a shear-line PL and simulated it with the Met Office Unified Model (MetUM). Hewson et al. (2000) investigated the mesoscale frontal features within four PL cases. All agree that a few case studies or model studies are not enough to fully determine the vertical structure of PLs and its variability, and stress the crucial importance of *in-situ* data to fully understand PLs three-dimensional dynamics.

Two other aspects of PLs which have only started to be studied are the moisture transport and the energetic aspects of PLs. Through heat and moisture transports, Melsheimer et al. (2016) evaluated the detectability of PLs via microwave humidity sounders. The study showed that PLs can be detected thanks to the brightness temperature of the water vapour channels of the sounders. However, as no minimum wind criterion was imposed, about double polar-low-like signatures were found compared to

other PL climatologies. In their study, Terpstra et al. (2015) quantified the contributions of both diabatic and baroclinic processes to PL development through idealised simulations. The study showed that disturbances need a "diabatic dominance during the early stage of development" in order to intensify. Thresholds (of moisture, baroclinicity and static stability) for which the diabatic amplification can occur, were found, though these thresholds should not be taken as absolute values as the thresholds are interdependent.

6.3.3 Polar lows: air-sea interaction and climate change

In Chapters 4 and 5, two climate models were used to investigate the interaction of PLs with the ocean and their response to climate change. However, results might be dependent on the ability of the models to represent the large- and meso-scale patterns of the ocean and atmosphere, and their ability to represent PLs. As observations are fairly sparse, the ability of the coupled HadGEM3-GC2 and atmospheric HadGEM3-GA3 climate models were assessed by comparing the results for PLs to those from the ERA-I and NCEP-CFS reanalyses. However, basing confidence in model results on the ones from reanalyses does not guarantee a truthful representation of "real world" PLs.

In Chapter 4, the interaction between PLs and the ocean was analysed by looking at monthly means. However, as PLs only last a few hours to a few days, the impact of PLs on the ocean might have been smoothed by the monthly average. To mitigate this problem, months with high and low PL numbers were compared to investigate if a cumulative effect of PLs could be seen to have an impact on the ocean. As most global climate models only output monthly ocean data due to issues with storing the increasingly large multi-level data, this method, although not ideal, represents the current best recourse. An alternative analysis to investigate the interaction of PLs with the ocean could be to perform an analysis similar to that of Condron and Renfrew (2013), to see if the depth of the mixed-layer of the Nordic Seas is affected by the passage of PLs within coupled climate models. However, this would require higher frequency ocean data than the current monthly data available.

Finally, in Chapter 5, to examine the response of PLs to climate change, three ensemble members for each of the three HadGEM3-GA3 resolutions were used. Future work could involve investigating the response of PLs with more ensemble members, and from more than one climate model. The High Resolution Model Intercomparison Project (or HighResMIP, Haarsma et al. 2016) applies a multi-model approach to evaluate the impact of horizontal resolution on the atmosphere and ocean. As results depend strongly on the ability of the chosen model to represent PLs and their environ-

ment, this future work would be of great value to enhance the results from previous studies and this thesis. Furthermore, the RCP 8.5 scenario was employed to assess the future climate conditions. As this RCP is the most extreme scenario of the current RCPs available, looking at other scenarios (e.g. RCP 4.5) would allow to evaluate the possible range of future response of PLs to climate change. Hence, experiments such as the Coupled Model Intercomparison Project 6 (or CMIP6, Eyring et al. 2016) will be of great value to reinforce our knowledge in depth analysis of the structure and energetic aspects of PLs and on PLs activity under our changing climate.

BIBLIOGRAPHY

N. Ahmed, T. Natarajan, and K. R. Rao. Discrete cosine transform. *IEEE Transactions on Computers*, C-23(1):90–93, Jan 1974. ISSN 0018-9340. doi: 10.1109/T-C.1974.223784.

M. D. Albright, R. J. Reed, and D. W. Ovens. Origin and structure of a numerically simulated polar low over Hudson Bay, 1995. ISSN 16000870.

L. Bengtsson, K. I. Hodges, and E. Roeckner. Storm tracks and climate change. *Journal of Climate*, 19(15):3518–3543, 2006. ISSN 08948755. doi: 10.1175/JCLI3815.1.

P. Berrisford, D. Dee, K. Fielding, M. Fuentes, P. Kållberg, S. Kobayashi, and S. Uppala. The era-interim archive. Shinfield Park, Reading, August 2009.

M. J. Best, M. Pryor, D. B. Clark, L. M. Mercado, S. Sitch, C. D. Jones, N. Gedney, G. G. Rooney, R. L. H. Essery, E. Blyth, O. Boucher, R. J. Harding, and P. M. Cox. The Joint UK Land Environment Simulator (JULES), Model description - Part 2: Carbon fluxes and vegetation. *Geoscientific Model Development Discussions*, 4(1):641–688, 2011. ISSN 1991-962X. doi: 10.5194/gmdd-4-641-2011.

A. M. Blechschmidt. A 2-year climatology of polar low events over the Nordic Seas from satellite remote sensing. *Geophysical Research Letters*, 35(9):2003–2007, 2008. ISSN 00948276. doi: 10.1029/2008GL033706.

R. Blender, K. Fraedrich, and F. Lunkeit. Identification of cyclone-track regimes in the North Atlantic. *Quarterly Journal of the Royal Meteorological Society*, 123(539):727–741, 1997. ISSN 00359009. doi: 10.1256/smsqj.53909.

N. A. Bond and M. A. Shapiro. Polar Lows over the Gulf of Alaska in Conditions of Reverse Shear. *Monthly Weather Review*, 119(2):551–572, 1991. ISSN 0027-0644. doi: 10.1175/1520-0493(1991)119⟨0551:PLOTGO⟩2.0.CO;2.

T. Bracegirdle. *The role of convection in the intensification of polar lows*. PhD thesis, University of Reading (UK), 2006.

T. J. Bracegirdle and S. L. Gray. An objective climatology of the dynamical forcing of polar lows in the Nordic seas. *Encyclopedia of Atmospheric Sciences*, 4(December 2007):1549–1555., 2008. ISSN 1476-4687. doi: 10.1002/joc.

T. J. Bracegirdle and S. L. Gray. The dynamics of a polar lows assessed using potential vorticity inversion. *Quarterly Journal of the Royal Meteorological Society*, 135:880–893, 2009. ISSN 00359009. doi: 10.1002/qj.411.

J. F. Bresch, R. J. Reed, and M. D. Albright. A Polar-Low Development over the Bering Sea: Analysis, Numerical Simulation, and Sensitivity Experiments. *Monthly Weather Review*, 125(1989):3109–3130, 1997. ISSN 0027-0644. doi: 10.1175/1520-0493(1997)125⟨3109:APLDOT⟩2.0.CO;2.

D. H. Bromwich, A. B. Wilson, L. S. Bai, G. W. K. Moore, and P. Bauer. A comparison of the regional Arctic System Reanalysis and the global ERA-Interim Reanalysis for the Arctic. *Quarterly Journal of the Royal Meteorological Society*, 142(695):644–658, 2016. ISSN 1477870X. doi: 10.1002/qj.2527.

D. H. Bromwich, A. B. Wilson, L. S. Bai, and Lui. Arctic System Reanalysis version 2. *Bulletin of the American Meteorological Society*, 2017.

K. Bryan. A numerical method for the study of the circulation of the world ocean. *Journal of Computational Physics (Reprinted from the Journal of Computational Physics, vol 4, pg 347-376, 1969)*, 135(2):154 – 169, 1997. ISSN 0021-9991. doi: http://dx.doi.org/10.1006/jcph.1997.5699.

S. Businger. The synoptic climatology of polar low outbreaks over the Gulf of Alaska and the Bering Sea. *Tellus A*, 39 A(4):307–325, 1987. ISSN 16000870. doi: 10.1111/j.1600-0870.1987.tb00310.x.

S. Businger and J.-J. Baik. An Arctic Hurricane over the Bering Sea. *Monthly Weather Review*, 119(9):2293–2322, 1991. ISSN 0027-0644. doi: 10.1175/1520-0493(1991)119⟨2293:AAHOTB⟩2.0.CO;2.

S. Businger and R. J. Reed. Cyclogenesis in Cold Air Masses. *American Meteorological Society*, 4(2):133–156, 1989. ISSN 0882-8156. doi: 10.1175/1520-0434(1989)004⟨0133:CICAM⟩2.0.CO;2.

A. Carleton. Satellite climatological aspects of cold air mesocyclones in the arctic and antarctic. *Global Atmosphere and Ocean System*, 5(1):1–42, 12 1996. ISSN 1023-6732.

A. M. Carleton. Satellite climatological aspects of the "polar low" and "instant occlusion". *Tellus A*, 37 A(5):433–450, 1985. ISSN 16000870. doi: 10.1111/j.1600-0870.1985.tb00442.x.

A. M. Carleton and D. A. Carpenter. Satellite climatology of 'polar lows' and broad-scale climatic associations for the Southern Hemisphere. *International Journal of Climatology*, 10(3):219–246, 1990. ISSN 10970088. doi: 10.1002/joc.3370100302.

J. F. Carrasco, D. H. Bromwich, and A. J. Monaghan. Distribution and Characteristics of Mesoscale Cyclones in the Antarctic: Ross Sea Eastward to the Weddell Sea. *Monthly Weather Review*, 131(2):289–301, 2003. ISSN 0027-0644. doi: 10.1175/1520-0493(2003)131⟨0289:DACOMC⟩2.0.CO;2.

J. L. Catto. *Extratropical Cyclones in HiGEM : Climatology , Structure and Future Predictions*. PhD thesis, University of Reading (UK), 2009.

J. Charney and A. Eliassen. On the growth of the hurricane depression. *Journal of Atmospheric Sciences*, 21:68–75, 1964.

C. Claud, G. Heinemann, E. Raustein, and L. McMurdie. Polar low *le Cygne*: Satellite observations and numerical simulations. *Quarterly Journal of the Royal Meteorological Society*, 130(October 1993):1075–1102, 2004. ISSN 00359009. doi: 10.1256/qj.03.72.

J. Cohen, J. A. Screen, J. C. Furtado, M. Barlow, D. Whittleston, D. Coumou, J. Francis, K. Dethloff, D. Entekhabi, J. Overland, and J. Jones. Recent Arctic amplification and extreme mid-latitude weather. *Nature Geoscience*, 7(9):627–637, 2014. ISSN 17520908. doi: 10.1038/ngeo2234.

M. Collins, K. R., J. Arblaster, J.-L. Dufresne, T. Fichefet, P. Friedlingstein, X. Gao, W. Gutowski, T. Johns, G. Krinner, M. Shongwe, C. Tebaldi, A. Weaver, and M. Wehner. *Long-term Climate Change: Projections, Commitments Group, and Irreversibility. In: Climate Change 2013: The Physical Science Basis. Contribution*

of Working I to the Fifth Assessment Report of the Intergovernmental Panel on Climate Change. Cambridge University Press, Cambridge, United Kingdom and New York, NY, USA, 2013.

W. J. Collins, N. Bellouin, M. Doutriaux-Boucher, N. Gedney, P. Halloran, T. Hinton, J. Hughes, C. D. Jones, M. Joshi, S. Liddicoat, G. Martin, F. O'Connor, J. Rae, C. Senior, S. Sitch, I. Totterdell, A. Wiltshire, and S. Woodward. Development and evaluation of an Earth-system model - HadGEM2. *Geoscientific Model Development Discussions*, 4(2):997–1062, 2011. ISSN 1991-962X. doi: 10.5194/gmdd-4-997-2011.

A. Condron and I. a. Renfrew. The impact of polar mesoscale storms on northeast Atlantic Ocean circulation. *Nature Geoscience*, 6(1):34–37, 2013. ISSN 1752-0894. doi: 10.1038/ngeo1661.

A. Condron, G. R. Bigg, and I. A. Renfrew. Polar Mesoscale Cyclones in the Northeast Atlantic: Comparing Climatologies from ERA-40 and Satellite Imagery. *Monthly Weather Review*, 134(5):1518–1533, 2006. ISSN 0027-0644. doi: 10.1175/MWR3136.1.

A. Condron, G. R. Bigg, and I. A. Renfrew. Modeling the impact of polar mesocyclones on ocean circulation. *Journal of Geophysical Research: Oceans*, 113(10):1–17, 2008. ISSN 21699291. doi: 10.1029/2007JC004599.

G. C. Craig and S. L. Gray. CISK or WISHE as the Mechanism for Tropical Cyclone Intensification. 53(23):3528–3540, 1996. ISSN 0022-4928. doi: 10.1175/1520-0469(1996)053⟨3528:COWATM⟩2.0.CO;2.

H. F. Dacre, M. K. Hawcroft, M. A. Stringer, and K. I. Hodges. An Extratropical Cyclone Atlas. *Bulletin of the American Meteorological Society*, pages 1497–1502, 2012. doi: 10.1175/BAMS-D-11-00164.1.

P. Dannevig. Meteorologi for Flygere. *Aschehoug*, 1954.

D. P. Dee, S. M. Uppala, A. J. Simmons, P. Berrisford, P. Poli, S. Kobayashi, U. Andrae, M. A. Balmaseda, G. Balsamo, P. Bauer, P. Bechtold, A. C. M. Beljaars, L. van de Berg, J. Bidlot, N. Bormann, C. Delsol, R. Dragani, M. Fuentes, A. J. Geer, L. Haimberger, S. B. Healy, H. Hersbach, E. V. Hólm, L. Isaksen, P. Kållberg, M. Kähler, M. Matricardi, A. P. Mcnally, B. M. Monge-Sanz, J. J. Morcrette, B. K. Park, C. Peubey, P. de Rosnay, C. Tavolato, J. N. Thépaut, and F. Vitart. The ERA-Interim reanalysis: Configuration and performance of the data assimilation system. *Quarterly Journal of the Royal Meteorological Society*, 137(656):553–597, 2011. ISSN 00359009. doi: 10.1002/qj.828.

B. Denis, J. Côté, and R. Laprise. Spectral Decomposition of Two-Dimensional Atmospheric Fields on Limited-Area Domains Using the Discrete Cosine Transform (DCT). *Monthly Weather Review*, 130(7):1812–1829, 2002. ISSN 0027-0644. doi: 10.1175/1520-0493(2002)130⟨1812:SDOTDA⟩2.0.CO;2.

C. J. Donlon, M. Martin, J. Stark, J. Roberts-Jones, E. Fiedler, and W. Wimmer. The Operational Sea Surface Temperature and Sea Ice Analysis (OSTIA) system. *Remote Sensing of Environment*, 116:140–158, 2012. ISSN 00344257. doi: 10.1016/j.rse.2010.10.017.

M. W. Douglas, L. S. Fedor, and M. A. Shapiro. Polar Low Structure over the Northern Gulf of Alaska Based on Research Aircraft Observations. *Monthly Weather Review*, 119(1):32–54, 1991. ISSN 0027-0644. doi: 10.1175/1520-0493(1991)119⟨0032:PLSOTN⟩2.0.CO;2.

C. Duncan. Baroclinic instability in a reversed shear flow. *Meteorology Magazine*, 107: 17–23, 1978.

E. T. Eady. Long Waves and Cyclone Waves. *Tellus*, 1(3):33–52, 1949. ISSN 0040-2826. doi: 10.3402/tellusa.v1i3.8507.

S. Eckermann. Hybrid σ - p Coordinate Choices for a Global Model. *Monthly Weather Review*, 137(1):224–245, 2009. ISSN 0027-0644. doi: 10.1175/2008MWR2537.1.

K. A. Emanuel. An Air-Sea Interaction Theory for Tropical Cyclones. Part I: Steady-State Maintenance. *Journal of the Atmospheric Sciences*, 43(6):585–605, 1986. ISSN 0022-4928. doi: 10.1175/1520-0469(1986)043⟨0585:AASITF⟩2.0.CO;2.

K. A. Emanuel and R. Rotunno. Polar lows as arctic hurricanes. *Tellus A*, 41 A(1): 1–17, 1989. ISSN 16000870. doi: 10.1111/j.1600-0870.1989.tb00362.x.

H. Ertel. Ein neuer hydrodynamischer Wirbelsatz. *Meteorol. Z.*, 59:277–281, 1942.

V. Eyring, S. Bony, G. A. Meehl, C. A. Senior, B. Stevens, R. J. Stouffer, and K. E. Taylor. Overview of the Coupled Model Intercomparison Project Phase 6 (CMIP6) experimental design and organization. *Geoscientific Model Development*, 9(5):1937–1958, 2016. ISSN 19919603. doi: 10.5194/gmd-9-1937-2016.

J. Fletcher, S. Mason, and C. Jakob. The climatology, meteorology, and boundary layer structure of marine cold air outbreaks in both hemispheres. *Journal of Climate*, 29 (6):1999–2014, 2016. ISSN 08948755. doi: 10.1175/JCLI-D-15-0268.1.

I. Fore, J. E. Kristjansson, E. W. Kolstad, T. J. Bracegirdle, O. Saetra, and B. Rosting. A 'hurricane-like' polar low fuelled by sensible heat flux: high-resolution numerical simulations. *Quarterly Journal of the Royal Meteorological Society*, 138(666):1308–1324, 2012. ISSN 00359009. doi: 10.1002/qj.1876.

R. Frehlich and R. Sharman. The Use of Structure Functions and Spectra from Numerical Model Output to Determine Effective Model Resolution. *Monthly Weather Review*, 136(4):1537–1553, 2008. ISSN 0027-0644. doi: 10.1175/2007MWR2250.1.

P. Gachon, R. Laprise, P. Zwack, and F. J. Saucier. The effects of interactions between surface forcings in the development of a model-simulated polar low in Hudson Bay. *Tellus, Series A: Dynamic Meteorology and Oceanography*, 55(1):61–87, 2003. ISSN 02806495. doi: 10.1034/j.1600-0870.2003.201267.x.

M. Gervais, J. Shaman, Y. Kushnir, M. Gervais, J. Shaman, and Y. Kushnir. Mechanisms Governing the Development of the North Atlantic Warming Hole in the CESM-LE Future Climate Simulations. *Journal of Climate*, pages JCLI–D–17–0635.1, 2018. ISSN 0894-8755. doi: 10.1175/JCLI-D-17-0635.1.

J. D. Gibbons and S. Chakraborti. *Nonparametric Statistical Inference*, pages 977–979. Springer Berlin Heidelberg, Berlin, Heidelberg, 2011. ISBN 978-3-642-04898-2. doi: 10.1007/978-3-642-04898-2_420.

S. L. Gray. *Intensification and Eye Dynamics of Tropical Cyclones and Polar Lows*. PhD thesis, University of Reading (UK), 1996.

S. L. Gray and G. C. Craig. A simple theoretical model for the intensification of tropical cyclones and polar lows. *Quarterly Journal of the Royal Meteorological Society*, 124(547):919–947, 1998. ISSN 00359009. doi: 10.1002/qj.49712454713. URL `http://doi.wiley.com/10.1002/qj.49712454713`.

R. J. Haarsma, M. J. Roberts, P. L. Vidale, A. Catherine, A. Bellucci, Q. Bao, P. Chang, S. Corti, N. S. Fučkar, V. Guemas, J. Von Hardenberg, W. Hazeleger, C. Kodama, T. Koenigk, L. R. Leung, J. Lu, J. J. Luo, J. Mao, M. S. Mizielinski, R. Mizuta, P. Nobre, M. Satoh, E. Scoccimarro, T. Semmler, J. Small, and J. S. Von Storch. High Resolution Model Intercomparison Project (HighResMIP v1.0) for CMIP6. *Geoscientific Model Development*, 9(11):4185–4208, 2016. ISSN 19919603. doi: 10.5194/gmd-9-4185-2016.

J. M. Harold, G. R. Bigg, and J. Turner. Mesocyclone activity over the North-East Atlantic. Part 1: Vortex distribution and variability. *International Journal*

of Climatology, 19(11):1187–1204, 1999a. ISSN 08998418. doi: 10.1002/(SICI)1097-0088(199909)19:11⟨1187::AID-JOC419⟩3.0.CO;2-Q.

J. M. Harold, G. R. Bigg, and J. Turner. Mesocyclone activity over the Northeast Atlantic. Part 2: An investigation of causal mechanisms. *International Journal of Climatology*, 19(12):1283–1299, 1999b. ISSN 08998418. doi: 10.1002/(SICI)1097-0088(199910)19:12⟨1283::AID-JOC420⟩3.0.CO;2-T.

T. W. Harrold and K. A. Browning. The polar low as a baroclinic disturbance. *Quarterly Journal of the Royal Meteorological Society*, 95(406):710–723, 1969. ISSN 1477870X. doi: 10.1002/qj.49709540605.

M. K. Hawcroft, L. C. Shaffrey, K. I. Hodges, and H. F. Dacre. How much Northern Hemisphere precipitation is associated with extratropical cyclones? *Geophysical Research Letters*, 39(24):1–7, 2012. ISSN 00948276. doi: 10.1029/2012GL053866.

G. Heinemann. Mesoscale vorticies in the Weddell Sea region (Antarctica). *Monthly Weather Review*, 1990.

G. Heinemann. A wintertime polar low over the eastern weddell sea (Antarctica): A study with AVHRR, TOVS, SSM/I and conventional data. *Meteorology and Atmospheric Physics*, 58(1-4):83–102, 1996. ISSN 0177-7971. doi: 10.1007/bf01027558.

G. Heinemann, C. Claud, and T. Spengler. Polar Low Workshop Summary. *Bulletin of the American Meteorological Society*, 98(6):ES139–ES142, 2018. ISSN 00030007. doi: 10.1175/BAMS-D-16-0207.1.

T. D. Hewson, G. C. Craig, and C. Claud. Evolution and mesoscale structure of a polar low outbreak. *Quarterly Journal of the Royal Meteorological Society*, 126(564):1031–1063, 2000. ISSN 00359009. doi: 10.1002/qj.49712656411.

K. Hodges, A. Cobb, and P. L. Vidale. How well are tropical cyclones represented in reanalysis datasets? *Journal of Climate*, 30(14):5243–5264, 2017. ISSN 08948755. doi: 10.1175/JCLI-D-16-0557.1.

K. I. Hodges. A General-Method For Tracking Analysis And Its Application To Meteorological Data. *Monthly Weather Review, American Meteorological Society*, 1994. ISSN 0027-0644. doi: 10.1175/1520-0493(1994)122⟨2573:AGMFTA⟩2.0.CO;2.

K. I. Hodges. Feature Tracking on the Unit Sphere. *Monthly Weather Review, American Meteorological Society*, 123(12):3458–3465, 1995. ISSN 0027-0644. doi: 10.1175/1520-0493(1995)123⟨3458:FTOTUS⟩2.0.CO;2.

K. I. Hodges. Spherical Nonparametric Estimators Applied to the UGAMP Model Integration for AMIP. *Monthly Weather Review, American Meteorological Society*, 124(12):2914–2932, 1996. ISSN 0027-0644. doi: 10.1175/1520-0493(1996)124⟨2914:SNEATT⟩2.0.CO;2.

K. I. Hodges. Adaptive Constraints for Feature Tracking. *Monthly Weather Review*, 127(6):1362–1373, 1999. ISSN 0027-0644. doi: 10.1175/1520-0493(1999)127⟨1362:ACFFT⟩2.0.CO;2.

K. I. Hodges. Confidence Intervals and Significance Tests for Spherical Data Derived from Feature Tracking. *Monthly Weather Review*, 136(5):1758–1777, 2008. ISSN 0027-0644. doi: 10.1175/2007MWR2299.1.

K. I. Hodges, R. W. Lee, and L. Bengtsson. A comparison of extratropical cyclones in recent reanalyses ERA-Interim, NASA MERRA, NCEP CFSR, and JRA-25. *Journal of Climate*, 24(18):4888–4906, 2011. ISSN 08948755. doi: 10.1175/2011JCLI4097.1.

J. R. Holton and G. J. Hakim. *An introduction to dynamic meteorology*. Academic Press, Fifth Edition, 2013. ISBN 978-0-12-384866-6.

B. J. Hoskins and K. I. Hodges. New Perspectives on the Northern Hemisphere Winter Storm Tracks. *Journal of the Atmospheric Sciences*, 59(6):1041–1061, 2002. ISSN 0022-4928. doi: 10.1175/1520-0469(2002)059⟨1041:NPOTNH⟩2.0.CO;2.

B. J. Hoskins, M. E. McIntyre, and a. W. Robertson. of the Meteorological October 1985. *Quarterly Journal of the Royal Meteorological Society*, 111(6):877–946, 1985. ISSN 00359009. doi: 10.1002/qj.49711147002.

E. C. Hunke, W. H. Lipscomb, A. K. Turner, N. Jeffery, and S. Elliott. CICE : the Los Alamos Sea Ice Model Documentation and Software User ' s Manual LA-CC-06-012. page 115, 2015.

B. Ingleby and M. Huddleston. Quality control of ocean temperature and salinity profiles - Historical and real-time data. *Journal of Marine Systems*, 65(1-4 SPEC. ISS.):158–175, 2006. ISSN 09247963. doi: 10.1016/j.jmarsys.2005.11.019.

IPCC. *Working Group I Contribution to the IPCC Fifth Assessment Report (AR5), Climate Change 2013: The Physical Science Basis*. 2013.

D. R. Jackett and T. J. Mcdougall. Minimal Adjustment of Hydrographic Profiles to Achieve Static Stability. *Journal of Atmospheric and Oceanic Technology*, 12(2):381–389, 1995. ISSN 0739-0572. doi: 10.1175/1520-0426(1995)012⟨0381:MAOHPT⟩2.0.CO;2.

C. D. Jones, J. K. Hughes, N. Bellouin, S. C. Hardiman, G. S. Jones, J. Knight, S. Liddicoat, F. M. O'Connor, R. J. Andres, C. Bell, K. O. Boo, A. Bozzo, N. Butchart, P. Cadule, K. D. Corbin, M. Doutriaux-Boucher, P. Friedlingstein, J. Gornall, L. Gray, P. R. Halloran, G. Hurtt, W. J. Ingram, J. F. Lamarque, R. M. Law, M. Meinshausen, S. Osprey, E. J. Palin, L. Parsons Chini, T. Raddatz, M. G. Sanderson, A. A. Sellar, A. Schurer, P. Valdes, N. Wood, S. Woodward, M. Yoshioka, and M. Zerroukat. The HadGEM2-ES implementation of CMIP5 centennial simulations. *Geoscientific Model Development*, 4(3):543–570, 2011. ISSN 19919603. doi: 10.5194/gmd-4-543-2011.

T. Jung, S. K. Gulev, I. Rudeva, and V. Soloviov. Sensitivity of extratropical cyclone characteristics to horizontal resolution in the ECMWF model. *Quarterly Journal of the Royal Meteorological Society*, 132(619):1839–1857, 2006. ISSN 00359009. doi: 10.1256/qj.05.212.

T. Jung, S. Serrar, and Q. Wang. The oceanic response to mesoscale atmospheric forcing. *Geophysical Research Letters*, 41(4):1255–1260, 2014. ISSN 19448007. doi: 10.1002/2013GL059040.

S. Kobayashi, Y. Ota, Y. Harada, A. Ebita, M. Moriya, H. Onoda, K. Onogi, H. Kamahori, C. Kobayashi, H. Endo, K. Miyaoka, and K. Takahashi. The JRA-55 Reanalysis: General Specifications and Basic Characteristics. *Journal of the Meteorological Society of Japan. Ser. II*, 93(1):5–48, 2015. ISSN 0026-1165. doi: 10.2151/jmsj.2015-001.

E. W. Kolstad. A new climatology of favorable condition for reverse-shear polar lows. *Tellus A*, 58A:344–354, 2005. ISSN 00359009. doi: 10.1002/qj.888.

E. W. Kolstad. *Extreme winds in the Nordic Seas: polar lows and Arctic fronts in a changing climate*. PhD thesis, University of Bergen (Norway), 2007.

E. W. Kolstad. A global climatology of favourable conditions for polar lows. *Quarterly Journal of the Royal Meteorological Society*, 137(660):1749–1761, 2011. ISSN 00359009. doi: 10.1002/qj.888.

E. W. Kolstad and T. J. Bracegirdle. Marine cold-air outbreaks in the future: An assessment of IPCC AR4 model results for the Northern Hemisphere. *Climate Dynamics*, 30(7-8):871–885, 2008. ISSN 09307575. doi: 10.1007/s00382-007-0331-0.

E. W. Kolstad, T. J. Bracegirdle, and I. A. Seierstad. Marine cold-air outbreaks in the North Atlantic: Temporal distribution and associations with large-scale atmospheric circulation. *Climate Dynamics*, 33(2-3):187–197, 2009. ISSN 09307575. doi: 10.1007/s00382-008-0431-5.

J. E. Kristjansson, I. Barstad, T. Aspelien, I. Fore, Godoy, Hov, E. Irvine, T. Iversen, E. Kolstad, T. E. Nordeng, H. McInnes, R. Randriamampianina, J. Reuder, Saetra, M. Shapiro, T. Spengler, and H. Olafsson. The Norwegian IPY-THORPEX: Polar lows and arctic fronts during the 2008 Andya Campaign. *Bulletin of the American Meteorological Society*, 92(11):1443–1466, 2011. ISSN 00030007. doi: 10.1175/2011BAMS2901.1.

J. E. Kristjánsson, S. Thorsteinsson, E. W. Kolstad, and A. M. Blechschmidt. Orographic influence of east Greenland on a polar low over the Denmark Strait. *Quarterly Journal of the Royal Meteorological Society*, 137(660):1773–1789, 2011. ISSN 00359009. doi: 10.1002/qj.831.

A. Kumar, J. Perlwitz, J. Eischeid, X. Quan, T. Xu, T. Zhang, M. Hoerling, B. Jha, and W. Wang. Contribution of sea ice loss to Arctic amplification. *Geophysical Research Letters*, 37(21):2–7, 2010. ISSN 00948276. doi: 10.1029/2010GL045022.

T. Laffineur, C. Claud, J.-P. Chaboureau, and G. Noer. Polar Lows over the Nordic Seas: Improved Representation in ERA-Interim Compared to ERA-40 and the Impact on Downscaled Simulations. *Monthly Weather Review*, 142:2271–2289, 2014. ISSN 0027-0644. doi: 10.1175/MWR-D-13-00171.1.

T. Linders and Ø. Saetra. Can CAPE Maintain Polar Lows? *Journal of the Atmospheric Sciences*, 67(8):2559–2571, 2010. ISSN 0022-4928. doi: 10.1175/2010JAS3131.1.

G. Madec and the NEMO team. NEMO Ocean Engine. Note du Póle de modélisation. (27):1–332, 2008.

J. Mailhot, D. Hanley, B. Bilodeau, and O. Hertzman. A numerical case study of a polar low in the Labrador Sea. *Tellus, Series A: Dynamic Meteorology and Oceanography*, 48(3):383–402, 1996. ISSN 02806495. doi: 10.3402/tellusa.v48i3.12067.

P.-E. Mallet. *Polar lows dans l'hémisphère Nord : influence de l'environnement de grande échelle, de sa variabilité et de ses modifications avec le changement climatique.* PhD thesis, École Polytechnique (France), 2014.

P.-E. Mallet, C. Claud, and M. Vicomte. North Atlantic polar lows and weather regimes: do current links persist in a warmer climate? *Atmospheric Science Letters*, 18(8):349–355, 2017. ISSN 1530261X. doi: 10.1002/asl.763.

D. A. Mansfield. Polar lows: The development of baroclinic disturbances in cold air outbreaks. *Quarterly Journal of the Royal Meteorological Society*, 100(426):541–554, 1974. ISSN 1477870X. doi: 10.1002/qj.49710042604.

J. Marshall and F. Schott. Open-ocean convection: Observations, theory, and models. *Reviews of Geophysics*, 37(1):1–64, 1999. ISSN 87551209. doi: 10.1029/98RG02739.

J. Marshall, A. Adcroft, C. Hill, L. Perelman, and C. Heisey. A finite-volume, incompressible Navier Stokes model for studies of the ocean on parallel computers. *Journal of Geophysical Research: Oceans*, 102(C3):5753–5766, 1997. ISSN 01480227. doi: 10.1029/96JC02775.

C. Mauritzen. Production of dense overflow waters feeding the North Atlantic across the Greenland-Scotland Ridge. Part 1: Evidence for a revised circulation scheme. *Deep-Sea Research Part I: Oceanographic Research Papers*, 43(6):807–809, 1996. ISSN 09670637. doi: 10.1016/0967-0637(96)00038-6.

G. D. McCarthy, D. A. Smeed, W. E. Johns, E. Frajka-Williams, B. I. Moat, D. Rayner, M. O. Baringer, C. S. Meinen, J. Collins, and H. L. Bryden. Measuring the Atlantic Meridional Overturning Circulation at 26°N. *Progress in Oceanography*, 130:91–111, 2015. ISSN 00796611. doi: 10.1016/j.pocean.2014.10.006.

K. McGuffie and A. Henderson-Sellers. *A climate modelling primer*. John Wiley & Sons, 2005.

H. McInnes, J. Kristiansen, J. E. Kristjánsson, and H. Schyberg. The role of horizontal resolution for polar low simulations. *Quarterly Journal of the Royal Meteorological Society*, 137(660):1674–1687, 2011. ISSN 00359009. doi: 10.1002/qj.849.

S. T. Meehl, G.A., W. Collins, P. Friedlingstein, A. Gaye, J. Gregory, A. Kitoh, R. Knutti, J. Murphy, A. Noda, S. Raper, and A. Watterson. *Global Climate Projections. In: Climate Change 2007: The Physical Science Basis. Contribution of Working Group I to the Fourth Assessment Report of the Intergovernmental Panel on Climate Change*. Cambridge University Press, Cambridge, United and Kingdom and New York, NY, USA. Weaver and Z.-C. Zhao, 2007.

A. Megann, D. Storkey, Y. Aksenov, S. Alderson, D. Calvert, T. Graham, P. Hyder, J. Siddorn, and B. Sinha. GO5.0: The joint NERC-Met Office NEMO global ocean model for use in coupled and forced applications. *Geoscientific Model Development*, 7(3):1069–1092, 2014. ISSN 19919603. doi: 10.5194/gmd-7-1069-2014.

N. Melia, K. Haines, and E. Hawkins. Sea ice decline and 21st century trans-Arctic shipping routes. *Geophysical Research Letters*, 43(18):9720–9728, 2016. ISSN 19448007. doi: 10.1002/2016GL069315.

C. Melsheimer, T. Frost, and G. Heygster. Detectability of Polar Mesocyclones and Polar Lows in Data from Space-Borne Microwave Humidity Sounders. *IEEE Journal of Selected Topics in Applied Earth Observations and Remote Sensing*, 9(1):326–335, 2016. ISSN 21511535. doi: 10.1109/JSTARS.2015.2499083.

C. Michel, A. Terpstra, and T. Spengler. Polar Mesoscale Cyclone Climatology for the Nordic Seas based on the ERA-Interim Reanalysis. *Journal of Climate*, pages JCLI–D–16–0890.1, 2017. ISSN 0894-8755. doi: 10.1175/JCLI-D-16-0890.1.

M. S. Mizielinski, M. J. Roberts, P. L. Vidale, R. Schiemann, M. E. Demory, J. Strachan, T. Edwards, A. Stephens, B. N. Lawrence, M. Pritchard, P. Chiu, A. Iwi, J. Churchill, C. Del Cano Novales, J. Kettleborough, W. Roseblade, P. Selwood, M. Foster, M. Glover, and A. Malcolm. High-resolution global climate modelling: The UPSCALE project, a large-simulation campaign. *Geoscientific Model Development*, 7(4):1629–1640, 2014. ISSN 19919603. doi: 10.5194/gmd-7-1629-2014.

M. T. Montgomery and B. F. Farrell. Polar Low Dynamics. 49:2484–2505, 1992. ISSN 0022-4928. doi: 10.1175/1520-0469(1992)049⟨2484:PLD⟩2.0.CO;2.

G. W. K. Moore, M. C. Reader, J. York, and S. Sathiyamoorthy. Polar lows in the Labrador Sea. A case study, 1996. ISSN 0280-6495.

G. W. K. Moore, K. Våge, R. S. Pickart, and I. A. Renfrew. Decreasing intensity of open-ocean convection in the Greenland and Iceland seas. *Nature Climate Change*, 5(9):877–882, 2015. ISSN 1758-678X. doi: 10.1038/nclimate2688.

R. Moss, M. Babiker, S. Brinkman, E. Calvo, T. Carter, J. Edmonds, I. Elgizouli, S. Emori, L. Erda, K. Hibbard, R. Jones, M. Kainuma, J. Kelleher, J. F. Lamarque, M. Manning, B. Matthews, J. Meehl, L. Meyer, J. Mitchell, N. Nakicenovic, B. O'Neill, R. Pichs, K. Riahi, S. Rose, P. Runci, R. Stouffer, D. van Vuuren, J. Weyant, T. Wilbanks, J. P. van Ypersele, and M. Zurek. Towards new scenarios for analysis of emissions, climate change, impacts and response strategies. *IPCC Expert Meeting Report*, page 25, 2008. ISSN 0022-2372. doi: 10.1086/652242.

R. J. Murray and I. Simmonds. A numerical scheme for tracking cyclone centres from digital data. Part I: Development and operation of the scheme. *Australian Meteorological Magazine*, 39(3):155–166, 1991. ISSN 0894-8755. doi: 10.1175/JCLI4203.1.

P. J. Neiman and M. a. Shapiro. The life cycle of an extratropical marine cyclone. Part I: frontal-cyclone evolution and thermodynamic air-sea interaction. *Monthly Weather Review, American Meteorological Society*, 121(8):2153–2176, 1993. ISSN 0027-0644. doi: 10.1175/1520-0493(1993)121⟨2153:TLCOAE⟩2.0.CO;2.

K. Ninomiya. Polar / Comma-Cloud Lows over the Japan Sea Pacific in Winter and the Northwestern. *Meteorological Society of Japan*, (February):83–97, 1989.

K. Ninomiya and K. Wakahara. Meso-a-scale Low Development over the Northeastern Japan Sea under the Influence of a Parent Large-scale and a Cold Vortex Aloft Low. 1993.

G. Noer, Ø. Saetra, T. Lien, and Y. Gusdal. A climatological study of polar lows in the Nordic Seas. *Quarterly Journal of the Royal Meteorological Society*, 137(660): 1762–1772, 2011. ISSN 00359009. doi: 10.1002/qj.846.

A. P. Orimolade, S. Larsen, and O. T. Gudmestad. Vessel stability in polar low situations: case study for semi-submersible drilling rigs. *Ships and Offshore Structures*, 13(3):303–309, 2018. ISSN 17445302. doi: 10.1080/17445302.2017.1372959.

Orimolade A.P., Furevik B.R., Noer G., Gudmestad O.T., and S. R.M. Waves in Polar lows. *American Geophysical Union*, (2):3372–3380, 2016. ISSN 21699275. doi: 10.1002/2015JC011421.Received.

M. Pagowski and G. W. K. Moore. A Numerical Study of an Extreme Cold-Air Outbreak over the Labrador Sea: Sea Ice, Air-Sea Interaction, and Development of Polar Lows. *Monthly Weather Review*, 129(1):47–72, 2001. ISSN 0027-0644. doi: 10.1175/1520-0493(2001)129⟨0047:ANSOAE⟩2.0.CO;2.

L. Papritz. Synoptic environments and characteristics of cold air outbreaks in the Irminger Sea. *International Journal of Climatology*, 37(January):193–207, 2017. ISSN 10970088. doi: 10.1002/joc.4991.

L. Papritz, S. Pfahl, H. Sodemann, and H. Wernli. A climatology of cold air outbreaks and their impact on air-sea heat fluxes in the high-latitude South Pacific. *Journal of Climate*, 28(1):342–364, 2015. ISSN 08948755. doi: 10.1175/JCLI-D-14-00482.1.

C. L. Parkinson and N. E. DiGirolamo. New visualizations highlight new information on the contrasting Arctic and Antarctic sea-ice trends since the late 1970s. *Remote Sensing of Environment*, 183:198–204, 2016. ISSN 00344257. doi: 10.1016/j.rse.2016.05.020.

J. Perlwitz, M. Hoerling, and R. Dole. Arctic tropospheric warming: Causes and linkages to lower latitudes. *Journal of Climate*, 28(6):2154–2167, 2015. ISSN 08948755. doi: 10.1175/JCLI-D-14-00095.1.

A. Pezza, K. Sadler, P. Uotila, T. Vihma, M. D. S. Mesquita, and P. Reid. Southern Hemisphere strong polar mesoscale cyclones in high-resolution datasets. *Climate Dynamics*, 47(5-6):1647–1660, 2016. ISSN 14320894. doi: 10.1007/s00382-015-2925-2.

J. G. L. Rae, H. T. Hewitt, A. B. Keen, J. K. Ridley, A. E. West, C. M. Harris, E. C. Hunke, and D. N. Walters. Development of the Global Sea Ice 6.0 CICE configuration for the Met Office Global Coupled model. *Geoscientific Model Development*, 8(7): 2221–2230, 2015. ISSN 19919603. doi: 10.5194/gmd-8-2221-2015.

E. Rasmussen. The polar low as an extratropical CISK disturbance. *Quarterly Journal of the Royal Meteorological Society*, 105(445):531–549, 1979. ISSN 1477870X. doi: 10.1002/qj.49710544504.

E. A. Rasmussen and J. Turner. *Polar Lows: Mesoscale Weather Systems in the Polar Regions*. Cambridge University Press, 2003. ISBN 9780521624305.

I. A. Renfrew and G. W. K. Moore. An Extreme Cold-Air Outbreak over the Labrador Sea: Roll Vortices and Air-Sea Interaction. *Monthly Weather Review*, 127(10):2379–2394, 1999. ISSN 0027-0644. doi: 10.1175/1520-0493(1999)127⟨2379:AECAOO⟩2.0.CO;2.

K. Riahi, S. Rao, V. Krey, C. Cho, V. Chirkov, G. Fischer, G. Kindermann, N. Nakicenovic, and P. Rafaj. RCP 8.5-A scenario of comparatively high greenhouse gas emissions. *Climatic Change*, 109(1):33–57, 2011. ISSN 01650009. doi: 10.1007/s10584-011-0149-y.

M. J. Roberts, P. L. Vidale, M. S. Mizielinski, M. E. Demory, R. E. S. Schiemann, J. A. N. E. S. Strachan, K. E. H. Hodges, R. A. Y. B. Bell, and J. O. C. Camp. Tropical Cyclones in the UPSCALE Ensemble of High-Resolution Global Climate Models *. *Journal of Climate*, pages 574–596, 2014. doi: 10.1175/JCLI-D-14-00131.1.

J. Robson, D. Hodson, E. Hawkins, and R. Sutton. Atlantic overturning in decline? *Nature Geoscience*, 7(1):2–3, 2014. ISSN 1752-0894. doi: 10.1038/ngeo2050.

M. Rojo, C. Claud, P. E. Mallet, G. Noer, A. M. Carleton, and M. Vicomte. Polar low tracks over the Nordic Seas: A 14-winter climatic analysis. *Tellus, Series A: Dynamic Meteorology and Oceanography*, 67(1):1–20, 2015. ISSN 16000870. doi: 10.3402/tellusa.v67.24660.

R. Romero and K. Emanuel. Climate Change and Hurricane-Like Extratropical Cyclones: Projections for North Atlantic Polar Lows and Medicanes Based on CMIP5 Models. *Journal of Climate*, 30(1):279–299, 2017. ISSN 0894-8755. doi: 10.1175/JCLI-D-16-0255.1.

R. Rotunno and K. a. Emanuel. An Air-Sea Interaction Theory for Tropical Cyclones. Part II: Evolutionary Study Using a Nonhydrostatic Axisymmetric Numerical Model. *Journal of the Atmospheric Sciences*, 44(3):542–561, 1987. ISSN 0022-4928. doi: 10.1175/1520-0469(1987)044⟨0542:AAITFT⟩2.0.CO;2.

B. Rudels. Haline convection in the greenland sea. *Journal of Marine System*, 37: 1491–1511, 09 1990.

B. Rudels and D. Quadfasel. Convection and deep water formation in the Arctic Ocean-Greenland Sea System. *Journal of Marine Systems*, 2(3-4):435–450, 1991. ISSN 09247963. doi: 10.1016/0924-7963(91)90045-V.

O. Saetra, T. Linders, and J. B. Debernard. Can polar lows lead to a warming of the ocean surface? *Tellus, Series A: Dynamic Meteorology and Oceanography*, 60 A(1): 141–153, 2008. ISSN 02806495. doi: 10.1111/j.1600-0870.2007.00279.x.

J. Safarov, F. Millero, R. Feistel, a. Heintz, and E. Hassel. Thermodynamic properties of standard seawater: extensions to high temperatures and pressures. *Ocean Science*, 5:235–246, 2009. ISSN 1812-0792. doi: 10.5194/os-5-235-2009.

S. Saha, S. Nadiga, C. Thiaw, J. Wang, W. Wang, Q. Zhang, H. M. Van den Dool, H. L. Pan, S. Moorthi, D. Behringer, D. Stokes, M. Peña, S. Lord, G. White, W. Ebisuzaki, P. Peng, and P. Xie. The NCEP Climate Forecast System. *Journal of Climate*, 19 (15):3483–3517, 2006. ISSN 08948755. doi: 10.1175/JCLI3812.1.

S. Saha, S. Moorthi, H. L. Pan, X. Wu, J. Wang, S. Nadiga, P. Tripp, R. Kistler, J. Woollen, D. Behringer, H. Liu, D. Stokes, R. Grumbine, G. Gayno, J. Wang, Y. T. Hou, H. Y. Chuang, H. M. H. Juang, J. Sela, M. Iredell, R. Treadon, D. Kleist, P. Van Delst, D. Keyser, J. Derber, M. Ek, J. Meng, H. Wei, R. Yang, S. Lord, H. Van Den Dool, A. Kumar, W. Wang, C. Long, M. Chelliah, Y. Xue, B. Huang, J. K. Schemm, W. Ebisuzaki, R. Lin, P. Xie, M. Chen, S. Zhou, W. Higgins, C. Z. Zou, Q. Liu, Y. Chen, Y. Han, L. Cucurull, R. W. Reynolds, G. Rutledge, and M. Goldberg. The NCEP climate forecast system reanalysis. *Bulletin of the American Meteorological Society*, 91(8):1015–1057, 2010. ISSN 00030007. doi: 10.1175/2010BAMS3001.1.

P. D. Sardeshmukh and B. I. Hoskins. Spatial Smoothing on the Sphere, 1984. ISSN 0027-0644.

A. Schmittner, J. C. H. Chiang, and S. R. Hemming. Introduction: The Ocean's Meridional Overturning Circulation. *Ocean Circulation: Mechanisms and Impacts - Past and Future Changes of Meridional Overturning*, pages 1–4, 2013. doi: 10.1029/173GM02.

J. A. Screen and I. Simmonds. The central role of diminishing sea ice in recent Arctic temperature amplification. *Nature*, 464(7293):1334–1337, 2010. ISSN 0028-0836. doi: 10.1038/nature09051.

D. E. Sergeev, I. A. Renfrew, T. Spengler, and S. R. Dorling. Structure of a shear-line polar low. *Quarterly Journal of the Royal Meteorological Society*, 143(702):12–26, 2017. ISSN 1477870X. doi: 10.1002/qj.2911.

M. C. Serreze. Climatological aspects of cyclone development and decay in the Arctic. *Atmosphere - Ocean*, 33(1):1–23, 1995. ISSN 14809214. doi: 10.1080/07055900.1995.9649522.

M. A. Shapiro, L. S. Fedor, and T. Hampel. Research aircraft measurements of a polar low over the Norwegian Sea. *Tellus A*, 39 A(4):272–306, 1987. ISSN 16000870. doi: 10.1111/j.1600-0870.1987.tb00309.x.

U. Shimada, A. Wada, K. Yamazaki, and N. Kitabatake. Roles of an upper-level cold vortex and low-level baroclinicity in the development of polar lows over the Sea of Japan. *Tellus*, 66A:24694, 2014. ISSN 1600-0870. doi: 10.3402/tellusa.v66.24694.

G. Siedler, J. Church, and J. Gould. *Ocean Circulation and Climate - Observing and Modelling the Global Ocean*. Internatio edition, 2001a. ISBN 0126413517.

G. Siedler, J. Church, and J. Gould. *Ocean circulation and climate*. Academic p - international geophysics series edition, 2001b. ISBN 0126413517.

B. Silverman. *Density Estimation for Statistics and Data Analysis*. Chapman & Hall/CRC Monographs on Statistics & Applied Probability. Taylor & Francis, 1986. ISBN 9780412246203.

B. Sinha, D. A. Smeed, G. McCarthy, B. I. Moat, S. A. Josey, J. J.-M. Hirschi, E. Frajka-Williams, A. T. Blaker, D. Rayner, and G. Madec. The accuracy of estimates of the overturning circulation from basin-wide mooring arrays. *Progress in Oceanography*, 160:101–123, 2018. ISSN 00796611. doi: 10.1016/j.pocean.2017.12.001.

W. C. Skamarock. Evaluating Mesoscale NWP Models Using Kinetic Energy Spectra. *Monthly Weather Review*, 132(12):3019–3032, 2004. ISSN 0027-0644. doi: 10.1175/mwr2830.1.

W. C. Skamarock, S.-H. Park, J. B. Klemp, and C. Snyder. Atmospheric Kinetic Energy Spectra from Global High-Resolution Nonhydrostatic Simulations. *Journal of the Atmospheric Sciences*, 71(11):4369–4381, 2014. ISSN 0022-4928. doi: 10.1175/jas-d-14-0114.1.

J. Smirnova and P. Golubkin. Comparing polar lows in atmospheric reanalyses: Arctic System Reanalysis versus ERA-Interim. *Monthly Weather Review*, pages MWR–D–16–0333.1, 2017. ISSN 0027-0644. doi: 10.1175/MWR-D-16-0333.1.

J. E. Smirnova, P. A. Golubkin, L. P. Bobylev, E. V. Zabolotskikh, and B. Chapron. Polar low climatology over the Nordic and Barents seas based on satellite passive microwave data. *Geophysical Research Letters*, 42(13):5603–5609, 2015. ISSN 19448007. doi: 10.1002/2015GL063865.

J. E. Smirnova, E. V. Zabolotskikh, L. P. Bobylev, and B. Chapron. Statistical characteristics of polar lows over the Nordic Seas based on satellite passive microwave data. *Izvestiya, Atmospheric and Oceanic Physics*, 52(9):1128–1136, 2016. ISSN 0001-4338. doi: 10.1134/S0001433816090255.

T. Spengler, C. Claud, and G. Heinemann. Polar low workshop summary. *Bulletin of the American Meteorological Society*, 98(6):ES139–ES142, 2017. ISSN 00030007. doi: 10.1175/BAMS-D-16-0207.1.

P. Stoll, R. G. Graversen, G. Noer, and K. Hodges. An objective global climatology of polar lows based on reanalysis data. *Quarterly Journal of the Royal Meteorological Society*, 2018. ISSN 00359009. doi: 10.1002/qj.3309.

H. V. Storch and F. W. Zwiers. Statistical Analysis in Climate Research. *Journal of the American Statistical Association*, 95:1375, 1999. ISSN 01621459. doi: 10.1017/CBO9780511612336.

J. Stroeve, M. M. Holland, W. Meier, T. Scambos, and M. Serreze. Arctic sea ice decline: Faster than forecast. *Geophysical Research Letters*, 34(9):1–5, 2007. ISSN 00948276. doi: 10.1029/2007GL029703.

J. C. Stroeve, V. Kattsov, A. Barrett, M. Serreze, T. Pavlova, M. Holland, and W. N. Meier. Trends in Arctic sea ice extent from CMIP5, CMIP3 and obser-

vations. *Geophysical Research Letters*, 39(16):1–7, 2012. ISSN 00948276. doi: 10.1029/2012GL052676.

R. Stull. *An Introduction to Boundary Layer Meteorology*. Atmospheric and Oceanographic Sciences Library. Springer Netherlands, 1988. ISBN 9789027727695.

K. E. Taylor, R. J. Stouffer, and G. A. Meehl. An overview of CMIP5 and the experiment design. *Bulletin of the American Meteorological Society*, 93(4):485–498, 2012. ISSN 00030007. doi: 10.1175/BAMS-D-11-00094.1.

A. Terpstra. *Dynamical Perspectives on the Formation and Intensification of Polar Lows*. PhD thesis, University of Bergen (Norway), 2014.

A. Terpstra, T. Spengler, and R. W. Moore. Idealised simulations of polar low development in an Arctic moist-baroclinic environment. *Quarterly Journal of the Royal Meteorological Society*, 141(691):1987–1996, 2015. ISSN 00359009. doi: 10.1002/qj.2507.

A. Terpstra, C. Michel, T. Spengler, A. Terpstra, C. Michel, and T. Spengler. Forward and Reverse Shear Environments during Polar Low Genesis over the Northeast Atlantic. *Monthly Weather Review*, 144(4):1341–1354, 2016. ISSN 0027-0644. doi: 10.1175/MWR-D-15-0314.1.

N. Tilinina, S. Gulev, and D. Bromwich. New view of Arctic cyclone activity from the Arctic system reanalysis. *Geophysical Research Letters*, pages 4068–4074, 2014. doi: 10.1002/2014GL059980.Received.

M. Tous, G. Zappa, R. Romero, L. Shaffrey, and P. L. Vidale. Projected changes in medicanes in the HadGEM3 N512 high-resolution global climate model. *Climate Dynamics*, 47(5-6):1913–1924, 2016. ISSN 14320894. doi: 10.1007/s00382-015-2941-2.

Unesco. The Practical Salinity Scale 1978 and the International Equation of State of Seawater. Technical report, 1981.

S. M. Uppala, P. W. Kallberg, A. J. Simmons, U. Andrae, V. D. C. Bechtold, M. Fiorino, J. K. Gibson, J. Haseler, A. Hernandez, G. A. Kelly, X. Li, K. Onogi, S. Saarinen, N. Sokka, R. P. Allan, E. Andersson, K. Arpe, M. A. Balmaseda, A. C. M. Beljaars, L. V. D. Berg, J. Bidlot, N. Bormann, S. Caires, F. Chevallier, A. Dethof, M. Dragosavac, M. Fisher, M. Fuentes, S. Hagemann, E. Hólm, B. J. Hoskins, L. Isaksen, P. A. E. M. Janssen, R. Jenne, A. P. Mcnally, J.-F. Mahfouf, J.-J. Morcrette, N. A. Rayner, R. W. Saunders, P. Simon, A. Sterl, K. E. Trenberth, A. Untch,

D. Vasiljevic, P. Viterbo, and J. Woollen. The ERA-40 re-analysis. *Quarterly Journal of the Royal Meteorological Society*, 131(612):2961–3012, 2005. ISSN 00359009. doi: 10.1256/qj.04.176.

K. Våge, R. S. Pickart, M. A. Spall, H. Valdimarsson, S. Jónsson, D. J. Torres, S. Østerhus, and T. Eldevik. Significant role of the North Icelandic Jet in the formation of Denmark Strait overflow water. *Nature Geoscience*, 4:723, aug 2011.

K. Våge, R. S. Pickart, M. A. Spall, G. W. Moore, H. Valdimarsson, D. J. Torres, S. Y. Erofeeva, and J. E. Ø. Nilsen. Revised circulation scheme north of the Denmark Strait. *Deep-Sea Research Part I: Oceanographic Research Papers*, 79:20–39, 2013. ISSN 09670637. doi: 10.1016/j.dsr.2013.05.007.

K. Våge, G. W. Moore, S. Jónsson, and H. Valdimarsson. Water mass transformation in the Iceland Sea. *Deep-Sea Research Part I: Oceanographic Research Papers*, 101: 98–109, 2015. ISSN 09670637. doi: 10.1016/j.dsr.2015.04.001.

S. Vavrus, J. E. Walsh, W. L. Chapman, and D. Portis. The behavior of extreme cold air outbreaks under greenhouse warming. *International Journal of Climatology*, 26 (9):1133–1147, 2006. ISSN 08998418. doi: 10.1002/joc.1301.

P. Verezemskaya, N. Tilinina, S. Gulev, I. A. Renfrew, and M. Lazzara. Southern Ocean mesocyclones and polar lows from manually tracked satellite mosaics. *Geophysical Research Letters*, 44(15):7985–7993, 2017. ISSN 19448007. doi: 10.1002/2017GL074053.

H. Von Storch and F. W. Zwiers. *Statistical Ananlysis in Climate Research*, volume 29. Cambridge edition, 1999. ISBN ISBN 0 521 45071 3. doi: 10.3354/cr029001.

D. Walters, I. Boutle, M. Brooks, T. Melvin, R. Stratton, S. Vosper, H. Wells, K. Williams, N. Wood, T. Allen, A. Bushell, D. Copsey, P. Earnshaw, J. Edwards, M. Gross, S. Hardiman, C. Harris, J. Heming, N. Klingaman, R. Levine, J. Manners, G. Martin, S. Milton, M. Mittermaier, C. Morcrette, T. Riddick, M. Roberts, C. Sanchez, P. Selwood, A. Stirling, C. Smith, D. Suri, W. Tennant, P. Luigi Vidale, J. Wilkinson, M. Willett, S. Woolnough, and P. Xavier. The Met Office Unified Model Global Atmosphere 6.0/6.1 and JULES Global Land 6.0/6.1 configurations. *Geoscientific Model Development*, 10(4):1487–1520, 2017. ISSN 19919603. doi: 10.5194/gmd-10-1487-2017.

S.-i. I. Watanabe and H. Niino. Genesis and Development Mechanisms of a Polar Mesocyclone over the Japan Sea. *Monthly Weather Review*, 142(6):2248–2270, 2014. ISSN 0027-0644. doi: 10.1175/MWR-D-13-00226.1.

S.-i. I. Watanabe, H. Niino, and W. Yanase. Climatology of Polar Mesocyclones over the Sea of Japan Using a New Objective Tracking Method. *Monthly Weather Review*, 144:2503–2515, 2016. ISSN 0027-0644. doi: 10.1175/MWR-D-15-0349.1.

S.-i. I. Watanabe, H. Niino, and W. Yanase. Structure and Environment of Polar Mesocyclones over the Northeastern Part of the Sea of Japan. *Monthly Weather Review*, 145(6):2217–2233, 2017. ISSN 0027-0644. doi: 10.1175/MWR-D-16-0342.1.

K. Wilhelmsen. Climatological study of gale-producing polar lows near Norway. *Tellus A*, 37 A(5):451–459, 1985. ISSN 16000870. doi: 10.1111/j.1600-0870.1985.tb00443.x.

D. S. Wilks. *Statistical methods in the atmospheric sciences*. Elsevier s edition, 2005. ISBN 9780127519661.

K. D. Williams, C. M. Harris, J. Camp, R. E. Comer, D. Copsey, D. Fereday, T. Graham, R. Hill, T. Hinton, P. Hyder, S. Ineson, G. Masato, S. F. Milton, M. J. Roberts, D. P. Rowell, C. Sanchez, A. Shelly, B. Sinha, D. N. Walters, A. West, T. Woollings, and P. K. Xavier. The Met Office Global Coupled model 2.0 (GC2) configuration. *Geoscientific Model Development*, 0:1509–1524, 2015. doi: 10.5194/gmd-88-1509-2015.

T. Woollings, B. Harvey, M. Zahn, and L. Shaffrey. On the role of the ocean in projected atmospheric stability changes in the Atlantic polar low region. *Geophysical Research Letters*, 39(24):1–5, 2012. ISSN 00948276. doi: 10.1029/2012GL054016.

B. L. Xia, M. Zahn, K. I. Hodges, F. Feser, and H. V. Storch. A comparison of two identification and tracking methods for polar lows. *Tellus, Series A: Dynamic Meteorology and Oceanography*, 64(1):1–11, 2012a. ISSN 02806495. doi: 10.3402/tellusa.v64i0.17196.

B. L. Xia, M. Zahn, K. I. Hodges, F. Feser, and H. V. Storch. A comparison of two identification and tracking methods for polar lows. *Tellus, Series A: Dynamic Meteorology and Oceanography*, 64(1), 2012b. ISSN 02806495. doi: 10.3402/tellusa.v64i0.17196.

W. Yanase, H. Niino, S. I. I. Watanabe, K. Hodges, M. Zahn, T. Spengler, and I. A. Gurvich. Climatology of polar lows over the sea of Japan using the JRA-55 reanalysis. *Journal of Climate*, 29(2):419–437, 2016. ISSN 08948755. doi: 10.1175/JCLI-D-15-0291.1.

M. Zahn and H. Von Storch. (a). A long-term climatology of North Atlantic polar lows. *Geophysical Research Letters*, 35(22):1–6, 2008. ISSN 00948276. doi: 10.1029/2008GL035769.

M. Zahn and H. von Storch. (b). Tracking polar lows in CLM. *Meteorologische Zeitschrift*, 17(4):445–453, 2008. ISSN 09412948. doi: 10.1127/0941-2948/2008/0317.

M. Zahn and H. von Storch. Decreased frequency of North Atlantic polar lows associated with future climate warming. *Nature*, 467(7313):309–12, 2010. ISSN 1476-4687. doi: 10.1038/nature09388.

M. Zahn, H. Von Storch, and S. Bakan. Climate mode simulation of North Atlantic polar lows in a limited area model. *Tellus, Series A: Dynamic Meteorology and Oceanography*, 60 A(4):620–631, 2008. ISSN 02806495. doi: 10.1111/j.1600-0870.2008.00330.x.

G. Zappa, L. Shaffrey, and K. Hodges. Can Polar Lows be Objectively Identified and Tracked in the ECMWF Operational Analysis and the ERA-Interim Reanalysis? *Mon. Wea. Rev.*, 142(8):2596–2608, 2014. ISSN 0027-0644. doi: 10.1175/mwr-d-14-00064.1.